

THE UNIVERSITY OF HULL

River Dunes in Unsteady Conditions

being a Thesis submitted for the Degree of Doctor of Philosophy
in the University of Hull

by

Christopher Adam Unsworth, MRes, Bsc.

February 2015

Thesis abstract

This thesis explores the nature of river dunes in unsteady conditions. River dune research has two main philosophical approaches that are necessitated by the nature of dunes; they are individually dynamic features emergent from the interaction between flow and sediment transport, whilst this dynamism is restricted by a mixture of instantaneous and historical flow and sediment boundary conditions.

This thesis has applied both philosophical approaches to the investigation of river dunes in unsteady conditions and highlights key areas where flow and sediment processes at the laboratory scale overlap that of the larger scale river, such as in the suspension of sediment, and importance of velocity profile shape on dune shape. Normalising the downstream velocity with shear velocity was repeatedly found to simplify and explain the fluid processes over dunes across a range of conditions and indicates that the dominant processes controlling dune shape and sediment mobility are hydraulically smooth, despite hydraulically rough grain sizes. The existence of a turbulent wave over dunes reduces the magnitude of flow velocity that reaches the bed and effectively changes the grain Reynolds number.

This turbulent flow structure was extensively measured in this thesis, with detailed instantaneous flow velocity measurements, across a range of flow conditions over fixed bedforms with the use of Particle Imaging Velocimetry. This also revealed that the well-known equilibrium turbulent flow structure over dunes is dramatically altered when in transient flow-morphology conditions. It was found that the wake and stacked wake, changes location and intensity with flow depth and discharge, and that reattachment length is strongly related to U/u^* as measured at the dune crest. This research provides descriptions of the causal mechanisms behind many bedform adaptations to flow unsteadiness, such as the formation of humpback dunes in high shear stress conditions.

A second set of laboratory experiments explored the mean scaling of dunes with a mobile bed in a recirculating flume. The mean velocity profile shape was adjusted to move the point of maximum downstream velocity toward the bed, whilst keeping depth and depth averaged velocity- two variables used in almost all bedform stability diagrams, the same. It was found that dune height scaled with

bed shear stress in a parabola, whilst dune wavelength scaled linearly. This indicates that dune height is primarily controlled via flow separation and dune wavelength scales most well is shear velocity and grain size (i.e. sediment transport lengths).

Lastly, dunes were measured in the field during the falling leg of the monsoonal wet season floods on a section of the Mekong River in Cambodia. The river bed consisted of large dunes with superimposed bedforms. The geometry of the large dunes showed no relationship with the hydraulic conditions present; however the secondary dunes size responded to the variations in flow depth. All large dunes migrated at a constant rate, despite variation in height, and it was hypothesised that the superimposed bedforms provided any excess sediment for the host dune migration.

Large dune height was half that predicted from empirical equations using flow depth. Variations in suspended sediment did not match those predicted via the Rouse number, instead, plotting U/u^* , across variations in discharge and depth showed a good relationship with suspended sediment concentration. This relationship between flow structure and suspended sediment, with the concurrent variation secondary dune size indicated that the large dunes were depth limited. This is despite the consistent presence of secondary dunes at the crest of the host bedform or strong free surface interaction and suggests that dune height in rivers with superimposed bedforms is controlled by the existence of superimposed bedforms.

Contents

Chapter 1	1
Introduction	1
1.1 The importance of understanding rivers	1
Chapter 2	9
Literature Review	9
2.1.1 Scaling of bedform morphology	9
2.1.2 Shape of dunes	22
2.1.3 Flow structure and grain & form roughness	24
2.1.4 Sediment movement with dunes	27
2.2 Current issues	31
2.2.1 Shear and reattachment	31
2.2.2 Hysteresis	32
2.2.3 Local Sediment Supply	36
2.3 Thesis aims, hypothesis and objectives	37
2.4 Thesis outline	39
Chapter 3	41
A Primer on using Particle Imaging Velocimetry in Geomorphological Research	41
3.1 Introduction	41
3.2 Methodological Overview	45
3.3 General Advantages and Limitations	47
3.4 Assessment of Data Collection Parameters	51
3.5 Data Quality & Post processing	52
3.6 Examples of PIV in Geomorphological Research	54
3.7 Summary	56
Chapter 4	57
Flow Structures over Fixed 2D Bedforms in Transient States	57
4.1 Introduction	57
4.2 Methods	62
4.2.1 Flume setup and experimental conditions	62
4.2.2 Analysis of turbulent flow statistics	66
4.3. Results	68
4.3.1 Depth Averaged Velocities	68

4.3.2 Mean flow velocity profiles	69
4.3.3 Reattachment length.....	74
4.3.4 Reynolds Stress	78
4.3.5 Quadrant Analysis.....	81
4.4 Discussion	88
4.4.1 Implications for the stability of dunes	94
4.4.2 Implications for sediment transport	98
4.4.3 Implications for dunes in transient conditions & impacts on superimposed bedforms.....	101
4.5 Limitations	104
4.6 Conclusions	105
4.6 Synthesis	107
Chapter 5.....	108
On the scaling and definitions of unidirectional bedforms.....	108
5.1 Introduction.....	108
5.2.1 Experimental setup.....	116
5.2.2 Post Processing of data	121
5.2.3 Flume conditions.....	123
5.3 Results	127
5.3.2 Intermittent Dune-Upper Stage Plane Bed	141
5.4 Discussion	144
5.4.1 Dune scaling	145
5.4.2 Upper stage plane bed transitions	151
5.5 Addendum	152
5.6 Limitations	155
5.7 Conclusions	155
5.8 Synthesis	156
Chapter 6	159
Dune Dynamics at the Field Scale	159
6.1. Introduction.....	159
6.2. Methods.....	162
6.2.1. Study Area	162
6.2.2. Data Collection Instruments, accuracy and correction.....	164
6.2.3. Collection area.....	165
6.2.4. MBES and aDcp Post-Processing	168

6.2.5. Calibration of aDcp Backscatter to Suspended Sediment Concentrations	168
6.3 Results	170
6.3.1 Dune field morphology	170
6.3.2 Overall Flow Field	180
6.3.3 Dune lee side flow	183
6.3.4 Suspended sediment	193
6.4 Discussion	192
6.4.1 Controls on Large Dune height	192
6.4.2 Scale of bed features and rates of change	198
6.4.3 Mode of sediment transport	186
6.5. Limitations	203
6.5. Conclusions	204
6.5. Synthesis.....	205
Chapter 7.....	207
Thesis Synthesis.....	207
7.1 Hypotheses and Conclusions.....	207
7.2 Key Thesis Synthesis	210
Reference list	211

List of figures

Figure 1-1	Distribution of flooding hazard frequency between the tropics, 1985-2003, superimposed on drainage basin boundaries. The figure shows that heavily populated regions, such as Bangladesh, S.E. Asia and China, North America and Eastern South America also have particularly high flood hazard frequency. From Syvitski et al.(2014).	p2
Figure 1-2	The relationship between flow depth and discharge across a transition from lower flow regime (ripples and dunes) to upper flow regime (flat bed and anti-dunes). Flow depth in the rising leg rises substantially whilst dunes are present, then falls sharply at $\sim 12 \text{ cf/s-1}$, when the dunes disappear. From Simons & Richardson 1962.	p3
Figure 1-3	From Cohen et al., (2014). Southeast Asia riverine normalized departure from mean for 1971 for; (top) sediment flux overlaying a lithology factor map, derived according to Syvitski and Milliman (2007), and (bottom) water discharge overlaying precipitation normalized departure from mean map, comparing annual precipitation of 1971 with 50 year average precipitation (1960–2010). Black line is an outline of the Ganges River Basin.	p6
Figure 1-4	Perspectives of River Dunes.	p8
Figure 2-1	A synthesis of bedform initiation via burst and sweeps. From Best (1992).	p11
Figure 2-2	Experimental existence fields for aqueous bedforms under equilibrium conditions, shown in the non-dimensional mean bed shear stress (wall-corrected)-grain size plane at 25°C. (From Allen 1982 pp 340, References for data points therein).	p14
Figure 2-3	From Van Rijn 1984. Bed state stability diagram for lower and transitional regime.	p15
Figure 2-4	Scatter of group mean height and mean water depth for dunes in river and marine or marine-influenced settings, with the relative dune height (H/h) as a parameter. There is a general trend for longer bedforms and deeper water, but there is considerable scatter. (From Allen 1982 pp333, references for data therein.)	p18
Figure 2-5	Correlation between group mean wavelength and water depth for dunes in river and marine or marine-influenced setting. The scatter is large, particularly at the larger water depths, but the scale of dunes clearly increases with increasing scale of flow. (From Allen 1982 pp331, references for data therein).	p19
Figure 2-6	Group mean dune height relative to mean water depth as a function under equilibrium conditions of the non-dimensional boundary shear stress and sediment calibre. Stress corrected for wall effects by procedure of G.P. Williams (1970). These plots show that dune height responds strongly to the boundary shear stress, with scatter less than when plotted against depth (Figure 8). From Allen 1982, pp334, data references therein.	p20
Figure 2-7	Effect of grain size on non-dimensional group mean dune wavelength and Froude number. The plotted line fits the dunes in the coarsest sand the best. (From Allen 1982, pp 332- references therein).	p21
Figure 2-8	Dune shape and definitions for steep and diminished dunes. (From Carling et al., 2000a. Modified from Allen 1968.	p23
Figure 2-9	Schematic diagram of the principal regions of flow over asymmetrical, angle-of-repose dunes. From Best 2005.	p25
Figure 2-10	Plots of mean dune height versus discharge (top row), mean dune length versus discharge (second row), mean dune steepness versus discharge (third row) and mean dune migration rate (U_s) versus discharge (bottom row). From Gabel (1993).	p33
Figure 2-11	Conceptualization of bedform growth and decay processes. (From Martin	p34

	and Jeolmack (2013).	
Figure 2-12	Diagram describing interactions in the bed-form merger growth model. From Martin and Jeolmack (2013).	p35
Figure 3-1	A typical monoscopic (2D-PIV) system overview. Figure adapted from Adrian (2005).	p41
Figure 3-2	Instantaneous 2D flow field over the centreline of a 2D dune shape. Axis are normalised by the dune height d . Vector arrows have been doubled in size, and the downstream (u) component suppressed by 68% (Tomkins & Adrian 1999; Adrian et al. 2000b) to highlight the rotational flow over the bedform. Flow direction is left to right. Flow separation downstream of the crest can be seen in the shorter vector magnitudes and reversed direction.	p41
Figure 3-3	Instantaneous 2D PIV data. The flow field is revealed though downstream, vertical velocities, Reynolds stress and Vorticity, illustrating how PIV can display a host of flow field information including detailed structure of the turbulence. The field of view is over the centreline of a 2D dune shape fixed to the base of a flume. Axis are normalised by the dune height d . Taken at the same instantaneous point in time as Figure 3-2	p42
Figure 3-4	An example of a raw image of lab 2D-PIV, illuminated from below. Field of view is downstream of a large bar fixed to the bed, flow is left to right.	p44
Figure 3-5	(above) example of 2D-PIV in a recirculating flume. Here the laser case and optics are outside the flume. A transparent flume floor and walls facilitate illumination and image capture. Image credit, C.A. Unsworth.	p47
Figure 3-6	(above) example of Large Scale Surface PIV, with calculated vectors superimposed in red. Image credit, Rui M.L. Ferreira.	p48
Figure 3-7	(above) example of a Volumetric PIV setup from TSI ©. This is a 3 camera system. Image credit, Gianluca Blois.	p48
Figure 4-1	Best (2005)'s summary conceptual diagram of flow over equilibrium dunes.	p56
Figure 4-2	Scaled schematic of laboratory dunes. The PIV field of view (large dashes) is centred over the middle dune. Mean bed level is 40mm as the dunes are triangular.	p61
Figure 4-3	Diagram of Quadrant definitions. The two axis are centred at 0,0 (the mean value for \bar{U} and \bar{V}). Dashed lines represent the threshold for quadrant classification, instantaneous values outside (away from 0,0) the dashed lines are above the Hole size and therefore count toward the quadrant percentage.	p65
Figure 4-4	Figure 4-4 Depth averaged velocities at the crest	p66
Figure 4-5	Time-averaged velocity profiles of streamwise velocity component \bar{U} (top panels) and vertical component \bar{V} (bottom panels) for conditions H14,M14 & L17.	p68
Figure 4-6	Time-averaged velocity profiles of streamwise velocity component U (top panels) and vertical component V (bottom panels) for conditions H76, M83 L73. A-B = at crest; C-D at trough; E-F near reattachment. + = 0.76ms^{-1} at 280mm, o = 0.83ms^{-1} at 240mm, x = 0.73ms^{-1} at 200mm depth.	p71
Figure 4-7	Flow reattachment lengths.	p73
Figure 4-8	Eddy shedding vs \bar{U}	p75
Figure 4-9	Wake Flapping vs \bar{U}	p76
Figure 4-10	Scaled images of the percentage of positive downstream velocity for all conditions at 280mm & 200mm depth. Flow direction is left to right. At the 280mm depth (left panels) reattachment length shortens slightly with higher \bar{U}_c , but this is inconsistent. The more significant change here is at the crest, where the flow reversal occurs higher in the flow with higher \bar{U}_c , leading to recirculation events occurring above the crest at the highest \bar{U} conditions here.	p76
Figure 4-11	2D contour plots of Reynolds Stress. Contours are normalised by the maximum Reynolds Stress value for each run. For the maximum Reynolds Stress magnitude see Table 4-1. Conditions naming: H=280mm depth, M= 240mm depth, L= 200mm depth. The number after the depth = \bar{U} in cms^{-1} . Dashed Black Lines shown on the L conditions indicate highlight how the angle of the area of high Reynolds stress changes with \bar{U} .	p78
Figure 4-12	Scaled images of significant ($H>1$) Quadrant 2 event contributions (colour	p83

	axis %). Contour levels are equal across images. Image naming: H=280mm depth, M= 240mm depth, L= 200mm depth. The number after the depth = \bar{U}_c in cms^{-1}	
Figure 4-13	Scaled images of significant ($H>1$) Quadrant 4 event contributions (colour axis %). Contour levels are equal across images. Image naming H=280mm depth, M= 240mm depth, L= 200mm depth. The number after the depth = \bar{U}_c in cms^{-1}	p84
Figure 4-14	Reattachment lengths compared to previous research	p88
Figure 4-15	Summary conceptual diagram of turbulent flow over dune in transient conditions. See conclusions for explanation of numbers. See introduction and Best 2005(a) for explanation of the Best 2005a diagram (middle, equilibrium condition)	p102
Figure 5-1	Conceptual diagram of sediment and fluid variables over migrating dunes in open channel flow. Modified and adapted from Raudikivi (1963), Allen (1982, their Figure 7-6) & Omid & Piomelli (2011 their Figure 5).	p106
Figure 5-2	From Milburn and Prowse (2002). Repeated measurements of downstream velocity under ice cover. Hay River, Northwest Territories, Canada, Station HR7, April 1–17, 1998. The Parabola shaped mean velocity profile is consistent across discharges.	p108
Figure 5-3	From Blanckaert (2011). Idealized downstream (v_s) and cross stream (v_n) velocity profiles in a meander bend. Note the downstream (pink) velocity maximum occurs around 50% flow depth, with a high gradient toward the bed.	p109
Figure 5-4	From Sequeiros et.al., (2010). Measured velocity profile and sediment densities in a laboratory flume. The height of high sediment density (0.04 in A, 0.03 in B) is strongly linked to the position of the velocity maximum. The consistent sediment density in B effectively shows a large moving sediment layer which reduces in velocity toward 0.	p109
Figure. 5-5	From Southard and Boguchwal, (1990). A Plot of bed state stability as defined by mean depth and velocity. Black X and red arrow indicate where in this stability field all the present experiments are.	p110
Figure 5-6	A Drying bed after the Open Channel Condition. Flow was top to bottom. Picture taken ~6.5m downstream of baffle. B ~1 hour into the 15mm Spikes condition. Long and tall dunes have already been produced. Suspended sand in the shear layer is quite clear (bottom left). C Flume design, showing locations of depth sounders and ADV's. To scale.	p112
Figure 5-7	Distribution of sand size used in all experiments	p113
Figure 5-8	Example of the location of velocity measurements above the mean bed level. Data from EXP3.	p115
Figure 5-9	Depth sounder filtering and bedform identification. A blue line are the original data, Red lines the interpolated bed after filtering. Bedforms are moving right to left. Substantial suspended sand can obscure the dune trough (black arrows). B shows that these are not recognized due to minimum dune size thresholds on the bedform identification algorithm. Black circles are dune crests and Red circles are troughs.	p117
Figure 5-10	Water surface slope, or energy slope, measured for all equilibrium conditions.	p119
Figure 5-11	Test section equilibrium. Water surface slope was aimed as close as possible to the to the flume slope to ensure equilibrium flow conditions in the test section.	p119
Figure 5-12	Bed shear stress τ_b (using depth slope product) plotted against the distance of downstream velocity maximum to mean bed level for all conditions, showing excellent agreement.	p120
Figure 5-13	displays the mean bedform height (m) along the flume measured from URS and Vectrino II depth soundings. Note, there are 2 data points per meter as two URS depth sounders were positioned at each meter, Figure 5-7. The data at 5.5m is from the Vectino II. The 30mm Spikes conditions data is omitted.	p121
Figure 5-14	displays the mean bedform translation rate along the flume as measured by the URS depth sounders (whole intervals) and vectrino II (5.5m only). The	p121

	30mm Spikes conditions data is omitted.	
Figure 5-15	displays the mean downstream velocity profiles for all conditions. The mean downstream velocity profile is the calculated from the four mean profile locations (Figure 8). The concurrent ADV measurements at the top of the profiles are then added to produce the final mean profile, covering >80% of the flow depth. Profiles do not reach near the free/top surface at ~0.125m as flow compression of ~0.02m was common over the dunes- thereby restricting velocity measurement close to the flow top/free surface.	p123
Figure 5-16	Bed Scans for all conditions, test sections are ~4.5-6.5 m downstream of the flume baffle. Colour of the bed is the elevation (vertical axis), scaled to each condition.	p125
Figure 5-17	Centreline profiles of the equilibrium bed scans (Figure 5-14) in the test section area. Note the vertical exaggeration.	p126
Figure 5-18	Mean downstream velocity is normalised by the Shear Velocity and plotted against distance above the mean bed level for each condition. Dashed line indicates where the stable dune forming conditions (EXP1-4) profiles converge.	p127
Figure 5-19	Mean bedform geometries and flow conditions. A shows the lack of relationship between depth and distance of the velocity maximum to mean bed level in these experiments. B Displays the parabolic relationship of bedform height and distance of Velocity max to mean bed level. The 30mm conditions are represented by three data points, the mean (+), dune only height (-) and USPB only heights (-). C Bedform length and distance of Velocity max to mean bed level. 30mm Spikes is not represented here due to no bedform scan measurement of this non-equilibrium condition.	p129
Figure 5-20	displays normalised histograms of bed elevation from the Vectrino II depth sounder and mean downstream velocity profiles all plotted around each runs' mean bed level. Large red X's indicate the location of the maximum downstream velocity for each condition. Closely spaced blue x's are Vectrino II measurements, Sparsely spaced x's are the Vectrino+ measurements.	p131
Figure 5-21	displays the mean elevation of crest and trough heights, as detected by the above bedform detection methods, around the mean bed level for all dune forming conditions (the 30mm Spikes condition only measured the dunes, USPB bed waves are not included in these mean calculations).	p132
Figure 5-22	Mean bedform height and translation rate, using all depth sounder data across the flume length. The 30 mm Spikes conditions data is omitted. The 30 mm Spikes conditions data is not plotted.	p134
Figure 5-23	displays the mean Migration rate for each condition (except 30 mm Spikes due to a lack of bedform wavelength measurement) vs distance of the velocity maximum to mean bed level	p135
Figure 5-24	displays the mean sediment transport rate for each condition (except 30 mm Spikes due to a lack of bedform wavelength measurement) vs distance of the velocity maximum to mean bed level. When the upper stage plane bed condition (50 mm Spikes) is omitted a good power law relationship occurs.	p135
Figure 5-25	displays the bed level elevation around the mean bed level for ~30 minutes for four locations along the flume, 1 m downstream (URS12), 3 m downstream (URS8), 5 m downstream (URS8) and 6 m downstream (URS1). For URS probe location see Figure 5-7.	p137
Figure 5-26	A displays the amplitude of depth sounder return through a dune-USPB-Dune transition. Colour contours in Decibels. B displays the depth averaged damplitude of depth sounder return for the A. The figure demonstrates that higher suspended sediment (inferred from amplitude) is a consequence of dunes. USPB produces little suspended sediment. Flow right to left.	p138
Figure 5-27	From Allen (1982, page 334) Group mean height relative to mean water depth as a function under equilibrium conditions of the non-dimensional boundary shear stress ad sediment calibre. Stress corrected for the wall effects by procedure of G.P. Williams (1970).	p141
Figure 5-28	Dune height adjustment factors. From Williams 1970, pp20	p143

Figure 6-1	Overview of the field site with an inset view of the wider river. The town of Kratie is to the east of the channel. Satellite imagery from the dry season shows the sand bar with relict dunes that extend into the water and the bed survey MBES data from Day 314. The DEM presented here is MBES data from Day 31, contoured to depth below water surface. Flow in top to bottom. Satellite imagery credit Esri, DigitalGlobe, GeoEye, i-cubed, Earthstar Geographics, CNES/Airbus DS, USDA, USGS, AEX, Getmapping, Aerogrid, IGN, IGP, swisstopo, and the GIS User Community.	p152
Figure 6-2	River stage Levels at Kratie during the wet season of 2013. Measurement period is highlighted in Red. Inset graph is a closer view of the measurement period. Mekong River Commission, http://ffw.mrcmekong.org/historical_rec.htm	p154
Figure 6-3	Grain size distribution of bed sediment measured at Kratie obtained on the 16/01/2013.	p155
Figure 6-4	Calibration curve of acoustic backscatter (dB) and suspended sediment concentration (mg/l) for the 1200 kHz ADCP unit. $P < 0.05$. Courtesy of C. Hackney.	p157
Figure 6-5	Multibeam bathymetry measured on day 314 in the channel near Kratie (seen in Figure 1). Flows is from top to bottom of the page. Depth is scaled to meters below water surface at the time of measurement. Grid resolution is 0.40 m.	p160
Figure 6-6	Local bed slope measured in degrees of the MBES bathymetry in Figure 6-5.	p161
Figure 6-7	Bed translation measured by repeated MBES surveys between days 314 and 319. The gap near the top of the survey is due to error on day 319 corrupting that line of data.	p162
Figure 6-8	Bedform translation and adaption. Profiles taken from the three MBES surveys, along the axis of aDcp transects displayed in Figure 1. 6-8(A) displays the flow stage corrected profiles of bedforms along the aDcp transect. 6-8(B) shows the same profile with the translation removed. Between day 314 and 315 8 m of translation was removed, and between day 314 and 319 22 m of translation was removed. Figures 6- 8 C,D,E and F shows selected larger dunes from Figure 6-8(B) to highlight the secondary bedforms on the stoss and crests of these larger dunes. Their location in Figure 6-8(B) can be found on their y axis distances.	p163
Figure 6-9	Distribution of secondary bedform height (top) and cumulative percentage of secondary bedform Height (bottom) for days 314,315 and 319 (MBES survey days). Bedform sizes are measured from all the profiles shown in Figure 6-8.	p168
Figure 6-10	aDcp transect from day 314. aDcp transect location is shown in Figure 6-1, 0m at the southern extent of the dune field in Figure 6-1. Flow magnitude and direction shows a variation across the transect due to flow convergence and steering at the northern extent (~700 to 1300m).	p170
Figure 6-11	Mean flow profiles for selected aDcp transects. Multiple profiles for days 314 and 315 are displayed to show the measurement range for similar flow conditions. Cross stream velocities (F) were calculated from rotating the downstream (A) vector to the mean streamline for each transect.	p171
Figure 6-12	aDcp transect and MBES data from day 314. aDcp transect location is shown as A to A', with A at 0m and A' at 1250m.	p173
Figure 6-13	aDcp transect and MBES data from day 315. aDcp transect location is shown as A to A', with A at 0m and A' at 1250m.	p174
Figure 6-14	aDcp transect and MBES data from day 319. aDcp transect location is shown as A to A', with A at 0m and A' at 1250m	p176
Figure 6-15	Correlations between vertical velocity, bed shape and suspended sediment for the day 314 aDcp transect. Orange bars identify periods where lee side separation can be identified where the value of vertical velocity drops and suspended sediment rises. Although the majority of dunes have measured lee side flow separation, not all dunes measured here had identifiable lee side separation and appear vertical rather than closer 45° due to vertical exaggeration.	p178
Figure 6-16A	Mean flow profiles for selected aDcp transects. Multiple profiles for days	p181

	314 and 315 are displayed to show the measurement range for similar flow conditions. Day 319 shows a higher gradient toward lower U/u^* values that are comparable to day 314.	
Figure 6-16B	The relationship between Y/U^* and suspended sediment concentration	p181
Figure 6-16C	An aDcp profile measured at peak flood at Kraite is plotted alongside the data of Figure 6-16B to show how a change in Rouse number affects the relationship found in Figure 6-16B.	p181
Figure 6-17	Mean large dune height / depth for the corresponding day vs. suspended sediment concentration for the corresponding day. A log fitted line is applied to attempt to show how well these variables are related.	p187
Figure 6-18	An attempt to correlate suspended sediment concentration over dunes (top) with Rouse number (middle) and the depth averaged suspended sediment concentration across an aDcp transect (bottom). Using day 314. Rouse number was calculated using the shear velocity estimated from the law of the wall on each profile. Rouse number inversely and incorrectly matches the changes in suspended sediment concentration	p189
Figure 7-1	Conceptual diagram of the interconnected variables defining sediment transport, for a given grains size and distribution.	p193
Figure 7-2	Time average downstream velocity profiles at the Crest, Trough and reattachment for 6 separate conditions. Top panels all show data from slow \bar{U} experiments (H14,M14,L18) whilst the bottom panels are from high \bar{U} conditions (H76, M83, L73). Vertical axis is normalised by the dune height of 0.08m. Downstream velocity profiles show a dramatic change in velocity profile shape accords the variations in depth and \bar{U} and demonstrate the significant variability in velocity profiles over dunes in out-of-equilibrium conditions.	p194
Figure 7-3	The Relative percentage (by magnitude) of quadrant events $\sim 13.5\text{mm}$ above the bed for three conditions in the experiments of chapter 3. The relative contribution of each quadrant changes as \bar{U} is increased at the same depth. Particularly, where Q4 and Q2 individually become dominant may indicate where morphological change would occur in mobile sediment conditions.	p196
Figure 7-4	A plot of the slope and intercept of a linear regression performed on the linear portion of Reynolds stress profiles across the dune under investigation in chapter 4. This conditions is H76. Flow reattachment is $\sim 3 D_H$ downstream here as the dune crest is 0 (rather than 1). The shape of the slope line is similar to that of Skin friction over dunes, whilst the intercept is most similar to turbulence.	p197
Figure 7-5	Selected Reynolds Stress profiles over the dune in chapter 4, from the same condition as Figure 7-4 (H73). Here the Reynolds Stress profiles are in Black, whilst the portion of the profile used to perform linear regression is highlighted in Red.	p198
Figure 7-6	Examples of Instantaneous streamwise-velocity fluctuations on a plane $0.05h$ above the bed. Solid lines represent the mean separation and reattachment lines. The ovals highlight regions in which the streamwise vortices cause upwash. From Omid, 2013, pp132	p202
Figure 7-7	Bed form evolution simulated by numerical model for run RT39. (a) The bed begins from a flat bed, (b) later ripples appear. These ripples grow in size and (c) the dunes begin its formation. (d) These dunes are merged and (e) larger dunes in both length and height are formed. Finally, (f) the bed forms reach their steady state and migrate in the form of two-dimensional dunes. From Nabi et al 2013b	p203
Figure 7-8	Flow, velocity quadrant, and transport variables at a time instant. (a) Downstream velocity at $z = 1\text{mm}$ as shown in Fig. 1. (b) Downstream force, f_x on particles. Particles with $ f_x < 2 \times 10^{-6}\text{ N}$ are not shown. (c) Downstream particle velocity. Particles with $ U < 0.007\text{ms}^{-1}$ are not shown. (d) Sweeps and outward interactions at $z = 5\text{ mm}$. Areas with $ u'w' < 0.0004\text{m}^2\text{ s}^{-2}$ are not shown. (d) Bursts and inward interactions at $z = 5\text{ mm}$. Areas with $ u'w' < 0.0004\text{m}^2\text{ s}^{-2}$ are not shown. (d) Near-bed pressure fluctuation at $z = 1\text{mm}$ From Schmeckle (2014).	p204

List of tables

Table 4-1	List of experimental conditions. No. =run number, Naming conventions- depths H=high (280mm) M=medium (240mm) L= low (200mm). D=average flow depth (m) above the mean bed level, \bar{U}_c & \bar{V}_c =depth-averaged mean downstream and vertical velocity at the crest, respectively (ms-1), Fr=Froude number, Re=Reynolds Number, Q=discharge (m ³ s-1).	P61
Table 4-2	Reattachment lengths and Strouhal numbers for all runs.	P74
Table 5-1	Experimental conditions.	P113
Table 6-1	Grain size distribution data	P155
Table 6-2	aDcp transect collection statistics and hydraulic measurements	P158
Table 6-3	Large Dune Geometry	P165
Table 6-4	Significance of large dune geometrical shape change	P166
Table 6-5	Comparison of Dune size with Empirical Estimations	P166
Table 6-6	Secondary Dune Geometries and Significance Tests	p168
Table 6-7	Details of bedforms and bed shear stress over selected aDcp transects	P179
Table 6-8	Self-Similar characteristic scales of bedform features	P186

Nomenclature

\bar{U}_c = Depth averaged mean downstream velocity at the crest

\bar{V}_c = Depth averaged mean vertical velocity at the crest

\bar{u} = mean fluctuating component of downstream velocity at a point

u_i = instantaneous downstream velocity

\bar{v} = mean fluctuating component of vertical velocity at a point

\bar{V} = time averaged vertical velocity

v_i = instantaneous vertical velocity

τ_b = bed shear stress

τ_r = Reynolds Stress

C_b = the volume concentration of grains in the bed

C_{fd} = form drag coefficient empirically found to be 0.19

u_R = the mean velocity at one dune height (H) above the crest

τ_{fd} = shear stresses attributed to form drag

τ_{gd} = shear associated with granular drag

τ_{sf} = shear associated from granular movement

τ_{tb} = boundary shear stress

τ_f = flume shear stress

c = bed-wave celerity
 d = flow depth
 D_{50} = median grain size
 D_{86} = 86th percentile of grain size (coarser)
 D_{14} = 14^h percentile of grain size (finer)
 D_H = dune height
 f = Frequency of vortex shedding
 Fr = Froude number
 f_v [Hz] = Eddie shedding frequency;
 f_w [Hz] = Shear layer flapping;
 g_B = Total sediment Transport Rate
 H = hole size in quadrant analysis
 h = bed height
 i_{bo} = bed-load transport rate
 K = acceleration parameter
 L = characteristic length [e.g. hydraulic diameter]
 M_r = bedform migration rate
 n = the number of observations.
 Q = Discharge
 Re = Reynolds Number
 St = Dimensionless Strouhal number
 u = downstream velocity
 \bar{U} = time averaged downstream velocity
 u^* = shear velocity
 U_o is mean velocity upstream of step; also \bar{U}_c
 V = velocity of the free flow
 v = vertical velocity
 W = Flume width
 x_r is the mean length of the separation zone [i.e. reattachment point length].
 Θ_{cr} = Shield's critical bed shear stress for sediment motion
 λ = bedform wavelength
 ρ = fluid density

List of Equations

$$Re_* = \frac{u_* D}{\nu} \quad 1.1$$

$$u_* = (\tau/\rho)^{0.5} \quad 1.2$$

$$W_s = \frac{RgD^2}{C_1\nu + (0.75C_2RgD^3)^{0.5}} \quad 1.3$$

$$Rouse = \frac{W_s}{ku_*} \quad 1.4$$

$$\frac{D_H}{d} \leq \frac{1}{6} \quad 1.5$$

$$\frac{D_H}{d} = 2.5 \left(\frac{d_{50}}{D_H} \right)^{0.3} \quad 1.6$$

$$\frac{D_H}{\lambda} = 0.016d^{0.84} \quad 1.7$$

$$\tau_b = \tau_{fd} + \tau_{sf} + g_d \quad 1.8$$

$$\tau_{fd} = \frac{1}{2} \rho C_{fd} u_R^{-2} \frac{H}{\lambda} \quad 1.9$$

$$-C_b \frac{dh}{dt} = \frac{di_b}{dx} \quad 1.10$$

$$\frac{-dh}{dt} = \frac{cdh}{dx} \quad 1.11$$

$$\frac{di_b}{dx} = \frac{C_b cdh}{dx} \quad 1.12$$

$$i_b - i_{bo} = C_b c (h - h_o) \quad 1.13$$

$$\tau_r = -\rho \bar{u} \bar{v} \quad 4.1$$

$$-\bar{u} \bar{v} = \frac{1}{n} \sum_{i=1}^n (u_i - \bar{U})(v_i - \bar{V}) \quad 4.2$$

$$-\bar{u} \bar{v}_Q = \frac{1}{n} \sum_{i=1}^n S(u_i - \bar{U})(v_i - \bar{V}) \quad 4.3$$

$$St = \frac{fL}{\nu} \quad 4.4$$

$$f_v < 0.8 \frac{\bar{U}_c}{X_r} \quad 4.5$$

$$f_w < 0.1 \frac{\bar{U}_c}{X_r} \quad 4.6$$

$$\tau_B = \rho g y_o S \quad 5.1$$

$$M_r = \frac{\lambda (\text{test section scan})}{\text{Translation Rate (at 5.5m)}} \quad 5.2$$

$$g_B = M_r W D_h \quad 5.3$$

$$\text{Wall Corrected Bed Shear stress} = W^{\wedge 2} / W^{\wedge 2} + 0.055d \quad 5.4$$

Acknowledgements

Christopher Adam Unsworth would like to thank the University of Hull for the PhD scholarship to conduct this thesis and my supervisor Daniel Parsons, for whom this thesis would not exist. I am forever in debt to Dan for the opportunity to peruse a PhD thesis and the many opportunities he has organised for me and for introducing me to many people along the way. Alongside Dan there are many other academics that have helped me in the past four years. Arjan Reesink was a Post-doc in Hull for some time and he has helped me become more focused and critical of my work, which usually produced new and better results that I originally had. I thank Robert Thomas for his consistent help, patience, stimulating discussion and guidance over the past three years. Richard Hardy and Stuart McLellend for honest opinions, quality control and encouragement. Phil Ashworth for constantly asking me questions that I never think of (and usually don't have answers for at the time). Tom Coulthard for many good discussions on emergence and complexity in dynamical systems. And Hugh Patrick Rice for discussion of dunes in pipe flow.

I thank the University of Hull for financial support in attendance of a 10 day environmental fluid mechanics course in Switzerland. I would like to thank Alfred Wuest, Dieter Etling, Fernando Porté Agel, George Constantinescu, Heidi Nepf, Vladimir Nikora, Greg Lawrence and Peter Davies for their lectures and lecture material.

In Hull I would like to thank Dr Lucy Clarke, Dr Rebecca Williams, Dr Sally Litte, Dr Carl Lewis, Leiping Yi, Dr Mike Rogerson, Dr Jane Bunting, Dr David Milan and Professor Jeff Blackford, and Linda Love, as well as the excellent technical staff in Hull: Brendan Murphy, Kim Rosewell, Paul McSherry, Mark Anderson and Mike Dennett.

Additionally, there are many people I have met at conferences that have been excellent to talk with that I would like to highlight; Chris Hackney, Colin Throne, Douglas Jerolmack, Eva Kwooll, Jeff Nittrouer, Jeremy Venditti, Jim Best, John Shaw, Ugo Piomelli, Mahammad Omidyeganeh, Steve Darby and Esther Sumner.

Below I have highlighted the help I received from people for specific chapters:

- Chapter three received helpful reviews from Dr Rich Hardy and Dr Rui Ferreira which greatly aided the clarity of the chapter.
- For the experiments in Chapter four I would authors would like to thank Dr. Gareth Keevil for his work in collection of the data in the Sorby Laboratory, University of Leeds. In Addition I would also like to thank Dr Rich Hardy and Dr Timothy Marjoribanks for their help in processing the data.
- For the experiments in Chapter five I would like to thank Prof. Steve Rice for very kindly lending the Vectrino + instrument, Dr Gareth Keevil for the Cole-Prumer flow meter, Dr. Rob Thomas for the use of the Vectrino 2 processing code, for making the instrument available, and thanks to Mr Leiping Yei for his floor and excellent food.
- For the fieldwork in Chapter six I would like to thank Prof. Steve Darby, Dr Chris Hackney, Prof. Jim Best, Prof. Andrew Nicholas, Dr. Julien Leyland, Prof. Rolf Aalto, The Mekong River Commission and their boat drivers for the amazing opportunity to take part in their fieldwork on the Mekong River in 2013. I also thank Claire Keevil for here assistance in Mulibeam processing.

I would like to thank my Parents Brian Unsworth and Dr Bridget Unsworth and my sister Sarah Unsworth for being my family and supporting me. Anni Dunster for giving me perspective keeping me sane.

Chapter 1

Introduction

1.1 The importance of understanding rivers

Gravitational attraction and a spatial gradient provide the primary driver for most geophysical flow processes on Earth. Despite the majority of Planet Earth being flat, the generally low slope rivers that flow across vast lowland landscapes display astonishing levels of dynamism. Humans have attempted to manage these dynamic environments to their benefit (Thomas & Watt 1903), largely for agricultural irrigation (Ruddiman & Raymo 2003; Hooke 2006) and indirectly through biomass burning (Bintliff 2002). Often these changes have altered rivers in a negative way, especially for those living near or depending on rivers for their livelihoods. For example, early forest burning increased sediment input into rivers and consequently in-filled Mediterranean river deltas and harbours (Macklin *et al.* 1995; Bintliff 2002). In some cases irrigation led to rivers becoming more flood prone and more likely to avulse as a result of Holocene climate change (Wilkinson 1999), despite early human flood defensive efforts (Heyvaert & Baeteman 2008).

The projected changes in rainfall-runoff at a global scale over the next 50 years due to climate change are alarming. Rainfall-runoff in high northern latitudes and the wet tropics is expected to increase within the next 50 years, whilst the dry tropics are expected to see a reduction in runoff, and areas South East Asia

face very uncertain outcomes due to unpredictable changes in the EL Nino Southern Oscillation (IPCC Working Group 2 2014; Gray *et al.* 2014). Rivers that receive snow meltwater (e.g. Mississippi) are expected to receive some of the largest changes in annual discharge due to the large temperature changes predicted for the next 50 years (IPCC Working Group 2 2014). Considering that most of the world's large rivers receive water from snow-melt this is a serious problem as large population centres tend to be based next to the world's larger rivers (Ashworth & Lewin 2012).

Large population centres and places of industry historically, and presently locate around rivers due to their significance in providing a range of needs such as fresh water supply, food supply, power generation and as transport corridors (Ullman 1941; Harris & Ullman 1945; Nystuen & Dacey 1961). However, rivers are a double-edged sword, the dynamic and stochastic characteristics of rivers means their path and stage (water level height) can drastically change through time (Jordan 1965; Kuhnle 1992; Wilbers & Ten Brinke 2003), producing significant risk to local inhabitants (Figure 1-1).

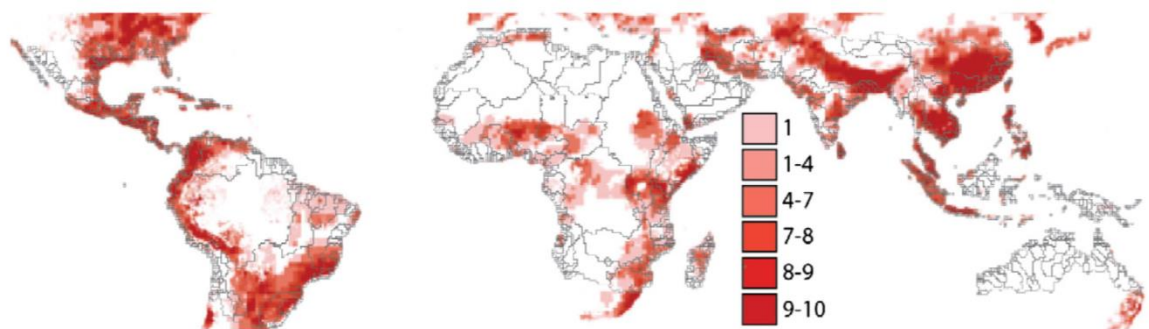


Figure 1-1: Distribution of flooding hazard frequency between the tropics, 1985-2003, superimposed on drainage basin boundaries. The figure shows that heavily populated regions, such as Bangladesh, S.E. Asia and China, North America and Eastern South America also have particularly high flood hazard frequency (From Syvitski *et al.* 2014).

In sand bedded rivers, prediction of river stage is complicated by the presence of a dynamic wavy sand bed. Sand waves are produced from the interaction of fluid and sediment, forming bedforms such as dunes, which add a significant amount of flow resistance to the moving water above. This extra resistance raises water levels for a given discharge (Figure 1-2) (Julien & Klasssen 1995; Amsler & Garcia 1997; Holmes & Garcia 2008; Wilbers & Ten Brinke 2003; Paarlberg *et al.* 2010). The extra resistance to flow is because, in addition to the friction of the sand grains to moving fluid, sediment pile-ups like dunes induce

form roughness produced from flow separation in the lee of the bedform. This separated flow is related to the size and shape of the bedform, and accelerates and decelerates the flow going over it, inducing a pressure gradient in the primary flow direction (Einstein & Barbarossa 1952; Vanoni & Brooks 1957; Brownlie 1983; McLean *et al.* 1999; Prent & Hickin 2001). It is this extra roughness with makes dunes the most rough bedform for rivers (Van Rijn, 1987; Garcia, 2008) and therefore important for flood prediction. Additionally, the turbulence produced from form roughness mixes the entire water column, re-distributing sediment, nutrients and as well as producing this greater fluid friction (Jordan 1965; Kostaschuk & Church 1993; Dimas 2008; Shugar *et al.* 2010; Robert 2011).

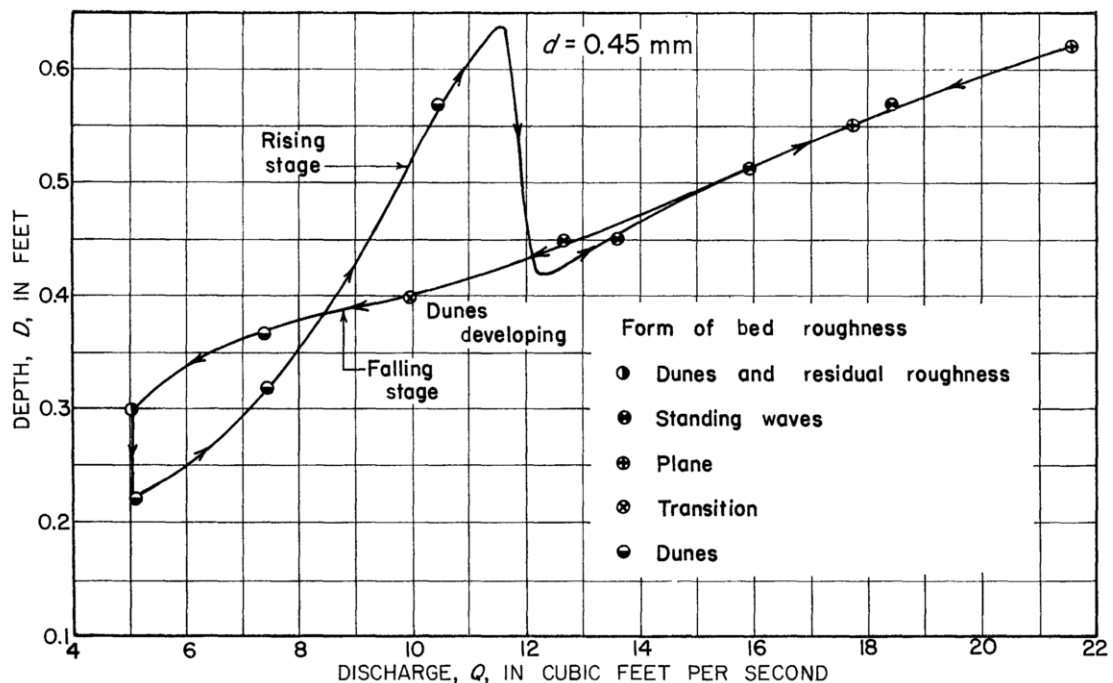


Figure 1-2: The relationship between flow depth and discharge across a transition from lower flow regime (ripples and dunes) to upper flow regime (flat bed and anti-dunes). Flow depth in the rising leg rises substantially whilst dunes are present, then falls sharply at ~ 12 cf/s^{-1} , when the dunes disappear (From Simons & Richardson 1962).

River dunes contribute the highest amounts of roughness and energy dissipation in rivers (relative to the other bedforms types) (Vanoni & Brooks 1957; Moog and Whiting, 1998b; Prent and Hickin, 2001; Ryu *et al.*, 2007; Garcia, 2008; Huybrechts *et al.*, 2011; Niemann *et al.*, 2011; Robert, 2011). The magnitude of the flow resistance directly influences the river stage levels for a given discharge (Chézy 1775; Manning 1891; Einstein & Barbarossa 1952; Simons & Richardson 1966; Jordan 1965; Amsler & Garcia 1997; Fedele &

Garcia 2001; Shimizu *et al.* 2009). Therefore dune size is a key component in predicting how high river levels attain during flood events.

The successful prediction of river bedform size is an important consideration in civil engineering projects such as bridges and tunnels. The maximum scour depth of dunes is a crucial factor in how deep foundations and tunnels need to be to prevent undercutting of man-made structures. River bedform dimensions can change dramatically particularly during severe floods. For example, Amsler & Garica (1997) describe an example where an increase in dune scour during a large flood led to serious structural problems for a tunnel under the River Parana in Argentina. The tunnel was designed to need a minimum sediment overburden of 3 m to prevent the tunnel uplifting. However in 1983 a particularly large flood, due to a weather pattern associated with the El Eño effect, produced dunes up to 6.5m high. This was twice as high as the maximum predicted height of the dunes and left the roof of the tunnel exposed to the river flow in the deepest dune troughs. The tunnel needed to be closed and loaded with army trucks filled with sand to prevent tunnel destruction via uplifting.

The height and lateral extent of dunes also affects the navigability of rivers around the world. For example, the River Rhine in Europe requires groynes to increase flow depth into a major European industrial centre. In flood, however, the Rhine dunes grow substantially in height and length (Carling *et al.* 2000a,b; Wilbers & Ten Brinke 2003) which affected the flow stage during the flood. This is a major issue for the Netherlands and prediction of maximum flood depth is reassessed every 5 years as a matter of government policy. This reassessment in turn affects the suitability of present and future flood defences (Paarlberg *et al.* 2010). Dunes produced from the hydraulic conditions present at peak flood can remain oversized relative to the flow depth in the channel for weeks. So even though flow stage may have returned to pre-flood levels, navigable depth can remain too low for shipping along the Rhine because of the larger dunes left over from the flood peak (Wilbers and Ten Brinke, 2003, Wilbers, 2004).

On a global scale, the movement of sediment toward river deltas, the ocean and continental shelf is dominated by river sediment transport (Milliman and Meade 1983; Syvitski and Milliman 2014) and now more controlled by humans than ever due to dam construction (Syvitski *et al.* 2005, 2009) and levée building (Belt 1975; Tobin 1995; Sills *et al.* 2008). Yet the global models that

estimate and predict these sedimentation rates, that are used to define delta and shoreline stability and future response to climate changes and sea level rise, omit the first order dependence of sediment transport on fluvial processes. This interaction often produces isolated pulses of sediment transport rather than a constant conveyor belt of sediment toward the oceans (Aalto *et al.* 2003; Nittrouer *et al.* 2008). Many of these sediment pulses coincide with rapid bedform development- particularly dunes- during flood pulses (Carling *et al.* 2000a; Nittrouer *et al.* 2008). The production of large bedforms has been shown to not just coincide with increases in bedload sediment transport rate but also an increase in suspended load. Flow separation produced by dunes can produce depth-scale sediment pulse events. Such processes can greatly alter sediment suspension lengths and travel times in rivers (Kostaschuk & Church 1993; Naqshband *et al.* 2014a), thus increasing the amount of suspended load, which travels downstream considerably faster than bedload. Suspended sediments, particularly suspended sand, produces the majority of delta forming sediments and are crucial in their future stability (Edmonds & Slingerland, 2009; Syvitski *et al.* 2009; Blum & Roberts, 2009; Ramirez & Allison, 2013; Caldwell & Edmonds 2014; Unverricht & Nguyen, 2014). The effect of climate variation on sediment transport in river reaches and toward the ocean has recently been modelled on a global- but simplified- level (Figure 1-3). Figure 1-3 shows that major (up to 3x) departures from the mean annual discharge and sediment load can be driven through climate and lithology variability. For the example shown in Figure 1-3, India, China and S.E. Asia are heavily dependent upon tropical cyclones for the majority of large flood events (Syvitski *et al.* 2014) and although future (50 year) predications of tropical cyclone intensity, frequency and location are uncertain (IPCC Working Group 2 2014), it is likely that even small departures in cyclone frequency and intensity will have major impacts on the annual regime of these rivers (Gray *et al.* 2014). Any change in monsoon frequency and magnitude would dramatically alter the delivery of sediment to deltas, floodplains and bars, particularly in the development of the large dunes that increase suspended sediments quantities.

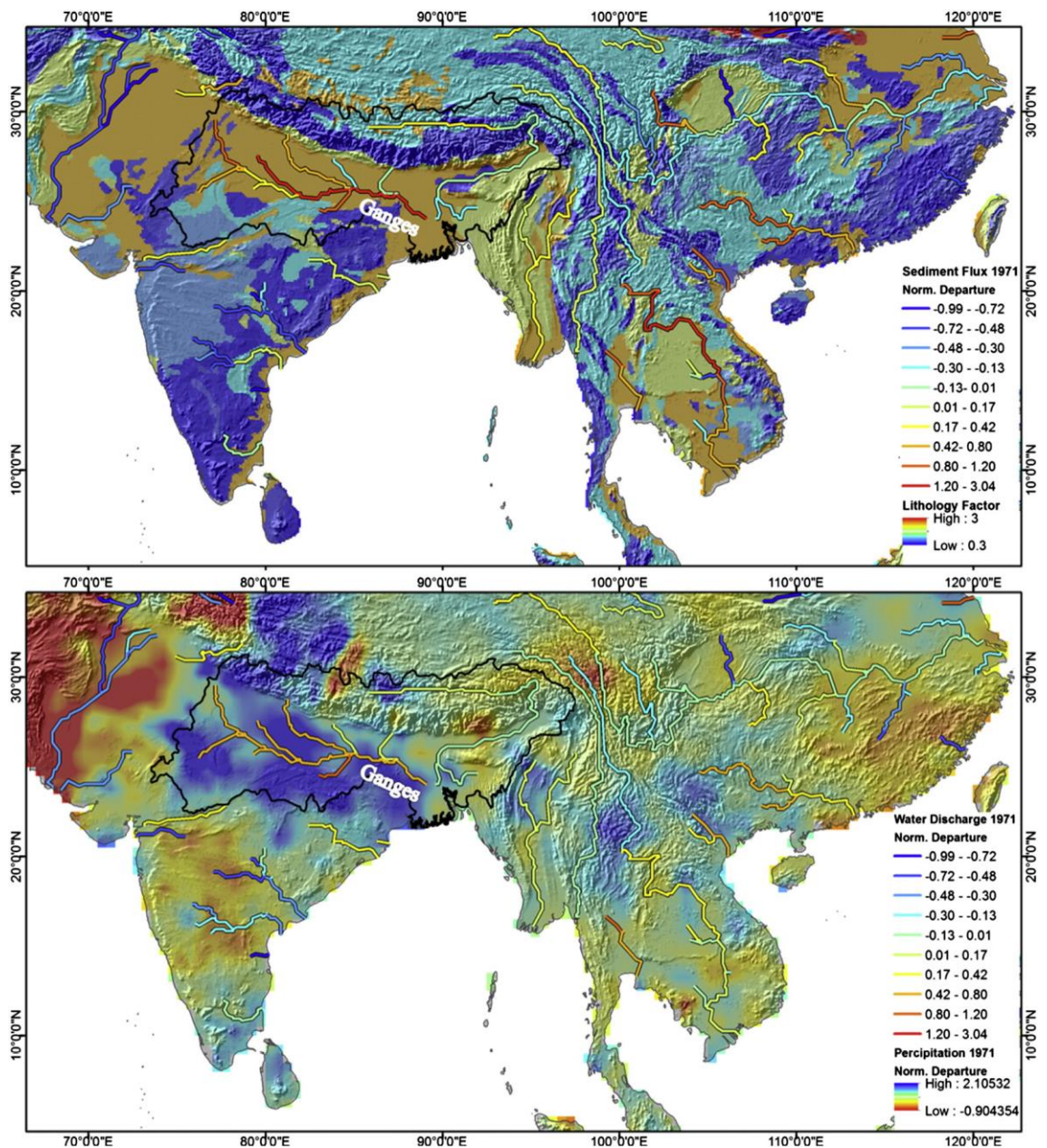


Figure 1-3, Southeast Asia riverine normalized departure from mean for 1971 for: (top) sediment flux overlaying a lithology factor map, derived according to Syvitski and Milliman (2007), and (bottom) water discharge overlaying precipitation normalized departure from mean map, comparing annual precipitation of 1971 with 50 year average precipitation (1960–2010). Black line is an outline of the Ganges River Basin (From Cohen *et al.* (2014).

The deposition of sand via river sediment transport forms an important part of the geology of Earth. Dune formed cross strata (or cross sets) deposits form a significant control of the world aquifer and petrochemical reservoirs properties. Additionally, producing hydraulic interpretations from dune cross strata are one of the most reliable ways of estimating paleo-river depth (Leclair 2002; Lunt *et al.* 2013). An estimate of paleo river depth can then be used to infer river and floodplain size (Bridge 1985; Bridge & Tye 2000; Leclair 2006). Yet a large

portion of dunes in the worlds large rivers display a stable distribution of multiple dune sizes (Fielding & Alexander 1996; Ashworth *et al.* 2000; Fielding *et al.* 2009), presumably caused by a tropical monsoonal climate, whilst present analogues that paleo-environmental interpretations are based upon assume one distribution of dunes sizes in equilibrium, steady, conditions (Leclair, 2002; Leclair 2011).

The sedimentology and preservation of cross strata produced from seasonal flood pulses requires attention as unsteady sediment transport, changes in primary sediment transport mechanism and production of dune hysteresis will all affect the style of cross strata preservation and reactivation surfaces (Carling *et al.* 2000a; Kleinhans *et al.* 2002; Reesink & Bridge 2007; 2009). Therefore understanding the processes behind how a river mobilises and deposits sediment, primarily in the form of sandy bedforms, such as dunes or ripples, is crucial for the accurate representation of such geological subsurface deposits and not just for present day predictions (Hand and Bartberger, 1988; Carling and Dawson, 1996; Bridge, 1997; Bridge and Tye, 2000; Reesink and Bridge, 2007; Leeder, 2009; Lunt *et al.*, 2013).

This thesis aims to improve our basic understanding of sandy bedforms, particularly dunes, because there is still paucity in understanding and predictive capability of these river bed features; yet their significance ranges from floods, sediment transport, from mountains to deltas and understanding numerous geological deposits. Some examples of these are shown in Figure 1-4.

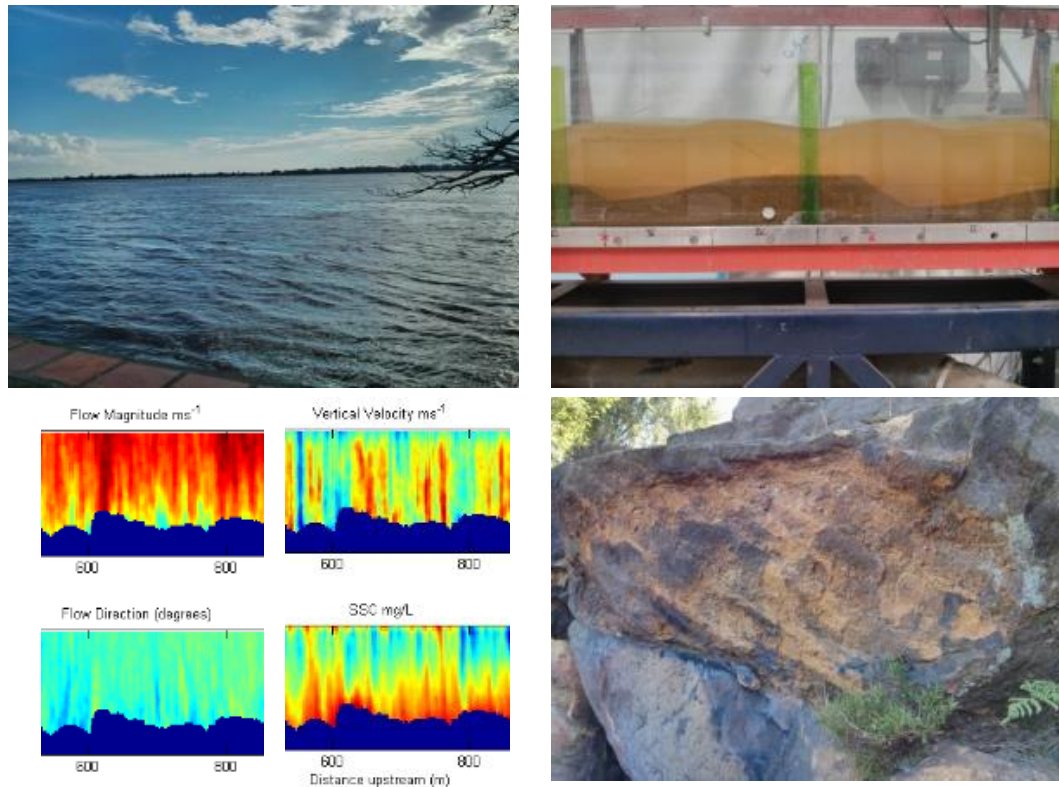


Figure 1-4: Perspectives of River Dunes:

- Top left, The Mekong River in Cambodia is in peak flood. September 2013, near Kratie. Underneath the water surface there is huge complexity and dynamism.
- Bottom Left: aDcp measurements of flow velocity magnitude, vertical velocity, flow direction and sediment suspension over sand dunes in the Mekong River, near Kratie from a 2013 field season, (Chapter 5). Notable features are, low velocity magnitude (light blue/green) pulses near the bed. Vertical velocity rises (more red) over the long stoss slopes of dunes, whilst they are more negative (blue) over steep lee faces. The Suspended sediment concentration (SSC) over dunes displays 1, large vertical pulses of suspended sediment, and 2, a high concentration layer close to the bed.
- Top Right, Sand dunes in a laboratory flume. Significant features are the lagging wavy reaction of the free water surface which responds to the shape and form roughness of dunes.
- Bottom Right, co-sets of repeating coarse sand and gravel (Carboniferous, Namurian). Formed in the lee slopes of dunes. In a disused Millstone Grit quarry, South Yorkshire Dales.

Literature Review

2.1.1 Scaling of bedform morphology

There is no single consensus on the controls and mechanisms of formation of ripples and dunes from a flat bed and current theory is split between three main avenues: 1) turbulent fluid motions (Jackson 1976a; Leeder 1983; Best 1992), 2) two-layer or mixing layer instabilities (Raudkivi 1998; Venditti *et al.* 2006), 3) emergence from granular transport mechanics (Bagnold 1966; Langbein & Leopold 1968; Coleman & Nikora 2009) - see Coleman and Nikora, 2009 for a recent summary. Bedforms are features produced in turbulent fluid flow over loose, granular, boundaries. In laminar flow conditions bedform “wavelets” form but do not reach the sizes reached of turbulent flow bedforms (Kuru *et al.*, 1995; Coleman & Fenton 2000). Therefore, turbulent flow characteristics are required for small wavelets produced from emergence in granular transport to develop into larger features, such as ripples or dunes (Coleman & Nikora 2009). As such, understanding the nature of dunes, their turbulent flow character and sediment dynamics are all important, as the nature of dunes is a mixture of emergence characteristics produced from the granular mechanics (Bagnold 1966; Langbein & Leopold 1968) and turbulent flow separation and effects on sediment transport (Best 1992; Nelson *et al.* 1993; Coleman & Nikora 2008). The mixing layer instability theory has been proposed many times but has never

gained traction, largely due to a lack of any significant quantifiable predictive or descriptive capability produced from the work.

The turbulent fluid motion concept of bedform development was a response from a burst in understanding of turbulent boundary layers in the 1970's and 80's (Jackson 1976b, Allen 1982; Leeder 1983), with further development by Best (1992; 1996). The development of horseshoe or hairpin vortexes in boundary layers has been well described in the fluid mechanics literature (Falco 1991; Adrian 2007) but there has yet to be a strong response from the sediment transport community to the repeating coherent flow structures described in Adrain (2007). The turbulent fluid motion concept is most commonly criticised for the unlikeliness of random turbulent events producing regular bedforms (Coleman & Nikora 2009). This is however a misunderstanding, turbulence is chaotic - which has structure - and is not random or structure-less (Swinney & Gollub 1981; Bogard & Tiederman 1986; Heslot *et al.* 1987; Meneveau & Sreenivasan 1987; Simpson 1989; Nezu & Nakagawa 1993; Adrian 2007). Although as yet, data illustrating the spatial distribution of both the boundary layer turbulent events and bedform scaling has yet to be shown.

The interaction of flow structure and bedload sediment transport occurs at the fluid-sediment boundary, where low speed streaks in the fluids' viscous sub layer vertically propagate into horse shoe/ hairpin vortexes. These are unstable on the order of \leq seconds and burst to produce a sharp upward and then downward fluid movement – commonly described as a burst and sweep (Jackson, 1976a,b; Nakagawa and Nezu, 1981; Laponite, 1992; Nezu and Nakagawa, 1993; Adrian *et al.*, 2000,a). The sweep of fluid down towards the bed temporarily penetrates the protective viscous sub layer and increases the bed shear stress to move the upper layer of sediment, producing sediment motion (Figure 2-1c).

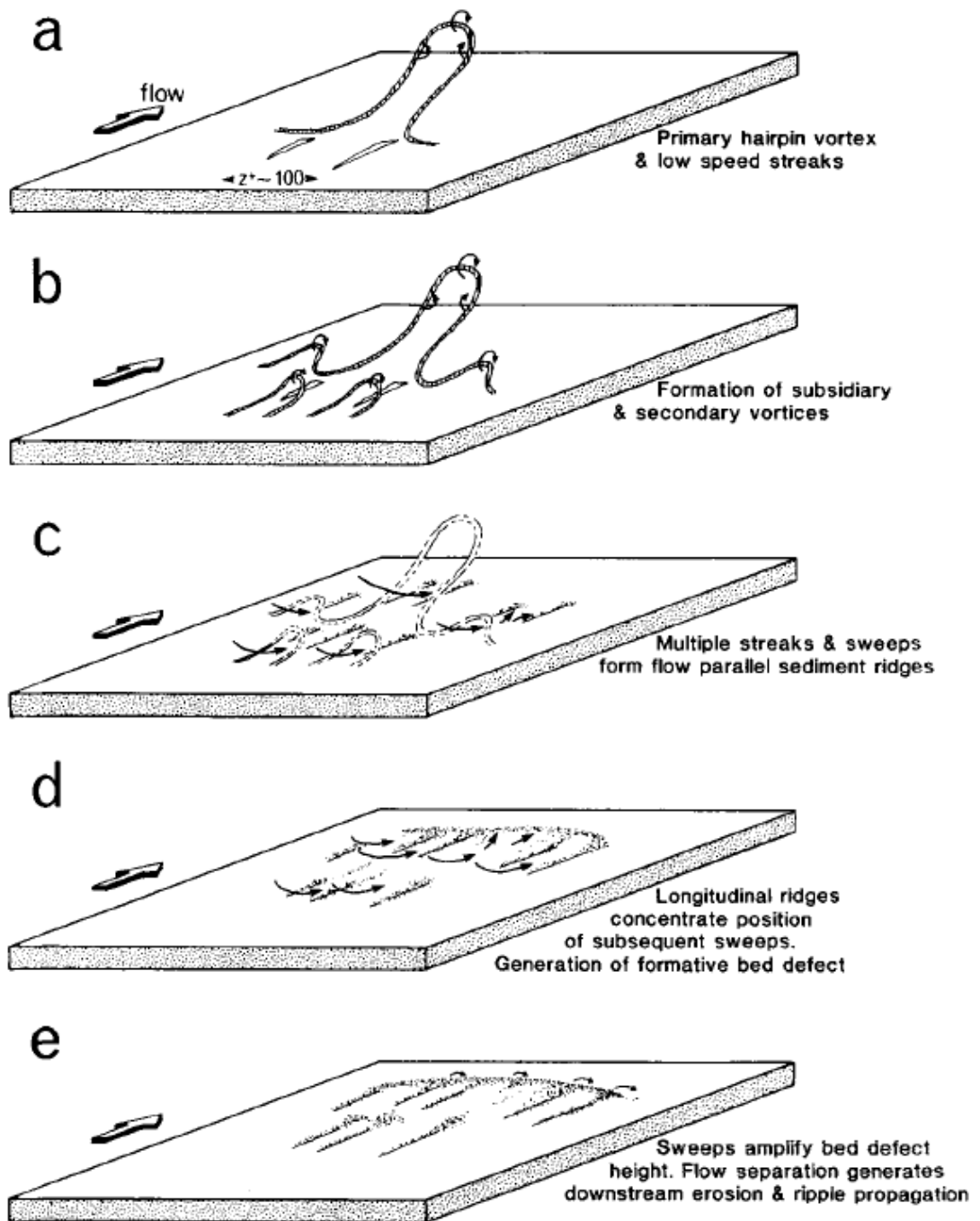


Figure 2-1: A synthesis of bedform initiation via burst and sweeps.

A, a hairpin vortex is present in the flow. Once the hairpin vortex has been generated within the boundary layer moves away from the bed secondary vortices are generated (b). These produce multiple sweeps that generate multiple entrainment corridors(c). These entrainment events are nested in the grouping around the larger vortex. The grouped sweep events produce multiple lineations of sediment on the bed forming transverse ridges (d). A critical height for producing flow separation is reached due to continued sediment build up on these ridges. The flow separation then controls the downstream propagation and growth of the bedform (e) (From Best, 1992).

This sediment motion is short lived and the sediment is deposited when the shear stress returns from the extreme of the sweep (Figure 2-1d-e). Flow

separation forms behind the bed defect and this sediment builds up and migrates (if it is not destroyed by another burst or bedform) until the sediment supply is reduced. Theoretically, due to the fractal nature of turbulence, flow separation can occur at any scale, even a height of one grain diameter. This is strongly dependent, however, on the ratio of grain size and shear velocity over the fluid viscosity, called the Grain Reynolds number Re_* :

$$Re_* = \frac{u_* D}{\nu} \quad 1.1$$

$$u_* = (\tau_b / \rho)^{0.5} \quad 1.2$$

where u_* =shear velocity, τ_b = bed shear stress, ρ = fluid density, D = grain size (mm) and ν = kinematic viscosity of the fluid. This therefore provides a combined sediment-fluid definition of the state/type of sediment and fluid interaction, assuming a perfectly flat bed with no elevation changes greater than one grain diameter. Further, to define the mode of sediment transport, the Rouse number is calculated. This requires a good estimate of the sediments fall velocity, w_s (after Ferguson & Church 2004):

$$w_s = \frac{RgD^2}{C_1\nu + (0.75C_2RgD^3)^{0.5}} \quad 1.3$$

where R = the submerged specific gravity (1.65 for quarts sand in water), g = acceleration due to gravity, D is the grain size in meters. For natural sand grains C_1 and C_2 are the constants 18 and 1 (Ferguson & Church 2004). Then to calculate the Rouse number;

$$\text{Rouse} = \frac{w_s}{ku_*} \quad 1.4$$

where k is the Von Karman constant 0.41. Values >2.5 indicate bedload dominated transport, 1.2 to 2.5 indicate sediment is 50% suspended, 0.85 to 1.2 indicates 100% of the sediment will be transported in suspension and <0.8 indicates the sediment is transported as the wash load (Allen 1982).

These equations highlight the significance of the variables shear velocity, grain size and fluid viscosity to granular transport. The interplay between these variables defines if sediment transport occurs and by what method. Subsequently, a substantial amount of the mechanisms of sediment transport in rivers is understandable from the perspective of these variables (Raudkivi

1998). Of these three, the shear velocity is the most difficult to estimate precisely (Petit 1987; Whiting & Dietrich 1990; Wilcock 1996; Biron *et al.* 1998; Hurther & Lemmin 2000; 2008). This can be due to measurement error (Pons & Davidson-arnott 2007; Bagherimiyab & Lemmin 2013;) and unsteady flow structure due to flow separation (Carling 1999; McLean *et al.* 1999a; Kostaschuk *et al.* 2004; Gmeiner *et al.* 2011).

Given a large enough grain, or group of grains, flow separation and eddies are produced which produces a local high in shear velocity and scours the bed. This deposits sediment further downstream as the flow settles and a new boundary layer forms. This causes another point of flow separation which auto-generates a new sediment pileup and often makes a train of bedforms behind a single depression/mound (Allen 1982; Best 1992,1996; Venditti 2003; Coleman & Nikora 2009).

Grain Reynolds number has also been used to differentiate between types of bedform. Ripples and dunes are often considered distinct from each other, despite similar geometric features (Allen 1982; Raudkivi 1998). A continuum of bedforms between ripples and dunes has been proposed several times (e.g. Jackson 1976a; Jerolmack *et al.* 2006), but there is convincing theoretical and experimental evidence that these bedform types are both hydrodynamically and sedimentologically separable (Yalin 1964; Simons & Richardson 1966; Allen 1980; Allen 1982; Van Rijn 1984c; Raudkivi 1998; Reesink & Bridge 2007; Aberle *et al.* 2010; Coleman *et al.* 2011). The key difference is that ripples scale most well with grain size (and thus grain Reynolds number) whilst dunes do not show a similar scaling pattern (Allen 1982). This is attributed to one key variable, grain roughness. Ripples are stable when the grains are smaller than the viscous sublayer (hydraulically smooth) which is why ripples do not form in hydraulically rough flows under normal (0-30°C water) viscosity conditions (Figure 2-2).

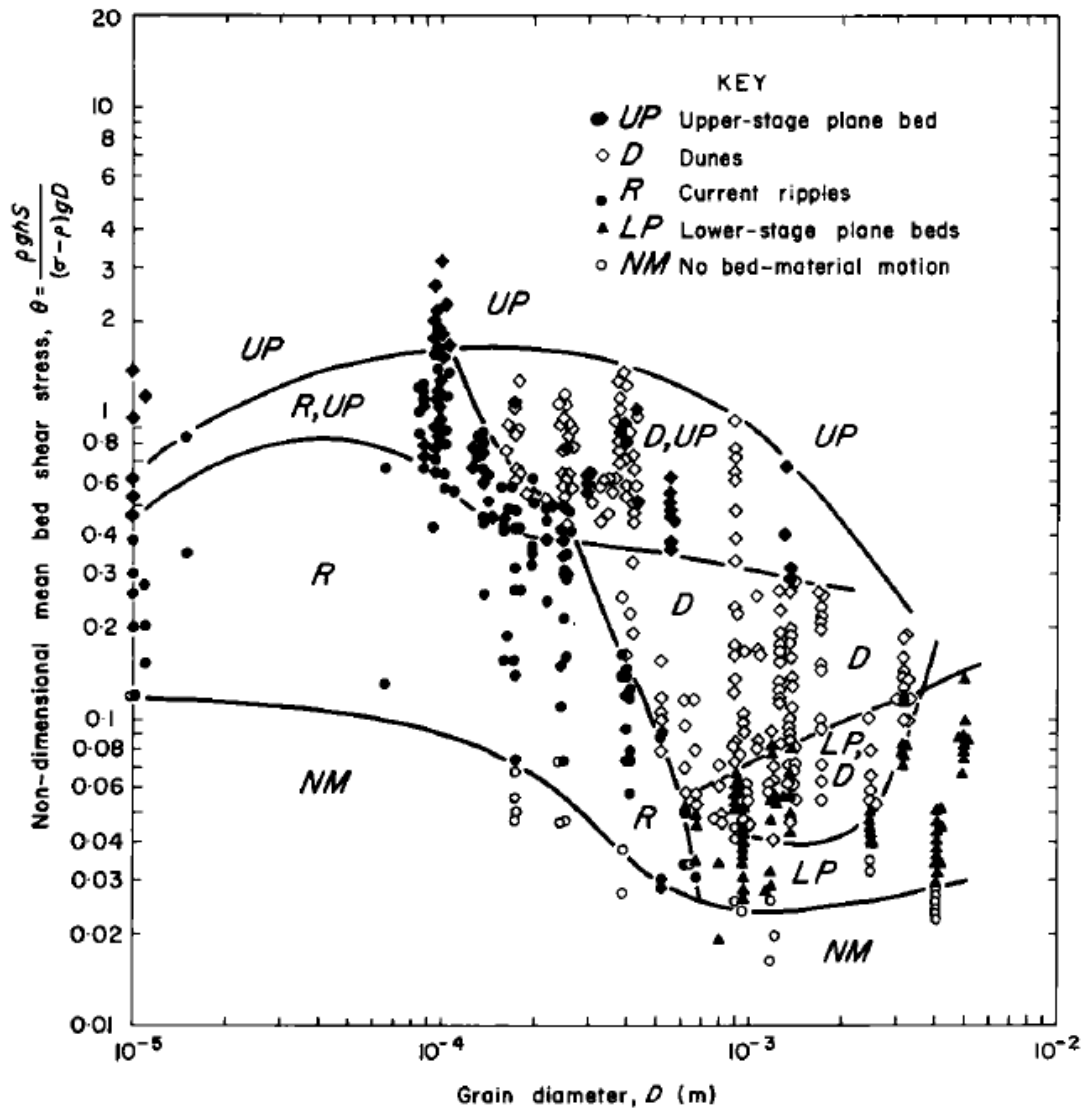


Figure 2-2: Experimental existence fields for aqueous bedforms under equilibrium conditions, shown in the non-dimensional mean bed shear stress (wall-corrected)-grain size plane at 25°C (From Allen 1982 pp 340, References for data points therein).

A second distinction between ripples and dunes are their effects on the water column. Ripples produce no free surface deformation whilst dunes, at least in shallow flows (Van Rijn 1984), produce an out of phase reaction in the local water surface slope (Allen 1982; Simons & Richardson 1966; McLean 1990; Bennett & Best 1996; Robert & Uhlman 2001; Fernandez *et al.* 2006). The free surface deformation produced by dunes is a result of flow acceleration and convergence over the dune stoss slope, and flow expansion over the lee and recirculation region (McLean 1990; Bennett & Best 1995; McLean *et al.* 1999a; Best 2005a; Fernandez *et al.* 2006). Therefore, these bedforms are pressure driven features. Whilst similar flow acceleration, deceleration and separation

occurs for ripples, their effects are different in one key way: they do not affect the free surface because ripple wavelength is never long enough to force flow convergence (McLean 1990; Maddux, *et al.* 2003a). It is interesting to note that, for the same shear stress, the development of either ripples or dunes appears strongly related to grain size (Figure 2-3), and therefore how hydraulically rough the sediment is.

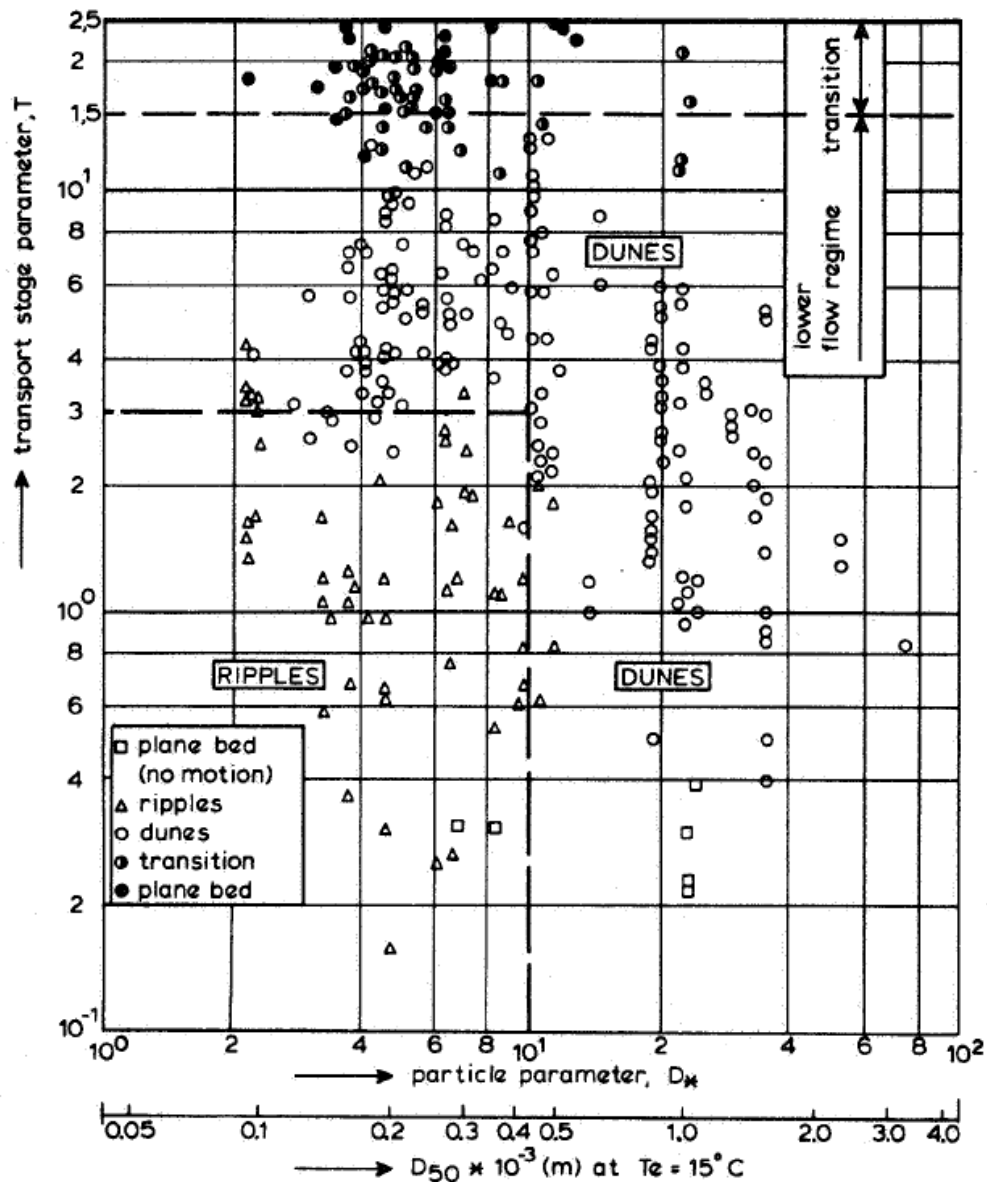


Figure 2-3, Bed state stability diagram for lower and transitional regime (From Van Rijn 1984c).

Many experiments have changed shear stress whilst keeping grain size constant to measure the transition of ripples to dunes out of practical necessity (Simons & Richardson 1966; Bennett & Best 1996; Robert & Uhlman 2001; Schindler & Robert 2005; Fernandez *et al.* 2006). It has been shown that the transition from

ripples to dunes produces clear increases in suspended sediment associated with greater turbulence intensity from flow separation (Schindler & Robert 2004). This is because the first morphological change from ripples to dunes is an increase in bedform height (Bennett & Best 1996; Uhlman 2001; Fernandez *et al.* 2006), which produces a longer and more powerful shear layer (Engel 1981; Muller & Gyr 1986). It is very rare to see evidence of an increase in ripple wavelength producing dunes (via producing greater topographic acceleration that increases shear layer intensity downstream) as new ripples tend to form in the gap. This indicates that a flow separation, rather than topographic acceleration, flow-sediment control, exists that separates ripples and dunes, and that this is also related to the relative grain roughness. Because ripples and dunes both show flow separation, the separation between these bedform types is likely to be a threshold between shear layer turbulence and relative size of the viscous sub layer and the grains, particularly around flow reattachment. Dunes that show no free surface effects (very deep dunes), like ripples, display similar magnitude and spatial location of flow separation shear stresses compared with the same dunes at an equilibrium flow depth (McLean *et al.* 1994). Therefore the key differentiator may be the ability of the viscous sub-layer to dampen the sediment transport initiation at flow reattachment - thus effecting bedform shape, rather than explicitly flow depth or free surface effects.

The difference between a strongly grain size dependent control (for ripples) to a more fluid based control (for dunes) should offer a clear distinction. Yet it is apparent that the steepness of these bedforms is (logarithmically) consistent across scales of 0.001 m to 1000 m (Flemming, 2000; Jerolmack *et al.* 2006). Therefore, whilst the primary fluid-sediment processes may differ, the emergent bedform shape is remarkably consistent. The distinct jump in bedform geometry through the ripple-dune transition discussed above does not necessarily require large changes in boundary condition (e.g. a 50% change in discharge), although both states are possible under the same hydraulic and sedimentological conditions (Figures 2-2 & 2-3), but this is commonly ripples being superimposed onto dunes stoss slope (Reesink & Bridge 2007) where the flow along the dune stoss slope is protected by the turbulent wake produced from flow separation and the adverse pressure gradient. Whilst the overall steepness of bedforms is continuous, the emergence of the bedforms along this continuum is not, as the dominant flow-sediment processes display a distinct

switch, rather than gradually alter (Bennett & Best 1996; Fernandez *et al.*, 2006).

A river dunes' limit in height and wavelength are currently seen to be dependent upon the flow depth and shear stress (Figures 2-4 & 2-5) (Allen 1982). If a bedform continues to grow in height and length for a set depth this will eventually enhance the topographic acceleration along the dune stoss side, increasing the flow velocity, shear stress and transport stage along the dune stoss until vertical deposition stops and any greater increase in shear stress can only result in greater sediment transport rate. This is why equilibrium dunes do not change shape much when discharge increases (when depth is kept relatively constant) (Nelson *et al.* 2011).

Garcia's (2008) recent review of dune geometry scaling affirmed that:

$$\frac{D_H}{d} \leq \frac{1}{6} \quad 1.5$$

here D_H = bedform height and d = Flow depth. A more useful definition is provided by Julien & Klassen (1995) that includes grain size effects:

$$\frac{D_H}{d} = 2.5 \left(\frac{d_{50}}{D_H} \right)^{0.3} \quad 1.6$$

where d_{50} = the median grain size. Figures 2-4 and 2-5 show a considerable amount of scatter around the classically defined ratios of dune height (Figure 2-4) and dune wavelength (Figure 2-5) to water depth. Defining dune geometry based upon flow depth is a useful simplification for engineering applications and geological interpretation of cross strata deposits, yet they do not show; i, a good correlation, and ii, the direct mechanisms behind dune height and length. Therefore, for the geomorphologist interested in the fundamental processes and morphodynamics of dunes, these definitions are perhaps not as useful.

Figure 2-6 displays considerably better correlation between dune height and boundary shear stress rather than depth, across several grain sizes. This figure appears to be a more useful tool in determining dune geometry as it facilitates the delineation of similar dune heights at different values of bed shear stress. However, it is not clear that the relationship remains intact if the shear stress is altered without a change in depth.

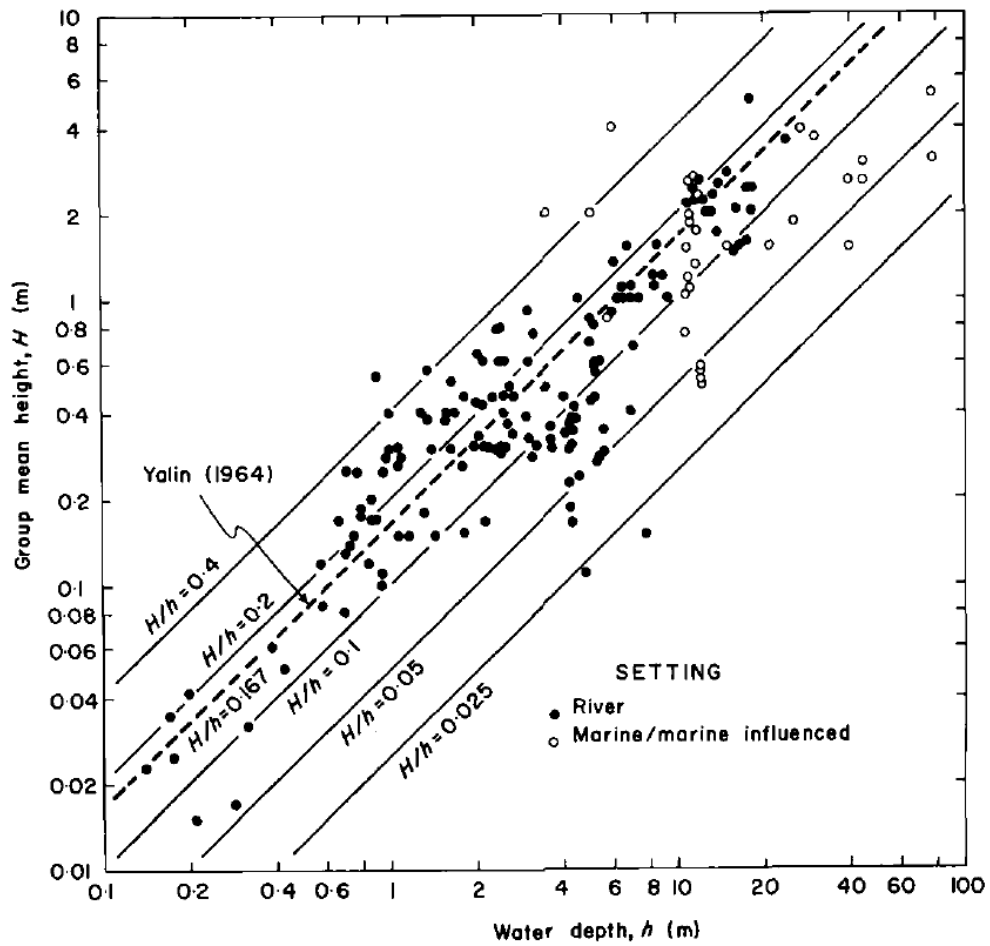


Figure 2-4. Scatter of group mean height and mean water depth for dunes in river and marine or marine-influenced settings, with the relative dune height (H/h) as a parameter. There is a general trend for longer bedforms and deeper water, but there is considerable scatter (From Allen 1982 pp333, references for data therein.)

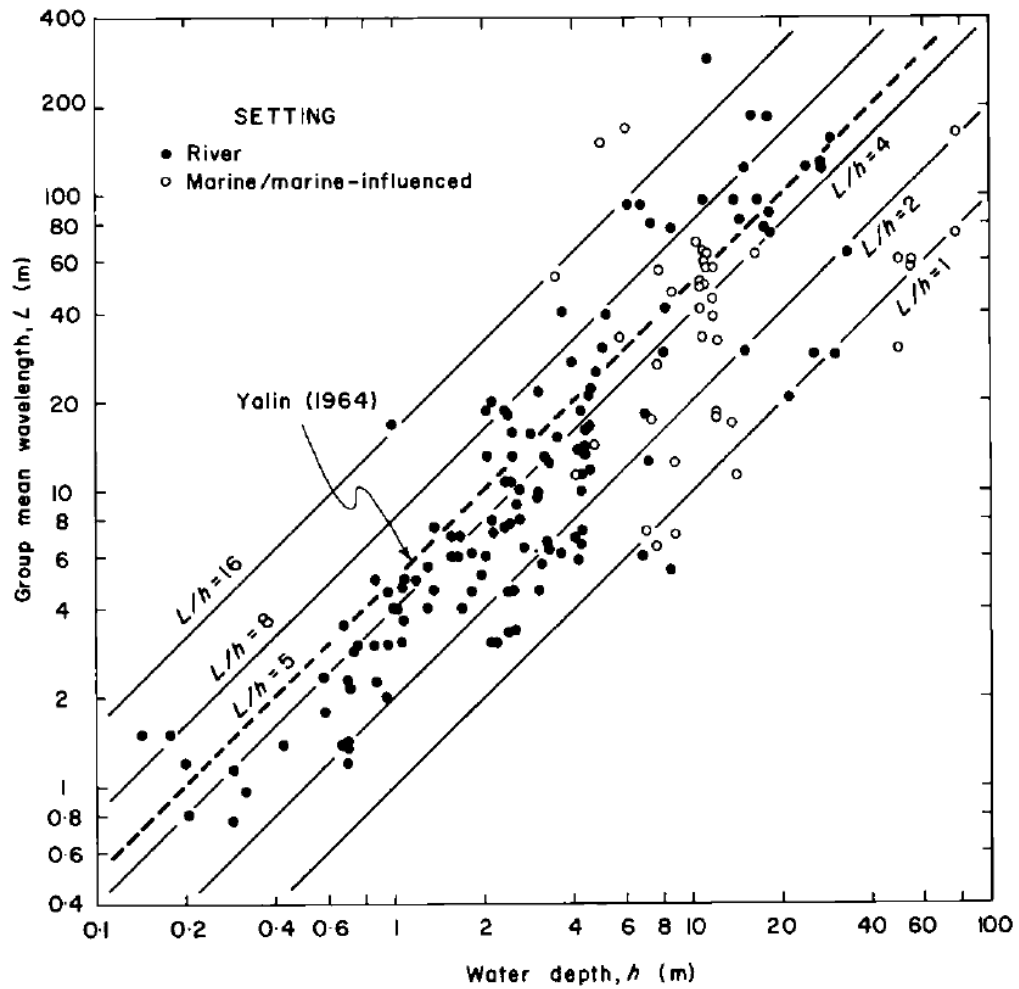


Figure 2-5: Correlation between group mean wavelength and water depth for dunes in river and marine or marine-influenced setting. The scatter is large, particularly at the larger water depths, but the scale of dunes clearly increases with increasing depth of flow (From Allen 1982 pp331, references for data therein).

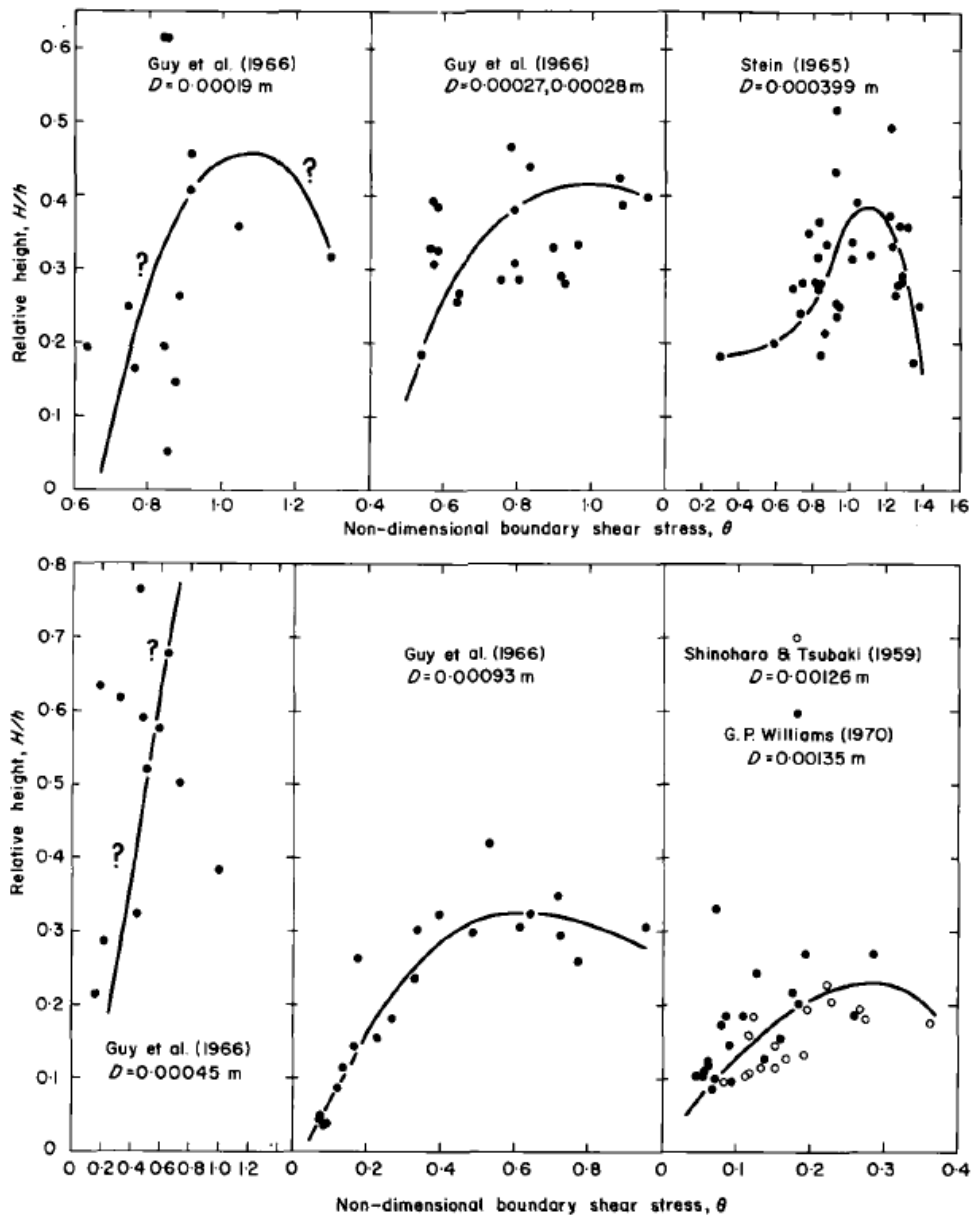


Figure 2-6: Group mean dune height relative to mean water depth as a function under equilibrium conditions of the non-dimensional boundary shear stress and sediment calibre. Stress corrected for wall effects by procedure of G.P. Williams (1970). These plots show that dune height responds strongly to the boundary shear stress, with scatter less than when plotted against depth (Figure 2-4) (From Allen 1982, pp334, data references therein).

Allen (1982) also notes the importance of grain size on dune geometry. Figure 2-7 displays the match between predicted non-dimensional wavelengths against Froude number. Here the best fit between prediction and observation is for the coarser grain sizes and Allen (1982) suggests this is due to the lack of sediment suspension at the largest grain sizes. Controversially, the actual wavelength decreases with increasing grain size, which is converse to the observations of

Rubin & McCulloch (1980) who found the longest bedforms were always the coarsest.

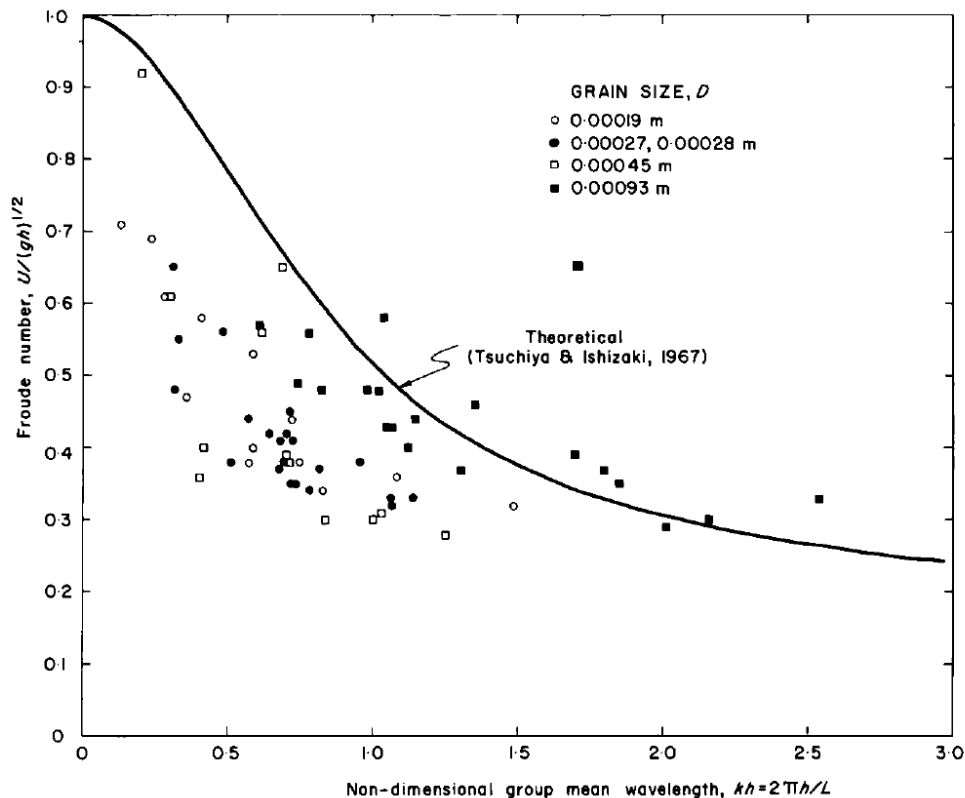


Figure 2-7: Effect of grain size on non-dimensional group mean dune wavelength and Froude number. The plotted line fits the dunes in the coarsest sand the best. (From Allen 1982, pp 332- references therein).

There have been many attempts at producing stability diagrams for ripples and dunes based upon sediment mobility (Allen 1982; Southard & Boguchwal 1990), dimensionless shear stress (Allen 1982; Southard & Boguchwal 1990), or sediment transport stage (Van Rijn 1984a; Van den Berg & Van Gelder 1993; Julien & Klassen 1995) vs. grain size. These stability diagrams can be useful, but caution should be exercised as there is considerable variation and scatter in the equilibrium heights, lengths and crestline curvatures of dunes and ripples within their own stability regimes (Allen 1982; Van Rijn 1984c; Ashley 1990; Southard & Boguchwal 1990). A key example is the existence of low-angle dunes, which are not dominated by bedload transport (unlike most laboratory experiments), as these do not plot correctly in stability diagrams (Kostaschuk & Villard 1996; Van den Berg & Gelder *et al.*, 1998). Other variations between predicted and measured bedform type and size has been attributed to 1: sediment type and sorting (uniformity or cohesion), 2: type of sediment

transport mechanisms prevalent (suspended bedload vs. bedload traction load),
3: hysteresis & unsteadiness affects.

2.1.2 Shape of dunes

Figure 2-6 displayed the change in dune height with bed shear stress. What is not shown on that diagram is how the bedform wavelength changes with bed shear stress. The change in dune height and wavelength with increasing bed shear stress produces different shaped dunes such that dunes of equal height will have different shapes dependent upon the bed shear stress (Allen 1982). The transition from low to high bed shear stress dune shapes for bedload dominated dunes can be summarised as:

1. Dunes (commonly highly 3D) (Venditti *et al.* 2005c)
2. High angle dunes (or maximum steepness dunes)(Allen 1968; Bridge & Best 1988)
3. Humpback dunes (or washed out/diminished dunes)(Allen 1968; Bennett *et al.* 1998; Carling *et al.* 2000a)
4. Upper stage plane bed (Best & Bridge 1992; Bennett *et al.* 1998)

Figure 2-8 illustrates the shape differences between the bedload dominated high angle dunes and humpback dunes (Carling *et al.* 2000a). The differences in relative length of the lee-side, crest and stoss side, change dramatically between these two dune shapes. These changes indicate that there is fundamental alteration of the dune processes. The diminished or humpback dunes display a short stoss slope, and long crest under high flow velocity and bed shear stress conditions. This is induced from the accelerated turbulence dissipation rate produced from the high downstream velocity over the stoss slope (Fredsoe 1979; Engelund & Fredsoe 1982). The long crest is essentially a temporary upper stage plane bed. Downstream crest length is controlled by the rate of dissipation produced from the grain roughness, once the downstream velocity drops, flow separation can become stable and the lee side is formed (Carling *et al.*, 2000b).

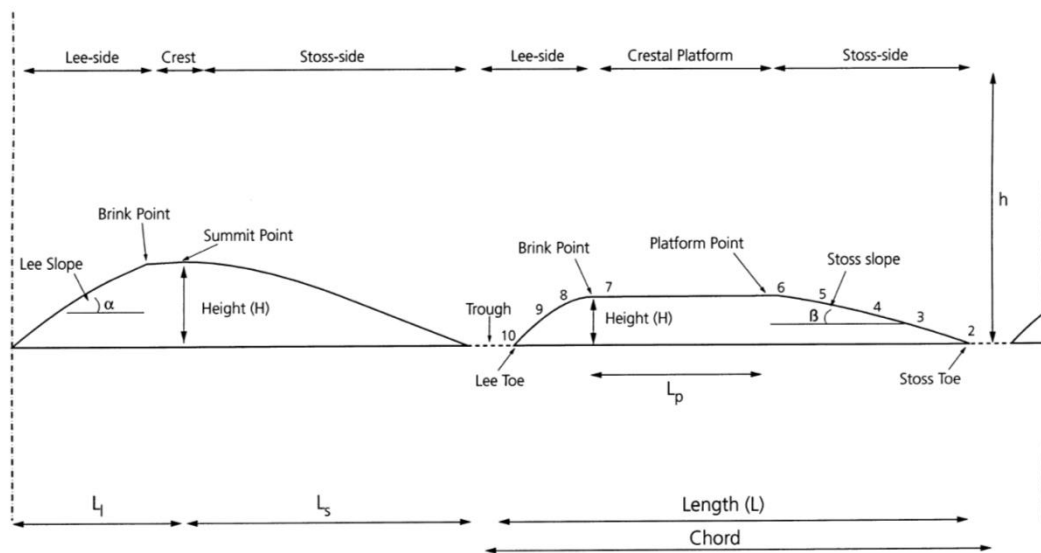


Figure 2-8. Dune shape and definitions for steep and diminished dunes. (From Carling *et al.*, 2000a(Modified from Allen 1968)).

The maximum steepness (height /length) of dunes is well constrained by empirical measurement from natural and laboratory measurements (Ashley 1990):

$$\frac{D_H}{\lambda} = 0.016d^{0.84} \quad 1.7$$

However whether a dune reaches this maximum steepness is dependent upon hysteresis effects, sediment supply and hydraulic constrains from depth limitation. Notably, certain dune types do not reach this limit, for example diminished/humpback dunes and low angle dunes never reach this maximum steepness value (Kostaschuk & Villard 1996; Carling *et al.* 2000a).

Diminished dunes and low angle dunes are an excellent example of a strong process control on the shape of the bedform that does not match those for classical bedload dominated dunes. Low angle dunes are thought to be caused by a high amount of suspended sediment concentration diminishing the intensity of the lee side shear layer, and thus reducing erosion at flow reattachment (Kostaschuk & Villard 1996; Best & Kostaschuk 2002). It is interesting to note that as yet, no-one has ever reported the creation of low angle dunes in a laboratory, and there are no reported records of the formation of low angle dunes from either a flat bed or higher angle dunes. The lack of laboratory formed low angle mobile dunes immediately indicates that free surface effects or width:depth ratio should be important. The small grain size

generally present for low angle dunes indicates that sediment cohesion may also play a role in reducing flow reattachment scour, due to the lower grain roughness number (Baas *et al.* 2011; Baas *et al.* 2013). In addition, it is not unlikely that bedform hysteresis effects play a role, as most low angle dunes have been found in estuaries (Kostaschuk & Villard 1996) and rivers with a monsoonal climate (Roden, 1998).

Humpback dunes are similar to low angle dunes in steepness due to their long stoss/crests and reduced height. Both bedforms show a strong influence on sediment transport from coherent flow structures suspending large amounts of sediment (Carling, *et al.*, 2000b; Bradley *et al.*, 2013;). The presence of flow separation precludes them being the same bedform but it may be that these are two examples of the same bedform processes but operating with different grain sizes and bed shear stresses.

2.1.3 Flow structure and grain & form roughness

It is clear from the above descriptions of bedform initiation and growth, that a key role in the stability of bedforms is the interaction of flow and bedform geometry with granular sediment transport (Bagnold; 1956; Bagnold; 1966; Allen, 1968; Allen, 1976; Allen, 1980; Best, 1996; Leeder, 2009). The vast majority of the time river flow is sub-critical and fully turbulent, therefore turbulent boundary layers form against walls and turbulent bursting can deform sandy layers by the relatively high shear stresses they create (Grass, 1970, 1983; Fredsoe, 1979,1982; Garcia *et al.*, 1996; Best, 1992; Muller and Gyr, 1996; Willians, 1996; Robert, 2003, 2011). Due to the subcritical nature of the flow, any change in the geometry of the boundary will lead to an out-of-phase adjustment by the flow (Nelson *et al.*, 1993, Bennett and Best, 1995, Smith, 1996, Fedele and Garcia, 2001, Maddux *et al.*, 2003b). As dunes migrate downstream, the surrounding flow structure will appear stationary as the geometry defines the reaction of the general flow structure.

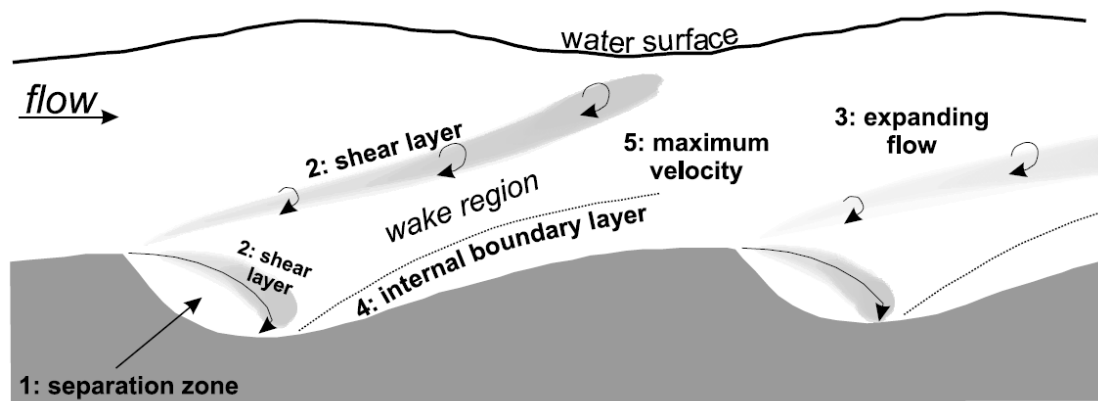


Figure 2-9. Schematic diagram of the principal regions of flow over asymmetrical, angle-of-repose dunes. 1: flow separation zone downstream of the angle of repose lee slope. 2: separation shear layer consists of eddies produced from the difference in velocity magnitude and direction from the outer flow and recirculating flow, a secondary shear layer above the wake is present due to the wakes lower velocity. 3 Above the shear layer a region of flow expansion occurs due to the high pressure inducted from flow separation. 4: a new internal boundary layer forms downstream of flow reattachment. 5: the wake and internal boundary layer merge at the crest, flow convergence up the stoss slope reduces turbulence intensity from the wake and downstream velocity is at a maximum, pressure is low. Body text has further description and references. (From Best 2005a).

On the lower angle (stoss side) the average flow velocity increases up the slope and creates a water surface depression over the crest of the dune, the flow surface then expands as the flow velocity decreases over the lee slope and lower stoss side of the next dune, as the water depth is larger (Figure 2-9), this creates the out-of-phase relationship between the dune geometry and water surface (Figure 2-9).

For flows over mobile beds there are two main causes of flow resistance, grain roughness and bedform form roughness (Einstein & Barbarossa 1952). The flow structure (Figure 2-9) that is produced over these asymmetric dune shapes has many important implications for flow resistance and sediment transport (Simons & Richardson 1966; Fedele & Garcia 2001; Prent & Hickin 2001; Holmes & Garcia 2008; Sandbach *et al.* 2012). The pressure difference between the stoss (lower pressure, accelerating flow) and lee side (higher pressure, decelerating and expanding flow) produces an overall net force on the dune which is the form roughness, or drag, of the bedform. For dunes this roughness is considerably larger than the grain roughness, although measurements of both are important in assessing the overall flow resistance for dunes (Raudkivi 1966; McLean & Smith 1986; McLean *et al.* 1999a; Maddux, *et al.* 2003a,b). The classic works of Raudkivi (1963, 1966) and Smith & McLean (1977), McLean &

Smith (1979) and McLean et al (1999a) demonstrate that form roughness does not contribute to overall sediment transport as the drag force is transmitted to the bottom boundary by fluid pressure as the force is integrated over the entire length of the bedform. The fluid pressure interacts with the native sediment transport hysteresis (Bagnold 1956) and affects the shape of the bedform, which may have indirect consequences on sediment transport rate across dunes.

One of the most significant features of flow over dunes is the presence of a shear layer caused by the sharp angle at the lee slope (Figure 2-9). The sharp velocity gradient over the dune lee produces a shear layer comprised of Kelvin-Helmholtz instabilities (Nagkagawa & Nezu 1981, Nezu & Nagkagawa 1993; Muller & Gyr 1986, 1996; Nelson *et al.* 1993; Bennett & Best 1995; Kadota & Nezu 1999) (Figure 2-9). These rotating vortices have higher than average instantaneous flow velocities and shear stresses; and thus greater ability to hold much more and/or larger sediment in the shear layer (Grass, 1983). Downstream of the shear layer a wake zone (zone of non-free flowing fluid) grows and dissipates the shear layer momentum deficit (Raudkivi 1963; McLean & Smith 1986; Maddux, *et al.* 2003b; Nelson *et al.* 1993).

This turbulent wake commonly carries pulses of fluid ejected from the shear layer and from a dune upstream (Figure 2-9) (Nelson & Smith 1989). This wake region therefore also has a velocity contrast to the free flow above and creates a secondary but weaker shear layer which sometimes interacts with the free surface as boils (Lapointe 1992,1996, Kostaschuk & Church 1993; Best 2005b). This wake effect is likely to be the primary mechanism of boil formation in rivers, but boils can form from a single shear layer and without multiple bedforms (Best 2005b; Chickadel *et al.* 2009) and/or from boundary layer turbulence (Jackson 1976b; Smith 1996).

When eddies in the shear layer hit the bed (at and around the flow reattachment point) the high turbulence intensities of eddies erode the dune stoss slope. This sediment is often piled up on the stoss slope in ripple, dunes or bed sheets due to the pulsed nature of the sediment movement (Parsons *et al.* 2005; Venditti *et al.* 2005b). This usually starts in the middle of the downstream dune because of the formation of a new turbulent boundary layer on the back of the downstream dune; thus starting with a laminar layer and transitioning to turbulence further up the stoss slope (McLean & Smith 1979; Rubin & McCulloch 1980; Reesink &

Bridge 2009; Best 2011). The combination of the new internal boundary layer, wake region and associated shear layer creates the expanding flow downstream of the dune crest (Figure 2-9). The dissipation of turbulence along the dune stoss layer also changes the velocity profile toward a classical open channel profile (Nezu & Nakagawa 1993; Fedele & Garcia 2001).

2.1.4 Sediment movement with dunes

Dunes migrate primarily through deposition of bedload sediment on the lee slope. This sediment arrives after being transported as either (or a combination of) sediment saltation or continuous traction (Allen 1980; Whiting *et al.* 1988; Schmeeckle & Nelson 2003; Aberle *et al.* 2012), as bedload sheets (Venditti *et al.* 2005a;) or through superimposed bedforms (Rubin & McCulloch 1980; Reesink & Bridge 2007) moving toward the crest. Suspended sediment does contribute to the migration of bedforms through settling onto the lee face in the flow recirculation region, but this quantity is relatively small. Naqshband *et al.* (2014a), and Kostaschuk *et al.* (2009) estimated that 17% of suspended sediment was deposited in the trough and added to dune migration.

The majority of suspended sediment is produced from flow separation and at reattachment (Nelson *et al.* 1995). Lapointe (1996) found that turbulent burst-like suspension events only took up 1-5% of the measurement duration but managed to account for 20-90% of all the suspension work in the mid Fraser River (Lapointe 1996). This highlights the importance of the eddies and coherent flow structures produced from flow separation to the maintenance of suspended sediment across dune fields (Jackson, 1976b; Nakagawa & Nezu, 1981; Muller & Gyr, 1986 1996; Laponite, 1992, 1996; Kostaschuk & Church, 1993; Babakaiff & Hickin 1996; Garcia *et al.*, 1996; Kadota & Nezu, 1999; Kostaschuk, 2000; Kostaschuk *et al.* 2009; Shugar *et al.*, 2010; Szupiany *et al.*, 2012; Bradley *et al.*, 2013).

The creation of these Coherent Flow Structures has broad implications; primarily that winnowing of smaller grains out of the bed and bedload layer increases the overall size of the grains that make up the dunes. An extreme

example of that has recently been found for ripples, where a sand-clay mix, given enough time, produced equilibrium sand ripples after the clay content was winnowed out through turbulent suspension (Baas *et al.*, 2011, 2013; Verhagen *et al.*, 2013). Secondly, the re-suspension of sediment into the water column has been suggested as the primary reason for the existence of low-angle dunes (Kostaschuk & Villard 1996; Best & Kostaschuk 2002; Best *et al.* 2004; Bradley *et al.* 2013). Increased concentration of suspended sediment dampens turbulence intensity (Baas & Best 2008; Baas *et al.*, 2009) and reduces the erosion of the stoss slope through flow separation, which also allows for enhanced deposition of fines on the lee side (Best & Kostaschuk 2002). The amount and intensity of turbulent bursting can therefore strongly control where sediment is transported across dunes and more research is needed to understand how this phenomena changes for various conditions, especially where dune height does not match empirical predictions, which is a surprisingly common occurrence (Jordan 1965; Williams 1970; Bridge & Jarvis 1977; Julien & Klaassen 1995). Additionally, these coherent flow structures can alter the quantity of sediment suspension over dunes whilst the spatially-averaged flow structure used to estimate bed shear stress may miss these locally and temporally high bed shear stress events (McLean *et al.* 1999a). Therefore the use of the Rouse number to determine sediment transport mode may oversimplify the sediment dynamics.

Recently, Keylock *et al.*, (2014) has been applying a new method of interpreting turbulent motions through a modification of the quadrant analysis approach (Bogard & Tiederman 1986) often used in turbulence studies of geophysical flows (Bennett & Best 1995; Sukhodolov *et al.* 2006; Balachandar *et al.* 2007; Hardy *et al.* 2009; Omidyeganeh & Piomelli 2011; Chapman *et al.*, 2012, 2013) that allows one to view the dependence between velocity and intermittency in the flow (Keylock *et al.* 2012; Keylock 2008, 2009). This approach is a somewhat similar, but more indicative, method of identifying sediment transport causing turbulent events than the flow exuberance methods used by Chapman *et al.* (2012 & 2013). The main implication of Keylock *et al.* (2014) is that sediment moving quadrant events happen in sequences of changing lateral (cross stream) flow direction and some of these sequences are more common than others. Importantly, particular turbulent events produce considerably

more bed shear stress than others (somewhat equivalent to quadrant 4 events). Application of this technique to flow over dunes has indicated that the turbulent wakes produced by dunes produces a unique turbulent signature that is comparable across experiments (Keylock *et al.* 2013, 2014). This observation can potentially be used to identify certain types or magnitudes of sediment transport events in natural rivers, but the relevance of this to the actual stability of dunes is, as-yet, unclear.

The implication that measurement and understanding of these instantaneous bed shear stress events is more important than the overall average bed shear stress is not new. Considerable laboratory work has detailed much of these flow events (Nelson *et al.* 1993, 1995; McLean *et al.* 1999a) and their sediment transport rates and sediment suspension dynamics (Nelson *et al.* 1995), therefore the control on the shape of the bed surface and water topography (Bennett & Best 1995; Best 2005a,b). Yet this research has yet to come to the fore and produce new process understanding that directly improves sediment transport predictions and any impacts on dune shape or scaling.

After the reattachment point, the amount of eddies hitting the bed reduces up the stoss slope of the downstream bedform as the wake rises, and internal boundary layer between the outer flow with its large low frequency turbulent events promoting vertical mixing is further away from the viscous sublayer and the bed (McLean & Smith 1986; McLean 1990; McLean 1994; Bennett & Best 1995). Here the sediment movement becomes largely related to the increase in downstream velocity, lower pressure and higher bed shear stress up the stoss slope (Raudkivi 1963, 1996). At the upper stoss slope and crest the flow and sediment dynamics are most comparable to classical (and flat) boundary layer theory, making the use of sediment transport formulae most applicable as the effects of the turbulent wake are least apparent in the flow structure (Fredsoe 1982; Nelson & Smith 1989; McLean *et al.* 1999a,b).

Estimating bed shear stress and sediment transport rate using velocity profiles near the crest has been moderately successful (Smith & McLean 1977), with a revision in McLean *et al.*, (1999a). This method involves partitioning the mean velocity profiles into two log-linear portions; the log-linear upper portion containing the total boundary shear stress, and a log-linear lower portion containing the form roughness. Measurement of this form roughness, rather

than skin friction as in Smith & McLean (1977), is more accurate as the turbulent wake still affects the velocity profile shape above the crest. As Einstein & Barbarossa (1952) detailed:

$$\tau_b = \tau_{fd} + \tau_{sf} + \tau_{gd} \quad 1.8$$

where τ_{tb} =total boundary shear stress, τ_{fd} = shear stresses attributed to form drag and τ_{sf} = shear associated from granular movement and τ_{gd} = shear associated with granular drag, usually ignored as it is commonly very small.

McLean et al (1999a) use a model to predict the velocity profile without the wake (a wake defect law) to predict the form drag to within +-15%:

$$\tau_{fd} = \frac{1}{2} \rho C_{fd} u_R^{-2} \frac{D_H}{\lambda} \quad 1.9$$

where C_{fd} = form drag coefficient empirically found to be 0.19; u_R is the mean velocity at one dune height (D_H) above the crest predicted from an analytical model developed in (McLean & Smith 1986; Nelson & Smith 1989; McLean *et al.* 1999a). Once calculated, the total boundary shear stress can then be predicted to within +-20% by estimating the grain roughness (Einstein & Barbarossa 1952).

The McLean *et al.*, (1999a) methods require detailed flow velocity profiles and assumes equilibrium 2D bedforms, although some adaptations for 3D bedforms have been produced (Maddux, *et al.* 2003a,b). However, the applicability of these will be heavily reliant on the particular morphology of the 3D dune, which is highly variable (Allen 1982, Venditti *et al.* 2005c, Venditti, 2007).

Producing one-dimensional models in geophysical research has proved very useful to the analysis and elucidation of dominant processes (Johannesson & Parker 1989; Parker 1990). Here, a method of estimating the sediment transport rate using one-dimensional sediment continuity equations for steady flow is used to illustrate this capacity:

$$-C_b \frac{dh}{dt} = \frac{di_b}{dx} \quad 1.10$$

and that:

$$\frac{-dh}{dt} = \frac{cdh}{dx} \quad 1.11$$

where C_b is the volume concentration of grains in the bed, c is bed-wave celerity and x is the downstream distance. i_b = variation in bedload transport rate over the stoss, h = bed height, this results in:

$$\frac{di_b}{dx} = \frac{C_b c d h}{dx} \quad 1.12$$

and is integrated into:

$$i_b - i_{b0} = C_b c (h - h_0) \quad 1.13$$

Where i_{b0} and h_0 are the bed-load transport rate and bed height in the bed wave trough (Exner 1920, Bridge 2003). As i_{b0} can be taken as zero (mean bed level) the above equation indicates that bed-load transport rate increases linearly with distance above the trough and reaches a maximum at the crest. Additional indications are that triangular bedforms will have the mean bedload transport rate half way up the stoss slope, and that bedwave height constantly increases with higher sediment transport rate for a constant migration rate: this last point is the converse of that described at the end of section 2.1 (page 17); whereby maximum dune height is achieved when the rising dune height increases topographic acceleration, which increases the sediment transport rate until no vertical deposition is possible (upper stage plane bed conditions). Any further increase in sediment transport rate is taken up purely with an increase in celerity, i.e. equilibrium conditions.

This general model for the scaling and growth of dunes forms the basis for many computational models (e.g. Jerolmack & Mohrig 2005a&b; Paarlberg *et al.* 2009; Shimizu *et al.* 2009) due to its relative computational simplicity. However, this removes much of the natural unsteadiness that one sees when watching dunes in laboratory conditions, such as bedform deformation (Mcelroy & Mohrig 2009), dune amalgamation (Best 2011; Best *et al.* 2013), calving/splitting (Warmink *et al.* 2014) and stranded or sheltered dunes (Jones 1977; Best *et al.* 2013); these dune dynamics are often parameterised into models based of thresholds. The thresholds for the initiation of e.g. bedform calving or a new bedform growing on a particularly long stoss slope are often based upon laboratory experiments that measured a constricted range of conditions for laboratory practicality (Warmink *et al.* 2014). Yet, these processes are most active, most important and most variable and dynamic

during periods of unsteady conditions (Allen 1976; Fredsøe 1979; Kuhnle 1992; Gabel 1993). In these situations the effects of bedform history, or hysteresis, can significantly complicate dune dynamics and can invalidate model assumptions (Hay 2011).

2.2 Current issues

2.2.1 Shear and reattachment

The transport of a significant amount of energy and sediment via eddies is one of the key modes of sediment transport in open channel flows (Muller and Gyr, 1996). Because of the temporal and spatial fluctuations in shear layers, defining the shear layer processes across space and time has been achieved by time averaging velocity data from flow visualisation and particle tracking studies (Nelson *et al.*, 1993, Bennett and Best, 1995). The shear layer flow reattachment point has been shown to vary through time even with a stable dune field or even fixed bedforms; this is due to two phenomena: eddy shedding and shear flapping (Figure 2-9) (Engel 1981; Nagkagawa & Nezu 1981; Levi 1983, 1991; Muller & Gyr 1986; Simpson 1989). Time averaging velocity data produces normalised reattachment lengths of five to seven bedform heights (Engel 1981; Ruderich & Fernholz 1986; Kadota & Nezu 1999) that are useful in bedform modelling and in the parameterisation of flow separation (Paarlberg *et al.* 2007). The drawback of this time-averaging method is that it removes any short term, high energy, processes and mechanisms from view, and therefore their evaluation in terms of influence of flow and sediment transport has been masked (Best 2005a; Muller & Gyr 1996). This view removes the natural variation that would occur during unsteady flow conditions, such as the role of superimposed bedforms on sheltering host bedform shear layers (Fernandez *et al.* 2006; Best 2011), unsteady sediment transport on dune stoss and lee sides (Reesink & Bridge 2007; 2009) the lack of consistent shear layers in low angle dunes (Kostaschuk & Villard 1996; Kostaschuk 2000; Best & Kostaschuk 2002; Bradley *et al.* 2013), and unsteady sediment transport and channel slope (Allen 1976, 1978a,b; Fredsøe 1979; Kuhnle 1992; Gabel 1993; Nezu & Nakagawa 1995; Tayfur & Singh 2012; Martin & Jerolmack 2013) where flow depth and depth averaged shear stress changes faster than the bedform adaption time, leaving the bedforms out-of-equilibrium.

2.2.2 Hysteresis

What happens when the flow regime changes but stays within the dune forming field (in standard stability plots) is less well understood despite being one of the more common types of condition change. Figure 2-10 displays typical bedform geometry vs discharge graphs found from bedform-discharge hysteresis during a flood (Gabel, 1993). In each survey there exists a non-linear response in dune characteristics and discharge, commonly forming a loop. This hysteresis is where the bedforms are smaller in the rising limb and larger in the falling limb of the flood due to the lag in bedform reaction to the changing flow state.

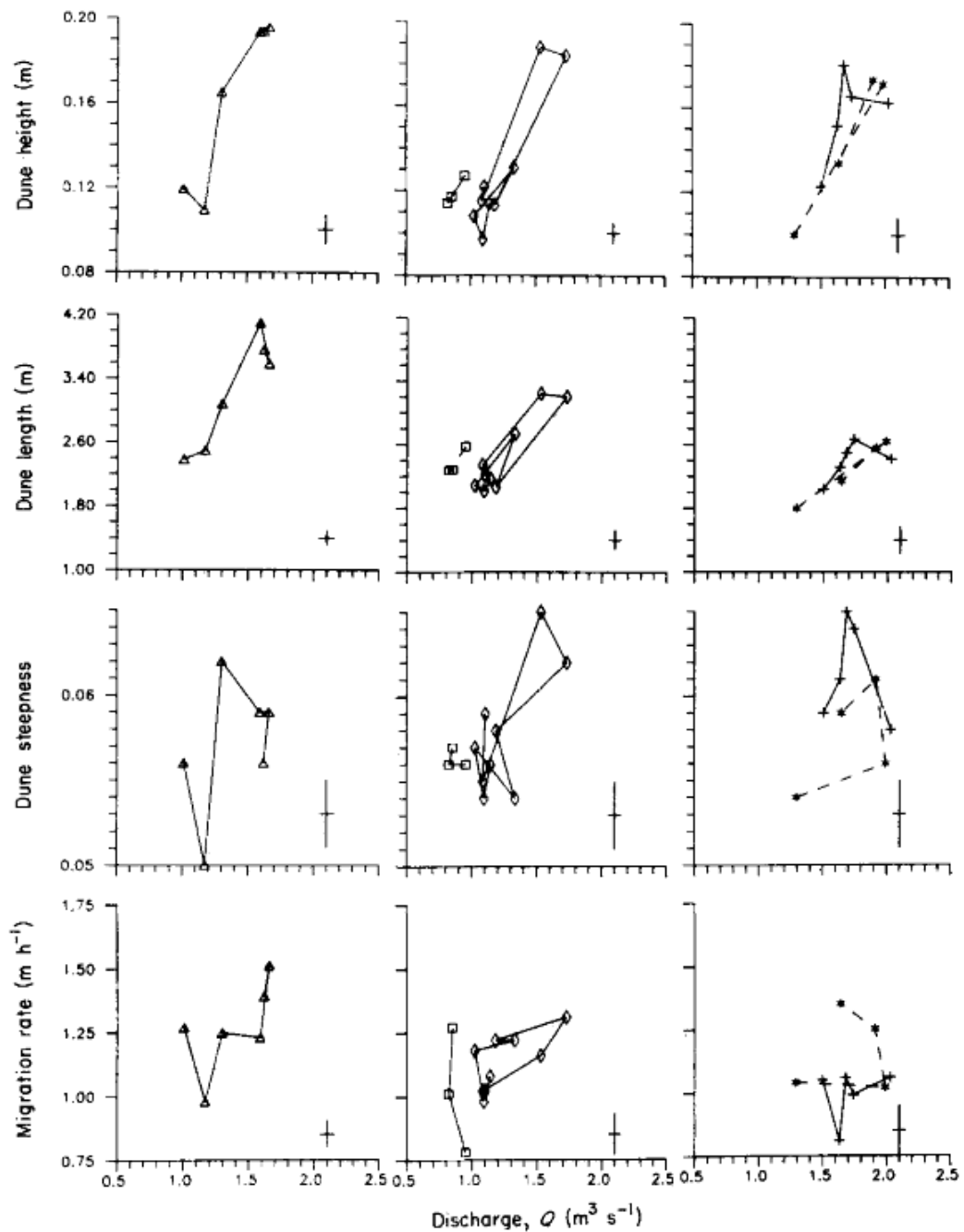


Figure 2-10. Plots of mean dune height versus discharge (top row), mean dune length versus discharge (second row), mean dune steepness versus discharge (third row) and mean dune migration rate (U_s) versus discharge (bottom row). In each row, the left-hand diagram shows data from spring 1986. The middle diagram shows data from spring and summer 1985 from the right channel. Data from both the left channel and the downstream area are plotted on the right-hand diagram in each row. On all diagrams, lines connect on consecutive surveys. Error bars are shown at lower right on each graph and represent the largest standard deviation of the mean measured from the data plotted on that graph (From Gabel 1993).

Martin and Jerolmack (2013) describe a flood wave impact on dune morphology and processes. Figures 2-11 & 2-12 shows the merging processes creating larger bedforms for the rising leg of a flood wave, and the cannibalisation processes for the falling leg. They investigated the difference in the rate of change in hydraulic and bedform state, and found that full flood flow can be produced without hysteresis, if the rise to peak flow is at the same rate as bedform adaption.

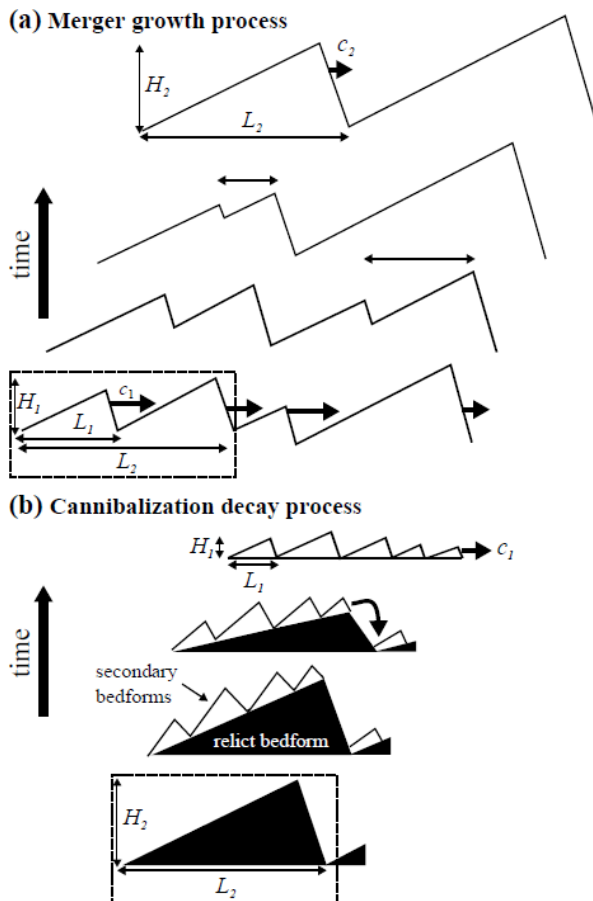


Figure 2-11. Conceptualization of bedform growth and decay processes. (a) For the growth process, differences among celerities cause bedforms to collide and merge into larger features until a new equilibrium is reached. (b) For the decay process, secondary bedforms (white) migrating across the larger relict flood peak bedform (black) erode the relict crest and the relict trough. H_1 , L_1 , and c_1 refer to low flow mean equilibrium bedform quantities, while H_2 , L_2 , and c_2 are for high flow. Dashed boxes outline reconstitution volumes V_1 for merger growth and V_2 for cannibalization decay (From Martin and Jerolmack 2013).

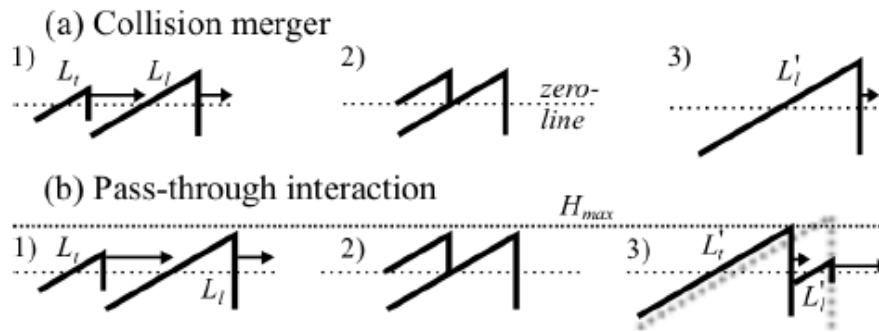


Figure 2-12. Diagram describing interactions in the bed-form merger growth model. Bedforms are treated as right angle triangles with constant steepness, $H=L$, which move with celerities inversely proportional to their sizes. For collision merger: 1) A small bedform (with length L_t) approaches a larger one (with length L_l) from behind. 2) When the small bedform is succinctly close, the intervening trough rises above the dashed zero-line, and they are considered merged. 3) Heights and lengths of colliding bedforms are combined additively to form the new merged bedform (with length L_{ol}). For pass-through interaction: 1) A small bedform approaches and 2) merges as before. 3) However, the resulting merged form would exceed H_{max} . Instead, a merged form at the maximum height line is formed (with length L_{ot}), and excess sediment is ejected as a small bedform in the front of the new merged bedform (with length L_{ol}) (From Martin and Jerolmack 2013).

While this conclusion seems obvious, it is not always applicable, as described in section 1.3.1 there are many bedform interactions that can occur and these two processes might not necessarily be the only ones that predominantly operating during a flood. Indeed, the effects of different transport stage on dune dynamics is a key factor in dune hysteresis (Prent & Hickin 2001). The ratio of bedload to suspended load can change migration rate and the typical grain size deposited on dune lee sides (Naqshband *et al.* 2014). As floods produce greater flow velocities it is generally true that they suspend greater amounts of suspended load compared with bedload (Jordan 1965; Nittrouer *et al.* 2008a; Ramirez & Allison 2013). Therefore bedform adaption rates can be strongly controlled by the amount of sediment suspended relative to bedload transport during the high flow velocities of floods and not falling into the lee face.

Rivers in tropical monsoonal climates typically display polymodal distributions of dune sizes (typically wavelength) due to the large variation in river stage between dry and wet season (Coleman 1969; Allen 1978b; Fielding & Alexander 1996; Fielding *et al.* 2009). This distribution indicates that the lag in bedform response to flow variability is so extreme that bedforms become some bedforms are only active during different parts of the year whilst being stable on timescales longer than a year. Yet it is likely that these different bedform scales

are produced through different processes that are dominant in either the peak flood or dry season. One key difference is the change in sediment suspension concentration between these two extremes (Bravard *et al.* 2014). The high sediment suspensions present during flood peak have the potential to alter flow separation (Baas *et al.* 2009) and the rate of sediment supply to the dune lee (Naqshband *et al.* 2014a). Additionally, the presence of secondary, superimposed, bedforms alters sediment transport delivery to the dune crest (Reesink & Bridge 2007). Secondary bedforms tend to grow in size during floods, which produces more suspended sediment and alters the development of the internal boundary layer along the host dunes stoss, adding more difficulty in predicting bedform morphology during floods (Julien & Klasssen 1995; Yen & Lee 1995; Amsler & Garcia 1997; Carling, *et al.*, 2000a,b). So, whilst sediment transport rates may be at their highest during peak flood, much of this will be as suspended sediment, thus limiting the bedforms ability to add volume and grow to the new hydraulic condition.

The predominantly bedload-based laboratory experiments of dune hysteresis have focused on dune splitting and merging during periods of unsteadiness. However, the effect of dominant sediment transport type needs to be taken into account as the change in phase between bedload dominated sediment transport and bedforms to suspended dominated sediment transport occurs (Nittrouer *et al.* 2008)

2.2.3 Local Sediment Supply

The above review of the role of turbulence and coherent flow structures indicates that there needs to be a better understanding of sediment routing over river dunes. The existence of low angle and diminished dunes indicates that sediment suspension has a very strong effect on the shape of dunes, and the processes present. The developing boundary layer and coherent flow structures present along the stoss of dunes has a huge potential to suspend more sediment than predicted from spatially-averaged estimates of bed shear stress. The additional presence of secondary bedforms on dune stoss slopes can also produce even greater quantities of suspended sediment (Rubin & McCulloch 1980; Fernandez *et al.* 2006; Best 2011). Depending on grain size this could

have various impacts, on bedform geometry; small sand sizes and coherent flow structures are linked with low angle dunes, whilst for larger grain sizes the impact of high sediment suspension from coherent flow structures and secondary bedforms may result in the increase of sediment suspension along the dunes stoss toward the crest. Such a gradual increase in suspension over bedload transport could result in the dune crest becoming supply limited, whilst the rest of the bedform remains relatively supply rich. This effect may be the reason why so many bedforms with superimposed secondary bedforms are lower in height than empirically predicted.

2.3 Thesis aims, hypothesis and objectives

The overall aim of the work presented herein is to assess the underlying processes that define the size, scaling and morphological response of river dunes to unsteady boundary conditions. Following the above literature review, the control of the fluid boundary conditions, particularly during periods of unsteady conditions, is of primary investigative importance. Therefore, this thesis will focus on controlling and varying the fluid boundary conditions over dunes in order to understand the variation in dune shape, size and the distribution and magnitude of sediment transport as bedload and suspended load. This will be achieved by using a reductionist approach whereby interrelated variables are picked apart and controlled or varied to elucidate the fluid and sedimentological processes that create the conditions for dune formation and maintenance in non-equilibrium conditions (Phillips, 2011). Through this overall aim, the thesis hopes to make the modelling of dunes in unsteady conditions easier via producing better parameterisations of flow-morphology relationships and processes that exist over dunes.

The hypotheses of this thesis are:

1. *The turbulent flow structure over bedforms in non-equilibrium conditions is considerably different from the turbulent flow structure for equilibrium conditions which has been previously researched, and that measuring these non-equilibrium flow states will illuminate why bedforms change shape to new flow conditions.*

2. *That dune leeside reattachment length over dunes varies with relative submergence.*
3. *That the relative effects of flow convergence and acceleration over a dune stoss slope is non-linear and affects the stability of dunes.*
4. *That using flow depth is a poor proxy for dune height and overall dune geometry, with bed shear stress being more representative of the processes that control dune height and length.*
5. *That superimposed bedforms can affect the maximum host dune height (rather than flow depth) through suspension of sediment along the host dune stoss slope.*
6. *That superimposed bedforms and their host bedform respond differently to changes in hydraulic conditions, i.e. they do not act as one single-or joint- unit of bedform.*

These hypotheses will be tested through completing the following research objectives:

1: Measure the mean flow fields and the location and intensity of turbulence over fixed two-dimensional dune fields at equilibrium and transient flow-morphology states, to assess the variation in location and intensity of turbulence production and dissipation produced in out-of-equilibrium conditions (hypothesis one)

2: To measure the median flow reattachment length across a suite of unsteady conditions (hypothesis two), to assess any variation with depth and mean flow velocity.

3: To measure the mean flow structure along a dune stoss slope across many conditions to assess the relative contributions of flow convergence, acceleration and turbulent dissipation on the mean flow structure and stability of dunes (hypothesis three).

4: Examine the relationship between velocity profile shape and bed shear stress on bedform shape and size in mobile bed conditions in equilibrium steady-states, without changing the flow depth (hypothesis two).

5: To measure the bedform morphology, turbulent flow field, flow structure and suspended sediment concentration in the field during unsteady conditions to be able to test hypothesis three & four and provide real world examples of the results found whilst investigating hypothesis one and two.

2.4 Thesis outline

The following chapters describe how the above hypothesis and research objective have been addressed, and how they contribute to the aim of the thesis.

Chapter four describes laboratory experiments in which high resolution turbulent flow structure over fixed bedforms across a wide range of hydraulic conditions was measured using a technique called Particle Image Velocimetry (see chapter three for a detailed review of the methodology of this technique). These experiments build but importantly expand upon the pioneering works of Nelson *et al.*, (1993) and Bennett & Best (1995) into unsteady flow conditions and in turn reveals relationships between relative submergence, flow velocity and reattachment length (hypothesis two); on major spatial shifts in turbulence production and dissipation (hypothesis one), which affect sediment transport mode, the dominant locations of erosion and deposition; and illustrates the importance of flow structure at a dune's crest on dune stability (hypothesis three). The results pave the way for increased parametrisation of the size and shape of dunes in computational models (overall thesis impact).

Hypothesis four is addressed in chapter five, which detailed the first experiments that adjust velocity profile shape, whilst controlling flow depth and discharge, in mobile bed conditions. This experiment investigated the impact of externally controlling velocity profile shape on dune size, curvature (three-dimensionality), their stability and sediment transport rate. This experiment add significant clarity to the scaling of fluvial dunes and argues that major adjustment needs to be made to dune height predictors to account for variations in velocity profile shapes in geophysical flows. The experiments also demonstrate how changes in flow structure affects the shape of dunes (as suggested in chapter four), with a mobile bed.

Objective three is detailed in chapter six, which presents research undertaken in the field on the Mekong River in 2013 during the falling leg of the rainy season. The chapter details repeated high resolution measurements of flow velocity, calibrated suspended sediment concentration and bathymetric quantification that reveals morphological and sediment transport mechanism responses changes in flow stage and discharge. The chapter attempts to answer hypothesis five and six whilst also providing a real-world analogue for the results of the research undertaken for hypothesis one to three.

Chapter seven provides a synthesis of the PhD's implications and concludes the thesis.

A Primer on using Particle Imaging Velocimetry in Geomorphological Research¹

Abstract

Particle Imaging Velocimetry (PIV) is one of the least intrusive methods for measuring flow fields. The key advantage of PIV is the ability to reveal temporal linkages in fluid motion on a scale from micrometers to meters, nanoseconds to minutes with measurement accuracy high enough to permit high order statistical analysis of flow turbulence. It is an ideal method for measuring flow conditions, turbulence and Coherent Flow Structures in a range of geophysical flows.

3.1 Introduction

For an array of environmental processes, fluid flow provides the medium for landscape change. Yet this fluid medium is not an inert passenger, flows also act and produce structures that play a key role in governing sediment movement. The measurement of these turbulent fluid flows is therefore critically important in understating many of the processes in geomorphology.

¹ The chapter is published in *Geomorphological Techniques*, Chapter. 3, Sec. 3.4 (2015)

Particle Imaging Velocimetry (PIV) is a measurement technique that was developed to measure wall bounded turbulent flows (Meinart, 1983, Yao & Adrian, 1984; Adrian & Yao, 1985; Adrian 1991; Adrian 2005). The advantage of PIV is whole flow field measurement with minimal intrusion from instrumentation. A typical 2D PIV system is illustrated in Figure 3-1. From full flow field visualisation, the structure and spatial linkages in turbulence can be observed, measured and proved, rather than inferred from single spatial point measurements (e.g. Bennet and Best 1995). This allows for spatial and temporal analysis techniques to be applied, from vorticity measurement (Lourenco & Krothapalli 1995; Adrian, *et al.* 2000a), to eddy detection (Chakraborty *et al.* 2005) and identification of Lagrangian Coherent Structures (LCS) (Haller & Yuan 2000; Hardy *et al.* 2010a,b; Haller & Sapsis 2011).

PIV systems are deployed in laboratories to provide 2D, 2.5D and full 3D flow measurements. In-field PIV can provide 2.5D and large scale water surface velocity measurements from UAV, Helium Balloon or a fixed position (e.g Coz *et al.* 2014). PIV provides instantaneous measurement of velocities across μm - mm - m sized areas have been used in geomorphological research areas such as; around vegetation (Cameron *et al.* 2013; Okamoto & Nezu 2013; Ricardo *et al.* 2014), turbulence & sediment transport (Coleman & Nikora 2009, Ferreira *et al.* 2010), flow in local scour cavities (Unger & Hager 2007; Ferreira 2011), Coherent Flow Structures (CFS) in rivers (Best 2005; Hardy *et al.* 2009, Cooper & Tait, 2010), secondary circulation in mender bends (Blanckaert *et al.* 2013) and surface velocity measurement through Large Scale PIV (LS-PIV) (Jodeau *et al.* 2008; Coz *et al.* 2014). Figure 3-2 displays an example of results from 2D PIV, showing an instantaneous vector field over a dune revealing flow separation in the dune lee. Figure 3-3 shows the same data decomposed into downstream and vertical velocities, Reynolds stress and Vorticity, revealing the larger turbulent structures in the flow.

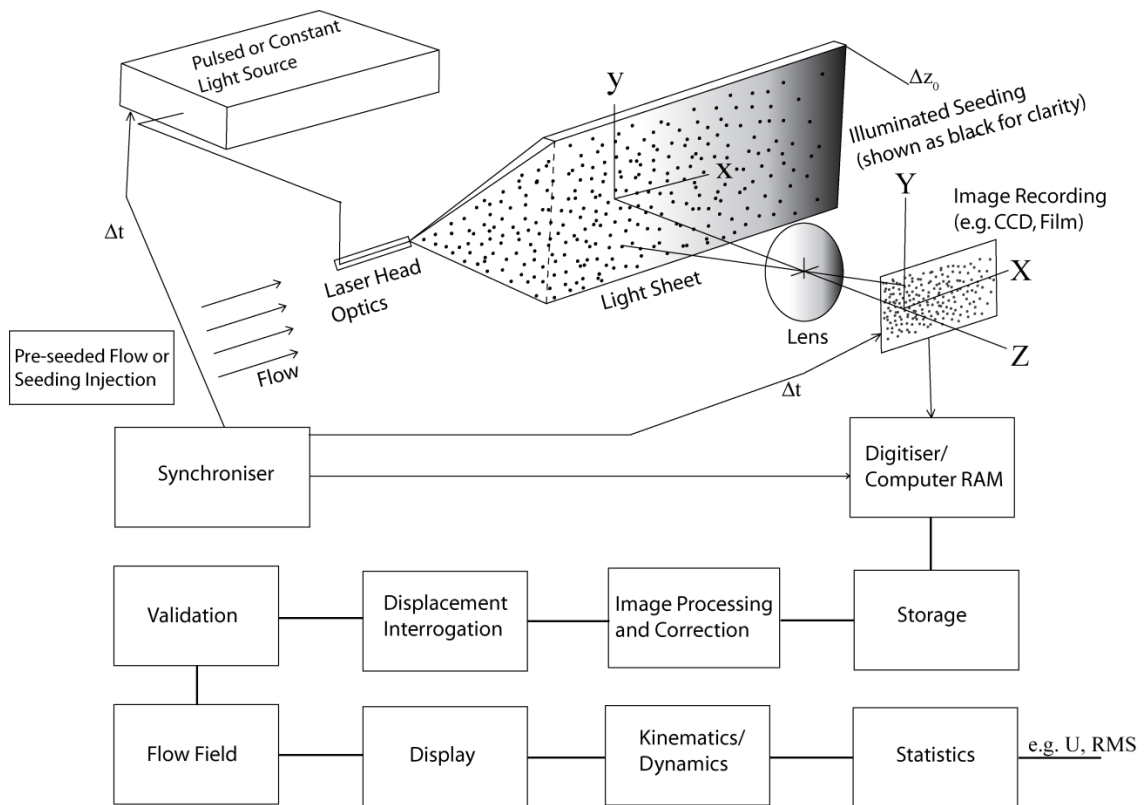


Figure 3-1 (above). A typical monoscopic (**2D-PIV**) system. Many aspects of this setup can be changed, such as light sheet illumination source, angle into the flow (e.g. through a transparent wall to further reduce flow impact), light sheet size, intensity and shape. Seeding can be injected into the flow at specific points or fully mixed into the flow. Multiple cameras can be used to increase spatial area and/or resolution. An additional camera mirroring the above light sheet-camera arrangement (i.e. both cameras facing each other) can be used to produce 3D velocity measurements in the light sheet plane (**Stereoscopic PIV**). Multiple Light sheets and cameras can be used to measure several planes of the flow simultaneously (**Tomographic or Holographic PIV**) (Figure adapted from Adrian, 2005).

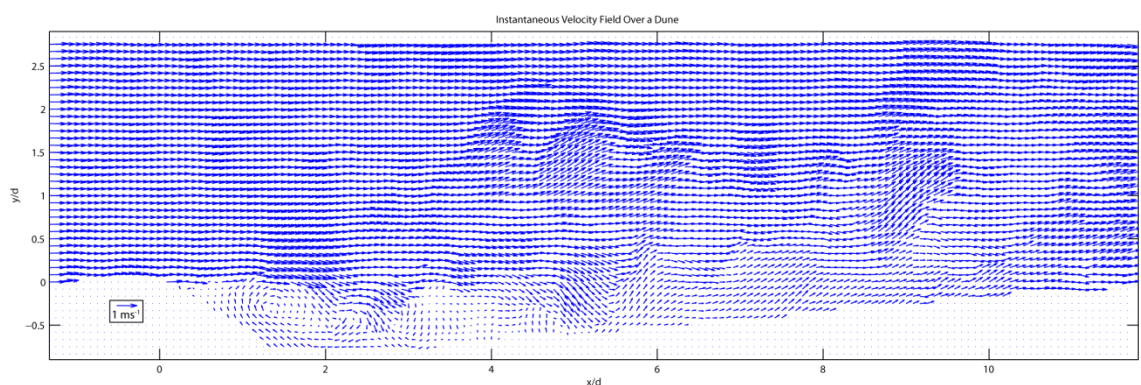


Figure 3-2: Instantaneous 2D flow field over the centreline of a 2D dune shape. Axis are normalised by the dune height d . Vector arrows have been doubled in size, and the downstream (u) component suppressed by 68% (Tomkins & Adrian 1999; Adrian *et al.* 2000b) to highlight the rotational flow over the bedform. Flow direction is left to right. Flow separation downstream of the crest can be seen in the shorter vector magnitudes and reversed direction. Data from Run H76 in Chapter 4.

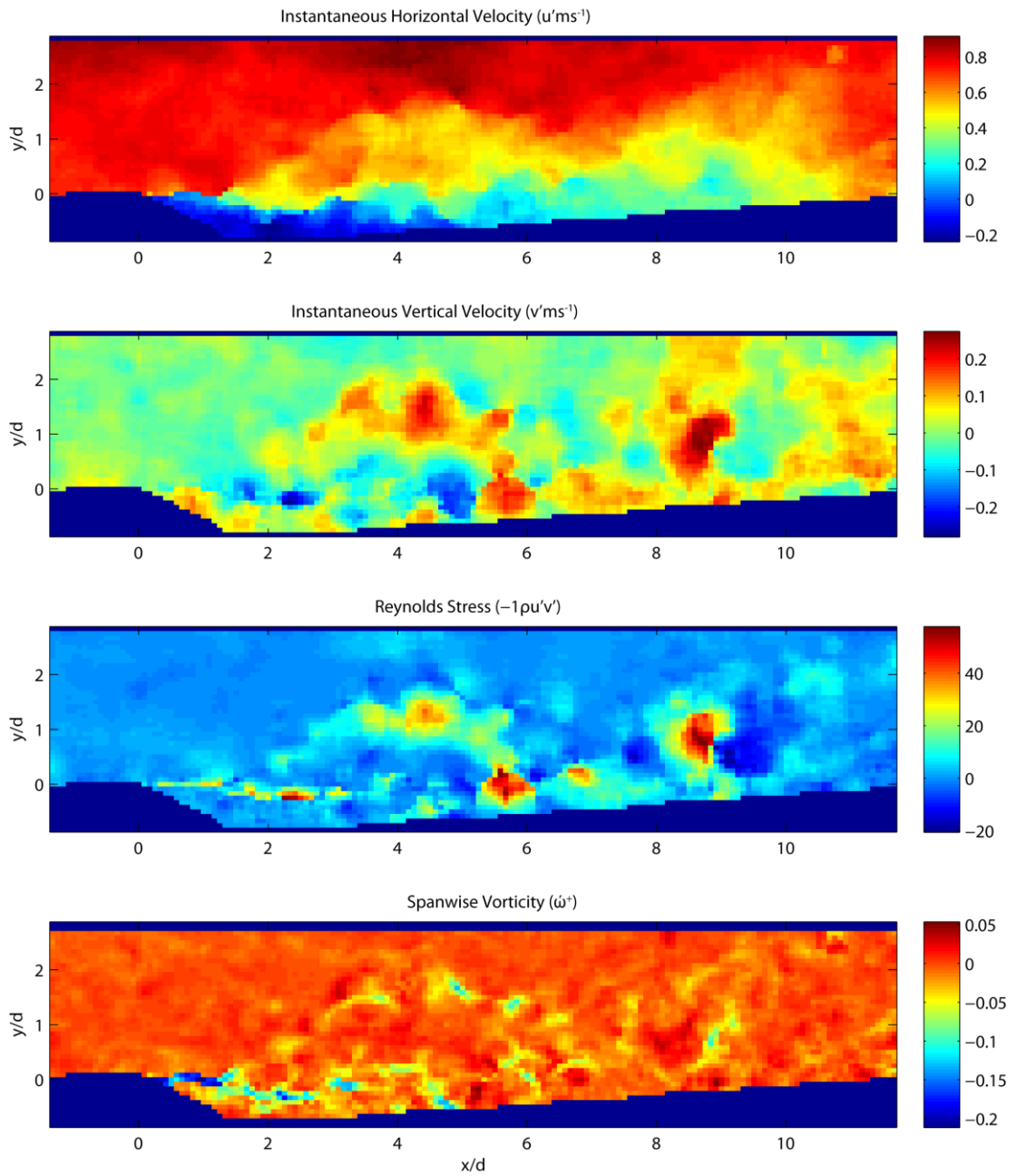


Figure 3-3: Instantaneous 2D PIV data. The flow field is revealed through downstream, vertical velocities, Reynolds stress and Vorticity, illustrating how PIV can display a host of flow field information including detailed structure of the turbulence. The field of view is over the centreline of a 2D dune shape fixed to the base of a flume. Axis are normalised by the dune height d . Taken at the same instantaneous point in time as Figure 3-2

3.2 Methodological Overview

For comprehensive reviews of standard PIV methodology and theory the books Raffell, et al (2007) and Adrian & Westerweel (2011) are applicable for beginners and advanced users.

The fundamental measurement in PIV is displacement and time, achieved through a now well-defined basic setup (Figure 3-1). Firstly, the fluid (water/air) of known density, viscosity and temperature is seeded with an even distribution of μm scale spherical particles/droplets. Particle seeding is of equal density to the fluid, small enough to respond to flow movements with minimal slip and faster than the measurement frequency whilst scattering enough light to be seen (see, Hjelmfelt & Mockros, 1966; Adrian 1991; Melling, 1997, among other solutions). Scattering particle refractive index is different from the fluid which they are seeded into, so light is scattered effectively (Adrian & Westerweel 2011). Secondly, a light sheet produced from laser or halogen bulb is focused into a thin plane with a series of optics. A thin plane of light is required so that a key assumption in the vector calculation is achieved: a spatially consistent grid of particles. Thirdly, a camera is placed perpendicular to the light sheet. Orthogonal camera to light sheet angles is possible but requires orthorectification (see Jodeau *et al.* 2008). The camera records light intensity with a high contrast ratio. Minimum measured pixel size, cost and availability tend to define camera resolution, which typically ranges from 1MP to 20MP. The camera sensor pixel size is an important consideration as smaller camera pixels improves the accuracy of each picture at a given resolution and reduces the error in vector calculation via a higher signal to noise ratio. Images produced look like a starry night sky (Figure 3-4). Finally, a synchroniser is required to keep the laser and image capture synchronous.

High density seeding (measurement via group displacement) is the typical method used in PIV (Adrian 1997; Westerweel 1997). A grid of interrogation regions is overlain over each image. The size of the grid can be varied to match particle seeding density, usually in powers of 2 starting at 8 (i.e. a grid of squares each 4x4 pixels).

The technique of measuring particle displacement in PIV is termed cross-correlation (Keane & Adrian 1992). Particle displacement is measured by finding the maximum spatial cross correlation between two interrogation region images separated in time. This provides a known direction and magnitude shift for each interrogation region in the field of view. Known time between images then produces the velocity vector. This process is performed repeatedly over the entire array of images via a 2D Fast-Fourier Transform (Adrian 1991; Keane & Adrian 1992; Westerweel 1993). If the particles in the interrogation window do not move with equal direction and magnitude then the calculated vector correlation coefficient will be low and is therefore easily removed in post-processing using a user defined threshold of correlation. Consequently, interrogation region size and measurement frequency is crucial for realistic measurements of highly turbulent flow, e.g. shear flow.

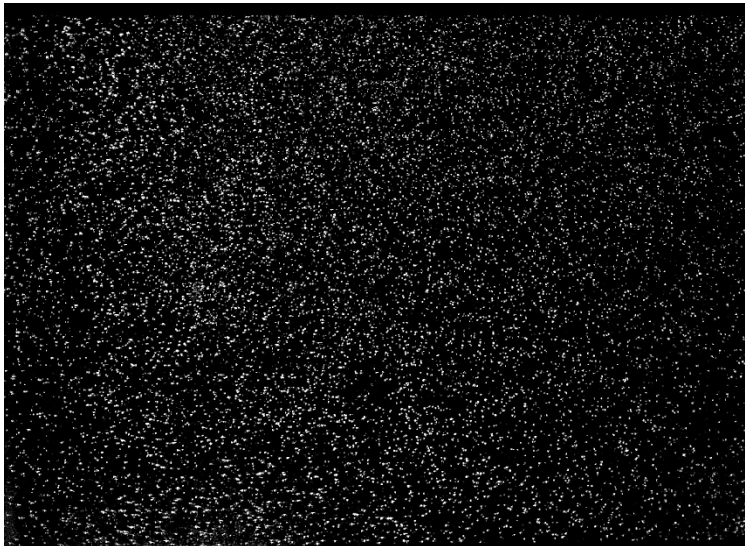


Figure 3-4. An example of a raw image of lab 2D-PIV, illuminated from below. Field of view is downstream of a large bar fixed to the bed, flow is left to right.

Interrogation regions are traditionally square and regular. However, as particles can sometimes move in and out of interrogation regions and thus reduce image correlation, an adaptive grid size and shape can be used to reduce this error. This also aids in measurement of poorly seeded areas, or areas with high shear (Gruen 1985; Lourenco & Krothapalli 1995; Theunissen *et al.* 2010). Recent algorithms can dynamically identify ideal window size and shape so that the number of particles in each window is above a user-defined threshold (Theunissen *et al.* 2007, 2010).

Illumination of seeding particles for photographic capture typically falls into two methods. Dual pulse pairs, which are two very closely spaced pulses of light that are recorded and used to produce a displacement map for a single time step.

The time displacement of the pulse pairs can be tuned to an expected amount of particle displacement and ideal interrogation window size. This allows for greater displacement measurement accuracy, but requires twice the data than single pulsed measurement. Single pulsed measurement uses the displacement between two single pulses at the output measurement frequency to derive displacement- therefore any tuning to the flow character changes the output measurement frequency. Single pulse does however allow for increased maximum length of measurement from halving the data required for each time step. Equally accurate measurements compared to dual-pulse are possible but measurement frequency needs to be carefully tuned to the range of probable instantaneous velocities.

3.3 General Advantages and Limitations

As stated, the principal advantage of PIV is whole flow field velocity measurement. This can be obtained across a wide range of measurement frequencies (e.g. 1-10-100-1000 Hz available) with a dynamic velocity range typically of 1:200 (Adrian 1997). PIV velocity accuracy ranges from 0.2%-2% of flow field of view size (e.g. +/- 0.08 mm s⁻¹, Hardy et al 2011). Although this is less good than LDA and LDV velocity measurements (e.g. ~0.002% of velocity range, Dantec 2014) it is still adequate for higher order statistical analysis such as vorticity (e.g. Chakraborty *et al.* 2005). Direct comparison between PIV and single point laser measurement's (LDA/LDV) is cumbersome as PIV accuracy scales with field of view size and LDA/LDV's accuracy scales with velocity range. It is certainly possible to obtain LDA/LDV accuracy measurements with PIV, but this may require small fields of view and/or very high resolution and low noise cameras.

Measurements can be made at high spatial resolution up to a μm scale, however there is usually a trade-off between spatial resolution and the size of the field of

view. This can be somewhat mediated if only mean flow measurements are needed- thus allowing for sections of a larger field of view to be measured individually then stitched together.

Flumes with transparent walls can be used to provide near-intrusion free measurement of the whole flow field. However, the addition of particle seeding, cameras, laser optics and flow stabilisers to the flow does reduce how unaffected the flow measurements are.

PIV can be used at microscopic scales (endoscopic PIV, e.g. Blois *et al.* 2014) up to 10's of meters (Large Scale PIV, e.g. Muste *et al.* 2008). Maximum measurement period is a combination of the amount of computer RAM, size of each digital image, number of images captured per second and the available on board camera memory. Typical measurement times are less than 10 minutes, occupying the Macro and Meso scales of velocity spectrum (Buffin-Bélanger & Roy 2005; Marquis & Roy 2011). The length of time that the laser can be operating may also be a factor as well as any potential experimental sensitivity to temperature change produced from the laser light.

Although lower-grade and cheaper systems are becoming available, PIV is usually very expensive. The high power class 4 Nd:YAG lasers often require extensive safety protocols and user training. The construction and setup of a PIV system is often very time-consuming with low tolerance for error. If flow around objects needs to be measured it should be noted that reflections can reduce data quality. Flow around transparent objects can be measured, however if the object's refractive index is not matched to the fluids' then the laser light will refract and illuminate out-of-plane areas. If the object is not transparent, flow down-view of the laser will not be illuminated.

Types of PIV Data Collection

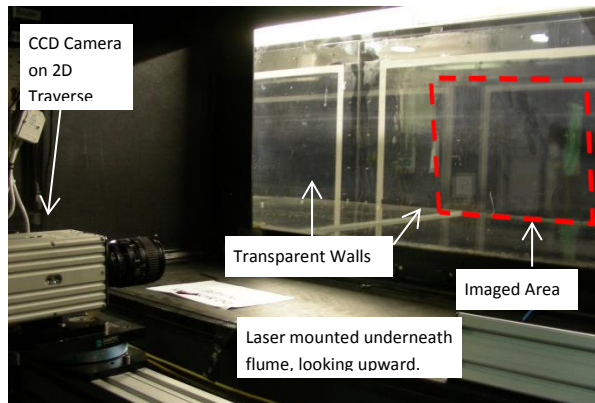


Figure 3-5. (above) example of 2D-PIV in a recirculating flume. Here the laser case and optics are outside the flume. A transparent flume floor and walls facilitate illumination and image capture. Image credit, C.A. Unsworth.

Standard 2D PIV produces vectors in two dimensions co-planer to the light sheet (e.g. Figure 3-2, 3-3, & 3-5) (Willert & Gharib 1991; Adrian 1997; Westerweel 1997). Stereoscopic PIV utilises two cameras positioned off-axis to a single light sheet whilst viewing the same area to produce depth of field (Wheatstone 1838; Arroyo & Greated 1991; Prasad & Adrian 1993; Soloff *et al.* 1997; Prasad 2000). This overcomes one of the main shortfalls of 2D PIV- the inability to simultaneously resolve all three components of velocity in a field of view. An especially significant drawback as turbulence is inherently three-dimensional (Gioia *et al.* 2010) and that geomorphological flows can produce strong flow three-dimensionality, e.g. river meanders (Bagnold 1960; Dietrich *et al.* 1979; Ferguson *et al.* 2003; Blanckaert 2011), bedforms (Maddux *et al.* 2003; Parsons *et al.*, 2005; Venditti 2007; Omid & Piomelli 2013) and at confluences and around bars (Best & Roy 1991; Biron *et al.* 1996; Fujita *et al.* 1998; Lane *et al.* 1998).

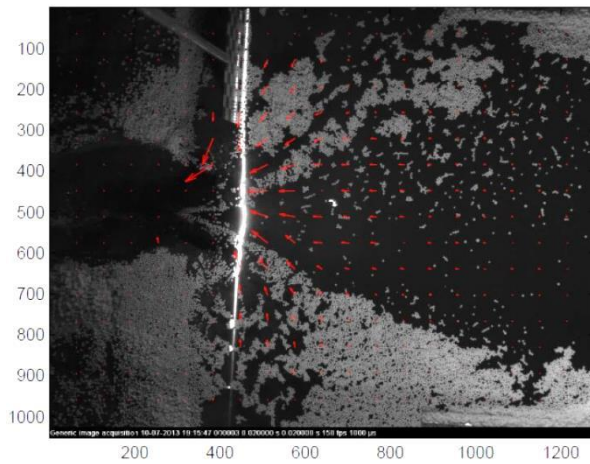


Figure 3-6. (above) example of Large Scale Surface PIV, with calculated vectors superimposed in red. From (Amaral et al. 2014).

Large Scale PIV (LS-PIV, Figure 3-6) differs from traditional PIV namely in scale and the cameras oblique angle to the measurement surface. Therefore images need to be orthorectified before image interrogation (Jodeau *et al.* 2008). Flow tracers also differ as they are required to float and have higher reflectance than laboratory scale PIV as the tracers are commonly illuminated by the sun or overhead lamps. Care is also needed to reduce glare from the water surface. LS-PIV has been used to measure flow discharge (Creutin *et al.* 2003; Jodeau *et al.* 2008; Muste *et al.* 2008) water movement in floodplains and around river engineering structures (Fujita *et al.* 1998).

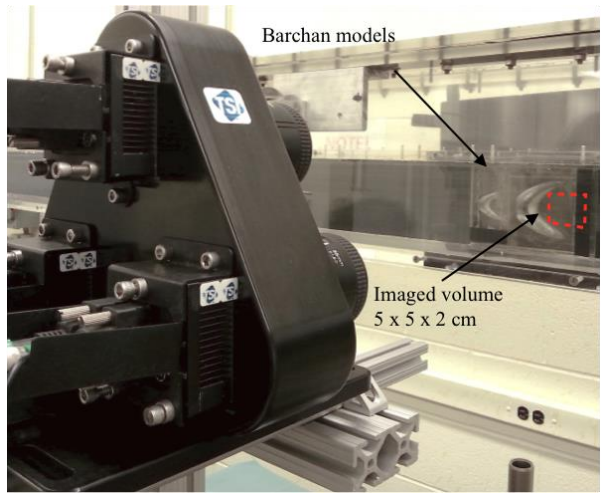


Figure 3-7. (above) example of a Volumetric PIV setup from TSI ©. This is a 3 camera system. Image credit, Gianluca Blois.

Volumetric (4D-PIV, Figure 3-7) velocity fields can be collected using Tomographic PIV (multiple camera) or holographic (infinite focal length camera) PIV methods. These techniques have been successfully used to measure

4D velocity fields in small volumes where distances between interrogation window measurement volumes are small enough that 3D cross correlation is possible (Barnhart *et al.* 1994; Elsinga *et al.* 2006; Kitzhofer *et al.* 2011; Schröder *et al.* 2011). Therefore the technique has generally been applied in micro-PIV studies (Malkiel 2003; Sheng *et al.* 2008). Recent advances in plenoptic (light field) cameras are allowing volumetric measurement in larger volumes- but with exponentially higher processing times (Fahringer & Thurow 2012; Lynch *et al.* 2012). In Geomorphology, volumetric flow measurement has recently been used to measure CFS over Barhcan dunes (Blois *et al.* 2012).

3.4 Assessment of Data Collection Parameters

Prior to collection of the desired flow data, an assessment of the capability of the PIV system and the data required to meet the needs of the researchers and their aims should to be performed. There are some practical trade-offs that need to be accounted for (See Chapter 10 in Adrian & Westerweel, 2011 for an extensive review of PIV set-up guidelines):

Field of view size: In general, a larger field of view will reduce the spatial resolution of vectors by increasing the area that each camera pixel is measuring. This can be somewhat mediated by camera resolution and lens type but this may be costly if new equipment needs to be purchased.

- Seeding: Seeding needs to follow the flow with minimal lag and slip whilst reflecting enough light to be visible. (See chapter 2 in Adrian & Westerweel 2011). There is a need for adequate seeding of the flow for the spatial resolution required. A minimum of 7 particles per interrogation area is recommended when using cross-correlation (Keane & Adrian 1992). Conversely, particularly high quantities of seeding may affect light intensity further away from the light source due to obscuration.
- Obstructions to the field of view: Unless the object under interrogation is transparent and the same reflective index as the fluid medium then flow

“downstream” of the light source will be darkened/obscured, curtailing measurements.

- Spatial resolution of vectors: This should be known prior to entering the lab. If the data is required to validate a model then vector grid size should ideally smaller than the numerical model grid (Hardy *et al.* 2005). High spatial resolution may require a reduction in field of view and scale of experiment, which may alter the scaling that can influence the experimental results (Peakall *et al.* 1996).
- Range of probable particle displacements: A known flow velocity is recommended so as to define sample rate, interrogation window size and overlap. The particle displacement between images-pulse pairs needs to be both large enough to be detectable but smaller than the interrogation region size possible. This can be mediated slightly with variable interrogation sizes and overlaps. This should also guide whether single or double pulse measured is used.

3.5 Data Quality & Post Processing

There are several common steps that are taken to improve data quality and are commonly available in PIV capture and processing software packages. The primary objective of pre-processing the images is to increase the signal to noise ratio in the FFT calculation. Some suggestions are: removing the mean intensity from each frame; Applying a high-pass filter to the images. Manipulate the image interrogation regions by applying a Gaussian filter. Use an interrogation area overlap, dependent on particle displacement length and interrogation grid size. A signal to noise ratio floor of 1.2 is very common and can be used to prevent vector calculation in poorly seeded/illuminated regions (Keane & Adrian 1992).

Post-processing of the calculated velocity vectors is essential as incorrect vector calculation from loss of pairs, phantom particles; poor seeding concentration will all produce spurious vectors. A known upper velocity magnitude limit based upon mean flow conditions can be used to remove obviously incorrect vectors.

Several vector outlier detection methods have been produced, of which the 2D median filter (Westerweel & Scarano 2005) is the most highly cited.

After the removal of poor vectors (quantity of which should be recorded as a gauge of data quality) there is the option of interpolating replacement vectors, of which there are many methods. These methods generally use the surrounding vectors to linearly interpolate replacement vectors (e.g. Garcia 2011). Some authors prefer not to interpolate vectors as the values of the interpolated values may not reflect the real fluid flow, particularly if there is strong rotation (e.g. Hardy *et al.* 2005).

High Cost Systems

High cost systems are usually based in well-funded laboratories and offer particularly high accuracy, precision and resolution as well as setup and collection experience. High cost PIV setups are generally purchased as an entire system (lasers and optics, camera (s), computers (s) and processing software) and often cost in the order of £100,000's. PIV systems can be purchased from companies such as Dantec©, TSI© and LaVision©, among others. Usually, additional equipment is required, such as a traverse and controller system and laser light shielding for safety. Software packages tend to provide support for acquisition and processing, with a large range of processing options available that can; filter/improve image quality, perform a wide range of PIV interrogation techniques, vector filtering and interpolation and even higher order statistical analysis like Proper Orthogonal Decomposition (Berkooz *et al.* 1993).

Low cost Systems

There is an established and growing low cost option than can offer very reasonable capabilities. These systems tend to be more “home-made” and use strobe lighting instead of lasers and general SLR-type cameras to reduce costs. Continuous lasers are also used, reducing the complexity of equipment (e.g. Aleixo, *et al.* 2012). Moreover, zero cost open access software is available, e.g. the free Matlab PIV toolbox (Thielicke 2014) for data collection and processing. Depending on the requirements of the research, a low cost option may have the capability to produce the desired dataset (e.g. Ryerson & Schwenk 2012) - but

Careful planning is certainly required. One advantage is that test runs can be performed at very low cost to establish the feasibility of a project.

3.6 Examples of PIV in Geomorphological Research

PIV tends to be used in Geomorphological research to measure CFS as well as general boundary conditions (mean velocities). In the section below, several papers that have used PIV and PIV based image interrogation are quickly summarized, and highlight how the application of PIV facilitated the authors' efforts to advance their subject.

Gravel beds

The particularly high bed roughness and irregularity of gravel beds, alongside their relatively shallow submergence in many environments exerts a significant control on the structure of fluid flowing over such beds (Wiberg & Smith 1991; Dinehart 1992, Cooper & Tait, 2010). Yet the understanding of the origin of macro turbulent CFS in gravel bed rivers had not been quantitatively measured until Hardy et al (2009, 2010a) used laboratory 2D PIV to capture the origin, scale and development of gravel clast produced CFS. The PIV data was used to produce mean flow, turbulence production, Reynolds Stress and Quadrant event statistics (Rao *et al.* 1971; Lu & Willmarth 1973; Bogard & Tiederman 1986; Nelson *et al.* 1993), with primary frequencies of eddy motion calculated via wavelet analysis (e.g. Torrence & Compo 1998). Hardy et al (2009) found that at a low Reynolds number near bed exerted a strong control on the outer flow via these near bed generated flow structures. With higher Reynolds numbers the length flow separation behind gravel clasts increased and the separated flow regions actually merged to form a layer of skimming flow over the bed (Hardy *et al.* 2009).

It has been observed that sediment entrainment in gravel beds occurs in patches rather than a continuum (Drake *et al.* 1988). Hardy et al (2010a) showed how the scale of bed roughness controlled the formation and character of macro-turbulent CFS. Indicating that large-scale CFS controlling these entrainment patches originate from bed generated turbulence and that outer flow layer flow structures are the result of flow topography interactions in the near bed region (Hardy *et al.* 2010a).

Channel shape

River meanders produce complex flow features, such as strong secondary circulation and flow separation (Jackson 1975; Bridge & Jarvis 1977; Ferguson *et al.* 2003; Seminara 2010; Blanckaert 2011; Dietrich *et al.* 1979; Zinger *et al.* 2013; Hooke 1975). Whilst the significance of flow separation in meanders had been noted for some time (Ferguson *et al.* 2003), the flow and channel shape controls on the occurrence of flow separation were ambiguous. Blanckaert *et al.* (2013) define some the formative conditions for flow separation in meanders via the use of 3D PIV and LS-PIV to measure surface velocity and thus identify locations of flow separation in a flume facility. The LS-PIV velocity measurements were calculated using a version of “SuperPIV” whereby PIV cross-correlation calculated velocity and direction in a grid- aiding a particle tracking algorithm which produced velocity vectors per particle. The result was then interpolated onto a grid producing average flow velocity across the meander bends (Blanckaert *et al.* 2013).

The stereoscopic PIV system used facilitated non-intrusive measurement of the three components of velocity in the highly three-dimensional flow structure of an idealised sharp meander bend. This was particularly useful in revealing locations of flow stagnation, local (shear) and global (secondary flow) rotation, and the location of impinging flow both in a flat bed and with an immobile bed. In combining these PIV techniques the authors were able to reveal some of the formative conditions for flow separation in meander bends that had previously been inferred.

Surface manifestation of coherent flow structures

Water flows over rough beds are often perturbed by upwelling fluid which often contains more suspended sediment than the surrounding flow (Matthes 1947; Coleman 1969; Jackson 1976; Lapointe 1992; Kostaschuk & Church 1993; Best 2005). These structures are generated at the rough bed boundary and mix fluid across the entire water depth (Muller & Gyr 1986; Best 2005; Kadota & Nezu 1999). Whilst qualitative description of boil types has been made (Babakaiff & Hickin 1996) it has been very difficult to quantitatively measure their size, shape and velocity.

Talke *et al.* (2013) used PIV algorithms on Infer-Red (IR) camera data of these upwelling boils in a tidal river. Temperature difference between a cooler surface and warmer sub-surface waters from the ebb tide that were upwelling were used to differentiate between normal flow and boils and facilitated a contrast that could be measured with PIV image interrogation (see Chickadel *et al.* 2011). Talke *et al.* (2013) were able to successfully measure the rate of Turbulent Kinetic Energy production and dissipation at the water surface and compare it to the rates of TKE production beneath and link this to the existence, size and intensity of boils to the unbalanced TKE budget. Best *et al.* (2010) used a similar technique on the acoustic backscatter from a multibeam sonar to identify and measure CFS under water in the Mississippi River (Best *et al.* 2010).

Other geomorphological areas that have utilised PIV include: Tracking sediment movement (Coleman & Nikora 2009), and Numerical Model Validation (Hardy *et al.* 2005). Recent advances in PIV have involved measurement of flow around vegetation (Cameron *et al.* 2013; Yager & Schmeeckle, 2013; Okamoto & Nezu 2013), volumetric measurements of turbulence over river bedforms (Blois *et al.* 2012), endoscopic measurement of hyporheic flow (Blois *et al.* 2014), and coupled measurements of flow and sediment transport (e.g. Amir *et al.* 2014, Schmeeckle 2014). Additionally, LS-PIV from fixed or mobile (UAV) positions has been developed in the past 5 years and facilitates measurement of velocities over very large areas (Coz *et al.*, 2014), around engineered structures (Jodeau *et al.*, 2008) and surface velocities (Chickadel *et al.*, 2011).

3.7 Summary

PIV is one of the least intrusive methods of measuring flow fields. Using PIV can be expensive, time consuming and complicated but it has the ability to provide velocity measurement across a range of geomorphological scales, even volumetrically, with accuracy sufficient to determine higher order statistical analysis. It is able to reveal temporal linkages in fluid motion on a scale from micrometres to meters, nanoseconds to minutes. It is an incredibly powerful research tool that has been- and continues to be- revolutionary in nearly every subject it used, including geomorphology.

Flow Structures over Fixed 2D Bedforms in Transient States

Abstract.

Flow processes measured in the laboratory over fixed, 2D or 3D bedforms have mostly been conducted at one flow depth and with bedform dimensions set by scaling laws based upon equilibrium flow conditions. These results thus have limited applicability to many natural situations where bedforms and flow fields are co-evolving at different rates in response to transient conditions, such as changes in flow depth and flow discharge associated with a flood. The research presented herein investigates flow processes over 2D fixed bedforms under a range of non-equilibrium, transient, states in order to quantify the spatial-temporal changes in turbulence associated with steady conditions that are set at non-equilibrium depths and velocities. Flow field information was obtained at steady states for a range of flow depths and mean flow velocities, mimicking conditions during the transient evolution of flow and bedforms during a flood wave. This procedure allowed quantification of flow fields over bedforms under transient boundary conditions, including shear stress profiles and the spatial variation in the dynamics of the separation zone. These findings provide data for a preliminary assessment of the link between sediment transport lag and transient flow dynamics, and facilitate an analysis of the implications of variable dune height: flow depth for flood wave propagation and bedform response.

4.1 Introduction

Dunes often produce the highest amount of bedform roughness to river flow and dynamically change their shape and roughness to the bed shear stress applied (Einstein & Barbarossa 1952; Simons & Richardson 1962, 1966; Prent & Hickin 2001; Wilbers 2004; Aberle *et al.* 2010; Paarlberg *et al.* 2010; Lefebvre *et al.* 2011). The successful prediction of dune size is important for 1: river stage prediction during floods when bedform size changes considerably (Kuhnle 1992; Gabel 1993; Julien & Klasssen 1995; Amsler & Garcia 1997; Fedele & Garcia 2001; Shimizu *et al.* 2009; Chen *et al.* 2012), 2: prediction of drought depth for

river navigation (Engelund & Fredsoe 1982; Wilbers & Ten Brinke 2003; Wilbers 2004; Paarlberg *et al.* 2010), 3: Prediction of dune migration rate and size is important in the costing of dredging (Dorst *et al.* 2013), and 4: accurate prediction of the scour depth of the dunes is important; as significant bedform scour can erode the foundations of sub-fluvial infrastructure such as tunnels (Amsler & Garcia 1997) or sub-marine infrastructure such as wind turbine bases and cables (Bolle *et al.* 2013).

To better understand the mechanics of dunes, their equilibrium flow structures have been extensively measured in laboratory conditions and there is a general agreement on the nature of the flow field over idealized 2D dune forms (Nelson & Smith 1989; Nelson *et al.* 1993; McLean *et al.* 1994; Bennett & Best 1995; Kadota & Nezu 1999; McLean *et al.* 1999a; Fedele & Garcia 2001; Best 2005b). Best 2005a summarized the recent research and produced the conceptual diagram (below) of the main flow features over equilibrium laboratory 2D dunes.

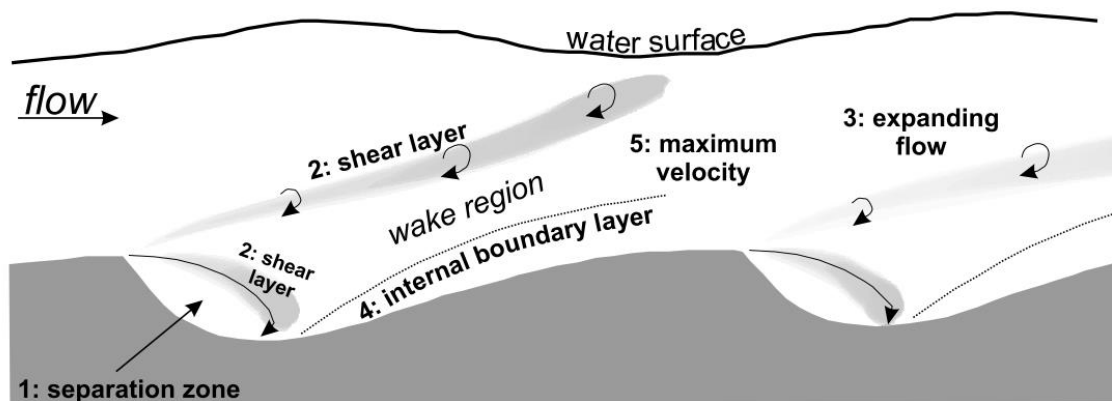


Figure 4-1: Conceptual diagram of flow over equilibrium dunes.

(1) Flow separation in the lee of the dune, with reattachment occurring approximately 4–6 dune heights downstream of the crest. (2) A shear layer is generated bounding the separation zone, large-scale turbulence is generated in the form of Kelvin-Helmholtz instabilities along this shear layer, and as the free shear expands, it creates a wake zone that grows and dissipates downstream. (3) A third region is one of expanding flow in the dune leeside. (4) Downstream of the region of reattachment, a new internal boundary layer grows as flow re-establishes itself and develops a more logarithmic velocity profile. (5) Maximum horizontal velocity occurs over the dune crest (From Best 2005).

Mean velocity at a dune crest is often the best developed, as the turbulent wake from the preceding dune has had the most time to merge with the developing internal boundary layer (Nelson *et al.* 1993; Nezu & Nakagawa 1993 (Figure 4-1, points 4&5). The mean profile at bedform crests are therefore often most similar to those from classical well-developed boundary layers and, for this reason, it

has been suggested that estimates of bed shear stress over dune bedforms should use the mean profile near the crest (McLean *et al.*, 1999b). Vertical profiles at dune troughs show the highest gradients and thus highest levels of turbulence production across dunes (Nelson *et al.*, 1993), with the bedform shape having a strong control over the flow structure (Kadota & Nezu 1999).

Flow reattachment is a critical zone on the development of flow over dunes (Engelund & Fredsoe 1982; Ruderich & Fernholz 1986; McLean 1990; Bennett & Best 1995). Turbulent eddies shed from the upstream shear layer hit the bed at the flow reattachment point ~four to six dune heights downstream of the crest (Engel 1981 Engelund & Fredsoe 1982; Bennett & Best 1995). These turbulent events quickly alter the magnitude and direction of bed shear stress, promoting sediment transport as bedload (Keylock *et al.* 2014) and sediment suspension events (Kuhnle & Wren 2009) for different sequences and direction of turbulent events. Sediment that falls onto the lee slope and sediment that is deposited within the flow recirculation region is used in the migration of the dune downstream (Naqshband *et al.* 2014a). Therefore, any variation in the sediment input into this region will affect the migration rate of bedforms, and also potentially influence the shape. Kostaschuk & Villard (1996) and Best & Kostaschuk (2002) demonstrate that high levels of suspended sediment reduce the intensity of flow separation over dunes, altering their lee slopes into low angle slopes ($\sim 12^\circ$) rather than angle of repose ($\sim 30^\circ$) lee slopes. The maintenance of the lee slope and spatial sediment transport hysteresis is therefore crucial in the formation and maintenance of dunes themselves (Yalin, 1977; Fredsøe, 1982; Bennett & Best, 1996; Bennett, *et al.* 1998; Best & Kostaschuk, 2002; Coleman & Nikora, 2009).

The standard model of the structure of flow over dunes was measured at a statistical equilibrium condition whereby depth and depth averaged velocity at successive fixed dune crests is constant. McLean *et al.* (1994) highlight how important it is to measure shear stress profiles at this condition, but they also describe how difficult it is to achieve such a condition in the laboratory, an approach taken in successive studies (e.g. Bennet & Best 1995). This issue highlights how narrow a window of flow conditions over dunes has been measured in previous research.

It is apparent that natural rivers rarely reach such a flow-morphology equilibrium condition due to constant changes in fluid discharge (Aberle *et al.* 2010). This instability commonly results in a flow-morphology hysteresis due to the relatively slower adjustment of bedform morphology in contrast to the change in flow depth and/or mean velocity (Allen 1978; Gabel 1993; Julien & Klasssen 1995; Amsler & Garcia 1997; Wilbers & Ten Brinke 2003; Aberle *et al.* 2010; Martin & Jerolmack 2013). The quantification of turbulent flow fields over dunes that are scaled to a *non-flow-morphology* equilibrium condition based upon empirical scaling (Guy *et al.*, 1966; Allen 1982) is of primary importance if we are to improve our understanding of dune morphological responses and flow resistance changes in river during unsteady flow conditions (Julien & Klasssen 1995; Paarlberg *et al.* 2010; Nelson *et al.* 2011).

The response of mobile dunes in rivers to these transient conditions can be manifested in four main categories that are defined by the four possible alterations in the components of flow 1: Increase in mean velocity produces greater bed shear stress and faster migration rate of dunes (Nelson *et al.*, 2011), 2: Decrease in mean velocity produces lower bed shear stress and slower dunes, 3: Higher depth induces amalgamation processes to increase dune height and length, whilst reducing overall number of bedforms (Carling *et al.* 2000a,b; Nelson *et al.* 2011; Martin & Jerolmack 2013; Warmink *et al.* 2014), 4: Lower depth induces calving/splitting process to increase dune population size whilst reducing the mean height and length of the dunes (Carling *et al.* 2000a,b; Nelson *et al.* 2011; Martin & Jerolmack 2013; Warmink *et al.* 2014). Realistically, these four components of discharge will almost never change independently (Simons & Richardson 1962). Flood pulses contain rising and lowering legs where depth and mean velocity concurrently increase and then decrease through time (at one location along a river). In extreme cases this can change the bed state of a river from ripples, to dunes and to an upper stage plane bed and back again through a flood pulse (Shimizu *et al.* 2009). Detailed experiments on the ripple to dune transition (Bennett & Best 1996; Schindler & Robert 2005; Fernandez *et al.* 2006) and the transition of dunes to upper stage plane bed (Bennett *et al.* 1998) clearly shows that the location and intensity of turbulence changes dramatically compared with the dune flow model of Best (2005a) (Figure 4-1). Currently little is known about the role of mean flow

structure and turbulence with transient conditions within the dune regime, yet the quantification of such flow-form interactions is vital to understand the unsteady dynamics and mutual adjustments that occur in natural flows.

Calculation of the bed shear stress and sediment transport rates over bedforms from experiments and field data is difficult, and using the traditional depth-slope product yields sediment transport predictions that can have significant error even for steady discharge at a flow-morphology equilibrium (see McLean *et al.*, 1994, Nelson *et al.*, 1995; Maddeux *et al.*, 2003a,b; McLean *et al.*, 1999b). This problem exists because the constant flow separation and wake disrupts the development of a fully-developed boundary layer over the stoss slope of a dune, introducing error into log-law, law of the wall, relationships (McLean *et al.* 1999a,b). These approaches are likely to be even less accurate for flows out of flow-morphology equilibrium as the re-distribution of flow momentum will change the shape of the mean velocity profiles.

Many experimental studies have used fixed bedforms to reduce complexity and the number of uncontrolled variables (e.g. Best 2005b; Fernandez *et al.*, 2006). The advantage of this technique is that it demonstrates how strongly the bedform geometry controls shear layer height and reattachment length (Engel 1981), and highlights how the stoss flow is less controlled by geometry and more controlled by interaction with the free surface (McLean *et al.* 1994). Free surface interaction manifests itself through enhanced topographic acceleration of the flow along the stoss slope of dunes downstream of flow reattachment, though 1) converging flow, and 2) dissipation of turbulence and transfer of momentum with downstream velocity (Nelson *et al.* 1993; McLean *et al.* 1994). Importantly, Nelson *et al.*, (1993) demonstrate that although the effect itself is reasonably weak (when compared to the shear layer), its effect and importance on the stability of dunes is much greater. Notably, the reattachment length has been shown to reduce with greater topographic acceleration changing the distribution of high and low pressure areas on the stoss of dunes (Engel 1981). The structure of the internal boundary layer and turbulent wake, which defines sediment transport over the dunes stoss, is dependent on the amount of topographic acceleration induced through flow convergence, turbulent dissipation, and the

Reynolds number (Nelson & Smith 1989; Nelson *et al.* 1993; McLean *et al.* 1994).

This research investigates how the mean turbulent structures over fixed, idealised, 2D dunes change with varying Reynolds number (through variations in flow depth and depth averaged flow speed at the dune crest) and will demonstrate how the formation and stability of dunes occurs. Whilst simultaneously demonstrating the influence of flow structure shape on dune stability in the more practical terms of depth and mean flow velocity.

4.2 Methods

4.2.1 Flume setup and experimental conditions

A large recirculating flume that had dimensions 1 m wide, 1 m deep, and 10 m long was used to conduct a series of detailed experiments on the flow structures over two-dimensional (straight crested) idealised dune forms. Three fixed dune forms, which were 80 mm high ($= D_H$) with an angle-of-repose lee face (~ 30 degrees), and a crest to crest wavelength of 0.995 m, were attached to the flume bed, (Figure 4-2). This high-angle type of dune is consistent with bedload dominated dunes rather than suspended load dominated dunes in nature (Kostaschuk & Villard, 1996; Best & Kostaschuk, 2002). A suite of experimental conditions were investigated using this set-up, where the depth and flow velocity were systematically changed over the same fixed bedforms. Herein, we present results from twelve conditions (Table 4-1). The flow depths measured were 280 mm for 3.5 dune heights (D_H), 240 mm for 3 D_H and 200 mm for 2.5 D_H as measured from the mean bed level (40 mm). The equilibrium depth of flow over dunes in laboratories is classically reported as 3 dune heights (Yalin 1964; Guy *et al.*, 1966; Allen 1982) and thus the study reported herein investigated conditions both above and below this depth. The reference, equilibrium, condition is M83 at 0.8 ms^{-1} and 240 mm depth.

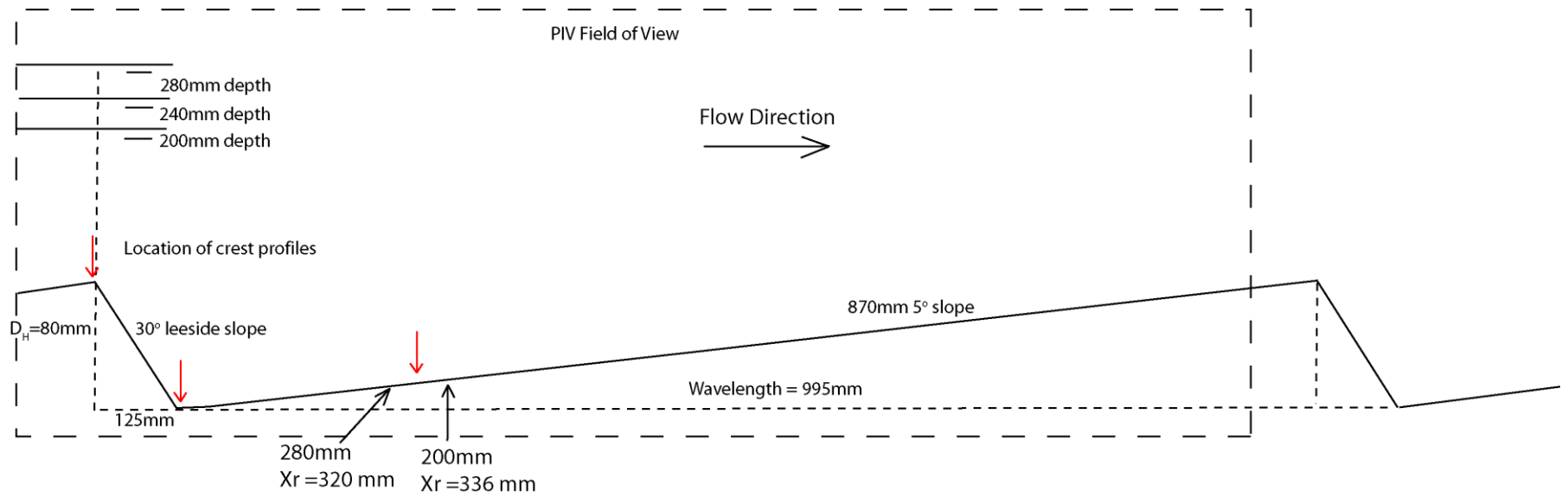


Figure 4-2: Scaled schematic of laboratory dunes. The PIV field of view (large dashes) is centred over the middle dune. Mean bed level is 40mm as the dunes are triangular. Red arrows indicate location of profiles shown in figures 4-5 & 4-6 X_r = reattachment length

Table 4-1: List of experimental conditions. No. =run number, Naming conventions- depths H=high (280mm) M=medium (240mm) L= low (200mm). D=average flow depth (m) above the mean bed level, \bar{U}_c & \bar{V}_c =depth-averaged mean downstream and vertical velocity at the crest, respectively (ms^{-1}), Fr=Froude number, Re=Reynolds Number, Q=discharge (m^3s^{-1})

No.	Name in text (Depth& Velocity)	Depth (mm) above mean bed level	\bar{U}_c (ms^{-1})	\bar{V}_c (ms^{-1}) crest	Fr	Re	Q (m^3s^{-1})	Temperature ($^{\circ}\text{C}$)	Reynolds Stress maximum
1	H14	280	0.14	0.0002	0.08	38842	0.038	19.4	0.3
2	H30	280	0.30	0.0081	0.18	83217	0.085	19.4	1.6
3	H61	280	0.61	0.0155	0.37	170347	0.17	19.4	6.2
4	H76	280	0.76	0.0108	0.46	213297	0.21	19.4	9.1
5	H92	280	0.92	0.0077	0.56	258427	0.25	19.4	16
6	M14	240	0.14	0.007	0.10	35041	0.035	19.7	0.28
7	M23	240	0.23	0.0079	0.15	55353	0.055	19.6	1
8	M83	240	0.83	0.0087	0.37	200359	0.20	19.6	8.2
9	L18	200	0.18	0.007	0.13	36826	0.037	19.4	0.45
10	L42	200	0.42	0.0106	0.30	84511	0.085	19.5	3.2
11	L62	200	0.62	0.0124	0.44	123892	0.12	19.5	6.3
12	L73	200	0.73	0.0099	0.53	147086	0.15	19.5	10

Detailed two-dimensional (streamwise (u) and vertical (v)) flow velocities were quantified for each condition using a Dantec™ 100 Hz Particle Imaging Velocimetry (PIV) system (see chapter 3). The laser was positioned so the field of view was along the centreline of the flume and centred on the mid-stoss of the second dune form. This set up illuminated the flow above the second dune over a horizontal distance of 1004 mm and a maximum height of 620 mm. The field of view for depths 240 & 200 mm is less (~ 10 mm) than the set flow depth; this is due to masking of the near surface flow to remove waves and unsteadiness from the PIV analysis. Movement of seeding particles was measured for 80 seconds per run, yielding an array of ~ 8000 two Mega Pixel images of the flow. The 80 second measurement time was long enough for mean flow statistics to converge to a statistically steady state (Buffin-Bélanger & Roy, 2005), and thus representative of the time averaged flow conditions. Image quality was improved by removing the mean run intensity image to remove constant reflections. To improve the signal to noise ratio, images were sharpened using a 3×3 high pass-filter. A signal to noise threshold of 7-1 was used to ensure that calculations in poorly seeded/illuminated areas did not occur. Flow vectors were calculated using an adaptive correlation algorithm (Theunissen et al, 2010) on a 32×32 pixel grid with a 75% overlap. One initial step at 64×64 pixel grid size was used to guide analysis. No sub-pixel refinement or deforming windows were used. This approach produced output interrogation grid cells of 8×8 pixels that were 6.4 mm^2 across the field of view, yielding 157 cells horizontally and 51, 36 & 27 pixels high for the three depths 280mm, 240mm and 200mm, respectively. Post-processing of the vector arrays used a 3×3 pixel median detection algorithm to locate and remove spurious vectors (Westerweel & Scarano 2005), with vectors replaced with the median (3×3) vector. Vector removal and interpolation changed an average of 1% of the vectors across all the runs. Particles moved no more than 6 pixels per timestep (or 4 ms^{-1}) which is less than 8 pixels limit defined from the 32×32 interrogation window and the $\frac{1}{4}$ rule (Adrian & Westerweel 2011). Therefore maximum particle displacement per interrogation window is $< 3.7\%$. Accuracy of velocities was therefore better than $\pm 0.001 \text{ ms}^{-1}$.

4.2.2 Analysis of turbulent flow statistics

Analysis of the 2D flow field vectors was performed using the conventional methods of calculating time average downstream velocity (\bar{U}) and time average vertical velocity (\bar{V}) for each pixel. Calculation of the Reynolds stress and Quadrant partitioning of the Reynolds stress followed Bennett & Best (1995). Thus, Reynolds stress was calculated as:

$$\tau_r = -\rho\bar{u}\bar{v} \quad (4.1)$$

$$-\bar{u}\bar{v} = \frac{1}{n}\sum_{i=1}^n(u_i - \bar{U})(v_i - \bar{V}) \quad (4.2)$$

Where τ_r = Reynolds Stress, ρ = the fluid density, $\bar{u}\bar{v}$ = the mean fluctuating components of velocity downstream and vertical respectively at each point. \bar{U} and \bar{V} are the time averaged velocities at each point, u_i and v_i are the instantaneous velocities t , and n is the number of observations.

Quadrant analysis was performed also using the methods outlined in Bennett & Best (1995) (cf. Lu & Willmarth, 1973; Bogard & Tiederman, 1986). Velocity fluctuations through time at each point were partitioned into four groups (or quadrants) dependent on their magnitude from the time average values at the same points, and above a user-set threshold. In this study a threshold value (hole size) of one standard deviation was used, others have used a hole size (H) of two, three or four to pick out larger magnitude events (c.f Bennett and Best 1995). The aim of this research was not to focus primarily on just the largest scale turbulent events but the mean values, so a value of one standard deviation ($H=1$) was chosen as this would contain a larger proportion of the turbulent events.

Figure 4-3 displays the four quadrants relative to the mean removed value (0,0). Quadrant 1 “outward” and 3 “inward” velocity fluctuations remove energy from turbulence and add to the mean flow, whilst quadrants 2 “ejection” and 4 “sweep” events describe velocity fluctuations that remove energy from the mean flow to produce turbulence. Q1 and 3 therefore reduce Reynolds stress and Q2 and 4 add to Reynolds Stress.

$$-\bar{u}\bar{v}_Q = \frac{1}{n} \sum_{i=1}^n S(u_i - \bar{U})(v_i - \bar{V}) \quad (4.3)$$

where a binary sorting factor S defines the quadrant type. The equation is repeated four times for each timestep and location:

S=1 for Quadrant 1 when $u_i > \bar{U}$ & $v_i > \bar{V}$,

S=1 for Quadrant 2 when $u_i < \bar{U}$ & $v_i > \bar{V}$,

S=1 for Quadrant 3 when $u_i < \bar{U}$ & $v_i < \bar{V}$, and

S=1 for Quadrant 4 when $u_i > \bar{U}$ & $v_i < \bar{V}$.

This situation pertains if $H=0$; when $H > 0$ then $S=1$ if $|uv| \geq H$ as well as matching the quadrant criteria above, otherwise $S=0$.

Quadrants are displayed as a percentage of the total time series that each point in time was within that quadrant. Increasing the hole size decreases the percentage as the threshold for $H \geq 0$ is raised.

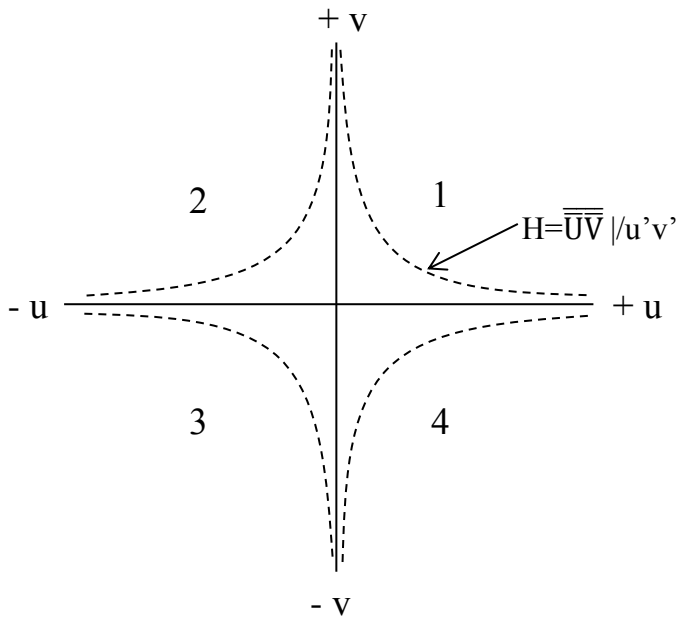


Figure 4-3: Diagram of Quadrant definitions. The two axis are centred at 0,0 (the mean value for \bar{U} and \bar{V}). Dashed lines represent the threshold for quadrant classification, instantaneous values outside (away from 0,0) the dashed lines are above the Hole size and therefore count toward the quadrant percentage.

In this study the bottom boundary is non-horizontal; therefore the mean streamline vector direction is not parallel to the bed; an assumption in traditional boundary layer research for which the technique was initially developed (Bogard & Tiederman 1986). Therefore the flow vectors were rotated

so that the resultant vector of \bar{U} was parallel to the mean streamline vector and \bar{V} at a right angle to the mean streamline for each vertical profile in the field of view. This adjustment produces a quadrant analysis that is more relevant to the flow itself, rather than the horizontal plane.

4.3. Results

4.3.1 Depth Averaged Velocities

The aim of these experiments was to measure the mean flow structure of dunes in non-equilibrium flow conditions; therefore flow depth was adjusted to above and below the equilibrium depth; and mean flow velocity was adjusted through a considerable range at each depth, rather than the one flow velocity used in most studies. The depth-averaged velocity over the crest for each condition is presented in Table 4-1. As the depth-averaged mean downstream velocity at the dune crest (\bar{U}_c) increases, the depth-averaged mean vertical velocity (\bar{V}_c) changes in a non-linear way (Figure 4-4). Initially, increases in \bar{U}_c depth averaged at the crest produces higher \bar{V}_c . The highest mean vertical velocity at the crest occurs at $\sim 0.60 \text{ms}^{-1} \bar{U}_c$ for both 280 mm and 200 mm depths, after which the increase in \bar{U}_c reduces the mean vertical velocity. Also notable is the near zero depth-averaged vertical velocity for condition H14 (280 mm, $0.14 \text{ms}^{-1} \bar{U}_c$).

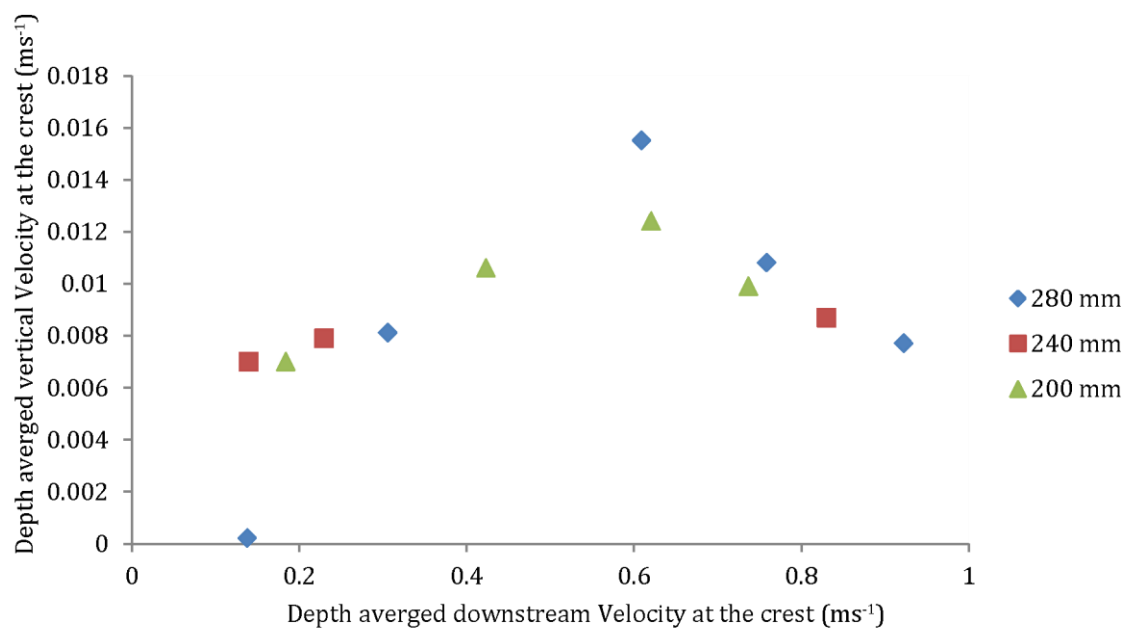


Figure 4-4. Depth-averaged velocities at the crest. The Figure illustrates a non-linear relationship between depth averaged vertical velocity with depth averaged downstream velocity at the dune crest for these transient conditions.

4.3.2 Mean flow velocity profiles

Profiles of the mean downstream component of velocity (\bar{U}) and the vertical component of velocity (\bar{V}) are compared in Figures 4-5 and 4-6 across all depths at the closest comparable \bar{U}_c condition. The positions along the dune of the streamwise (\bar{U}) and vertical (\bar{V}) profiles shown are shown in Figure 4-2. These results emphasise the relative changes in the profile shape and magnitude across the different flow depth conditions.

Crest Profiles

Across the different depth conditions there are significant changes in the shape of the mean time-averaged profiles at the crest. Figure 4-5A shows, for comparable depth-averaged velocities of the incoming flow that the absolute profile shape of downstream velocity (\bar{U}) changes considerably with flow depth. The deepest flow condition (H14) has the smallest gradient and maintains a classical two-step profile shape (McLean *et al.*, 1999b). The equilibrium depth condition (M14) has a considerable increase in mean velocity between the upper and lower flow sections (Around $2.5 D_H$), and the lower than equilibrium depth condition (L18) essentially has one high gradient slope to the profile.

The change in vertical velocity at comparable \bar{U} conditions across depths (Figure 4-5B) shows several important features; 1) that for all depths at this low \bar{U} condition the vertical velocity at the crest is always non-negative; 2) for H14, there is very little gradient in vertical velocity; 3) the equilibrium depth profile (M14) has both the highest gradient and highest magnitude of vertical velocity, and that; 4) reducing the depth further, to the lowest depth condition (L18), produces similar patterns in the vertical velocity profile but at a smaller magnitude than for the equilibrium (M14) condition.

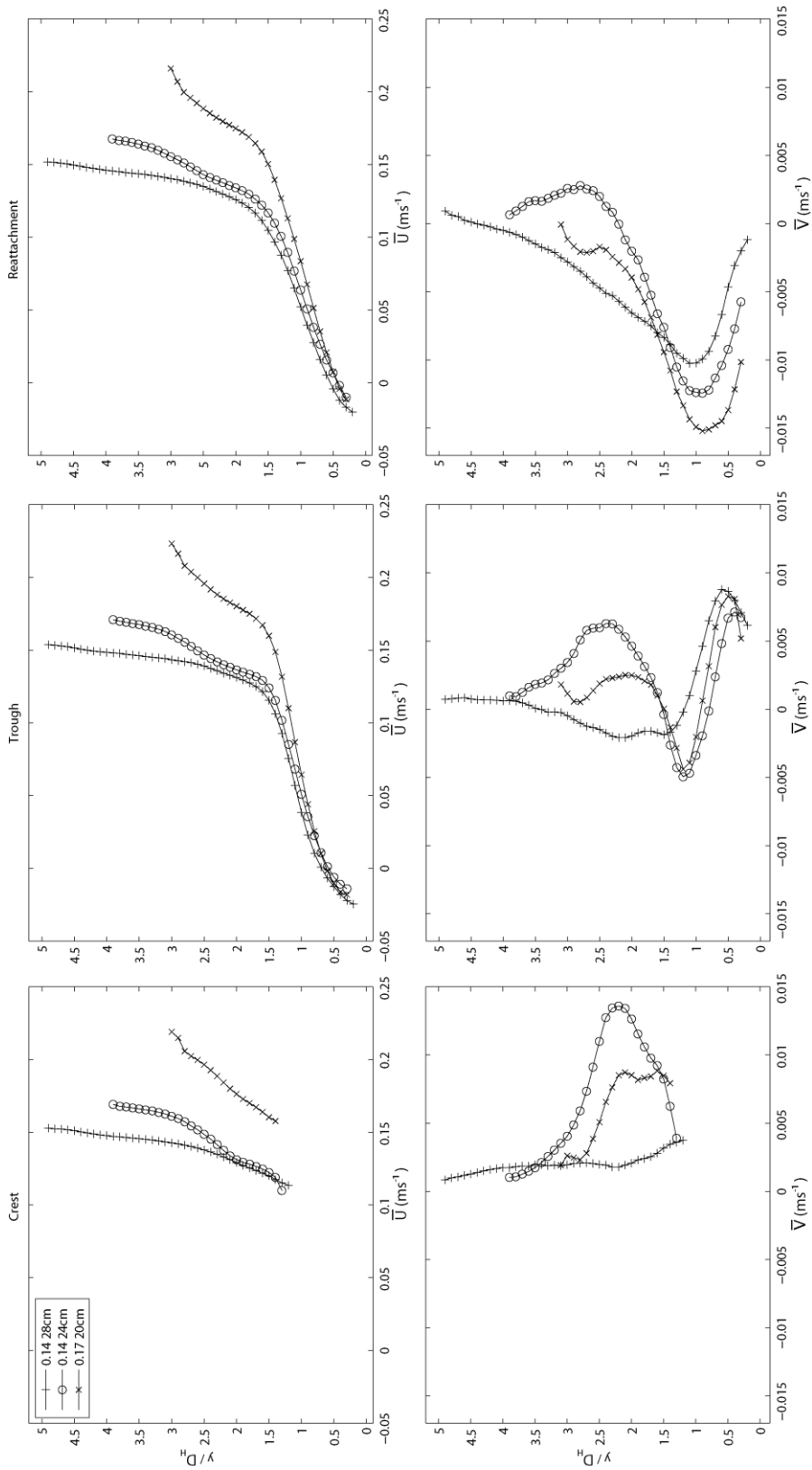


Figure 4-5: Time-averaged velocity profiles of streamwise velocity component \bar{U} (top panels) and vertical component \bar{V} (bottom panels) for conditions H14, M14 & L17. Left panels = profiles at crest; Middle panels = profiles at trough; Right panels = profiles at near reattachment. + = H14, o = M14, x = L17. Y axis = normalised profile height where 1 = the dune crest. X axis is the velocity magnitude in ms⁻¹. The Figure shows variations in profile shape with changes in depth with comparable depth averaged flow velocities and illustrates the significance of flow depth on the mean velocity profile shapes.

Interestingly, at the higher \bar{U}_c conditions (Figure 4-6B) the vertical velocity does become negative for sections of each profile. The switch from positive to negative occurs at a higher relative location in the profile with increasing flow depth; with the vertical velocity direction for the 200 mm condition switching at $2D_H$, 240 mm at $2.5D_H$ and for the 280 mm depth condition at $4D_H$. The increase in \bar{U}_c of $\sim 0.62 \text{ ms}^{-1}$ between Figure 4-6AB and Figure 4-6AB has also changed the mean downstream velocity profile at the crest. The equilibrium (240 mm) flow depths' profile changes from a log-linear profile shape at the lower \bar{U}_c condition (Figure 4- 5A) to a single, high, gradient profile at the higher \bar{U}_c condition (Figure 4-6A). This change in shape with higher \bar{U} is replicated at the lower than equilibrium (200 mm) condition. The low gradient free (or outer) flow seen in the upper profiles in Figure 4-5A is much less clear at higher \bar{U}_c and lower depth. The highest flow depth run in Figure 4-5A maintains its log-linear profile shape at the higher high \bar{U}_c condition.

Trough profiles

Figure 4-5, C&D shows the mean downstream and vertical velocity profiles at the trough, respectively. The shear layer produced from flow separation at the dune crest can be seen as a distinct kink in the downstream and vertical velocity profiles at $\sim 1.4D_H$. At all depths, there is a strong consistency in the mean downstream and vertical profiles' profile shape through the re-circulating flow and shear layer. Above this kink the profiles diverge toward the free surface in similar patterns seen at the crest (Figure 4-5, A&B), but with some key differences. For condition H14, the vertical velocity at the trough (Figure 4-5D) above the shear layer ($>1.4D_H$) is negative for a substantial portion of the profile. Whilst at lower depths for comparable \bar{U} the vertical velocity in the same section is positive (Figure 4-5D). Importantly, this outcome is maintained at the higher \bar{U} conditions (Figure 4-6D). The reduction in depth from the 280 mm condition H76 to M83 produces an alteration in the location of the change from negative to positive vertical velocity, which happens at $3D_H$ for 280 mm, $2.5D_H$ for 240 mm, and $1.5 D_H$ (vertical) for 200 mm.

Reattachment Profiles

Figure 4-5EF and 4-5EF plot the \bar{U} and \bar{V} velocity profiles around reattachment. The horizontal location of the profiles is a distance of $4 D_H$ downstream from

the crest. The average reattachment length across all conditions is $4.15 D_H$ downstream of the crest, (Table 4-2) therefore the profiles in Figures 4-5 & 4-6 E&F are slightly upstream of the mean reattachment point, so as to show the changes in recirculation magnitude and location in the vertical profiles.

For all sets of upstream flow velocities the downstream velocity is negative $\sim 0.5 D_H$'s above the bed, whilst the flow is downwelling for $2 - 4.5 D_H$ above the bed across all conditions shown in Figures 4-5 & 4-6 E&F. The vertical flow direction near the bed at reattachment is strongly negative across all depths (Figures 4-5F & 6F). Vertical velocity near the bed at the lower \bar{U}_c conditions (Figure 4-5F) shows a consistent pattern of increasing negative values with less depth. A reverse pattern occurs at the faster \bar{U}_c conditions (Figure 4-6F). Despite this, the shear layer height remains the same (around $1 D_H$ Figures 4-5F & 4-6F) across depths, showing that the bedform geometry has the strongest control on recirculation zone height, but the difference in vertical location and relative magnitude of upwelling and downwelling above the shear layer is controlled by a combination of depth and \bar{U}_c .

The increase in \bar{U} at each depth has substantially changed the location above the shear layer ($>1 D_H$ vertical axis) where the flow begins to upwell (Figure 4-5F & 4-6F), with upwelling starting $\sim 0.5-1 D_H$ closer to the bed at the higher \bar{U}_c conditions between the three depths.

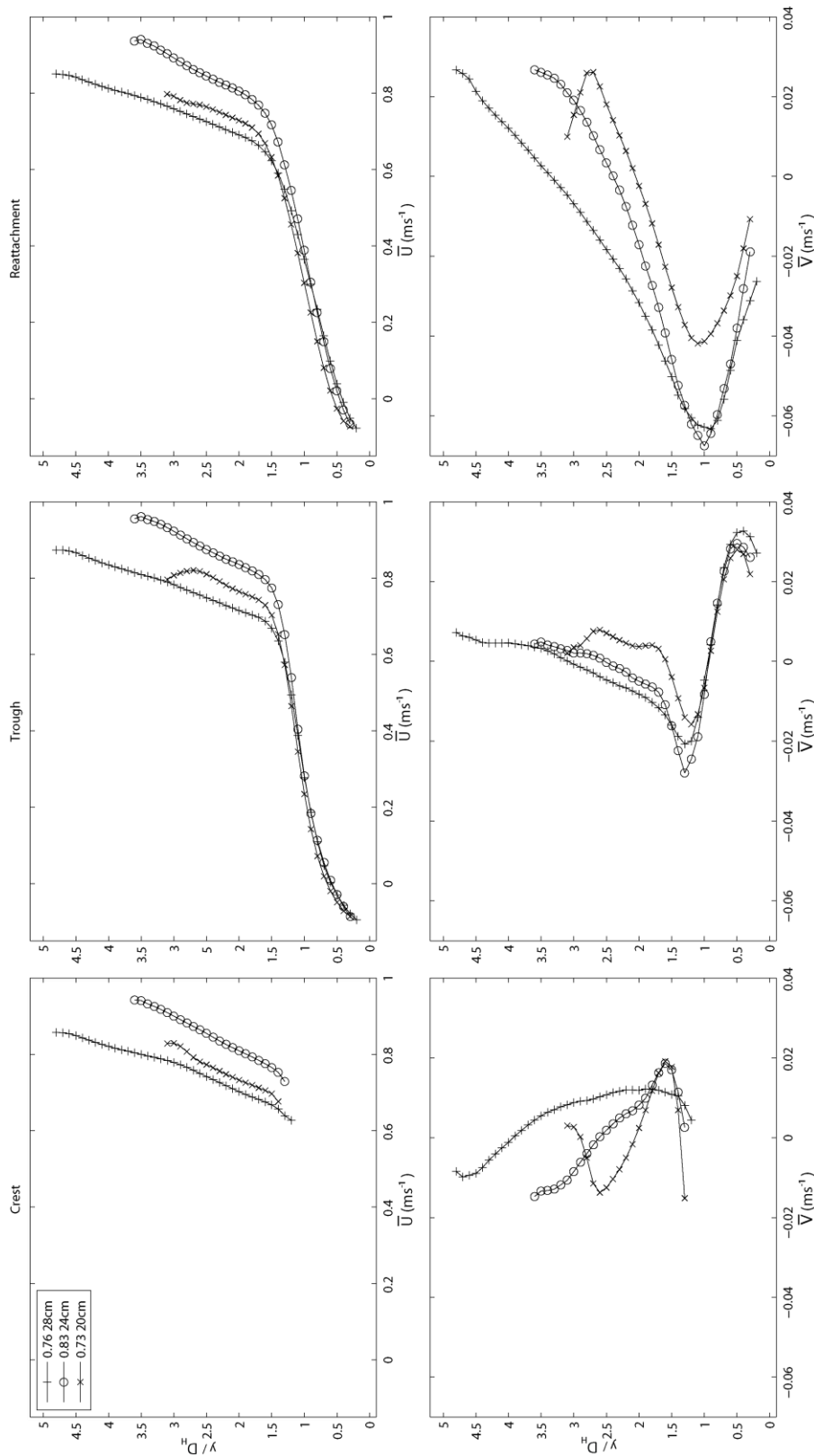


Figure 4-6: Time-averaged velocity profiles of streamwise velocity component U (top panels) and vertical component V (bottom panels) for conditions H76, M83 L73. A-B = at crest; C-D at trough; E-F near reattachment. + = 0.76ms⁻¹ at 280mm, o = 0.83ms⁻¹ at 240mm, x = 0.73ms⁻¹ at 200mm depth. Y axis = normalised profile height where 1 = the dune crest. X axis is the velocity magnitude in ms⁻¹. The Figure shows conditions with the most comparable high incoming mean flow velocity. Here the shape of the profiles has changed significantly compared to Figure 3 through the influence of higher \bar{U} . Changes in depth still produce significant alteration in mean profile shape, notably in the gradient of the profiles.

4.3.3 Reattachment length

Figure 4-7 and Table 4-2 display the calculated reattachment lengths for all runs using the median method of 50% negative flow velocities to define the median flow reattachment location on the bed (Simpson, 1996; Kadota & Nezu 1999). Figure 4-7 shows that the change in flow depth has a major impact on how median flow reattachment length responds to \bar{U}_c . Reducing depth to 200mm produces a linear relationship with \bar{U}_c . This adjustment happens somewhat at 240 mm flow depth, but more strongly for the shallower 200 mm condition (Figure 4-7).

The high gradient of the mean profiles at the crest at low depth 200 mm ($2.5D_H$) produces a considerably different reaction in the shear layer to the classic log-linear profile shape at the higher depths (e.g. H14,H76). Although the height of flow reversal near reattachment did not change with changes in flow depth or \bar{U}_c (Figure 4-5 & 4-6 E), the length of reattachment does increase with \bar{U}_c for the 200 mm conditions and the highest \bar{U} at 240 mm (Figure 4-7).

At 280 mm, there is variation in the reattachment length but it shows no consistent change with \bar{U}_c . Both behaviours can be seen at the equilibrium depth conditions (240 mm). At the low \bar{U}_c conditions (M14 & M23) there is variation but no consistent trend. Whilst the high \bar{U}_c condition (M83) has a very similar reattachment length to L73, of similar incoming \bar{U}_c , and shape of \bar{U} profile at the crest (Figure 4-6A). The profiles of mean downstream velocity at the crest in Figures 4-5 & 4-6A show subtle change in the profile shape at the crest between M83 & M14, with M83 loosing much of its log-linear profile shape; similarly to the conditions at the lower depths (L14,L30,L60,L76,&L96).

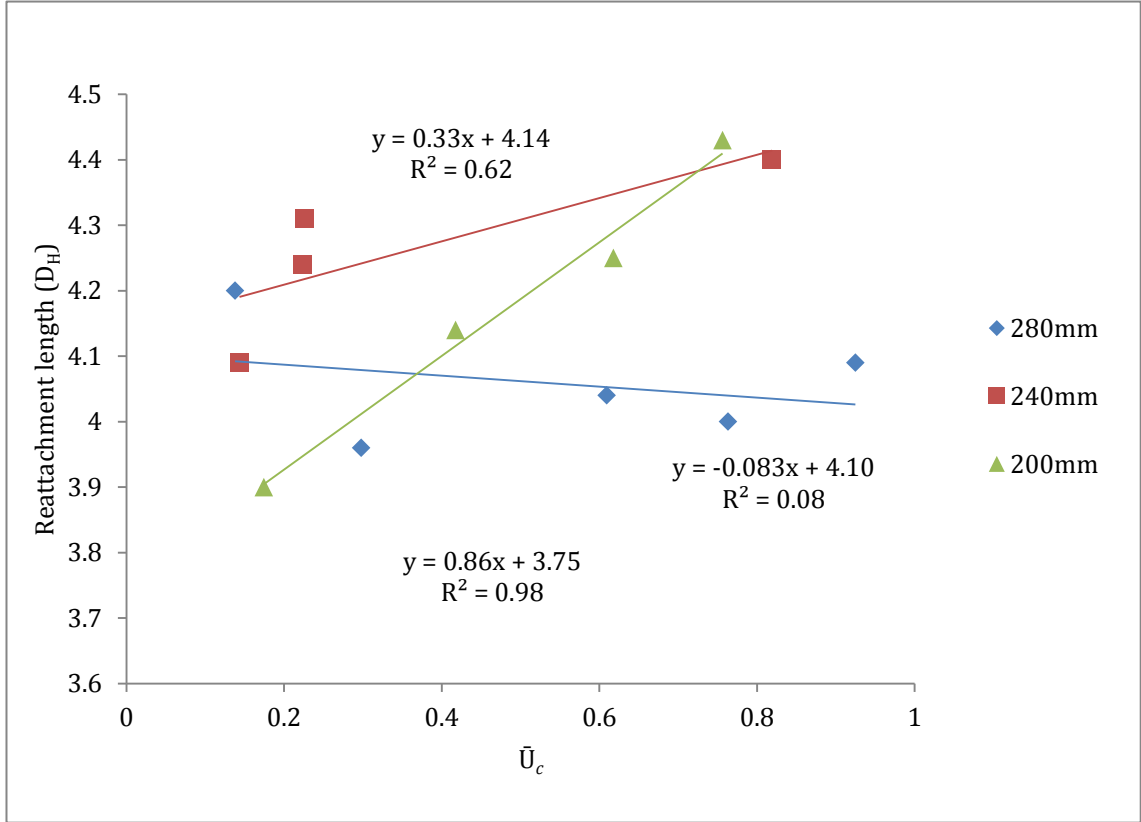


Figure 4-7: Flow separation reattachment lengths normalised by the dune height, where one Dune Height equals the dune crest.

Shear layers are known to “flap” from the rolling up of eddies in the shear layer (Levi, 1983; Rudericj & Fernholz, 1986; Muller & Gyr, 1986, 1996; Kostaschuk, 2000), the frequency of this shear flapping is directly related to \bar{U} and length of flow separation via the equations (Levi 1983; Levi 1991):

$$St = \frac{fL}{V} \quad (4.4)$$

$$f_v < 0.8 \bar{U}_c / x_r \quad (4.5)$$

$$f_w < 0.1 \bar{U}_c / x_r \quad (4.6)$$

where St = Dimensionless Strouhal number; f = Frequency of vortex shedding; L = characteristic length [e.g. hydraulic diameter]; V = velocity of the free flow; f_v [Hz] = Eddie shedding frequency; f_w [Hz] = Shear layer flapping; x_r is the mean length of the separation zone [i.e. reattachment point length].

Here, \bar{U}_c is changed across depths, but at the higher depth of 280 mm the reattachment length does not change with \bar{U}_c , therefore the Strouhal numbers calculated are largely unaffected (Figure 4-8 & 4-9). However, for the changing \bar{U}_c and reattachment length conditions at the lower depth of 200 mm, \bar{U}_c and Strouhal numbers for eddy shedding and wake flapping have a direction relation via the change in reattachment length with \bar{U}_c .

\bar{U}_c	Name	Reattachment Lengths (D_H downstream of crest)	Eddy Shedding f_v	Wake Flapping f_w	Strouhal Number (Shedding)	Strouhal Number (Flapping)
280 mm						
0.14	H14	4.2	0.0265	0.0033	0.0533	0.0067
0.30	H30	3.96	0.0602	0.0075	0.0566	0.0071
0.61	H61	4.04	0.1207	0.0151	0.0554	0.0069
0.76	H76	4	0.1527	0.0191	0.0560	0.0070
0.92	H92	4.09	0.1809	0.0226	0.0548	0.0068
Mean		4.058				
240 mm						
0.14	M14	4.09	0.0280	0.0035	0.0469	0.0059
0.23	M23	4.24	0.0422	0.0053	0.0453	0.0057
0.22	Not reported	4.31	0.0421	0.0053	0.0445	0.0056
0.83	M83	4.4	0.1489	0.0186	0.0436	0.0055
Mean		4.26				
280 mm						
0.18	L18	3.9	0.0358	0.0045	0.0410	0.0051
0.42	L42	4.14	0.0807	0.0101	0.0386	0.0048
0.62	L62	4.25	0.1163	0.0145	0.0376	0.0047
0.73	L73	4.43	0.1259	0.0157	0.0361	0.0045
Mean		4.18				

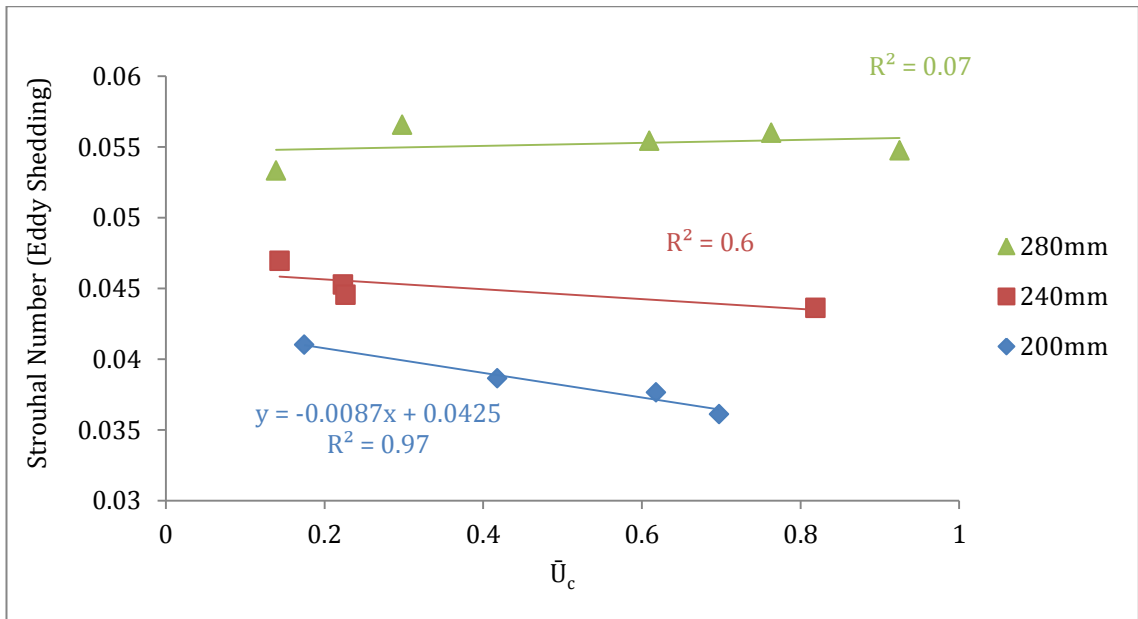


Figure 4-8: Strouhal Number for eddy shedding calculated from (4.4) and (4.5).

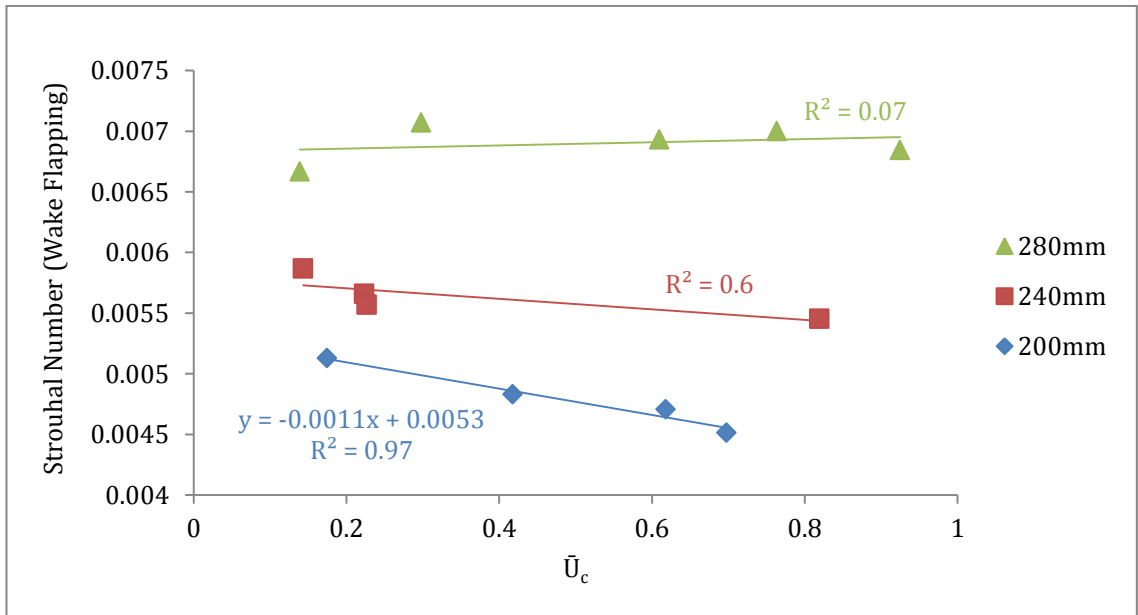


Figure 4-9: Strouhal Number for wake flapping calculated from (4.4) and (4.6).

To further investigate the changes in recirculation, the percentage of time the flow was reversed (negative u_i) during the measurement period is plotted in Figure 4-10 for a section of the field of view. Figure 4-10 clearly shows the change in length of the median recirculation region with \bar{U} at the lower flow depth (200 mm, right panels in Figure 4-10). Additionally, the area with some of instantaneous negative downstream velocities round the median (yellow) expands at higher \bar{U}_c . As \bar{U}_c is increased, the recirculating, upwelling flow, over the lee slope lifts the separated flow region above the dune crest. This effect also

occurs with higher \bar{U}_c at the 200 mm flow depth condition, despite the elongation of the reattachment length at this condition. Therefore the vertical height on the lee face where the flow separates altered, despite the fixed geometry, with \bar{U}_c . This change in flow separation height is ~ 3 pixels high from lowest to highest \bar{U}_c , which equates to $\sim 19\%$ of the dune height.

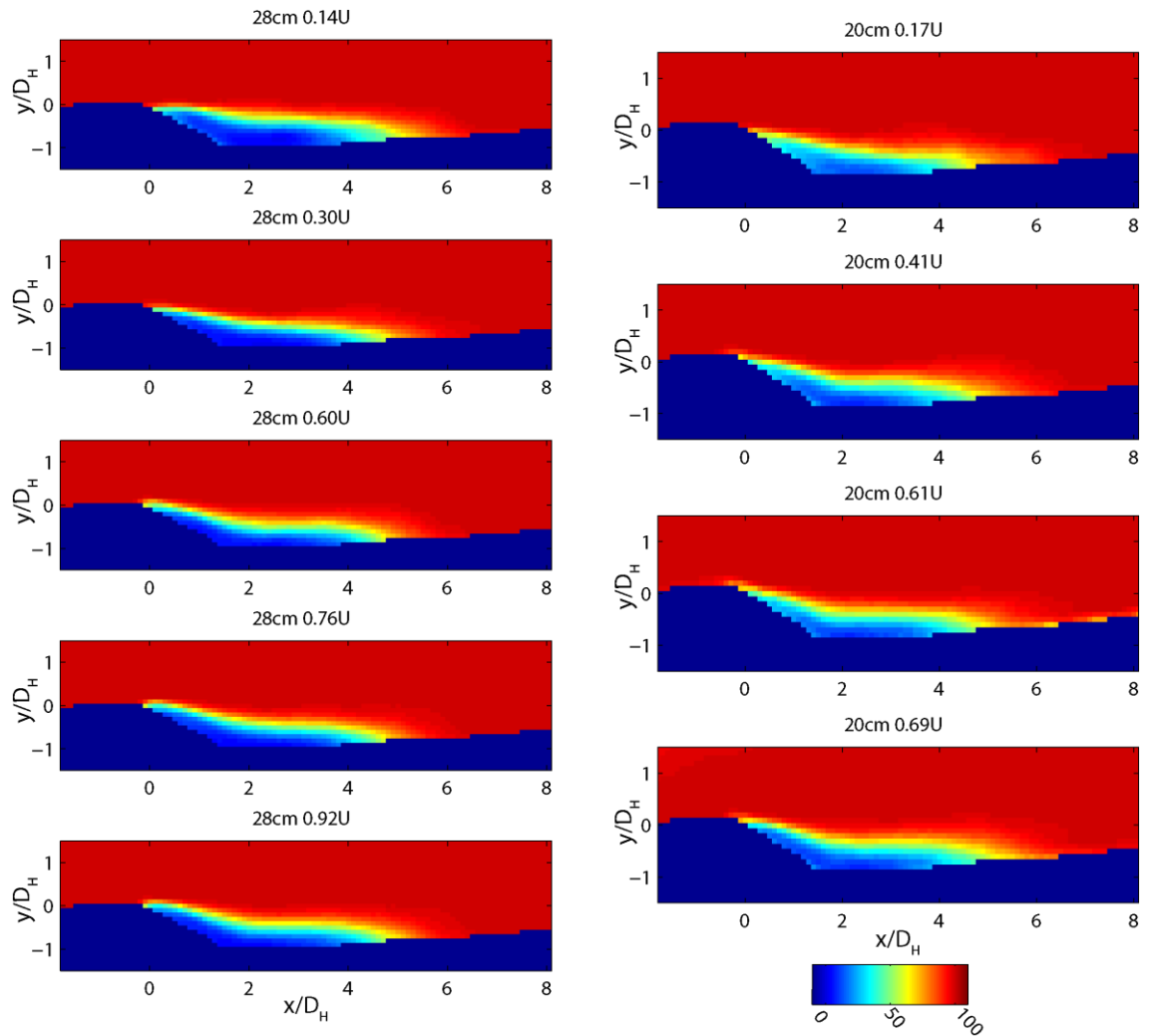


Figure 4-10: Scaled images of the percentage of positive downstream velocity for all conditions at 280mm & 200mm depth. Flow direction is left to right. At the 280mm depth (left panels) reattachment length shortens slightly with higher \bar{U}_c , but this is inconsistent. The more significant change here is at the crest, where the flow reversal occurs higher in the flow with higher \bar{U}_c , leading to recirculation events occurring above the crest at the highest \bar{U} conditions here.

4.3.4 Reynolds Stress

As described earlier, Reynolds stress is the sum of fluid density and the mean instantaneous fluctuations in u_i and v_i velocities for each point in the flow field (equation 4-1). The maximum Reynolds stress values increases linearly with \bar{U}_c

(Table 4-1) however this misses a key observation in Figure 4-11, that the locations and total area of high magnitude Reynolds stresses changes with both \bar{U}_c and flow depth. In these experiments, Reynolds stress changes considerably at the flow reattachment point, an important area where fluid momentum changes considerably (Raudkivi 1966). Despite a near-consistent reattachment length across the range of \bar{U}_c conditions at the higher depth of 280 mm (standard deviation of $0.08D_H$), the area of high Reynolds stress around reattachment ($\sim 5D_H$ in Figure 4-10, as the crest $=1D_H$) extends further downstream with increasing \bar{U} , showing an important change in the magnitude and location of turbulence near reattachment along the stoss slope (Figure 4-11, 4-8 D_H downstream). In contrast, the median reattachment point has remained generally constant at this depth (Figure 4-7).

To compare the effect of depth on the distribution of Reynolds stress the conditions have been grouped across depths but with similar \bar{U}_c . These are the low \bar{U}_c group, H14 M15 L18 (Figure 4-11: H14 M15&L18), a medium \bar{U}_c group H61 & L62 (Figure 4-11: H61 & L62), and a high \bar{U}_c group of conditions, H76, M83 & L73 (Figure 4-11: H76, M83 & L73).

Downstream of reattachment there is a consistent change in the spatial distribution of Reynolds Stress between depths for the lowest flow conditions measured here (Figure 4-11: H14 M15 L18). The turbulent wake as revealed by Reynolds stress rises in profile to around 1-1.5 D_H with a maximum height of $3D_H$ above the mean bed level, whereas in Figure 4-11, M15 and L18 for successively lower flow depths, the turbulent wake is found progressively closer to the bed over the dune stoss and remains close to the bed (within one dune height), normal to the stoss slope.

Figures 4-11, H61 and L62 show some important spatial differences in the patterns of Reynolds Stress at comparable \bar{U}_c . The highest Reynolds stress patterns at 280 mm (Figure 4-11 H61) covers a larger area, whilst both areas cover 0.5-5 D_H downstream of the dune crest, 280 mm extends higher into the flow, covering about $1.5D_H$ compared to $1D_H$ at 200mm vertically.

Conditions H76, M83 & L73 (Figure 4-11) are compared here to demonstrate the effects of depth changes at comparable \bar{U}_c (difference of $0.06\bar{U}$). For L73, the turbulence just downstream of reattachment extends to over 8DHs downstream of the crest, whilst at H76 the comparable Reynolds Stress values stop at 8DH. In contrast to this, the turbulent wake from the upstream dune at L73 is smaller and less intense than the higher depth.

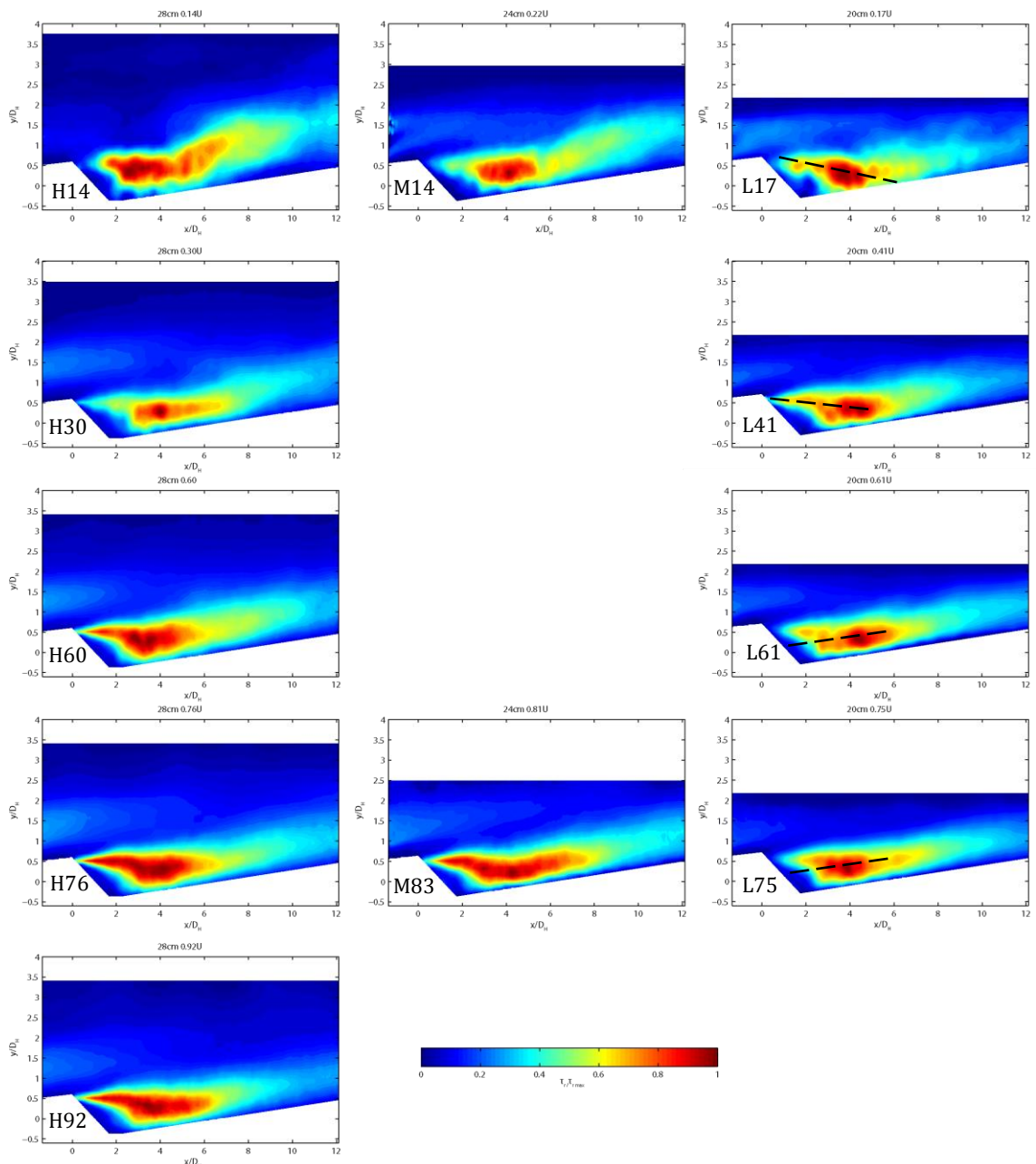


Figure 4-11: 2D contour plots of Reynolds Stress. Contours are normalised by the maximum Reynolds Stress value for each run. For the maximum Reynolds Stress magnitude see Table 4-1. Conditions naming: H=280 mm depth, M= 240 mm depth, L= 200 mm depth. The number after the depth = \bar{U} in cms^{-1} . Dashed Black Lines shown on the L conditions indicate how the angle of the area of high Reynolds stress changes with \bar{U} .

For the 200 mm flow depths there is an interesting change in the angle of the area of highest Reynolds stress areas with \bar{U}_c (Shown in Figure 4-11). At low flow speeds, the angle of the high Reynolds stress is perpendicular to the stoss slope (Figure 4-10 L18). With increasing \bar{U}_c this area becomes more parallel to the stoss slope, indicating that the area of highest stresses changes in their average spatial orientation to become more normal to the bed slope with higher \bar{U}_c conditions.

From the comparison of Reynolds stress between flow depths with similar \bar{U}_c , it is clear that depth has a considerable influence on the distribution of Reynolds stresses along a dune profile. For the 280mm flow depth conditions, the Reynolds stress is able to dissipate higher in the flow than at 200mm, this leads to a reduction in Reynolds stress along the upper stoss slope and crest at the higher flow depth. This difference is reduced at higher flow speeds (for the same depths) when flow acceleration over the same stoss slope is greater and high Reynolds stresses are appear along the dune stoss closer to the bed. For the lower flow depth, this trend is reduced and \bar{U}_c does not produce a spatial change of the same magnitude as the higher flow depth.

4.3.5 Quadrant Analysis

Traditional turbulent boundary layer studies used flat surfaces for measurements of uniform turbulent flow as the mean streamline vector is parallel to the bed (Lu & Willmarth 1973; Bogard & Tiederman 1986). However, here the bed is sloped so the parallel streamline assumption is not valid. Therefore, recent studies of near bed flow over dunes have rotated the quadrant definition to the bed slope angle (Omidyeganeh & Piomelli 2013ab), as flow very close to be bed also has a mean streamline parallel to bed. Here, as the whole flow field over an uneven bed is under investigation, the quadrant definitions are rotated to the depth-averaged mean streamline vector for each profile and experimental run. Therefore the u component is rotated parallel to the mean streamline, and v component at a right angle to the mean streamline. This rotation was performed to give a more correct quadrant analysis that is relevant to the mean flow conditions and not to an artificial horizontal plane which is not necessarily relevant to the mean flow above a non-flat surface. The most

significant rotation ($\sim -3^\circ$) is in the flow separation bubble. The highest positive rotation (1°) is around the crest and upper stoss. These are not major rotations (being less than the slopes of the bedform) so the major change is in capturing Quadrant 2 and 4 events that lie near the boundary between quadrant definitions (Omidyeganeh 2013). Figure 4-12 and 4-13 show quadrants 2 and 4 respectively for the higher 280mm depth (conditions H14,H30,H61,H76,&H96, left panels; top down), the middle 240mm, equilibrium, depth (M14 & M83, middle panels; top down), and the lower depth of 200mm (L18,L42,L62&L73, right panels; top down) the colour axis is constant per quadrant and across flow depths.

As found in previous research, there are three main areas of burst and sweep events (quadrants 2 and 4, +ve contributions to Reynolds stress), these are i) the shear layer downstream of the crest, ii) flow reattachment, iii) the wake downstream of reattachment (Figure 4-12 for Q2, Figure 4-13 for Q4). Whilst negative contributions to Reynolds stress (Q1 & 3, outward and inward interactions, not shown) are mainly present in, i) in the free flow above the bed, and ii) in the internal boundary layer beneath the wake downstream of reattachment toward the crest (McLean, 1990; Nelson, *et al.*, 1993; McLean *et al.*, 1994; Bennett & Best, 1995; Best, 2005a,b). Here, for flows that are not scaled to a flow-morphology equilibrium (although condition M83 is close), it is revealed the locations of turbulent production and dissipation, that are not the shear layer, change and are dependent on flow depth and velocity.

The shear layer downstream of the dune crest is spatially very consistent; however the intensity of the shear layer changes with \bar{U}_c and depth. Changing \bar{U}_c has a noticeable effect on the intensity (percentage contribution over one standard deviation), which a more intense (more red) shear layer appearing with higher \bar{U}_c at both depths (Figure 4-12); this is also the case for quadrant 4 events (Figure 4-13). The effect of rotating the quadrant definition to the depth averaged streamline vector does modify the spatial coherence of the shear layer, this is because the recirculating flow produces a rotation of $\sim 3^\circ$ (the largest rotation across the dune). A method that resolved this might be to rotate the quadrant definition to the streamline vector for each point. This method was not

performed as it would make interpretation of the flow structure considerably more complex.

Eddy shedding and wake flapping increase with \bar{U}_c (Levi 1983; Simpson 1989; Levi 1991; Bennett & Best 1995), therefore greater intensity of wake turbulence produced from the shear layer is expected. In fact, the major changes between the conditions measured here are in the wake region as the flow is less controlled by the bed morphology than the shear layer.

Viewing Figures 4-12 & 4-13, an increase in \bar{U}_c and/or reduction in depth shows a remarkable change in the structure of the wake and internal boundary layer. Figures 4-12 & 4-13 (H14,M14&L18) demonstrates several key changes in the wake from the reduction in depth, the wake produced in the field of view (Q2 & Q4) moves toward the bed along the stoss, ii, the stacked wake (from upstream) is almost non-existent at the highest depth and becomes more intense and larger with decreasing depth. This overlying stacked wake may well be why the wake produced in the field of view moves toward the bed; as an extra region of high pressure turbulence sits between the wake and the free surface. The two turbulent wakes meet downstream of reattachment at $\sim 8D_H$ downstream in condition H30. Interestingly, both Q2 and Q4 show that at L18, the upstream wake is interacting with the shear layer produced in the field of view and producing some of the highest percentage contributions of Q2 and Q4 at L18.

The effect of increasing \bar{U} at constant depth and slope is shown in Figure 4-12 and 4-13. The intensity and spatial extent the percentage contribution of Q2 & Q4 events in the wake and stacked wake change considerably across the different depth conditions (Figure 4 12&13, conditions H14,H30,H61,H76&H96). At the lowest \bar{U}_c condition of 0.14 ms^{-1} (Figure 4- 12 H14) the highest percentage of Q2 events are in the wake zone, whilst just downstream of reattachment ($6-10 D_H$) there is no noticeable upstream wake. Increasing \bar{U}_c by 0.16 to 0.30 ms^{-1} (Figure 4-12 H30) produced a large and intense stacked wake that is dominated by Q2 events. Interestingly this stacked wake has few (%) Q4 events and is comparable in percentage contribution to the free surface events. The stacked wake as revealed by Q2 events merges with the wake produced in the field of view at around $8D_H$. This merger influences the

Q4 event distribution of the wake produced in the field of view, with an increase in both intensity and height of Q4 events at around 8-9 D_H downstream, showing that wake interaction does alter the location of turbulent events. The next three increases in \bar{U}_c (Figures 4-13 H61,H76 & H96) produce smaller upstream wakes of gradually reduced intensity. The percentage contribution of significant ($H>1$) Q2 events in the shear layer and at reattachment increases with higher \bar{U}_c (Figure 4-12 H61, H76 & H96). There is a concurrent reduction of percentage contributions in the wake produced in the field of view. Increasing \bar{U}_c also results in the stacked wake becoming more confined, extending less downstream and vertically than at H30. This appears to reduce the stacked wakes' interaction with the wake produced in the field of view. The distance of the stacked wake to the crest & shear layer reduces with increasing \bar{U}_c and it is likely that there is considerable interaction between the eddies in the stacked wake and shear layer. This has knock on effects for turbulence downstream of reattachment, as the peak in intensity produced from the wakes merging, described above, moves upstream, closer to the dune crest. Between conditions H30 to H96 (Figure 4-12, H30 H61 H76 H96) the peak in Q2 intensity moves upstream from $\sim 8-10D_H$ to $6-8D_H$, just downstream of reattachment. This shift also produces an increase in percentage Q2 events at around reattachment compared with the lower \bar{U}_c runs.

There is a moderately similar pattern in the spatial distributions of Q4 percentage contributions. Generally, the higher intensity Q4 areas in the wake move toward the bed with increasing \bar{U}_c for all cases, but the change in distribution of high Q4 events with different conditions \bar{U}_c is more complex. There is an initial increase in Q4 events in the stacked wake with \bar{U}_c (Figure 4-13 H14, H30), but similarly to Q2 reduces with increasing \bar{U}_c thereafter (Figure 4-12 H61 H76 H96). By H61 the stoss is evenly distributed in Q4 event intensity, but further increases in \bar{U}_c changes the distribution again, with the high Q4 events migrating towards reattachment at lower \bar{U}_c .

Increasing \bar{U}_c at the 200 mm flow depth (Figure 4-12, L18,L42,L62&L73) affects the distribution of Q2 events in different ways than for the 280 mm flow depth. At 200 mm, increasing \bar{U}_c results in increasing percentage contributions and size of the wake produced in the field of view, whilst the staked wake reduces

significantly in its intensity. This adjustment is shown well in the Q4 events (Figure 4-13, L18, L42, L62 & L73) which starts with have the highest percentage contributions in the stacked wake for all conditions (Figure 4-13 L18), but then reduces with increasing \bar{U}_c (Figure 4-13, L42, L62 & L73). At 200 mm, the wake is always near the bed and increases in intensity with increasing \bar{U}_c (both Q2 and Q4). This adjustment is shown well with both Q2 and Q4. Interestingly, the reduced depth also affected how the wake responds to higher \bar{U}_c ; for the 280 mm conditions (Figure 4-12 & 4-13 H14, H30, H61 H76 H96), Increasing \bar{U}_c produced high percentage events closer to reattachment, but at 200 mm the opposite pattern emerges, with high % Q2 events migrating downstream from around 6DH to 7-9DH (Figure 4-12, L42, L62 & L73) and ~8DH for Q4 events (Figure 4-13, L42, L62 & L73).

The stacked wake throughout the 200 mm depth conditions undergoes an interesting change with increasing \bar{U}_c . Whilst already larger and more intense than for the 280 mm conditions, the stacked wake does not appear to merge well with the wake produced in the field of view. Instead, the wake is angled normal to the stoss slope, unlike at 280 mm where after the crest the stacked wake becomes horizontal, showing the reduced influence of bed morphology. At 200 mm the wake maintains its angle over the stoss slope and reaches the free surface at around 4-8D_H downstream of the crest.

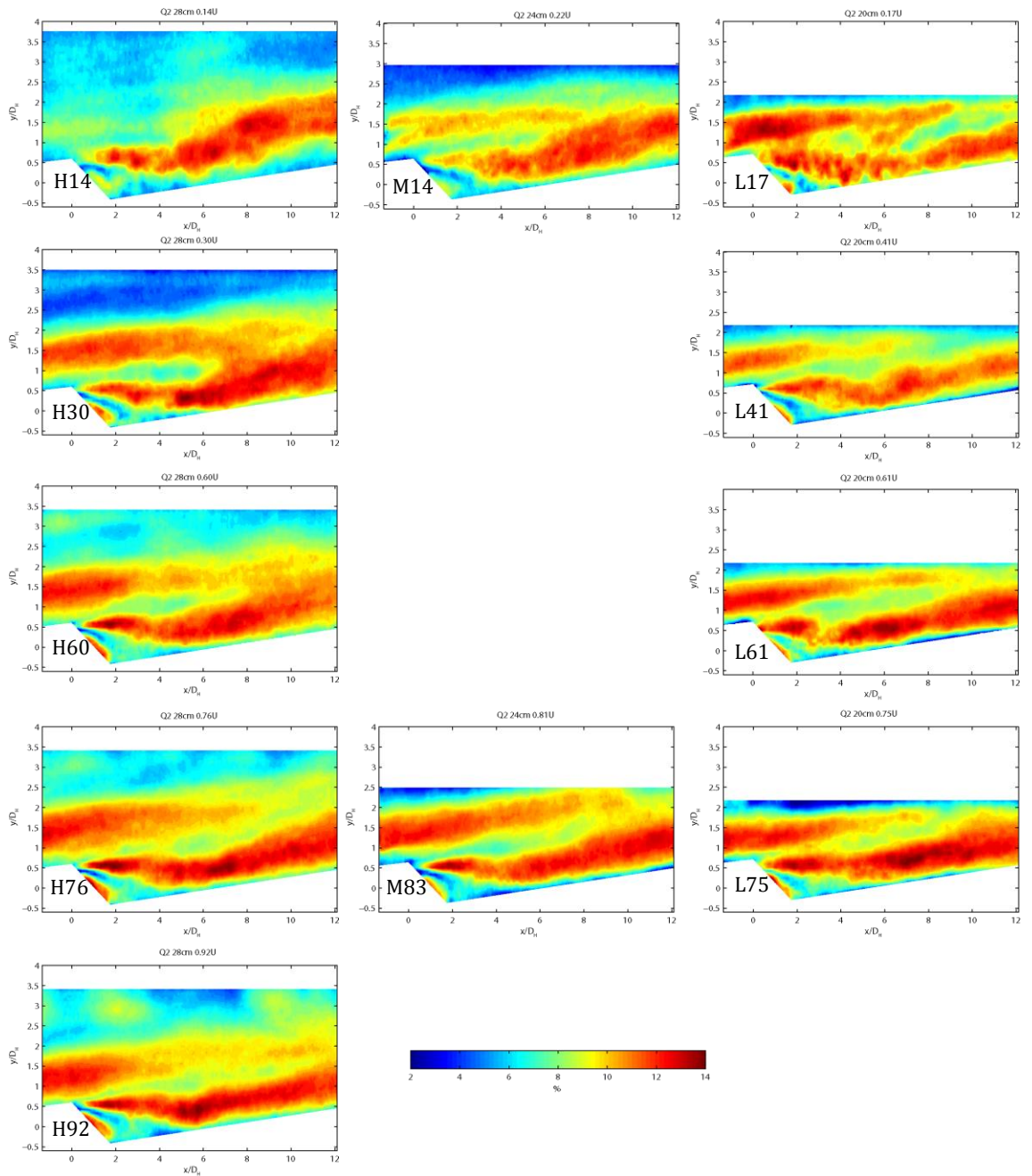


Figure 4-12: Scaled images of significant ($H > 1$) Quadrant 2 event contributions (colour axis %). Contour levels are equal across images. Image naming: H=280mm depth, M= 240mm depth, L= 200mm depth. The number after the depth = \bar{U}_c in cm s^{-1}

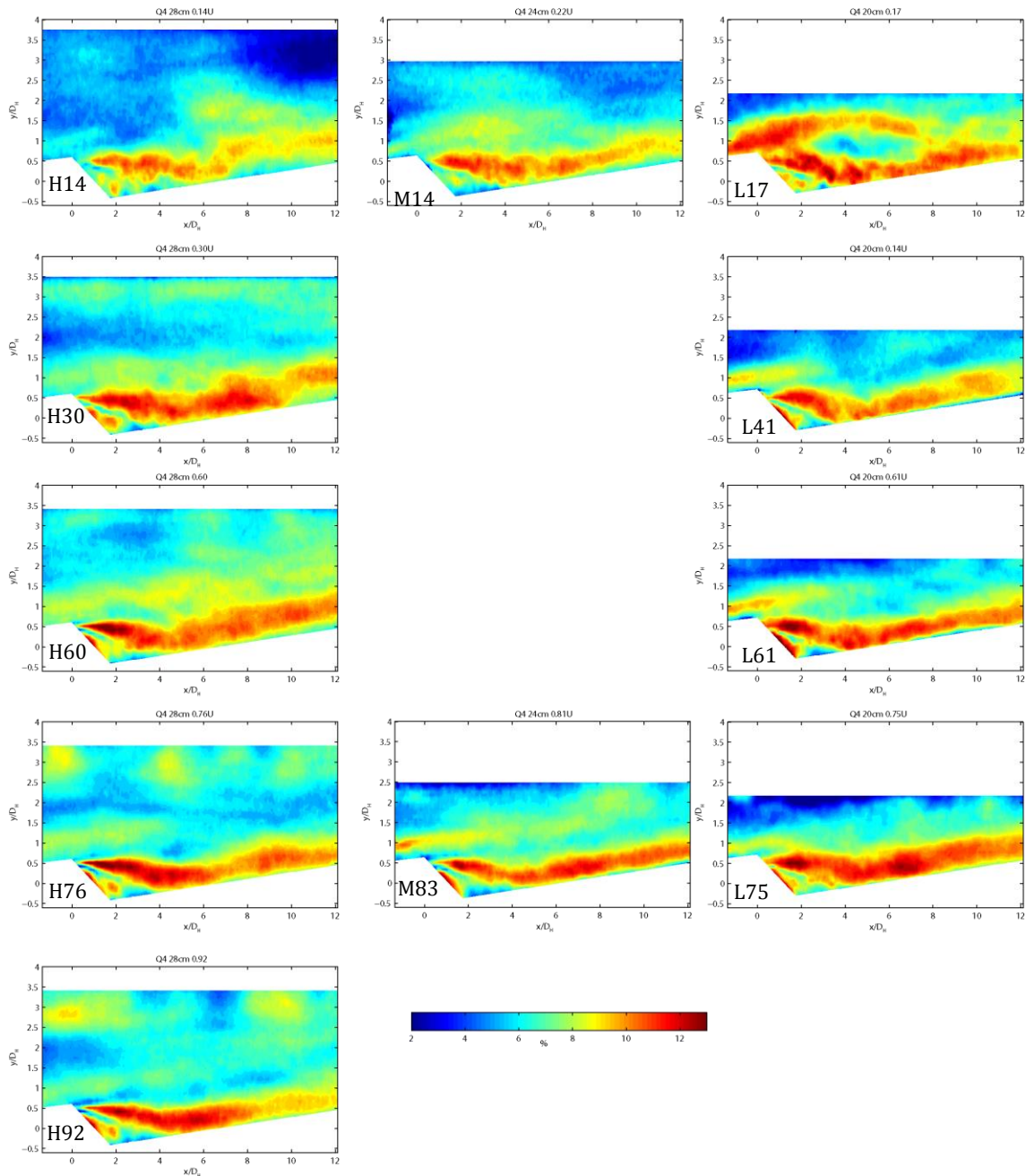


Figure 4-13: Scaled images of significant ($H > 1$) Quadrant 4 event contributions (colour axis %). Contour levels are equal across images. Image naming: H=280 mm depth, M= 240 mm depth, L= 200 mm depth. The number after the depth = \bar{U}_c in cm s^{-1}

There is a common theme through the variety of conditions tested here in the response of the wakes observed. That is, when the wake produced in the field of view becomes more intense, the stacked wake appears to be less intense. Assuming that the same flow conditions exist for the upstream dune, this indicates that turbulence production and dissipation occurs faster with higher shear layer intensity. The important finding here is that this can be caused by increasing \bar{U} as well as greater interaction between the stacked wake and shear layer. This interaction increases the percentage contribution of significant

turbulence events in the shear layer and at reattachment, as seen for conditions H61 H76 H96, L42, L62 & L73 (Figures 4-12 & 4-13, H61 H76 H96, L42, L62 & L73). The confinement of high Q2 and Q4 events toward reattachment happens in concurrence with a change in mean burst and sweep quadrant contributions in the stacked wake. Conditions at 280 mm (Figures 4-12 & 4-13, H14 H30 H61 H76 H96), demonstrate that the relationship between the stacked wake and shear layer influences the distribution of Q4 sweep events over the stoss and around reattachment.

4.4 Discussion

Previous studies on flow over dunes have generally measured flow-morphology for equilibrium conditions (e.g. Nelson *et al.* 1993; McLean *et al.* 1994; Bennet & Best, 1995). The Reynolds stress, and the quadrant partitioning of the Reynolds stresses measured in these studies therefore demonstrated the typical fluid processes of equilibrium flow conditions over a dune bed (e.g. Figure 4-12 in Bennet & Best, 1995). However, natural river flow conditions are subject to change across a range of scales, produced for example by seasonality or storms. As a result, much of the time the flow-morphology relationship is not in equilibrium and the channel bed is often adjusting in response to the prevailing flow conditions (Aberle *et al.* 2010). The response of a rivers' flow velocity and flow depth to an increase in discharge is often substantially faster than the bed morphology response to a change in flow conditions. This produces a flow-bedform hysteresis (Martin & Jerolmack 2013). The present research has measured the mean and fluctuating flow structures over a fixed dune bed in some of these transient states to observe how the mean flow structure changes with variations in flow depth (relative roughness) and mean flow velocity. These changes in turbulent flow field are summarised conceptually in Figure 4-14 where conditions H14,L18,H76 and L73 illustrate the variations. Several key points can be made:

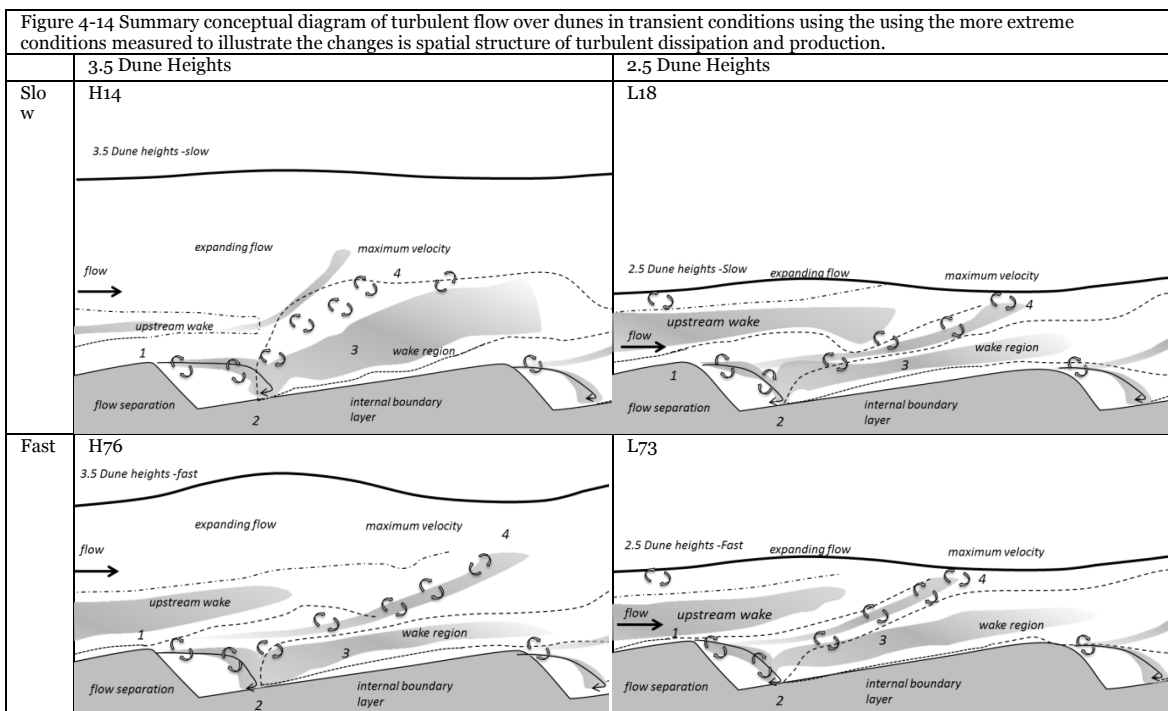
- 1: The stacked wake produced from the upstream dune interacts with the shear layer and wake produced in the field of view, this interaction increases the percentage of quadrant events in the stacked wake relative to the wake produced

in the field of view and is dependent upon variation in relative roughness and flow velocity.

2: Flow reattachment length did not change for flows that were deeper than classical equilibrium flow-morphology conditions. A shallower depth produced a strong linear relationship between mean downstream flow velocity and reattachment length as grain roughness become dominant over form roughness.

3: The flow field downstream of reattachment changes substantially with mean flow speed and flow depth. Increased topographic acceleration over the stoss slope and wake stacking changed the location of the most frequent turbulent events along the stoss, with the highest percentage Q2 and Q4 events migrating toward reattachment with higher mean downstream velocity and flow confinement from the stacked wake.

4: The position along the dune where turbulence reached the free surface changed considerably, due to the varying extent of wake produced by the upstream dune and topographic acceleration produced in the field of view. In some instances, where mean flow velocity was low and depth high, shear and wake turbulence did not reach the free surface. At low flow depth, turbulence reached the flow surface across all discharges.



Varying depth and \bar{U}_c in the experiments conducted herein has provided an insight into the relative importance of these two variables on the amount of flow convergence and topographic acceleration over dunes. It is clear that depth plays the more significant role in the shape of mean velocity profiles for the conditions measured here. Even at low \bar{U} there are significant changes to the downstream flow velocity profile shape across the three depths measured in this study (Figure 4-5). The mean downstream (\bar{U}) profiles at the crest overlap close to the solid boundary but diverge further away from the boundary (Figures 4-5 and 4-6). This adjustment is indicative of two main flow features, 1) that with less depth the skin friction layer (lower section) remains constant in height and 2) the free flow above adjusts to a higher velocity to compensate for depth reduction. As the lower than equilibrium depth (200mm) produces only one main (higher) gradient in the downstream velocity profile, the previous effects on the velocity profile of form roughness and skin friction have become considerably more obscured.

The differences in the profiles of the mean vertical (\bar{V}) component of velocity provide an indication of the scale of relative change in the location and intensity of the mean flow structures with increasing \bar{U}_c . The results also demonstrate how strongly the bedform shape controls the mean profiles in the recirculation region, with a constant shear layer height as well as a constant reattachment length across the range of incoming flow velocities for the 280 mm depth conditions (Figure 4-7). However, when the mean downstream velocity profiles merge into one gradient the shape, and importantly length of the shear layer, begins to adjust with \bar{U}_c (Figure 4-7). This change indicates that a threshold in the behaviour and response of the shear layer exists between 240 mm and 200 mm flow depths (2.5 and $3D_H$) for this bedform geometry. It is a key finding that with a wide range of conditions tested; a threshold for such a significant feature of dune flow exists very close to the typical equilibrium depth of $3D_H$. It is apparent that, as a relationship between reattachment length and \bar{U}_c occurs when the shape of the incoming downstream velocity profile no-longer has a log-linear profile shape, that this condition is unnatural for equilibrium dunes.

Engel (1981) found that for steep dunes (e.g. Bridge & Best 1988) the length of flow separation did not change, as form drag was dominant, whilst altering

dune morphology to low steepness dunes (Allen 1968, Carling *et al.*, 2000a, “washed out dunes”) increased the relative significance of sand grain roughness compared to form drag, resulting in a change to the reattachment length. As bedform shape is constant in these experiments, the relative roughness is increased by lowering flow depth and the associated change in reattachment length is therefore a reflection of the increase in the influence of skin friction over form drag in the total boundary stress equation (Engel 1981). Importantly, the velocity magnitude plots at low and high \bar{U}_c (Figures 4-5 & 4-6) show that with a reduction in flow depth, the profile shape at the dune crest and the flow recirculation region changes, reducing from a clear two-step gradient profile at the higher depth to high gradient profile shape for the 200 mm case with no clear change in gradient. Importantly, the skin friction portion of the profile shows little change when depth is reduced from 280 mm to 240 mm. The rest of the profile merely loses a portion of the freer flow above until it is lost completely at 200 mm. This change in the dominating form of friction can explain why the reattachment lengths increase with \bar{U}_c at 200 mm and they do not at 280 mm, because grain roughness becomes dominant over form drag at the lower depth condition (Engel 1981).

It is still unclear why a threshold for the length of flow separation occurs so close to the classical scaling of dune height (depth=3D_H). As these experiments used a fixed morphology no change in the depth of trough scour could be recorded. However, as the Reynolds stress and Quadrant plots indicate, the magnitude of turbulence at reattachment certainly increases with lower depth and/or higher \bar{U}_c and is likely lead to the larger trough scours found in humpback dunes (Carling, 2000a). What is clear is that if the incoming velocity profile does not have a classical log-linear velocity profile shape then the reattachment length will change with \bar{U}_c , and that this does not happen when classical scaling is achieved. Therefore the successful development of the lower gradient log-linear profile shape over the stoss is critical in defining the type of flow recirculation behaviour.

Balachandar *et al.* (2007) recently investigated the effect of flow depth on flow reattachment length and summarised their findings alongside previous research. Here, Figure 4-15 displays the mean reattachment lengths from

research herein compared with Balachandar *et al.* (2007)'s Figure. The results of the present study are similar to the results of Balachandar *et al.* (2007) where a reduction in flow depth produced longer reattachment lengths. There is no evidence, however, for their suggestion that reattachment length across these studies is tending toward a length $\sim 5D_H$ downstream of the crest. In fact, because of the considerable scatter in this diagram, with many similar roughness heights producing considerably different reattachment lengths, such a relationship may not be very informative. The potential reason for this discrepancy is the differing bedform geometries between the studies influencing the flow pressure field e.g. Kadota and Nezu (1999) found that longer spacing of bedforms meant longer flow reattachment lengths.

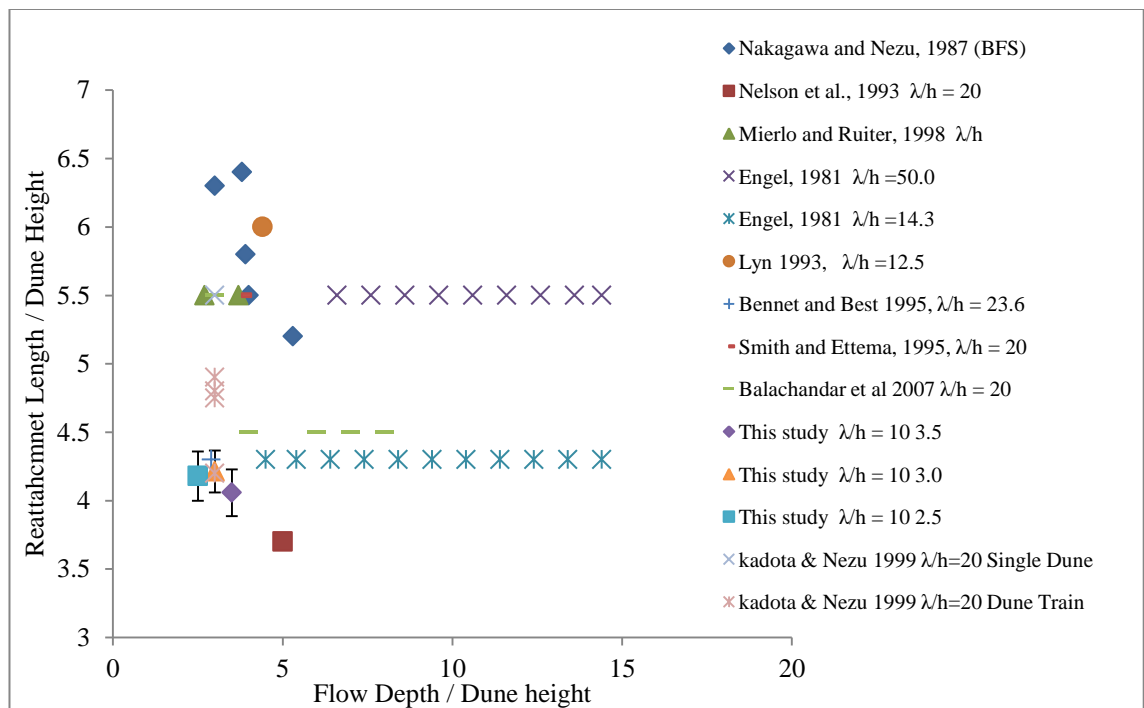


Figure 4-15: Reattachment lengths compared with previous research. Modified from Balachandar et al. (2007).

Figure 4-15, where dune height has normalised the depth and reattachment length scales, is actually demonstrating that dune height, although a major factor in determining the pressure field, is not the single factor affecting dune flow reattachment length. Additional factors influencing the length of flow separation are the shape and angle of the stoss slope, the angle of lee slope and the spacing of the dunes (Engel 1981; Simpson 1989; Allen 1968; Kadota and Nezu 1999; Venditti 2007), and as shown in this study \bar{U}_c can also change the

reattachment length when skin friction is dominant. Additionally, bedform crestlines and their orientation to main flow direction can also alter flow reattachment length as well as its 3D shape (Maddux, Nelson, *et al.* 2000ab; Venditti 2007; Omidyeganeh & Piomelli 2013ab), then more sophisticated predictors and descriptors of flow reattachment character are required for parameterisation of flow separation in computation models (e.g. Paarlberg *et al.*, 2007).

Figure 4-10 demonstrated that height of flow separation on the lee slope changes with \bar{U}_c at both depths shown. This adjustment is likely to be a manifestation of interactions between the shear layer, recirculation and stacked wake (as shown in Figures 4-12 & 4-13). With greater \bar{U}_c the stacked wake is closer to the crest and shear layer. This adjustment should produce; 1, more frequent eddy shedding and /or wake flapping through interaction of coherent flow structures in the stacked wake and 2, produce higher magnitude coherent flow structures through eddy merging. The Strouhal numbers for eddy shedding and wake flapping in Table 4-2 were calculated reattachment lengths, there is also a Strouhal dependency on \bar{U}_c for the 200 mm conditions that is not seen for 280 mm, due to the changes in reattachment length with \bar{U}_c . These Strouhal relationships were created with a fully developed boundary layer upstream, and not with a turbulent wake, it is as yet unclear whether the overlying wake directly affects the frequencies of eddy shedding or wake flapping.

Additionally, the higher flow separation point and influence of an overlying wake from the upstream dune are likely to be interlinked. The coherent flow structures that have developed in the wake upstream will have interacted with the shear layer in the field of view. These low pressure turbulent structures intermittently lift pulses of recirculating fluid higher up the lee slope and will likely have significant implications for how sediment is routed and preserved on the lee face of dunes in unsteady conditions (Reesink & Bridge 2007, 2009).

4.4.1 Implications for the stability of dunes

Figure 4-4 illustrates the variation in depth averaged mean vertical velocity at the crest across a range of incoming flow velocities and depths (also shown in Table 4-1). The magnitude in vertical velocity was shown to rise with \bar{U}_c at both 280 mm and 200 mm depths until $\sim 0.6 \text{ ms}^{-1} \bar{U}_c$, whereby any additional increase in \bar{U}_c results in a reduction in the magnitude of the depth averaged vertical velocity at the crest. The condition M83 is the condition tested here that is closest to the classical equilibrium conditions scaling for this geometry of dunes (Allen 1982; Yalin 1977). However, as the mean velocity profiles at the crest show (Figure 4-4 & 4-5A), the profile shape for condition M83 is not the classical log-linear profile shape, with a clear skin and form roughness partition (McLean 1990). Additionally, the depth-averaged vertical velocity at the crest for M83 is well past the peak in \bar{V} at around $\sim 0.6 \text{ ms}^{-1} \bar{U}$. This initial rise and then fall in \bar{V}_c with \bar{U}_c in Figure 4-4 is due to the increase in magnitude of downwelling flow near the free surface. This downwelling is due to increased flow contraction with \bar{V}_c and can be seen in the mean vertical velocity profiles at the crest between Figures 4-5 & 4-6B where the switch from positive (close the bed) to negative (close to free surface) vertical velocity occurs at a higher location in the profile with increasing depth. With the direction of vertical velocity for the 200 mm conditions switching at 2DH, 240 mm at 2.5DH and for the 280 mm depth condition at 4DH (Figures 4-6B). Comparing Figures 4-5B vs. 4-6B it is clear that depth strongly adjusts the shape of mean vertical velocity at the crest. However there is little difference in the relationship between in \bar{U} and \bar{V} between the depths shown in Figure 4-4, as the increase in negative \bar{V} is minimised by the additional upwelling near the bed (Figures 4-5B & 4-6B). The change of \bar{V} with \bar{U} in Figure 4-4 is therefore a result of the relatively less negative vertical velocities produced between 0.14 to $\sim 0.60 \text{ ms}^{-1}$, then the relatively higher magnitude and proportion of negative vertical velocities above $\sim 0.60 \text{ ms}^{-1}$.

This depth affect has a clear impact on the direction of the depth-averaged flow vector at the dune crest. The dune crest is a critical area, as the location, and direction, of maximum bed shear stress defines the type of bedform produced (Yalin 1977). Using linear stability analysis, McLean (1990) reiterates the importance of a phase lag between flow velocity and sediment flux on the

stability of dunes; whereby the maximum sediment flux is upstream of the crest, thus promoting vertical deposition of sediment as the bedform migrates downstream. Bennett *et al.* (1998) demonstrate that dunes lose stability and transition into upper stage plane beds when the location of maximum sediment transport flux moves downstream of the \bar{U} maximum (Bennett *et al.* 1998).

As the mean vertical distribution of momentum at the crest becomes more positive (vertically) with \bar{U}_c until $\sim 0.6 \text{ ms}^{-1}$ this indicates that the interplay between topographic acceleration over the rising stoss slope is dominant over the flow contraction effects that promote downward flux. Above this mean flow speed, the flow contraction effects start to become more dominant, and reduces the \bar{V}_c from the relatively higher magnitude and proportion of negative vertical velocities in the mean profile.

It is interpreted that for the set geometry of dunes studied here, the flow conditions above $\sim 0.6 \text{ ms}^{-1}$ gradually move away from equilibrium dune conditions. For Condition M83, the closest to classical equilibrium scaling, the incoming \bar{U}_c condition does not produce a classical log-linear profile shape at the crest. The high gradient in the mean vertical velocity indicates the presence of the wake seen in Figure 4-11, M83. The high positive, then negative gradient in mean vertical velocity at the crest (Figure 4-5 & 4-6B) clearly shows the wake becomes confined toward the bed whilst flow contraction above produces stronger downwelling as \bar{U}_c increases (Figure 4-5B vs. 4-6B). Such contraction of the wake and positive vertical velocity surely limits the vertical deposition of sediment for mobile dunes. Yalin (1977) demonstrates that dune height scales with dimensionless bed shear stress in a nonlinear way, with a peak in dune height at $\sim 10 \Theta / \Theta_{cr}$, where Θ = bed shear stress, and Θ_{cr} = critical bed shear stress for sediment motion. Here, it is demonstrated that a similar non-linear relation occurs with vertical velocity at the crest with \bar{U}_c that is possibly more demonstrative of the processes controlling dune height.

Flow contraction and topographical acceleration have a strong effect on the flow structure along the stoss slope. The dune stoss is a complicated area, subject to a developing boundary layer post flow reattachment and flow acceleration (McLean & Smith, 1986; Fredsoe, 1982). Eddies that emanate from the shear

layer produce a turbulent wake as flow attempts to stabilise and mix with the upper flow (Bennett & Best, 1995). This adjustment has a major impact on the consistency of the developing internal boundary layer, disrupting it with turbulent bursts directed toward the bed (Q4 events), and this disruption is crucial in the initiation and maintenance of sediment movement along the stoss which affects the development and stability of dunes (Nelson *et al.*, 1993, 1995).

Experiments conducted where bedform morphology and flow depth and velocity were in classical equilibrium have found that the wake region had a set height limit above the bed (Nelson *et al.*, 1993, Bennet & Best 1995). The above analysis of turbulent flow over fixed 2D dunes indicates that changing \bar{U}_c across a wide range of magnitudes, from incoming flow velocities that are too low to form dunes (e.g. H14,M14 &L18) to velocities near upper stage plane bed conditions (e.g. H96), does have an major impact on the height and location of highest turbulent intensities in the turbulent wake.

Changing \bar{U} at the 280 mm depth dramatically changed the spatial distribution of the wake produced in the field of view as well as the stacked wake from the upstream dune. As described above, at the lowest \bar{U}_c condition (H14) there is no significant wake from the upstream dune visible across the crest of the study dune. However, the wake from the study dune rises toward the free surface considerably more than at higher \bar{U}_c conditions. Interestingly, the next \bar{U}_c condition up (H30) produces the largest stacked wake for the 280mm conditions, reaching that of $\sim 8DH$ s downstream of the dune crest. As described above, when \bar{U}_c is increased still further, closer to equilibrium dune conditions (H61,L62), the highest Reynolds stresses and Q2 & Q4 events in the wake are both moved toward the flow reattachment point and toward the bed (Figures 4-12 & 4-13 H61,L62). As Nelson *et al.* (1995) found, the wake and flow reattachment downstream of a single backward facing step is longer than that over a train of bedforms, which is also similar to findings from Engel (1981). Both studies attributed this variation to the additional influence of topographic acceleration produced by the stoss slope (Maddux, et al, 2003a). When topographic acceleration is added via a downstream bedform the length of the wake decreased as the rate of decay in turbulence intensity is higher (Nelson *et al.*, 1993). Here, it is shown these topographic acceleration effects can also occur

without a bedform geometry change and with a change in relative roughness and \bar{U}_c . The stacked wake, as seen at the higher depth, was largest at H30, and became less intense moved upstream progressively with increases in \bar{U} . This change is likely due to the rate of decay in turbulence intensity increasing due to higher velocity gradients with higher \bar{U}_c conditions (Figures 4-5 & 4-6A). These results indicate that the stability of dunes is heavily reliant on the interaction between topographic acceleration and the position of the turbulent wake with the incoming flow velocity. Relatively higher proportions of Q2 and Q4 events closer to reattachment, caused by high \bar{U}_c conditions here, should promote larger dune troughs; potentially producing humpback dune shapes in mobile bed conditions at high bed shear stress (Carling *et al.* 2000a).

The importance of topographic acceleration has also be discussed and emphasised in studies on the ripple-dune transition (Robert & Uhlman 2001; Schindler & Robert 2005; Fernandez *et al.* 2006). The transition from ripples to dunes usually occurs when there is large topographic acceleration along a large “rogue” ripple producing considerable trough scour through a higher downstream velocity gradient at the crest (Bennett & Best 1996; Fernandez *et al.* 2006). This larger trough and wake changes the locations of turbulent events along the downstream ripple, thus promoting further growth downstream (Venditti *et al.* 2005a). The low \bar{U}_c conditions presented here helps to indicate why dunes do not form at low flow speeds - there is not enough topographic acceleration to promote bigger troughs though spatial confinement of: 1) the reattachment length, and 2) high magnitude turbulent events along the downstream stoss slope towards the reattachment point.

Topographic acceleration in depth-limited flows produces a notable free surface response that also promotes flow acceleration through flow convergence (McLean *et al.* 1990). However, dunes have been measured in deep flows with no free surface response (e.g. McLean et al 1994) and it has been found that the reduction in topographic acceleration (which was measured as a lower gradient in mean downstream velocity profile) produced little change in magnitude of shear stress over the stoss, McLean *et al.* (1994) write: “*It is interesting that this difference in acceleration does not seem to affect the shear stress at all.*” (pp 12,739). It is also noted in the present study where Reynolds stress magnitude only scaled with \bar{U}_c and not flow depth (i.e. relative roughness) (Table 4-1).

Importantly, what is shown in this study is that the locations of Reynolds stress, and particularly the highest Reynolds stresses events (Q2 & Q4), subtly changes with depth and \bar{U}_c as a result of different topographic forcing. In flows with free surface interaction it is likely that the additional flow acceleration over the stoss from free surface interaction via flow contraction is why higher \bar{U} conditions are needed to produce dunes in deeper flows, with constant grain size, in stability diagrams (Southard & Boguchwal, 1990, their Figure 2); as deeper flows would have less topographic acceleration produced from the free surface interaction, therefore moving the turbulent wake and stacked wake toward the free surface, and away from the bed.

Traditionally, dune height scales with flow depth (Simons & Richardson 1962, 1966; Yalin 1977; Fredsoe 1982). However, recent field surveys have found dune fields where the scales of the bedforms have a tendency to be smaller than expected given the flow depths, particularly those found in larger rivers with high width:depth ratios (Parsons *et al*, 2005). As Figure 4-5 & 4-6 demonstrate, even a relatively small increase of 0.5 dune heights above the equilibrium depth can produce a substantial change in the direction of vertical velocity above the shear layer (Figure 4-5 & 4-6D). This adjustment indicates that any suspended sediment is likely to be falling onto the shear layer at this depth. Depth changes of 0.5DH are common in natural rivers (Aberle *et al*. 2010) and this implication requires significant exploration. In particular, these non-scaling dunes tend to have low angle lee slopes and high suspended sediment concentrations in the flow (Kostaschuk & Villard 1996; Kostaschuk 2000). The present finding may illuminate why these dunes tend to form, in that high flow depths redistribute the negative vertical velocities at comparable \bar{U}_c conditions.

4.4.2 Implications for sediment transport

The Reynolds stress diagrams (Figures 4-11, 4-12 & 4-13) demonstrate there is considerable turbulence at and downstream of flow reattachment. Eddy shedding from around reattachment has been shown to produce large coherent flow structures that can reach the flow surface as boils, which often have higher levels of suspended sediment than the surrounding free flow (Jackson 1976; Muller & Gyr 1986; Kostaschuk & Church 1993; Bennett & Best 1995; Babakaiff

& Hickin 1996; Muller & Gyr 1996; Kadota & Nezu 1999; Kostaschuk 2000; Best 2005b; Shugar *et al.* 2010; Talke *et al.* 2010). This change in distribution of Reynolds stress and Q2 burst events around reattachment indicates that these large coherent flow structures increase in intensity with a reduction in flow depth and/or increase in \bar{U} . At the lower 200mm depths the frequency (based upon the Strouhal number, Table 4-2) of eddy shedding increases due to longer reattachment lengths.

Maximum eddy size generally scales with maximum depth in rivers (rather than width) and these larger events in deeper water have been shown to produce correspondingly larger sediment suspension events (Lapointe, 1992, 1996). Lapointe (1996) found that higher depths produced more frequent large sediment suspending events, this is likely to do with the increase in dune size (and therefore reattachment length) that accompanied the higher depth in Lapointe's field surveys increasing the eddy shedding frequency. Jackson (1976) and Babakaiff & Hickin, (1996) found that systematically reducing depth (and this increasing the relative roughness) increased the frequency of these events as the free surface was closer to the turbulent wake produced by the dunes (Jackson, 1976b; Babakaiff & Hickin, 1996). Importantly, at the lower flow depths, although the largest eddy size is reduced the distance of the wake above the bed is also reduced, as shown in Figure 4- 12. This effect is likely to lead to a larger area of relatively higher bed shear stress causing events for a greater proportion of time (Keylock *et al.* 2014). This adjustment will have important implications for i) the balance between sediment being transported in traction or as suspended load, and ii) the magnitude and distribution of that sediment transport across the stoss.

Additionally, it has been found that the wake from the upstream bedform is more intense at the lower depth measured here (200 mm) compared with a higher depth (280 mm) with comparable \bar{U}_c (Figures 4-11, 4-12 & 4-13 H14 L18). The impact of this stronger and more persistent wake at the lower depth will delay or even prevent the transition to a near-fully developed boundary layer at the crest, affecting the accuracy of log-law estimates of bed shear stress for bedload sediment transport estimates (Kostaschuk & Villard 1996; McLean *et al.* 1999; Kostaschuk *et al.* 2004). Additionally, the consecutively higher \bar{U}_c

conditions at a set depth shows that the angle of high Reynolds stress in the shear layer and wake changes; becoming more normal to the bed slope, rather than horizontal. Such an effect may produce greater turbulence anisotropy which is more able to induce sediment transport (Keylock *et al.*, 2014).

Recently, considerable advances in correlating sediment transport and turbulent events, or sequences of events, have been made (Nelson *et al.* 1995; Bennett *et al.* 1998; Venditti & Bennett 2000; Wren *et al.* 2007; Claudin *et al.* 2011, Chapman *et al.* 2012, 2013; Keylock *et al.* 2014; Schmeeckle 2014). Naqshband *et al.* (2014a) report that the bypass fraction of sediment at the crest of a dune changes considerably with increases in mean downstream flow velocity (10% to 27% bypass change) and when the bypass fraction was compared relative to the suspended sediment arriving at the dune crest then 16% to 39% of sediment is bypassed. Showing that a substantial part of the sediment flux is not used for bedform migration and this is related to the magnitude of \bar{U} (Naqshband *et al.* 2014a). Key variable they identify is the sediment excursion length. If the sediment excursion length is $<$ flow separation length then the sediment that has an excursion length $<$ then the flow separation length will be used for bedform migration. This is a change to Mohrig & Smith (1996) model where excursion length $>$ horizontal slip face distance is all bypassed (Naqshband *et al.* 2014a). Here, it is shown that the reattachment length can vary with \bar{U}_c in unsteady conditions where skin friction dominates over form drag (high \bar{U} and/or low depth conditions). This will have a significant effect on how much sediment transport is used for bedform migration via the flow separation region for mobile dunes.

The turbulent flow field results presented in the present chapter illustrate that, out of equilibrium, the areas where turbulence generally associated with bedload transport Q4 events (Nelson *et al.* 1995; Schmeeckle 2014) and sediment suspension events (Q2 events (Ninto & Garcia 1996; Garcia *et al.* 1996; Wren *et al.* 2007) dramatically change. Here, the most significant changes in quadrant event distribution is over the stoss and crest of the dune, whilst the magnitude of Q2 and Q4 events in the flow separation region is always relatively high.

4.4.3 Implications for dunes in transient conditions & impacts on superimposed bedforms

Realistically, \bar{U}_c and flow depth are interdependent (Simons & Richardson, 1962; 1966). However, here we attempted to pull apart these interdependent variables to reveal some of the similarities and differences that are generated when they are varied. In doing so we reveal important insights into the above four conditions (of flow velocity and depth) as well as the stability of equilibrium dunes (above).

When equilibrium dunes are subject to quick changes in discharge the main agents that alter the host dune shape are the processes of amalgamation or carving/splitting (Nelson *et al.* 2011). These processes of changing dune shape can further be separated into two categories, fast and slow. Nelson *et al.* (2011) showed that dune height changed quickly in response to a drop in depth. Here, it is asserted that the process behind such a change is revealed. As depth is dropped, the gradient of downstream velocity at the crest increased through greater free surface interaction and topographic acceleration along the stoss slope. This adjustment also produces a longer turbulent wake and a longer stacked wake relative to the higher flow depths (Figure 4-11 H14,M14&L18. H76,M83 &L73). Such a change would be very likely to induce greater bedload transport capacity at the crest and would either increase the celerity of the dunes or reduce the height of the dune (“washing out”), dependent on how much additional bed shear stress is applied (Allen 1982; Carling *et al.* 2000 a,b; Nelson *et al.* 2011).

Whilst changes in dune height are relatively quick, changes in bedform wavelength commonly require considerably more time (Allen 1978; Gabel 1993; Martin & Jerolmack 2013). Slower bedform adjustments are related to the presence of superimposed bedforms on the stoss of dunes (Nelson *et al.* 2011) which almost always exist over a dune’s stoss (Venditti *et al.* 2005b). Several observers have noted the presence of superimposed bedforms on dunes in the field and in the laboratory and these features have been classified using the usual bedform stability diagrams (e.g. Simons & Richardson, 1962; Southard & Boguchwal 1990); lower stage plane beds (Venditti *et al.* 2005b) and

superimposed ripples & dunes (Simons & Richardson 1966; Rubin & McCulloch 1980; Parsons *et al.* 2005; Reesink & Bridge 2007). The constant existence of these superimposed features means there is continuous unsteadiness in sediment transport and bedform geometry along the stoss- even at a statistical equilibrium (Aberle *et al.* 2010). The bedform scale interactions of amalgamation and carving/splitting (Kocurek *et al.* 2010) become the key processes of dune morphological change in unsteady conditions (Martin & Jerolmack 2013).

For the case of amalgamation with depth rises, the growth in bedform height is commonly from superimposed bedforms adding sediment to the crest (Carling, 2000a; Wilbers & Ten Brinke 2003; Martin & Jerolmack 2013). The turbulence and form drag from a superimposed bedform is often not enough to erode the host stoss completely, leaving the superimposed bedform to migrate toward the host crest, where sediment transport is greatly reduced via sheltering, producing a stalled host dune (Best 2011). The key implication of the present research here is that when depth increases, the turbulent wake and stacked wake both move away from the bed. The associated topographic acceleration reduces which results in less capacity to transport sediment, promoting deposition along stoss slopes and crests. This process tends to take longer than for reduction in flow depth because of the lag associated with the transport of sediment to the crest via superimposed bedforms (Carling *et al.* 2000a), whereas when depth rapidly reduces sediment transport capacity at the crest rapidly increases (Gabel 1993; Wilbers 2004). Importantly, in the converse situation where depth drops in natural rivers \bar{U}_c drops as well; this means that the depth effects on wake and stacked wake described above are somewhat mediated.

Superimposed bedforms are also crucial in the reduction of dune wavelength with reduction in depth through the process of carving (Martin & Jerolmack 2013; Carling 2000a), however not all superimposed bedforms carve the host dune when depth is reduced (Nelson *et al.*, 2011). When an equilibrium dune field is subject to a reduction in depth the superimposed bedforms produce greater trough scour (rather than crest height growth) (Martin & Jerolmack 2013; Warmink *et al.* 2014). Using a very similar set of reasoning used in the

above description of the importance of topographic flow acceleration on the stability of dunes, the carving superimposed bedforms and their erosive natures can be explained. When depth is lowered over dune bedforms topographic acceleration over their stoss increases due to greater interaction with the closer free surface and flow compression and acceleration, this will produce a higher downstream velocity gradient at the crest and therefore considerably more intense turbulence at reattachment, as seen from Figures 4-5 & 4-6A for velocity profiles and Figure 4-11 H14,M14 & L18 for low \bar{U}_c and Figure 4-11, H76,M83 & L73 for high \bar{U}_c conditions.

Amalgamating bedforms have been found to commonly have straight crestlines compared to the inherently 3D crests of carving superimposed bedforms (Warmink *et al.* 2014). This difference is not accounted for here as the present study only investigated 2D crest lines. Research on 3D crested dunes demonstrates that the locations of the most intense turbulence and burst and sweeps is heavily reliant on bedform morphology (Maddux, *et al.* 2003b; Venditti 2007; Omidyeganeh & Piomelli 2013b). The 3D shape of the crest and stoss slopes of carving bedforms will redistribute the effects of topographic acceleration and locations of high intensity turbulence (Omidyeganeh *et al.* 2013b) and is therefore likely to show a modified type of bedform behaviour in response to these unsteady flows. Importantly, for comparison with dunes where discharge is increasing (both \bar{U}_c and depth increasing), \bar{U}_c can be considerably higher than observed here without developing washed out dunes, because as the depth increases the topographic acceleration is reduced relative to a case where no depth change occurs, and therefore adjusting the stability range of dunes.

4.5 Limitations

The present study as not explored the effects of depth and velocity on the frequency of turbulent events and the direction of their energy. Turbulent flow

over dunes is known to be an-isotropic and this is a major control on the movement of sediment, particularly the suspension of sediment, over bedforms (Keylock et al., 2014, Wren et al., 2007, Wren & Kuhnle 2008, Kuhnle & Wren 2009). The higher spatial gradient of downstream velocity at the crest of the dune is likely to produce greater turbulent an-isotropy, but this is not analysed here, but it will form the basis on a future journal article.

Whilst the results of this chapter are discussed in reference to sediment transport and bedform shape, these effects are only inferred from the mean velocity and turbulent fields. This limitation was a necessity due to the requirement of P.I.V. needing clear flow, and a stationary bed to achieve converged mean velocities. It has been shown from other researchers that the moving bedload layer changes the instantaneous and mean velocities near the bed through greater dissipation of turbulent energy from fluid-particle interactions (Naqshband et al, 2014a, Muste et al, 2000), so the near bed velocities are perhaps unrepresentative of moving bed conditions. Moreover, the changes in mean flow and turbulent structure described above are only indicate of changes to sediment transport and bedform shape, the direct relationships shown here are not necessarily directly applicable into computation models (for example) due to the lack of dissipation from sediment motion which could dampen the effects relationships found here.

One major limitation of this study is the lack of measurement of cross stream velocities and a variation in dune shape. This is a particularly strong limitation as three-dimensional bedform shapes (e.g. Venditti 2007), alter the spatial distribution of momentum, shear and drag (Maddeux et al, 2003 a,b). The present laboratory study produced changes in the spatial distribution of shear but much less so momentum and drag. Three dimensional bedform shapes also produce secondary flow structures (Omidyeganeh & Piomelli, 2013) which produce different scour features on the bed in the dune lee sides (Venditti et al 2005c), when compared to purely 2D cases. Such morphological forcing also creates non-uniform flow reattachment lengths (Allen 1967; Maddeux et al, 2003 a,b), unlike those measured in the present study. These affects would substantially vary the flow-morphology relationships found in this chapter, and require further research to quantify these affects. A hypothesis of future

research would be that using U/u^* to predict reattachment length over 3D dunes would still produce a linear relationship, if the locations of U/u^* and reattachment length measurement are along the same streamline.

4.6 Conclusions

The detailed 2D flow fields over fixed 2D dune bedforms in unsteady, transient, conditions presented here reveals complex relationships between flow depth, and mean velocity with turbulence structure and flow reattachment.

1: The wake produced from upstream dunes interacts with the shear layer produced in the field of view. This occurred without a change in bedform geometry and will likely contribute to morphological adjustment on the dune stoss side in response to flow variability via altering the shape and intensity of the wake underneath over the stoss slope; particularly by increasing the percentage of significant turbulent events near the bed.

2: Spatial change in turbulence zonation does not extend to, and does not appear to have a significant impact on, the height and length of the shear layer and reattachment zone for the deeper than classical equilibrium flow-morphology conditions. Shallower depth produced a strong linear relationship between mean downstream flow velocity and reattachment length as grain roughness become dominant over form roughness.

3: The flow field downstream of reattachment changes substantially with mean flow speed and flow depth. The turbulent wake zone of Q2 and Q4 events extend downstream of the crest over the lee side separation region and also moves closer towards the bed over the subsequent dune stoss. This adjustment has significant implications for bed shear stress distributions and thus sediment transport mechanisms and magnitudes. Increased topographic acceleration over the stoss slope and wake stacking changes the location of the most frequent turbulent events along the stoss, with the highest % Q2 and Q4 events migrating toward reattachment with higher mean downstream velocity. As a consequence

larger troughs are promoted and possibly this is the mechanism behind the shape of humpback dunes. Thus the importance of topographic acceleration found in ripple-dune transition studies is emphasised.

4: The position along the dune where turbulence reached the free surface changed considerably, due to the varying extent of wake produced by the upstream dune and topographic acceleration produced in the field of view. In some instances, where mean flow velocity was low and depth high, shear and wake turbulence did not reach the free surface. At low flow depth, turbulence reached the flow surface across all discharges.

Additionally, the shape of mean downstream and vertical velocity varies considerably across the three depths measured. In particular, the log-law shape is much less clear at low depths or high mean downstream velocity, indicating that log-law bed shear stress relationships breakdown and prone to error for out of equilibrium conditions. The variation in reattachment length with mean downstream velocity (2) only occurred when the log-law profile was unclear, again indicating that grain roughness had become dominant.

The structure of mean turbulence and the impact of topographic acceleration and flow compression observed here provides important insight into the stability of dunes. Across the range in incoming flow velocities at the higher depth it was clear that there was not enough topographic acceleration at a very low flow velocity to produce turbulence over the stoss typically found over dunes (H14). Whilst the next mean flow velocity up (H30) displayed considerably more wake turbulence.

4.7 Synthesis

This study on flow structure over a fixed dune bed is, principally, taking the classic studies of Nelson et al., (1993) and Bennet & Best (1995) and altering the flow conditions to be deeper or shallower, and faster or slower than the

equilibrium conditions in these two papers. The simple method reveals how the turbulent flow structure shown in Nelson et al., (1993) and Bennet & Best (1995) changes with fluid boundary conditions - it does not remain spatially consistent as if it were totally dependent upon to the topography. This has revealed some controlling variables on this complicated system: principally the alteration of reattachment length as a function of the magnitude and spatial gradient of downstream velocity at the crest (U/u^*), and that flow compression and acceleration along the dune stoss slope and at the crest are dominant at separate conditions, which a peak in flow acceleration and convergence existing near the equilibrium flow conditions for this morphology. This relationship indicates that in equilibrium conditions, which these flow-morphology was based around, exist as a result of the interplay between upwelling and accelerating flow producing low pressure at the crest. This mechanism has been known for some time (e.g. Chézy 1775, Yalin 1966) and forms the basis of understanding dunes (Mclean 1990), but has not been investigated in such detail before. The addition of flow structure at the dune crest controlling reattachment length is novel and expands the importance of measuring flow structure at dune crests when trying to understand their dynamics.

This relationship does not improve methods of estimating bed shear stress, form roughness and skin friction as proposed by Mclean et al., (1999), which uses velocity profiles at the dune crest and stoss slope. The following chapter aims to tests these limitations by running a fully mobile bed. It is hoped that these experiments will reveal the same variation in dune height and tough scour that are inferred in this chapter from the mean velocities and location and magnitude of Reynolds stress.

On the scaling and definitions of unidirectional bedforms

Abstract

The past 100 years of research on fluvial dunes and their deposits has produced bedform scaling laws based on flow depth, grain size and flow velocity. Such flow-form-deposit scaling is used ubiquitously for a wide range of paleo-environmental interpretations and in predictions of river bed roughness in floods. Recent research from marine environments, density currents, and fluvial flows with strong secondary circulation shows that these laws are often extrapolated beyond the limits of the original research. In submarine density currents, for example, paleo-hydraulic reconstructions commonly predict dune forming flow conditions, but preserved dune cross strata are rarely found. One particular difference between these geophysical flows is the velocity profile shape and bed shear stress that results. In a series of novel laboratory experiments the shape of the mean downstream velocity profile was systematically altered so the velocity maximum was lowered toward the bed through the addition of roughness elements at the water surface; whilst maintaining flow depth and depth-averaged velocities. This procedure produced velocity profile shapes closer to those in density currents, and open-channel flows with strong secondary circulation. The initial lowering of the velocity maximum position increased dune height and length by 250%. The lowest velocity maximum position produced a stable upper-stage plane bed, whilst predictions based on flow depth and mean velocity remained within the dune regime phase-space. The results therefore demonstrate that the vertical position of the downstream velocity maximum can be a better predictor of equilibrium bedform geometries than flow depth or depth averaged velocity and also highlight that paleo-hydraulic reconstructions need to account for the possible variation in profile shape between geophysical flows. This research improves fundamental understanding of fluvial bedform stability and flow-form-deposit scaling laws for extrapolation into a broader variety of depositional environments beyond open-channel flows.

5.1 Introduction

The scaling of fluvial dunes is classically related to flow depth in the majority of stability diagrams and theoretical predictive formulae (Yalin, 1977; Allen, 1982; Fredsoe, 1982; McLean, 1990; Southard & Boguchwal, 1990; Bridge, 2003). Depth is defined as a mean water surface above a mean bed level and dune height (D_H) has been found to scale with water depth (D) by around $D_H \sim 1/6D$ (cf. Holmes & Garcia, 2008). There is a variety of empirical relationships between dune height and flow depth, with the majority of scaling falling within $3 < D/D_H < 20$ (Bridge, 2003). Despite a clear relationship across many

environments the overall correlation between dune height and flow depth is quite poor. This lack of correlation is because maximum dune height peaks not at the highest shear stress that forms dunes but in the middle of the shear stress existence field for dunes, and falls away either side as a parabola (Yalin, 1977). This effect produces the smallest dunes both at the lowest and highest shear stresses in dune forming conditions. Dune wavelength is slightly more strongly correlated with flow depth (Allen 1982, Ashley 1990). Prediction of dune geometry is of primary importance for hydraulic predictions of bed roughness, as the height and length of bedforms directly effects the form roughness dunes produce and consequently flow depth-discharge relationships (Allen 1974; Smith & McLean 1977; Wilbers 2004; Shimizu *et al.* 2009; Paarlberg *et al.* 2010; Nelson *et al.* 2011; Lefebvre *et al.* 2014). Additionally, the interpretation of cross strata for estimating paleochannel geometry is critically dependent on the empirical relations of equilibrium dune height and flow depth (Rubin & McCulloch, 1980; Paola & Borgman 1991; Bridge 1997; Leclair 2002; Straub *et al.*, 2012; Lunt *et al.*, 2013).

Whilst studies that derive empirical definitions have been numerous (Yalin, 1964,1977; Van Rijn, 1984c; Julien & Klassen, 1995), new tests of the processes behind the apparent scaling have been lacking (c.f. Bridge 2003). A recent example is Naqshband *et al.*, (2014b) where a re-analysis of a large number of studies produced a re-evaluation of the transition from dunes to upper stage plane bed, placed importance on the relative amount of suspended sediment and free surface effects. Whilst this interrogation of the literature is useful and welcome in identifying potential generic controls, there is a need to better understand the process linkages between suspension, free-surface and bedform evolution. For example, Naqshband *et al.* (2014b) commonly cite “free surface affects” as being very important, yet there is no description of this affect or how it may influence bedform size and dynamics. Such a flow-bedform process understanding is vital to progress understanding of bedform morphodynamics for all bedform-flow adjustments. Thus transitioning from empirical descriptions to a physical-based understanding and, ultimately, improved predictions (Lane & Richards 1997).

Such an improved understanding has been called for from recent bedform field surveys in large channels that have found examples of dunes that do not scale to flow depth as well as the empirical research suggests (e.g. Flemming, 2000, Bartholdy *et al.* 2002, Szupiany *et al.* 2009). This observation indicates that bedforms in many of the world's largest sand-bed rivers do not conform to the current predictions. It has been suggested that this is due too:

1: Non-equilibrium conditions during measurement (Ashley, 1990; Gabel, 1993; Kostaschuk, 2000)

2: High levels of suspended sediment (Kostaschuk & Villard 1996; Best & Kostaschuk 2002; Bradley *et al.* 2013)

3: The presense of secondary bedforms (Kostashcuk & Villard 1996; Amsler & Garcia, 1997; Carling *et al.*, 2000a,b)

4: Substrate sediment cohesion (Baas *et al.*, 2013)

5: Secondary circulation effects due to channel curvature and/or width: depth ratio (Bridge & Jarvis 1982; Bridge 2003; Szupiany *et al.* 2009)

6: Incorrect interpretations of bedform stability diagrams (Julien & Klassen 1995; Kostaschuk & Villard 1996, Van den Berg & Van Gelder, 1998).

The use of flow depth for dune scaling implies a significant flow-based definition on the maximum height of the bedform, whilst the definition of dune height itself depends upon accurate and precise definition of both the dune crest and trough. These two locations are essentially formed by different processes (Raudkivi 1966; Yalin 1977). The maximum possible height of the crest for a given mean depth should be defined by the capability of the flow to produce deposition at the crest. A condition close to this is essentially an upper stage plane bed with no vertical sediment transport flux and is perhaps best typified by humpback dunes, with long and flat stoss slopes (Carling *et al.*, 2000a).

The flow acceleration over the rising stoss slope produces a non-trivial upward flow component over the stoss and crest which promotes deposition whilst at the same time the downstream velocity and sediment transport rate increase. This parameter is termed the acceleration parameter K and is defined from the acceleration in the near surface flow velocity (Omidyeganeh & Piomelli 2011). As the pile up of sediment lowers the local depth, water surface slope and bed shear stress increase further and flatten the accumulation of sand. This feedback

reduces flow acceleration from the topographic forcing produced from the dune shape, and therefore the upward vertical component promoting deposition is greatly reduced. The flow acceleration also causes the water surface to contract at the crest and expand over the trough as flow decelerates over the undulating bed, indicating a switch from high to low pressure, from flow contraction to expansion and from upwelling flow to downwelling flow.

Figure 5-1 displays the fluid properties commonly used in the description of dunes, their formation and stability. The Figure displays several key features; 1) a lag between sediment erosion rate and turbulence (Allen 1982), 2) the decrease of the acceleration parameter K before the peak in bed shear stress due to the decrease in stoss slope angle (Raudkivi 1963; Omidyeganeh & Piomelli 2011)- leading to, 3) sediment drop out above the mean bed level producing a downstream sediment trough which induces flow separation. Flow separation is a key positive feedback as it amplifies the bedform height, largely through extra trough scour (e.g. McLean 1990). The formation of dunes further downstream is therefore dependent upon subsequent sediment accumulations produced from flow acceleration, then deceleration, post-flow separation and reattachment (Venditti *et al.* 2005a).

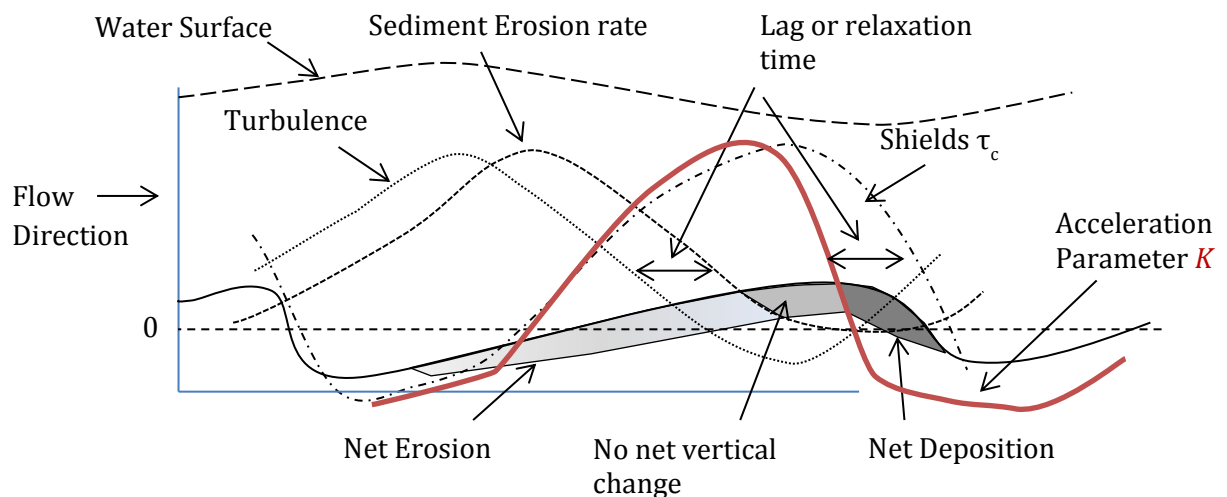


Figure 5-1 Conceptual diagram of sediment and fluid variables over migrating dunes in open channel flow. Modified and adapted from Raudkivi (1963), Allen (1982, their Figure 7-6) & Omid & Piomelli (2011 their Figure 5).

The dune trough is formed through flow separation and erosion of the downstream bedform stoss. It has been shown that eddies produced in the shear layer hit the bed at and around flow reattachment and can produce large

sediment entrainment and transport events (Kostaschuk & Church 1993; Bennett & Best 1995; Kostaschuk *et al.* 2009). The erosion of the downstream stoss slope is not equally matched by deposition in the trough, as many of the turbulent events have a greater than average downstream velocity (Bennett & Best 1995; Keylock *et al.* 2014), this reduces the amount of sediment avalanching on the dune lee slope. The amount of shear hitting the bed from turbulent events is dependent upon the gradient between the downstream flow above and the recirculating flow beneath the shear layer. This gradient is a combination of, 1) the mean depth and downstream velocity, and 2) the height of the bedform (Engel 1981; Simpson 1989). There is a strong feedback between bedform height and shear layer intensity and this is one of the major controls on the formation and maintenance of dunes. Moreover, an increase in trough scour as a bedform migrates is one of the more common ways a dune increases in height, rather than an increase in crest height above the mean bed level (Bridge 2003).

Bed shear stress has been shown to be linearly related to the distance of maximum velocity to the mean bed level in straight fully developed open channel flow (Nezu & Nakagawa 1993). Yet this distance is not always a consistent percentage of flow depth due to effects like secondary circulation and width to depth ratio (Jordan 1965; Williams 1970; Bridge & Jarvis 1977; Julien & Klaassen 1995; Szupiany *et al.* 2009, 2012). Flemming (2000) and Bartholdy *et al.* (2002) observe that grain size can be a more precise predictor of bedform geometry than mean depth. This conclusion is supported in the observations of Rubin & McCulloch (1980) where the largest bedforms found in San Francisco bay were always the coarsest. This outcome indicates that a bed shear stress-grain size relation should work better. Indeed, it has been found that dunes do not scale with flow depth where flow depth is not the primary control on the vertical position of the shear stress maximum. For example, secondary circulation produced in meanders, (e.g. Bridge & Jarvis 1982; Nittrouer *et al.*, 2008, Blanckaert *et al.*, 2013) or at confluence-diffuence sections (Szupiany *et al.*, 2012). In larger rivers (Ashworth and Lewin 2013) a wide variety of dune sizes has been found (Julien & Klaassen, 1995) often with a very weak relationship to flow depth (Leclair, 2011). On a more intermittent basis, rivers in cold climates often have frozen surfaces and or large blocks of ice floating on

them and research on bedforms with ice capped flows has demonstrated a range of considerably different dune geometries and sediment transport rates that require alterations to traditional sediment transport formulae and roughness calculation (Smith & Ettema 1995, 1997; Milburn & Prowse 2002; Ettema & Daly 2004). One of the main suggestions for a change in bedform dynamics under ice is the effect the ice cover has on altering the shape of the velocity profile from a normal log-profile shape to a parabolic shape (Figure 5-2).

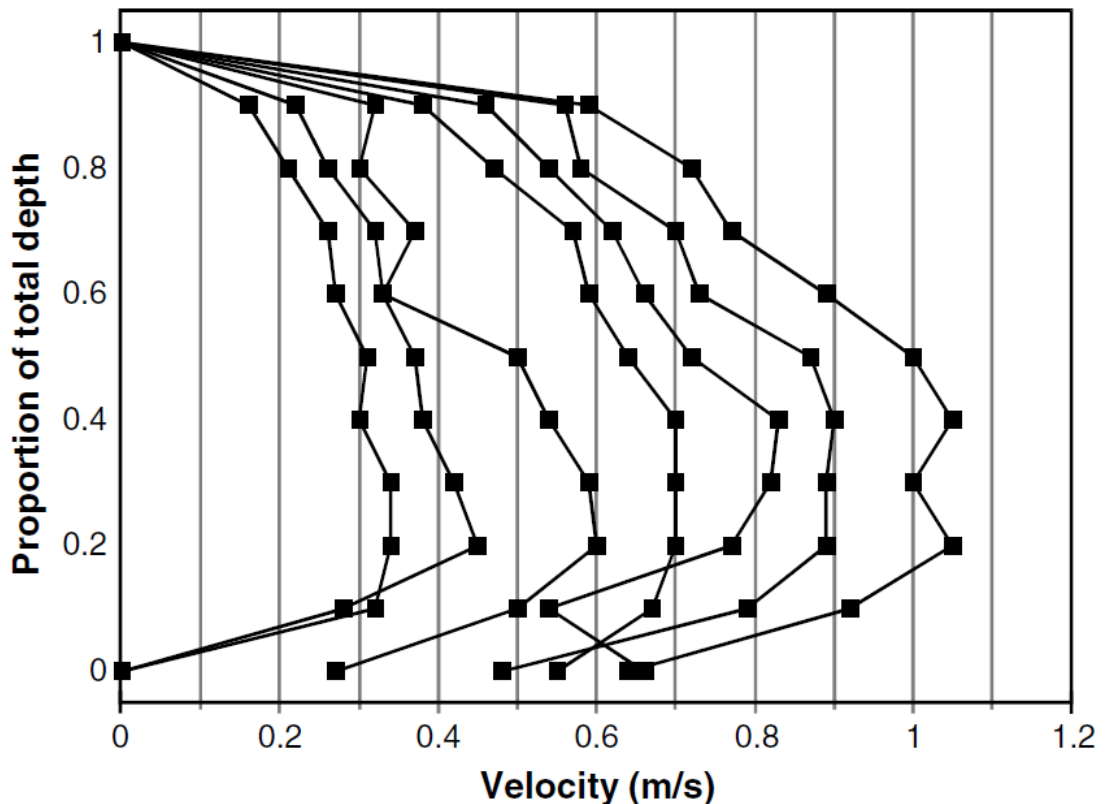


Figure 5-2 From Milburn and Prowse (2002). Repeated measurements of downstream velocity under ice cover. Hay River, Northwest Territories, Canada, Station HR7, April 1-17, 1998. The Parabola shaped mean velocity profile is consistent across discharges.

The distance of the velocity maximum can be moved further toward the bed when there is strong secondary circulation, producing skewed parabola profile of downstream velocity, in addition to the secondary circulation found in meanders (Figure 5-3). It has been found that mean dune size in meander bends are smaller than predicated, as well as compared with straighter sections before/after the bend (Bridge & Jarvis 1977, 1982). Additionally, dune size changes considerably across the channel cross section of meanders and mid channel bars (Jackson 1975b; Dietrich *et al.* 1979; Szupiany *et al.* 2009; Blanckaert 2010).

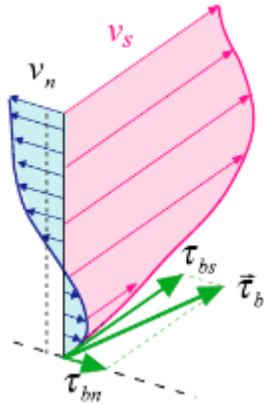


Figure 5-3 From Blanckaert (2011). Idealized downstream (v_s) and cross stream (v_n) velocity profiles in a meander bend. Note the downstream (pink) velocity maximum occurs around 50% flow depth, with a high gradient toward the bed.

In a very different sedimentary environment, submarine density currents (turbidity currents) also have highly skewed downstream velocity profiles with a velocity maximum very close to the bed/moving sediment layer due to being driven via a strong density contrast rather than water surface slope (Figure 5-4).

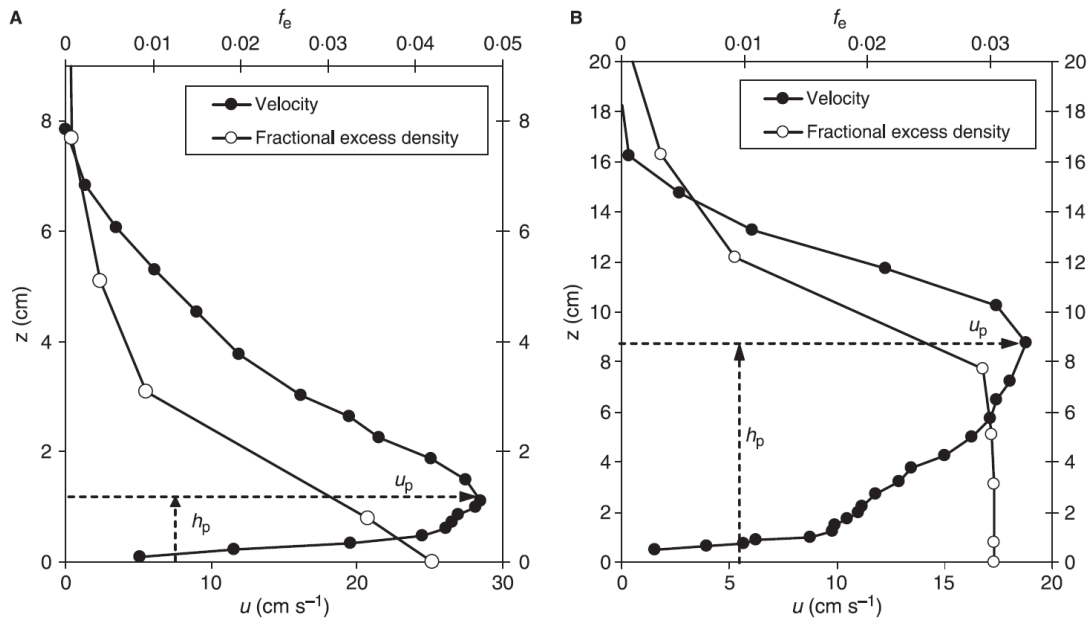


Figure 5-4 From Sequeiros et.al. (2010). Measured velocity profile and sediment densities in a laboratory flume. The height of high sediment density (0.04 in A, 0.03 in B) is strongly linked to the position of the velocity maximum. The consistent sediment density in B effectively shows a large moving sediment layer which reduces in velocity toward 0.

Interestingly, there is a paucity of sedimentary evidence for the existence of dunes in these environments, despite paleo-hydraulic indications of dune forming conditions (Arnott 2010; Sumner *et al.* 2012; Talling *et al.* 2012). This evidence suggests that the processes that define dune scaling to mean flow depth, which is driven through an assumed velocity profile shape, need to be

expanded and adapted to suit a wider range of flows and which implicitly incorporate other processes that affect the velocity profile shape.

A test of the significance of the shape of mean velocity profiles on the scaling of bedforms has yet to be achieved. This Chapter presents a suite of laboratory experiments to examine both the definition and delineation of dune size through the systematic alteration in the shape of the mean downstream velocity profile whilst, critically, maintaining constant depth and depth-averaged velocity (i.e. constant discharge). The response of bedform geometry to these changes in the velocity profile shape and thus bed shear stress were examined in detail.

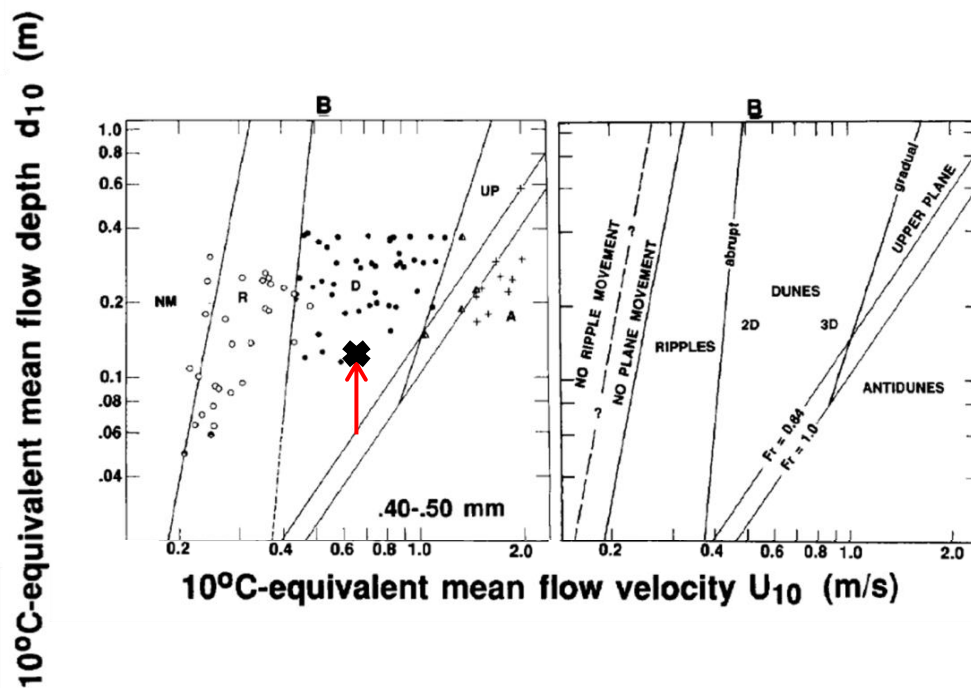


Figure. 5-5: A Plot of bed state stability as defined by mean depth and velocity. Black X and red arrow indicate where in this stability field all the present experiments are positioned (From Southard & Boguchwal, 1990).

5.2.1 Experimental setup

Six laboratory experiments were conducted using a glass-walled Armfield™ recirculating flume 10 m long x 0.3 m wide x 0.5 m deep at the University of Hull, UK (Table 5-1; Fig. 6). The experiments used well sorted, sieved medium coarse sand ($D_{50}=0.55$ mm, Std 0.34, Figure 5-7) that filled the flume to a flat bed level of 85 mm.

As dunes in flumes often scale with flow depth, the running water depth was held as constant as possible across all experiments at 125mm. However some minor variation from this was observed due to the remarkably high form roughness produced in some of the experiments. To ensure that the depth-averaged velocity was equal across all six experiments, a Cole-Parmer 32986-00 ultrasonic pipe flow meter was installed and the flume pump speed control adjusted to maintain a fixed discharge for all experiments of 0.0234 (m^3s^{-1}).

Equilibrium flow conditions were sought for each experiment. The exact flume slope required for equilibrium flow varied between the six experiments and the slope and pump frequency were adjusted iteratively over many hours and many repeated measurements to ensure the mean bed slope, mean water surface slope and flume slope were equal in the test section. To alter the mean velocity profile characteristics, whilst keeping both flow depth and the depth-average velocity (and thus discharge) constant, buoyant foam was placed on the water surface of the entire flume to provide a no-slip condition on the water surface, therefore inducing a flow profile resembling a parabola, similar to those under ice covered flows (Smith & Ettema 1997; Turcotte *et al.* 2011). The foam was rigid but some minor flex from horizontal was seen, particularly around dune crests. Overall the addition of the foam cover reduced small perturbations in the water surface often seen in flume experiments where surface waves are commonly associated with the relatively (compared with field prototypes) higher Froude numbers. Small holes were cut into the foam to allow instrumentation access to the water column.

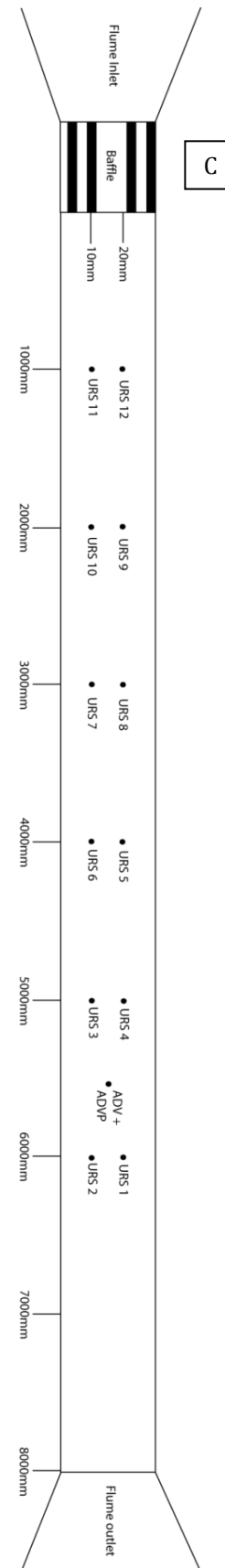
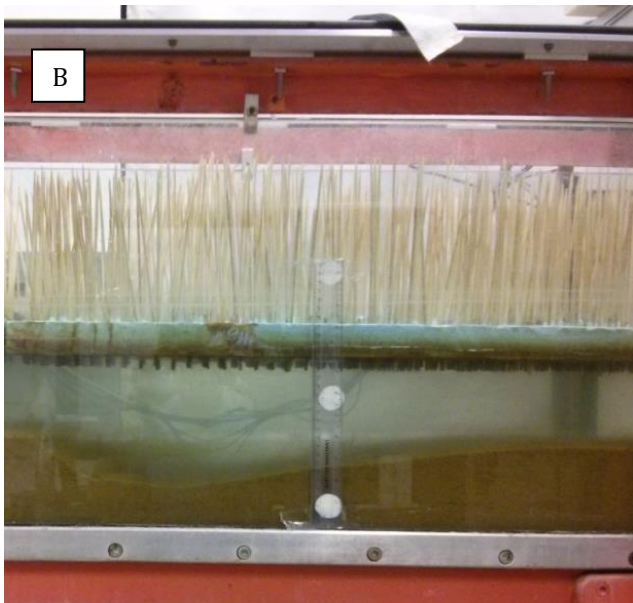


Figure 5-6: A: Drying bed after EXP1. Flow was top to bottom. Picture taken ~6.5m downstream of baffle. B: ~1 hour into the 15mm Spikes condition. Long and tall dunes have already been produced. Suspended sand in the shear layer is quite clear (bottom left). C Flume design (to scale), showing locations of depth sounders and ADV's. Test section is between 5000 mm and 6000 mm.

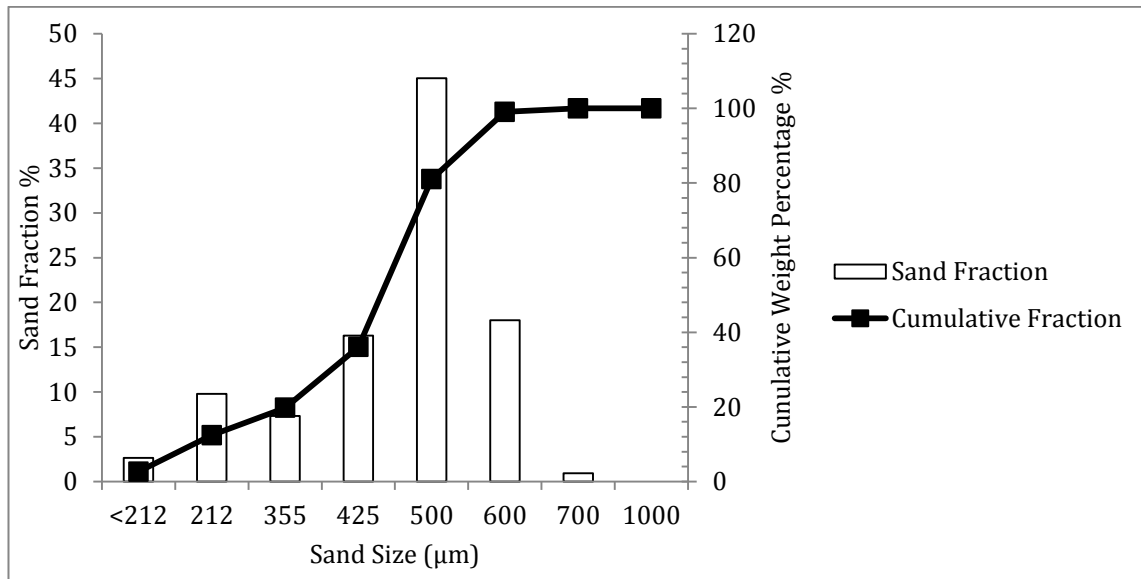


Figure 5-7: Distribution of sand size used in all experiments

Notes	Variable	EXP 1: Open channel	EXP2: Foam Cover	EXP3: 15mm spikes	EXP4: 25mm spikes	EXP5: 30mm spikes	EXP6: 50mm spikes
m^3s^{-1}	Q	0.0234	0.0234	0.0234	0.0234	0.0234	0.0234
ms^{-1}	U Depth Av	0.65	0.65	0.65	0.65	0.65	0.65
°c	Temperature	23.65	25.63	25.6	22.6	21.03	21
	Froude	0.58	0.58	0.58	0.56	0.59	0.59
	Reynolds	82899	84227	82567	88248	79855	80021
test section average (m)	Depth	0.128	0.13	0.127	0.136	0.1231	0.123
mm	Grain Diameter d_{50}	0.47	0.47	0.47	0.47	0.47	0.47
mm	Grain Diameter d_{90}	0.53	0.53	0.53	0.53	0.53	0.53
m	Velocity Max To Mbl	0.089	0.074	0.04947	0.046	0.036	0.021
%	Velocity Max / Depth*100	67.2	57.1	38.9	34.1	29.1	17.3
m/m	Water Surface Slope	0.0025	0.006	0.0115	0.0124	0.0153	0.0229
$=\rho * g * R * S$	Bed Shear Stress	0.96	7.61	14.31	16.61	18.01	27.74
Sqrt (ghS)	Shear Velocity U^*	0.056	0.048	0.066	0.071	0.074	0.091
m	Bedform Height	0.026	0.052	0.062	0.065	0.046	0.003
m	Bedform Length	0.533333	0.58	0.75	0.8		0.921
steepness	H/L	0.049	0.118	0.083	0.081		0.003
$D * U^* / \nu$	Grain Reynolds 1	26.5	22.4	30.7	33.1	35	43
$U^* * ks / \nu$	Grain Reynolds 2	76	106	119	126		25

The open-channel uniform flow condition required a flume slope of 0.0025 % (1/400) to account for the energy gradient produced from flow resistance from boundaries, grain roughness and form roughness (Einstien & Barbarossa 1952; Simons & Richardson 1962). The addition of roughness via the foam cover required a larger flume slope (0.0059% ~2.35x higher than the open channel slope) for uniform flow conditions, particularly as initial experiments showed that dunes often scoured to the bed in the downstream half of the flume channel. The next four conditions used several thousand wooden spikes (see Table 5.1) placed through the polystyrene foam in a regular 2x2 cm grid across the whole flume length and width to ensure uniformity of imposed roughness. These skewers intruded into the water from above at four lengths for five separate experiments. The skewers intruded the flow by 15 mm, 25 mm 30 mm, and 50 mm long across give experiments (EXP 3, 4, 5, and 6 respectively) and required correspondingly higher flume slope to achieve an equilibrium uniform flow (Table 4-1). Measurements of bed slope were facilitated though twelve calibrated (relative to datum) Seatek® URS depth sounders positioned in pairs at meter intervals along the flume channel from 1 m to 6 m downstream of the inflow baffle. These are accurate to ± 2 mm. Initially, side wall measurements of average bed level were undertaken at half meter increments in the test section (4-6m) to check the depth sounding results. Average water surface slope was measured through numerous repeat observations of calibrated sidewall mounted scales, accurate to ± 2 mm.

Once uniform flow and equilibrium bedform conditions had been achieved, three-dimensional flow velocities and bedform transects were measured for 4 hours by a downward-looking profiling ADV (Nortek Vectrino II®) at 5.5 m downstream of the flume baffle and 2.5 m upstream of the downstream end. The ADV measures a region 4 cm to 7.5 cm away from the probe head. Four consecutive 1 hour profiles were recorded (example in Figure 5-8), each 1 cm lower than the previous measurement to ensure measurement of a large proportion of the mean velocity profile. Simultaneous velocity measurements above the ADV measurement region (with a blanking distance of 4 cm + submerged probe head), a sideward facing ADV (Nortek Vectrino+ ®) was positioned above the ADV, with a vertical separation in sampling volumes of 4 cm. The side looking ADV facilitated measurement of flow velocities

considerably closer to the flow surface and therefore enabled collection across a considerably larger proportion of the velocity profile (Figure 5-8).

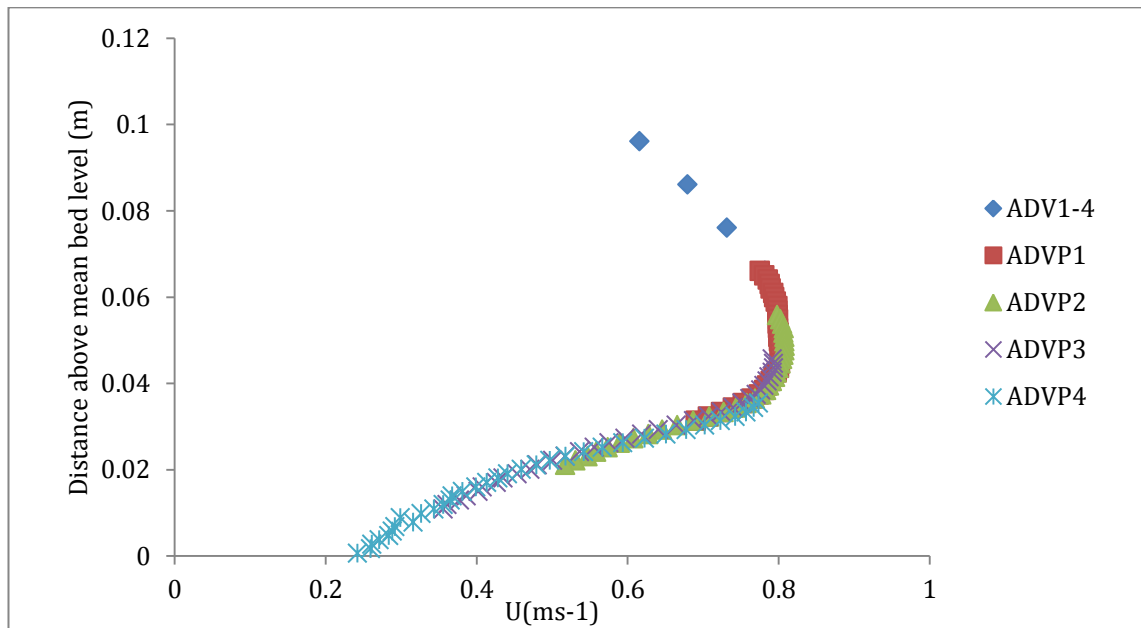


Figure 5-8: Example of the location of velocity measurements above the mean bed level. Data from EXP3.

The ADVP was set to a velocity range of 2.2 ms^{-1} as considerable phase wrapping occurred when set at the highest single-pulse-repetition frequency of 1.2 ms^{-1} . Although the high velocity range of 2.2 ms^{-1} is well above the maximum instantaneous velocity anticipated, setting a high velocity range reduced the difference in pulse frequencies and therefore amount of signal speckle from interface in the dual-frequency-repetition mode (Holleman & Beekhuis, 2003; Joe & May 2003). The potential loss of velocity resolution at the higher velocity range was considered preferential over the significant amount of phase wrapping found at the highest single pulse repetition frequency. Three-dimensional velocities were measured at this range for every condition, at a frequency of 100 Hz, cell size of 1 mm with the full calibrated range of 35 mm. The depth sounder function was enabled at 3hz which provided an additional bottom profile though the test section as well as providing profiles of amplitude of return from the 10Mz pulse which was well attenuated by the suspended sand.

The sideward facing ADV (Nortek Vectrino +) was set with a horizontal velocity range of 1.88 ms^{-1} and a vertical velocity range of 0.54 ms^{-1} which was the closest range to the actual velocities without producing velocity wrapping. To reduce signal noise, a transmit length of 2.4 mm with a sampling volume of 9.1 mm and

a sampling rate of 100 Hz were used to increase the amount of instrument averaging.

The final equilibrium 3D bed was measured with a laser scanner mounted on a traverse above the flume after the 4 hours of measurements were complete and the flume carefully drained. As short as time as possible between the end of profiling and pump disengagement was pursued so that the 3D bed scan was representative of the bed during flow measurements. This time was always <30 seconds. Scan measurements were made at a vertical and horizontal resolution of 2 mm. DEMs were calibrated by scanning a talcum powder covered still water surface at zero flume slope. This procedure found that the traverse system has a vertical undulation of ~6 mm across the flume length which was corrected in the final DEMs.

5.2.2 Post Processing of data

Suspended sand was able to obscure the bed in the URS depth sounder data and therefore post-processing of the data was required. Filtering of all zero values (from poor return voltages in the URS depth sounders) and spikes (due to suspended sand) in the data was undertaken. Noise was detected by setting a maximum threshold of the gradient between two pings of the bed return. This threshold was set to 0.5 times the standard deviation of each time series and was applied across a three bin wide moving window. Figure 5-9 shows the original signal (blue) and the filtered signal (red) for the end of the 15 mm spikes condition. This run had the tallest bedforms and significant amounts of suspended sand, the effect on the depth sounder output can be seen in the lee sides of the dunes in Figure 5-9A, (arrows), this is an extreme example. This high suspended sand concentration does sometimes obscure the lee side bed, e.g. at ~69500 seconds. Removed values are replaced with linearly interpolated values with a radius of 2 cells each side. Visual inspection (e.g. Figure 5-9) of the filtered and replaced data was undertaken to decide if further removal of noise was needed. This type of filter has the advantage that the crest and trough heights are unchanged, whereas standard smoothing techniques would reduce the amplitude of the bedforms.

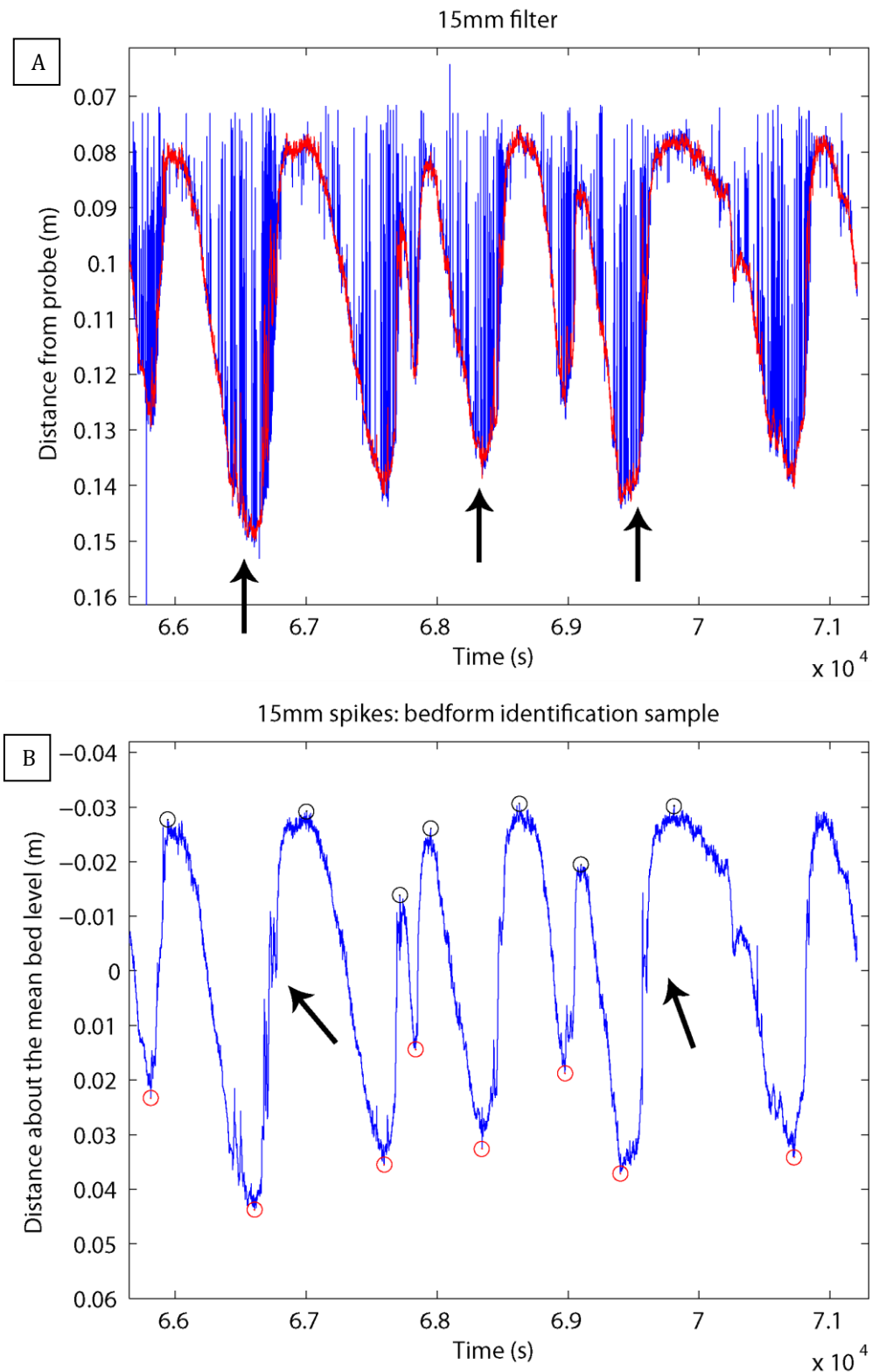


Figure 5-9: Depth sounder filtering and bedform identification. A: blue line are the original data, red lines the interpolated bed after filtering. Bedforms are moving right to left. Substantial suspended sand can obscure the dune trough (black arrows). B: shows that the large spikes original timeseries are not recognized due to minimum dune size thresholds on the bedform identification algorithm. Black circles are dune crests and Red circles are troughs.

Once filtering of the depth sounder data was complete, detection of bedforms and measurement of bedform geometry was undertaken using the following steps:

1. Removal of mean bed level
2. Zero crossings located (crossings <3 bins wide removed)
3. Location of zero crossings used to define windows to search for the maximum and minimum (crest and trough) locations in the timeseries and distance about the mean bed level.
4. Bedform height and translation calculated from zero crossing pairs (not from collective crest and trough means)

Figure 5-10 shows the crests (black circles) and trough (red circles) locations found a section of the 15 mm long spikes run measured by the ADVP. Small zero crossings, particularly on lee slopes, can be seen in Figure 5-10, e.g. ~69500 seconds, and are not identified as bedforms due to the removal of small zero crossings with a median filter prior to step 3.

Post processing of the velocities measured from the sideward looking ADV (Nortec Vectrino+) was conducted using the WinADV software (Wahl, 2000). Velocities with a minimum instantaneous signal to noise ratio of <5 or correlation <70% were removed and not replaced. De-spiking used the method of Goring & Nikora (2002). The combined filters removed no more than 15% of the data for each 1 hour collection run. ADVP data processing was conducted using the procedure of Thomas & McLellend (in review), which provided a correlation and de-spike filter for the velocity data using the methods of Goring and Nikora (2002) and Wahl (2003) for spike filtering, Wahl (2003) and (Cea *et al.* 2007) for velocity co-variance filtering and (Zedel & Hay, 2010) for the correlation with a confidence interval of 0.001. Removed vectors were replaced by linearly interpolated values based upon the local mean value of unfiltered vectors.

5.2.3 Flume conditions

Figure 5-10 displays the water surface slope for all conditions, with all but the open channel condition having very consistent slopes with $r^2 > 90$.

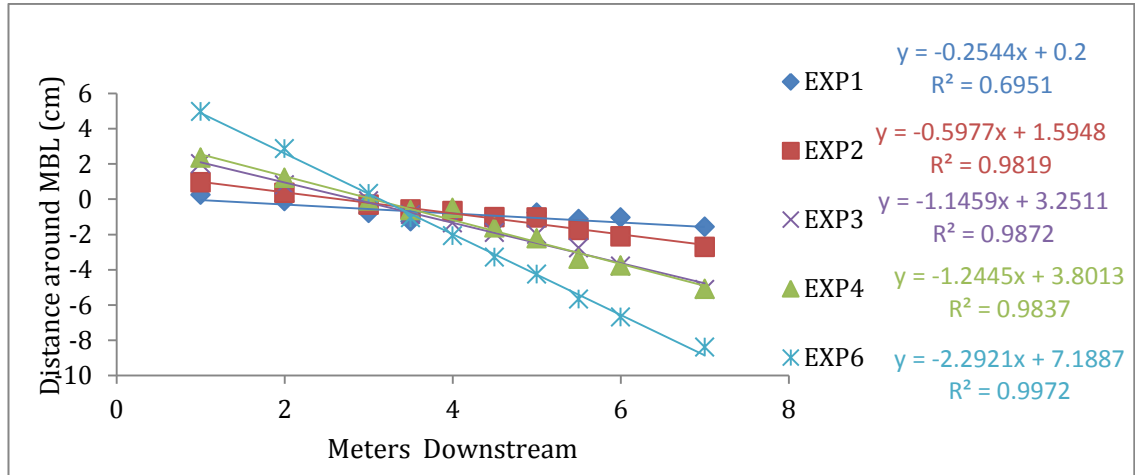


Figure 5-10: Water surface slope, or energy slope, measured for all equilibrium conditions.

The test section water surface equilibrium is displayed in Figure 5-11. Here the flume slope and running water surface slope are compared. The exact start of the test section varied by ~ 0.5 m due to different bedform size development along the flume (Figure 5-13).

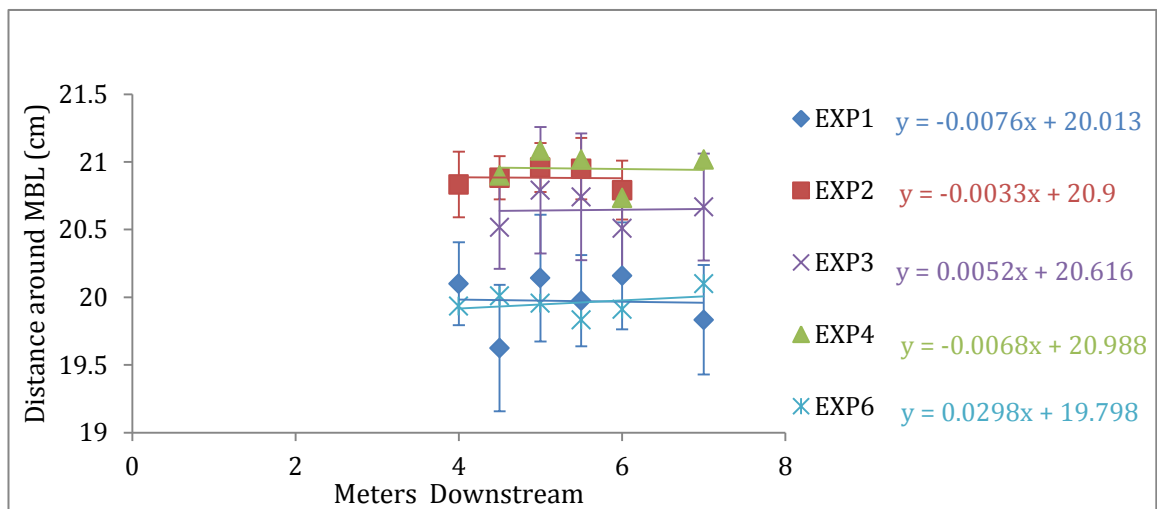


Figure 5-11: Test section equilibrium. Water surface slope was aimed as close as possible to the flume slope to ensure equilibrium flow conditions in the test section.

Bed shear stress was calculated using the water surface slope (Figure 5-10), then using the reach averaged method of calculating bed shear stress (τ_B):

$$\tau_B = \rho g y_o S \quad (5.1)$$

Where ρ =water density, g = acceleration due to gravity, y_o =depth and S =slope. Figure 5-12 compares this calculated bed shear stress to the distance between the downstream velocity maximum and mean bed level, with an excellent match. Therefore, despite the large variation in mean downstream velocity profile shape, the height of maximum downstream velocity above a surface still scaled linearly with bed shear stress and these two variables are therefore freely interchangeable.

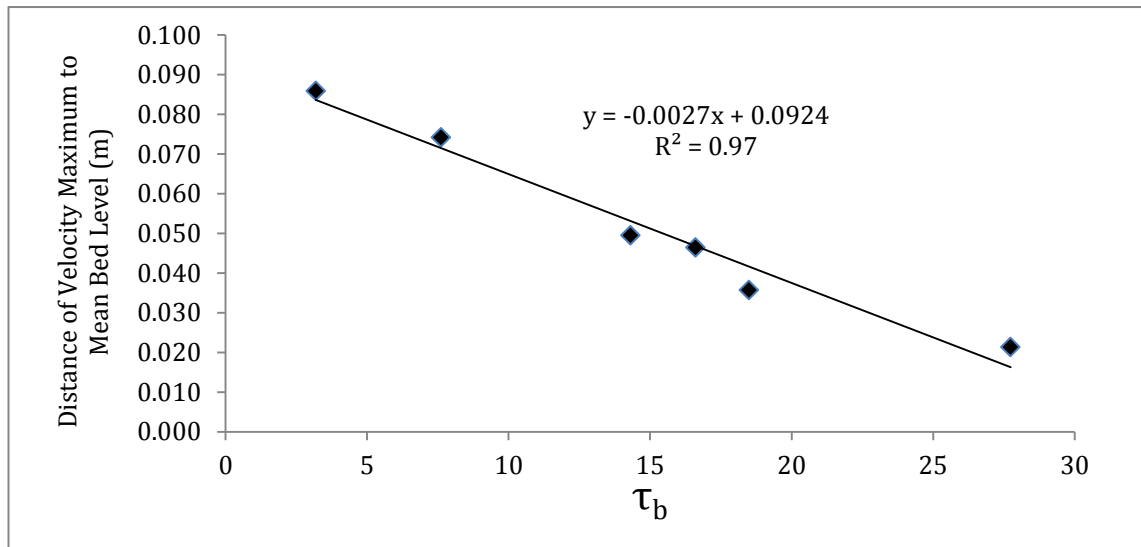


Figure 5-12: Bed shear stress τ_b (using depth slope product) plotted against the distance of downstream velocity maximum to mean bed level for all conditions, showing excellent agreement.

In EXP1, the open channel condition, a consistent mean dune height is found by ~ 4 m downstream of the flume inlet. The conditions with extra roughness added (EXP2-5) all display consistent increases in mean dune height with distance away from the flume baffle (Figure 5-13). The EXP5 condition presents very low amplitude bedforms along the flume length with a maximum variation (relative to maximum mean height) of 38%, which is approximately half that of the other conditions.

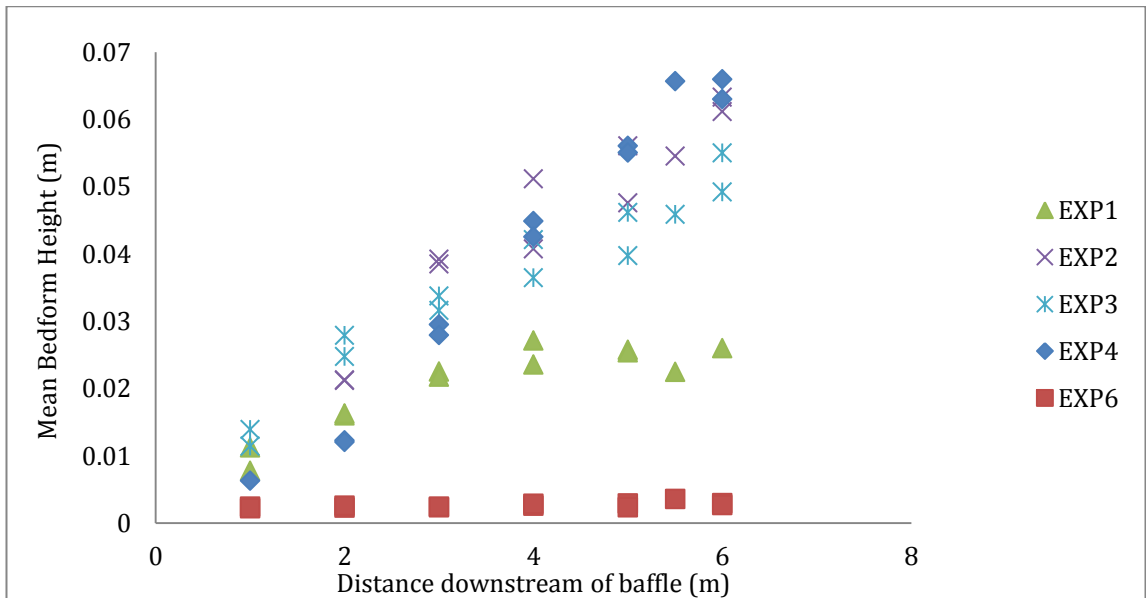


Figure 5-13 Mean bedform height (m) along the flume measured from URS and Vectrino II depth soundings. Note, there are two data points per meter as two URS depth sounders were positioned at each meter, Figure 5-7. The data at 5.5 m are from the Vectrino II. EXP5 data are omitted.

Figure 5-14 displays the mean bedform translation rates across 6 m of the flume. EXP1 has again achieved spatial equilibrium in translation rate at ~4 m downstream of the inlet, whilst for the higher roughness conditions the translation rates were found to be less spatially consistent.

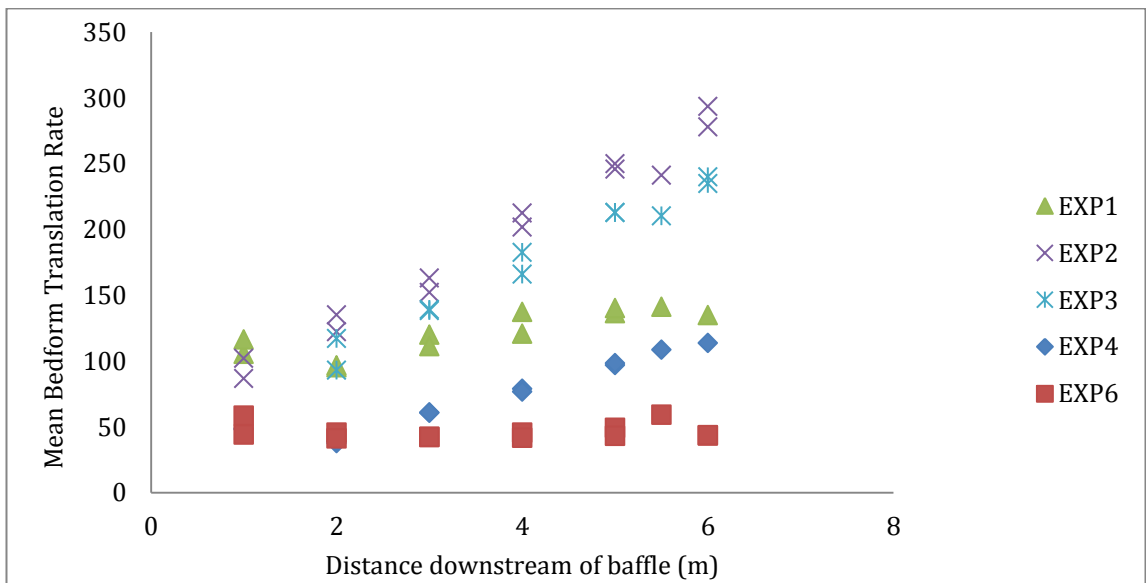


Figure 5-14 The mean bedform translation rate along the flume as measured by the URS depth sounders (whole intervals) and Vectrino II (5.5m only). EXP5 data are omitted.

Figures 5-13 to 5-14 indicate that the larger bedforms produced in the higher roughness conditions were reproduced with the spatial consistency of EXP1. Therefore the equilibrium bed state was defined as when the bed slope (as defined by mean bed level) in the test section was flat and the bedform size at each location was consistent in time. This approach ensured that the natural variation in sediment transport rate and migration rate produced by dunes was temporally consistent over a minimum of 1 hour.

5.3 Results

Figure 5-15 displays the mean downstream velocity profile shapes produced from the additional increases in surface roughness. The added surface roughness has clearly altered the shape of the mean downstream velocity profile, with the highest roughness condition (EXP6) producing a profile shape very similar to that of turbidity currents (Figure 5-4). The velocity maximum for EXP1 (Open Channel condition) is measured at 0.086 m (67% of depth) above the mean bed level; EXP2 = 0.074 m (57%), EXP3 = 0.049 m (39%), EXP4 = 0.046 m (34%), EXP5 = 0.036 m (29%) and EXP6 Spikes = 0.021 m (17.3%) above mean bed level. Interestingly, aside from the EXP6 condition, the gradient of mean downstream velocity below ~0.03 m changes little with the successive increase in surface roughness and lower maximum velocity condition.

The shape of the velocity profiles only begins to show a clear parabola for EXP3 the 15 mm Condition; this indicates that the foam cover had very little roughness compared to the form roughness produced from the dunes below. The flow shear produced by the foam roughness was not measured due to its proximity to the foam and the natural variation in water level with the passing of dunes.

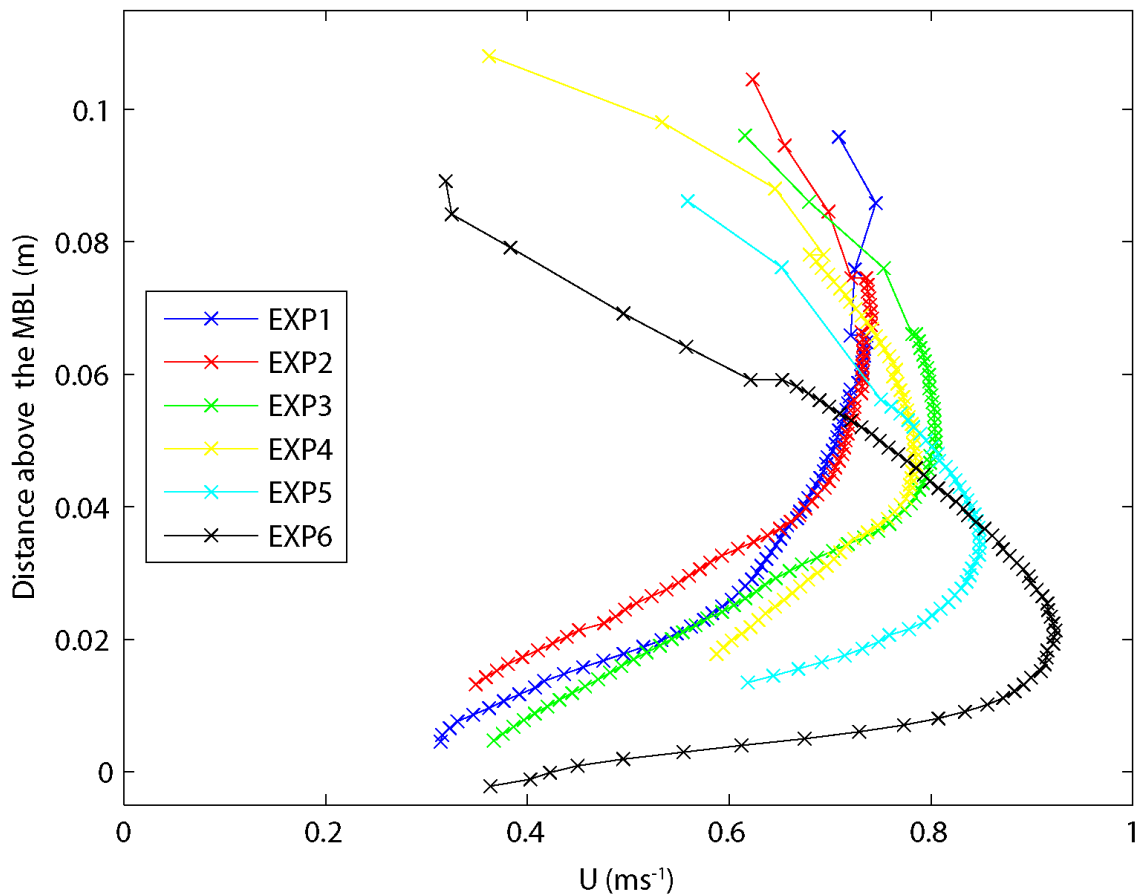


Figure 5-15 displays the mean downstream velocity profiles for all conditions. The mean downstream velocity profile is the calculated from the four mean profile locations (Figure 8). The concurrent ADV measurements at the top of the profiles are then added to produce the final mean profile, covering >80% of the flow depth. Profiles do not reach near the free/top surface at $\sim 0.125\text{m}$ as flow compression of $\sim 0.02\text{m}$ was common over the dunes- thereby restricting velocity measurement close to the flow top/free surface.

Figure 5-16 displays the final bed state for five experimental conditions as scanned by the flume mounted laser scanner. EXP5 was not scanned as an equilibrium condition was impossible to measure for a bed state in flux between two different stable conditions of dunes and an upper stage plane bed (USPB). Some of the results (velocity profiles and bedform heights) from EXP5 are shown here for completeness, but a separate results section that highlights this interesting condition follows the main results here. The successive increase in bed shear stress produced several changes in dune morphology and bed state. Firstly, the introduction of the buoyant foam cover reduced dune crestline three-dimensionality considerably (Figure 5-16), with EXP2-4 having almost no dune three-dimensionality at all. EXP2 also showed a reduction in the number of smaller, superimposed bedforms compared to EXP1. A consistent change from EXP1 to EXP4 is the increase in trough scours and crest height around the

mean bed level at ~ 5.5 m downstream. Alongside this, the length of dunes increases consistently though the higher bed shear stress conditions EXP2-4.

The downstream development of dune size also varies with the induced bed shear stress through the experiments. The largest bedforms for EXP1-4 are all located around 5.5 meters downstream. As Figure 5-13 showed, EXP1 reaches bedform size stability at around 4-5 m downstream. The final bed state scans show that this state is probably due to a lack of lee side scour, which is only seen to scour deeply at around 5.5 m in Figure 5-16. The higher bed shear stress conditions (EXP2-4) all show deeper trough scours from 2 m downstream onwards. EXP2 displays consistent, classically triangular, bedforms sizes that gradually change into humpback dunes at ~ 5 m, downstream. EXP3 shows humpback dunes existing as high up the flume at 3 m. EXP4 shows a different bedform development along the flume length. Here the upstream end of the flume is almost an upper stage plane bed, with small symmetrical undulations similar to that shown at the downstream end of EXP6. Downstream of this is rapid development of dunes. As Figure 5-13 showed, the bedform heights measured here are smaller than even the EXP1 dunes, until ~ 3 m when the mean bedform height increases rapidly.

EXP6 displays an upper stage plane bed (USPB) condition. Sand waves of mm scale amplitude and meter scale length are visible across the whole flume. There are shorter and higher amplitude undulating bedforms at the furthest point downstream; this is a result of a slow build-up of sediment hysteresis circulating around the flume over the ~ 6 hours of running bedform the flume was stopped and drained.

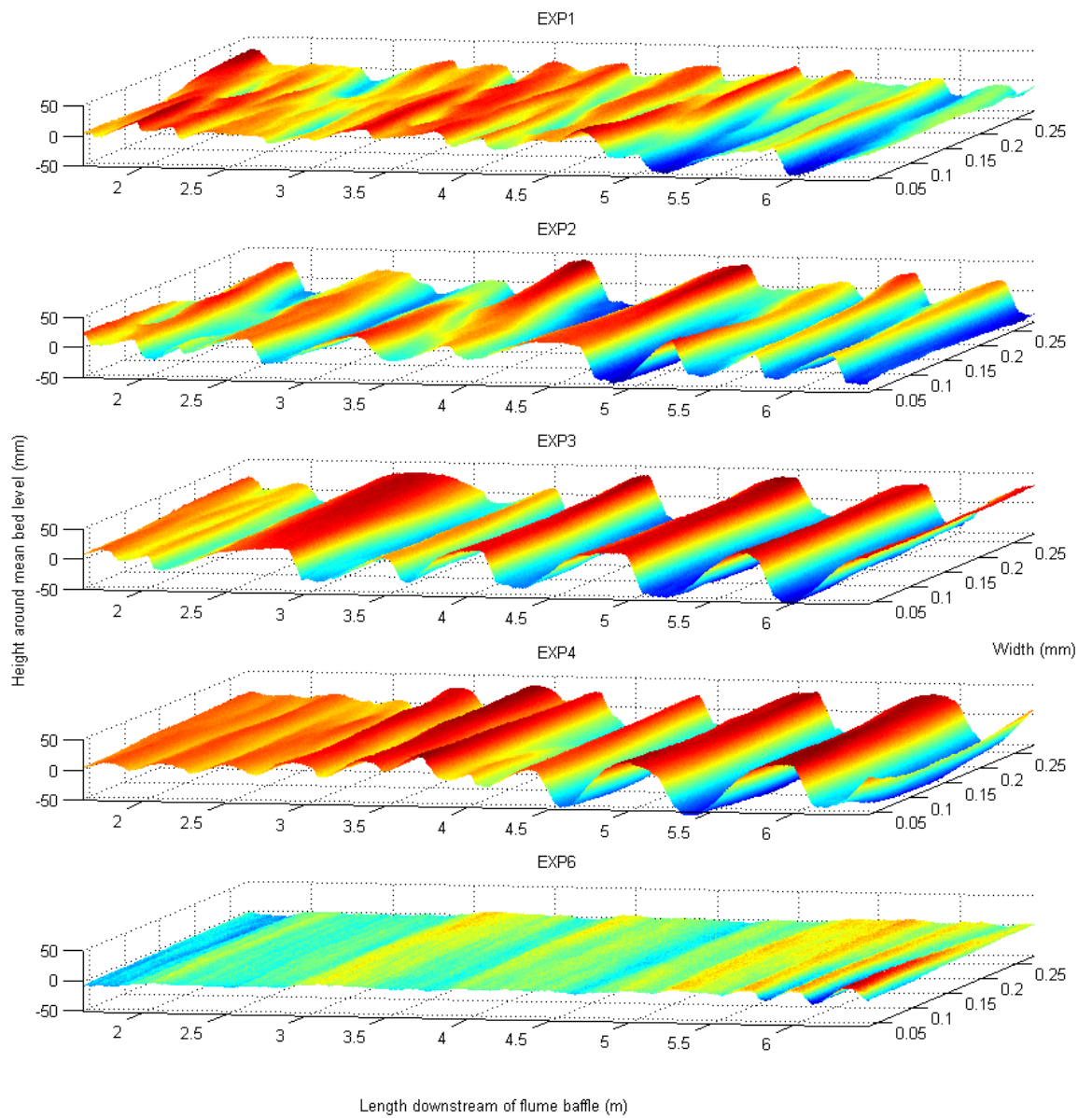


Figure 5-16: Bed Scans for all conditions, test sections are ~4.5-6.5 m downstream of the flume baffle. Colour of the bed is the elevation (vertical axis), scaled to each condition.

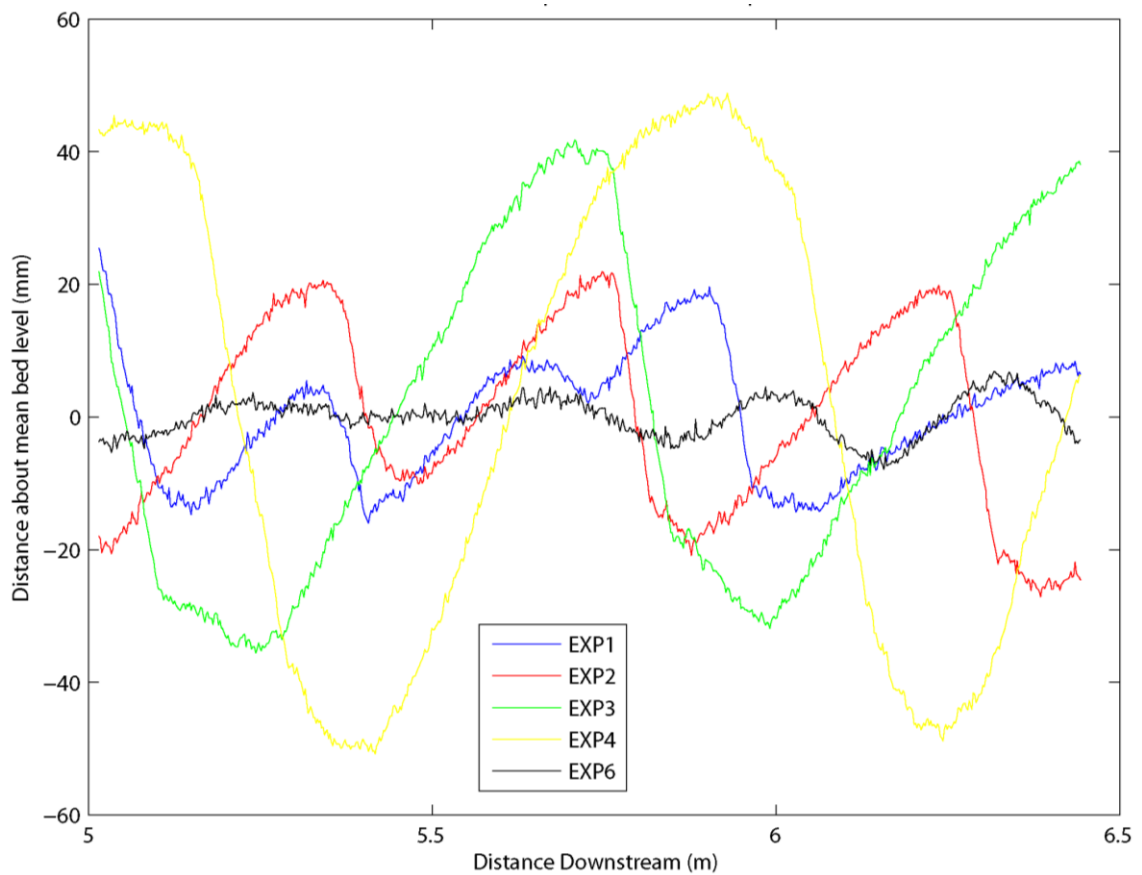


Figure 5-17: Centreline profiles of the equilibrium bed scans (Figure 5-14) in the test section area. Note the vertical exaggeration.

Figure 5-17 displays the centreline (150 mm) laser scan profile of the flume test section. Here, the 2D shape of the final test section bedforms is revealed, and the length of final equilibrium bedforms can also be quantified (Table 4-1, Figure 5-16). The height and length of the dunes increase considerably from EXP1 up to the ESP4 condition, with test section dune wavelengths changing from 0.53 m in EXP1 to 0.8 m in EXP4 (Table 4-1). To measure more than one bedform wavelength for EXP6, the entire scan length along the centreline was used as these bedforms were considerably longer than the dune test section, and Figure 5-16 indicates that these bed waves did not change in size further up or downstream of the flume inlet.

Normalising mean downstream velocity by the shear velocity (Figure 5-18), calculated using the reach averaged method, with the test section water surface slope, is sufficient to collapse the dune forming conditions from 0.03 m to the mean bed level. The gradient for each profile of U/u^* collapses from $\sim 0.3m$. Experiments EXP1 and EXP3 most clearly collapse near the bed, despite the

large change in bedform amplitude between these conditions., this indicates how strong an effect the grain roughness has on the velocity profiles across a wide range of bedform amplitudes. Measurement of the velocity profile for the EXP6 condition was considerably closer to the boundary as this bed shear stress level produced an upper stage plane bed. The absence of dunes meant that the ADVP probe head could be positioned closer to the mean bed level without risk of burial or damage to the instrument from the bedload layer. Consequently the normalised mean downstream velocity from EXP6, is the closest to u^* for all conditions (Figure 5-18). The lack of dunes in EXP6 produces a relationship between U/u^* that reaches comparable magnitude to the dune conditions at a lower elevation above the mean bed level. This result is due to the above mean bed level elevation of the long stoss slopes of the dunes.

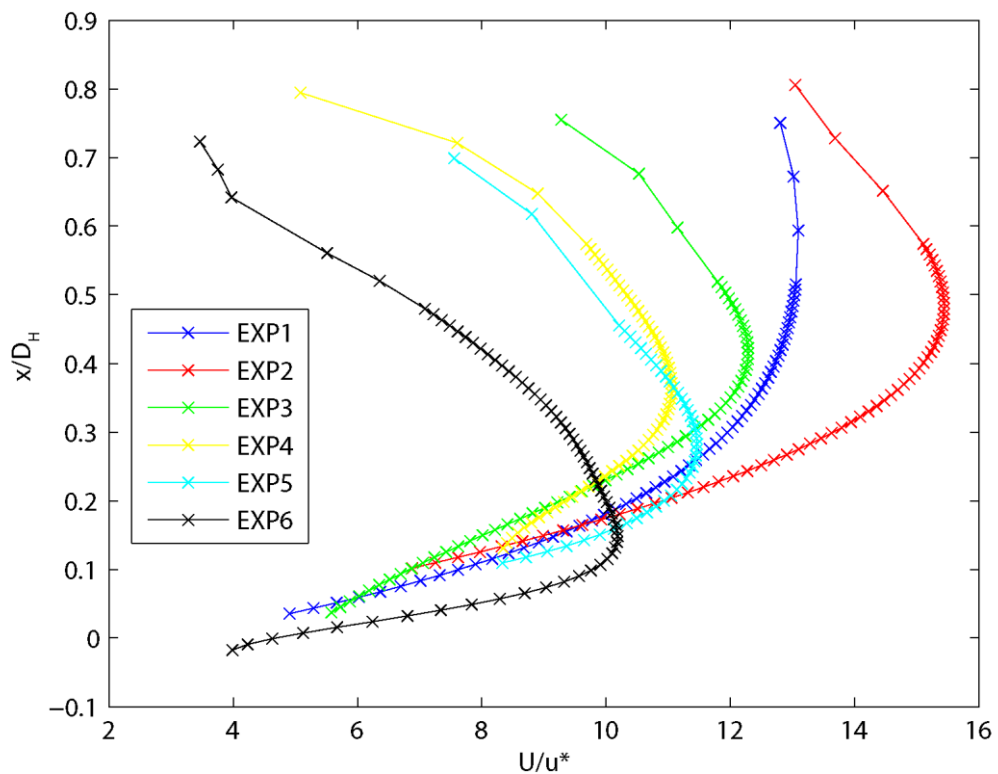


Figure 5-18 Mean downstream velocity is normalised by the shear velocity and plotted against distance above the mean bed level for each condition.

Figure 5-19A displays the relationship between flow depth and distance of the downstream velocity maximum to mean bed level for all conditions. Despite the variation in flow depth that did occur no consistent relationship is apparent (Figure 5-19A). This result reiterates the independence of bed shear stress and depth produced in these experiments. Figure 5-19B displays the strong non-

linear relationship between bed shear stress and dune height. Bedform height is lowest at the two extremes of bed shear stress and largest in the middle of the range of bed shear stresses measured. The EXP3 conditions produced the highest dune heights. The dune heights produced during the EXP4 and 5 conditions are progressively smaller in contrast to the EXP3 dune heights, but for a considerably different velocity profile shape and bed shear stress. The USPB parts of EXP5 and all of EXP6 produced very low amplitude bedforms (Figure 5-19B). The range of bedforms produced (represented as error bars of 1 standard deviation) across these conditions changes considerably. For EXP1 the distribution of bedform heights is strongly skewed to the mean value, whilst for EXP2 there is a near normal distribution of dune heights. At the peak mean bedform height (EXP3) the mean is skewed toward the higher bedform height. For EXP 4 and 5 (dune only) the gradually reducing mean height is skewed to the smaller sizes, and then near normally. Overall, the range of dune heights increases until the USPB is formed.

Figure 5-19C displays a strong linear relationship between bedform length and bed shear stress. Bedform length was as measured in the test section scans (Figure 5-17) for the dune forming conditions. Distributions of dune lengths are comparatively normally distributed, compared with the variation seen in dune height. There is no general trend in the range of standard deviation with higher bed shear stress. Measurement of dune length in the EXP6 condition used the entire scan length as the low amplitude bed waves seen in Figure 5-16 are on the order of 1 m. The short, higher amplitude, bed waves seen at the downstream end of the EXP6 condition scan were not representative of the USPB for the majority of the time measured (see bed elevation distribution in Figure 5-20 and Figure 5-13). There was no scan of the non-equilibrium EXP5 condition and therefore no bedform wavelengths are reported here for that condition.

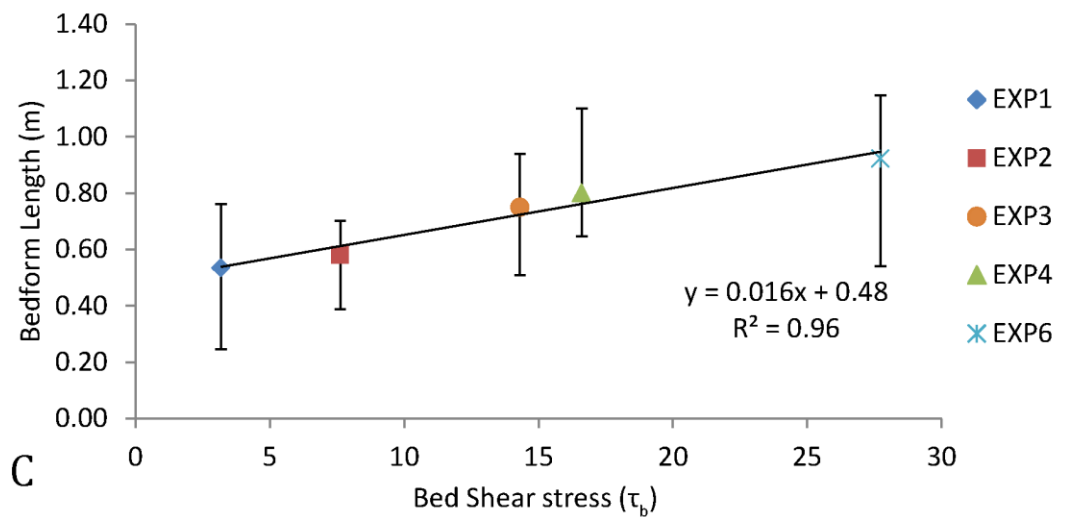
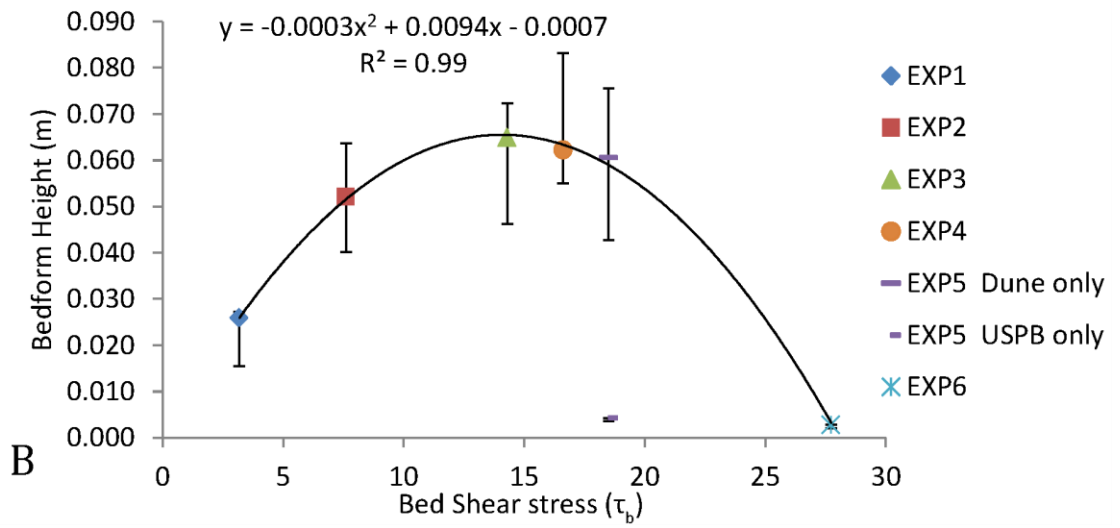
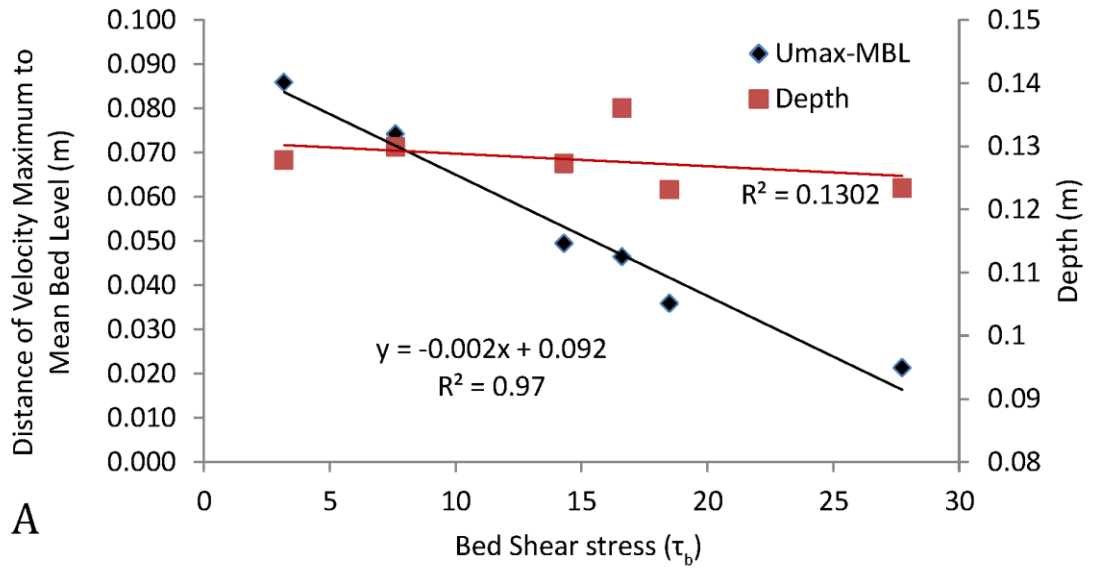


Figure 5-19 Mean bedform geometries and flow conditions.

A: The lack of relationship between depth and bed shear stress, whilst velocity maximum to mean bed level distance correlates well with bed shear stress. B: The parabolic relationship of bedform height and distance of velocity max to mean bed level. The EXP5 conditions are represented by two data points, dune only height (--) and USPB only bedform heights(-), the polynomial regression line does not include the USPB EXP5 data. C: Bedform length and bed shear stress. EXP5 Spikes is not represented here due to no bedform scan measurement of this non-equilibrium condition. Error bars represent one standard deviation around the mean, for (C) the error bars are more a measurement of bedform translation than real wavelength.

To better understand the relationship between bedform morphology and bed shear stress (and velocity profile shape) seen above, both the mean velocity profile and distribution of elevations measured from the Vectrino II depth sounder are combined into Figure 5-20 for all conditions. Several key observations can be made:

1. The bimodal distribution of bed elevations for the open channel condition reveals a clear crest height (~ 0.01) with the distribution skewed toward the crest. The second peak in the distribution is below the mean bed level (~ 0.01 m) and likely indicates a consistent trough height.
2. The addition of a foam top surface dramatically changes the shape of the bedforms; this produces a very flat distribution that is nearly 2x more spread than the open channel condition and has no obvious peak at all.
3. The addition of more surface roughness (EXP3) procures a clear peak in bed level at ~ 0.03 m but no peak below the mean bed level. The maximum scour level has increased again but the maximum crest height has not increased above that seen in the EXP2 condition.
4. For the EXP4 condition the peak in bed return around the crest is broader but less high overall than the EXP3 Condition. Trough scour depths have increased again but the overall distribution is fairly similar to that in the EXP3.
5. The EXP5 condition produces a very different distribution. The large peak at ~ 0.01 m indicates the level of the upper stage plane bed, which is higher than 0 due to the trough scour and crests from the dunes altering the mean bed level. The small peak at ~ 0.025 m is likely representative of the dune crests and upper stoss slopes and is very similar in height to the peak in the EXP3.

6. The bed elevation histogram for the EXP6 condition is a near perfect Gaussian distribution of very small range compared with the dune forming flows.

The velocity profile shapes show in Figure 5-20 all start to increase in gradient when the profiles start to overlap with the bed histograms. The distance between the velocity maximum (large red X's) and the bedform crests shortens for each additional increase in top surface roughness, rather than force the crest away from the velocity maximum, indicating that there is a strong dune stabilising process present. The EXP6 velocity profile has changed dramatically due to the high surface roughness and comparative lack of bedform form resistance.

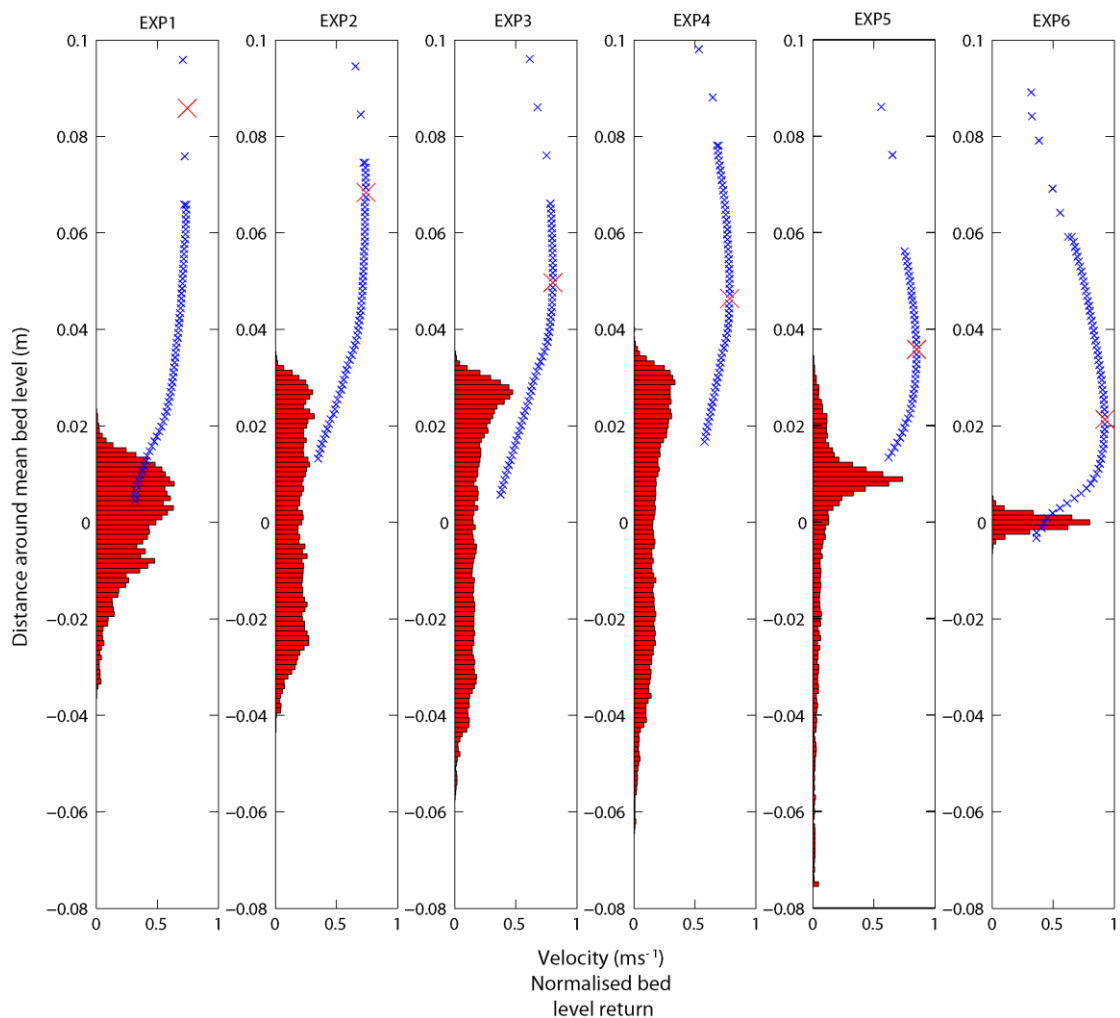


Figure 5-20. Normalised histograms of bed elevation from the Vectrino II depth sounder and mean downstream velocity profiles all plotted around each runs' mean bed level. Large red X's indicate the location of the maximum downstream velocity for each condition. Closely spaced blue x's are Vectrino II measurements, Sparsely spaced x's are the Vectrino+ measurements.

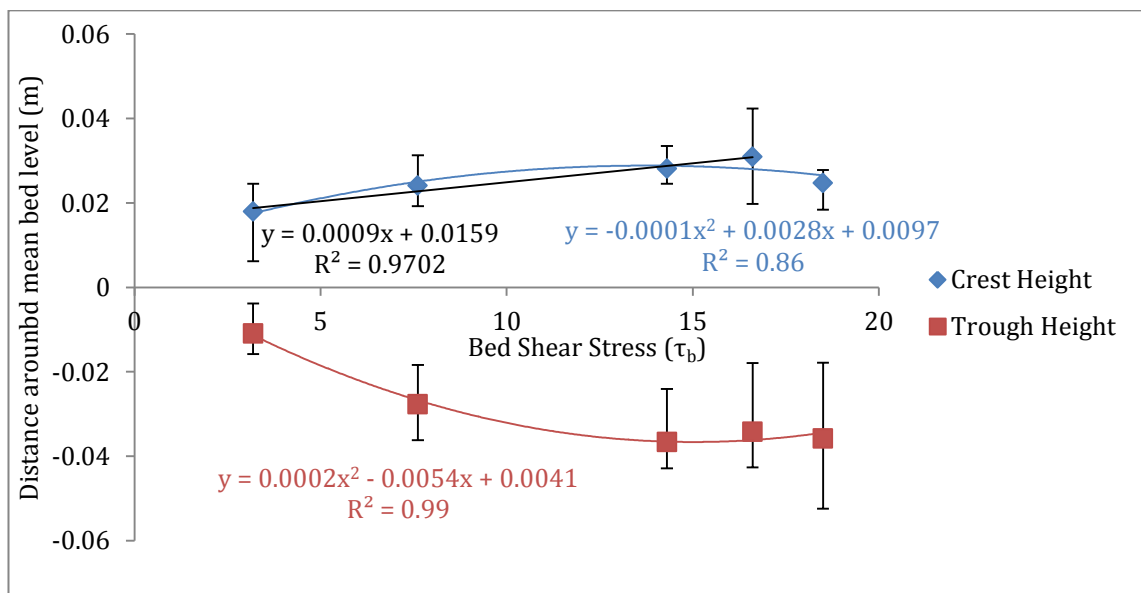


Figure 5-21 Mean elevation of crest and trough heights, as detected by the bedform detection methods, around the mean bed level for all dune forming conditions (EXP 5 condition here is displaying dunes, EXP6 bed waves are not included in these mean calculations).

To look at the relationship between velocity profile shape, bed shear stress and bedform geometry, Figure 5-21 displays the mean elevation of dune crest and trough locations around the mean bed level for all dune forming conditions (EXP1-5) against bed shear stress. Overall both features have a parabolic trend due to the presence of EXP5. However dune height elevation above mean bed level is a very strong linear relationship ($r^2=0.97$) between EXP1 and EXP4. The slopes of these fits indicate that the trough elevation moves away from the mean bed level at nearly twice the rate of that of the mean crest height with an increase in bed shear stress. This relationship is less clear in the histograms shown in Figure 5-20, probably as the amount of time spent at the crest and trough is small compared with the size of the long stoss slope, and therefore identification of crest and trough in those histograms is hindered somewhat by bedform stoss shape and length. Nevertheless, by ~ 15 Pascals, mean dune height, crest and trough elevation are essentially constant. The standard deviation of these features increases with bed shear stress until upper stage plane beds are produced. Therefore, the bed shear stress required to produce the largest dune for this grain size has been reached. It is notable that it takes an increase in bed shear stress of a further 15 Pascals to produce a stable USPB;

this indicates that the processes controlling dune formation and stability is very strong.

The bedforms shown in the bed scan (Figure 5-16) show that the changes in surface roughness affected the development of the bedform sizes. To investigate this further, bedform height (Figure 5-13) and translation rate (Figure 5-14) along the whole flume are plotted.

Figure 5-22 shows the mean bedform heights of Figure 5-13 against the mean bedform translation rates of Figure 5-14 (thus using all the depth sounding data along the flume). The height and translation rate of the bedforms in EXP1 are relatively clustered when compared with the high roughness conditions of the EXP2-4 conditions, but still show a trend for higher dunes equating to a longer translation rate. The EXP2 condition elongates this trend to higher dune heights and higher translation rates and displays the longest translation rates found. The EXP3 condition has slightly higher mean dune height across the flume, but lower translation rates. The EXP4 condition displays higher maximum mean bedform heights again but this higher roughness produces considerably shorter translation rates. When the bed state reached upper stage plane bed (EXP6) the translation rates and bedform heights cluster with some of the shorter bedform data points of EXP4. These points from EXP4 are located near the flume entrance (Figure 5-6) and therefore indicate that an upper stage plane bed did exist for a section of the EXP4 condition; this interpretation is reinforced in the bed scan of the final bed state (Figure 5-16).

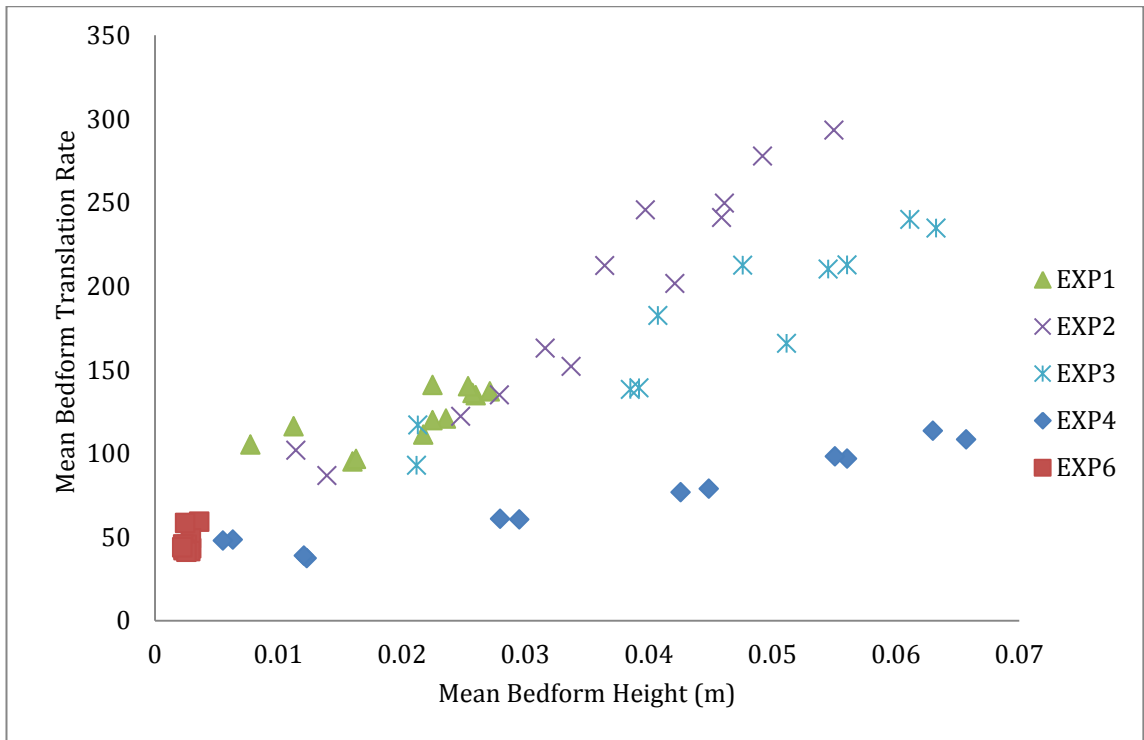


Figure 5-22 Mean bedform height and translation rate, using all depth sounder data across the flume length. The EXP5 conditions data are not plotted.

The migration rate of the bedforms in the test section was calculated by:

$$M_r = \frac{\lambda \text{ (test section scan)}}{\text{Translation Rate (at 5.5m)}} \quad (5.2)$$

where λ is the mean bedform wavelength. The total sediment transport rate (g_B) was calculated by

$$g_B = M_r W D_h \quad (5.3)$$

where W is the flume width and D_h is the mean dune height at 5.5 m.

The migration rate shows a good ($R^2 = 0.84$) exponential relationship with bed shear stress (Figure 5-23). When mean dune height and flume width is included to produce a total sediment transport rate, however, the relationship breaks down (Figure 5-24) due to the low amplitude of upper stage plane bed waves in EXP6 and the high amount of sediment transport transported in suspension, which is not detected. Ignoring the USPB condition data point produces a good ($R^2 = 0.92$) exponential relationship between bed shear stress and total sediment transport rate for the dune forming conditions only (Figure 5-26).

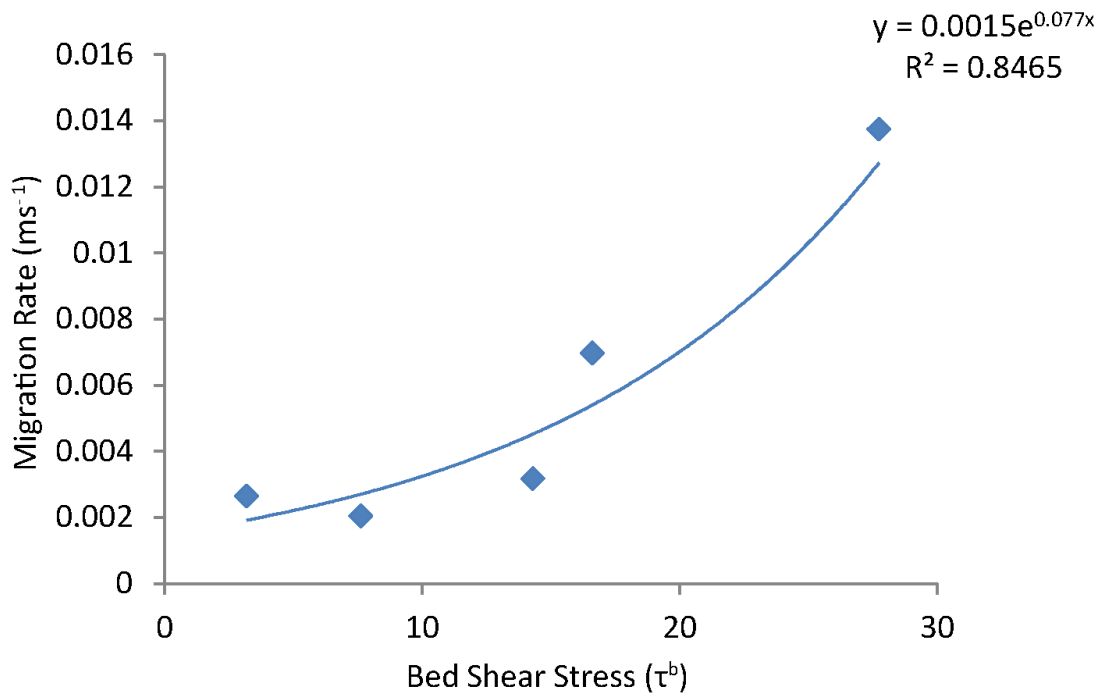


Figure 5-23. Mean Migration rate for each condition (except EXP5 due to a lack of bedform wavelength measurement) vs bed shear stress

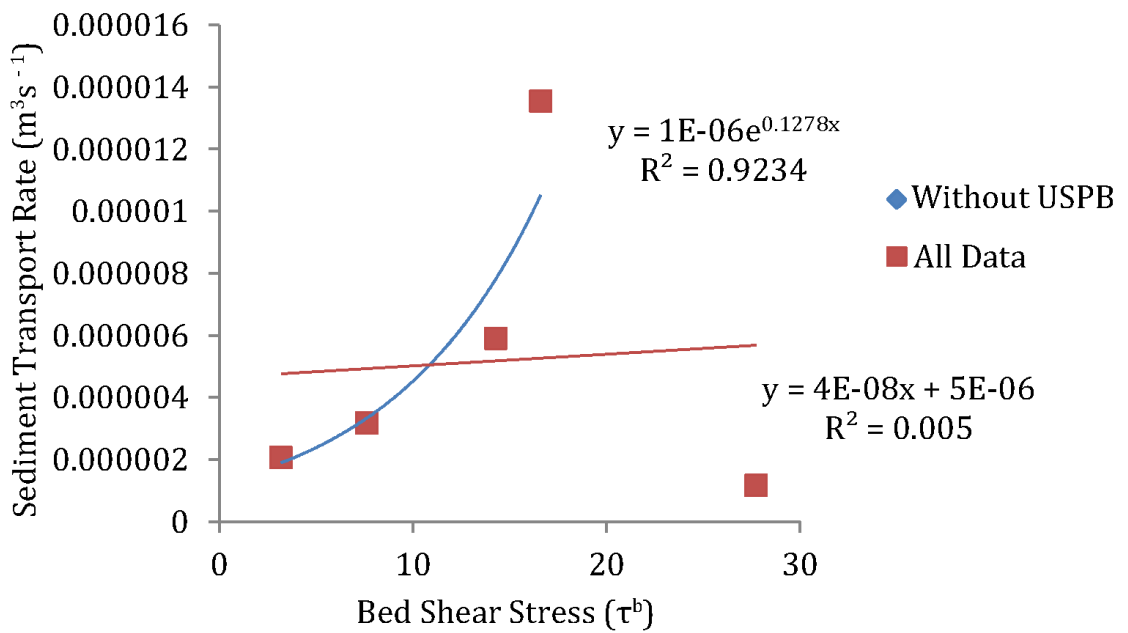


Figure 5-24 The mean sediment transport rate for each condition (except EXP5 due to a lack of bedform wavelength measurement) vs bed shear stress. When the upper stage plane bed condition (EXP6) is omitted a good exponential relationship is produced.

5.3.2 Intermittent Dune-Upper Stage Plane Bed

The intermittent transition from dunes to upper stage plane bed conditions in EXP5 was typified by a large lee face migrating downstream with no bedform development upstream of it. The re-formation of dunes was near spontaneous, but initial bed waves could be seen to build up on the upper stage plane bed prior to dune development (Figure 5-25). These pulses are seen at 1 m downstream of the inlet (Figure 5-25) and are of the scale of 1 cm either side of the mean bed level. The dunes form throughout the flume when there is an increase in depth on the order of 1 cm below the mean bed level at 1 m downstream (e.g. ~4000 seconds Figure 5-25). A subsequent decrease in flow depth by ~1 cm above the mean bed level at 1 m downstream prevents any further development of new bedforms at the upstream end of the flume and this lack of new bedforms eventually propagates through the flume channel. The recurrence interval for dune formation is on the order of ~2.7 to 3 minutes and was quite consistent over several hours.

Suspended sediment was not directly measured; however the vertical profiles (1 mm resolution) of depth sounder amplitudes from the Vectrino II can provide an indication of the level of suspended sand as the acoustic signal was well attenuated by suspended sand (e.g. Figure 5-9). Figure 5-26 displays vertical profiles (Figure 5-26A) and the depth-averaged (Figure 5-26B) amplitude of the depth sounder return during a dune to USPB and back to dune regime. This figure highlights the relatively higher magnitude of acoustic return through the depth profile when dunes are present. Indeed, the depth-averaged amplitude gradually increases when dunes are present (200-1000 seconds) and, when the bed state transitions to USPB, the depth averaged amplitude of return decreases (1000-1600 seconds).

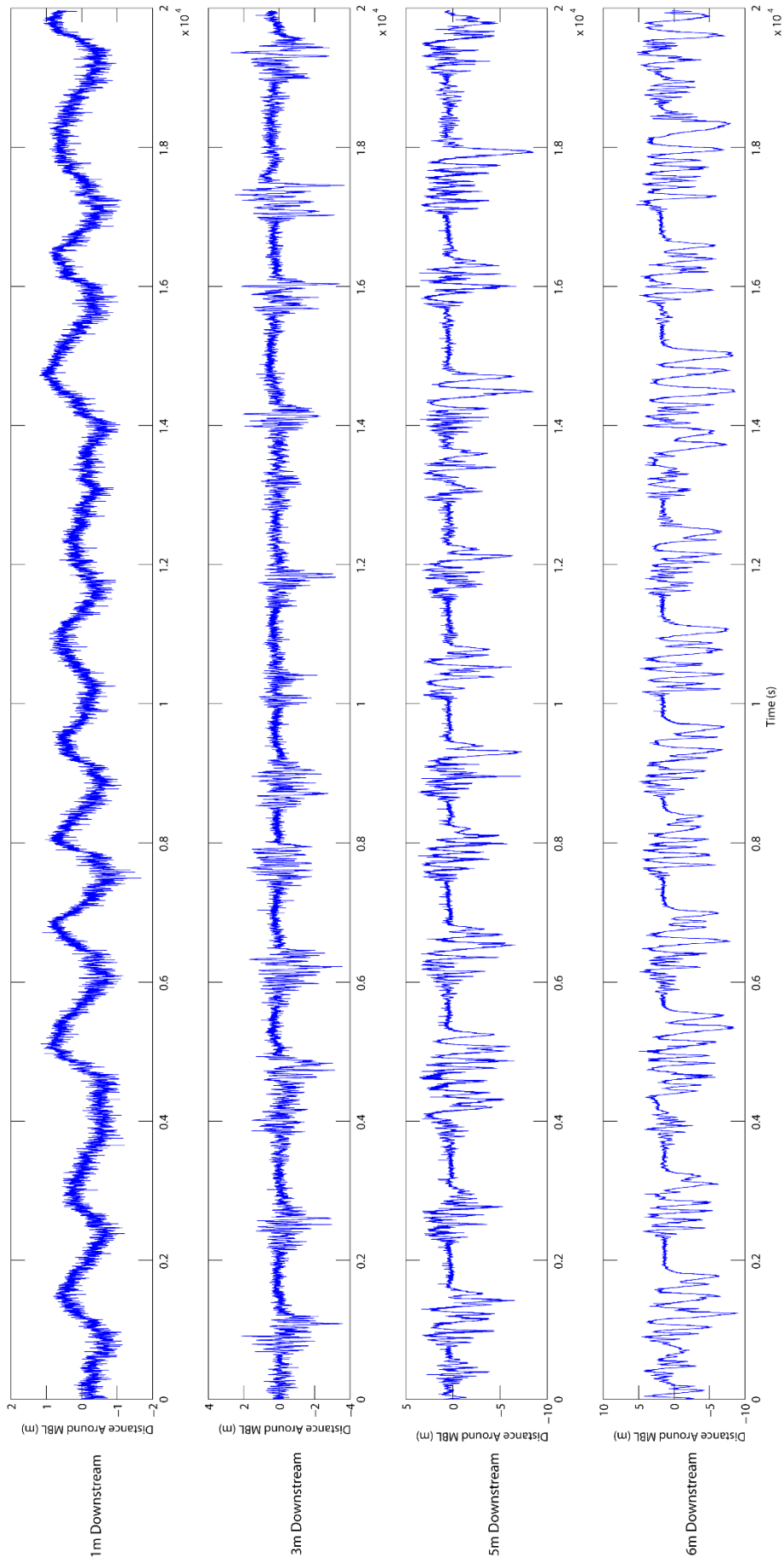


Figure 5-25 The bed level elevation around the mean bed level for ~30 minutes for four locations along the flume, 1 m downstream (URS12), 3 m downstream (URS8), 5 m downstream (URS8) and 6 m downstream (URS1). For URS probe location see Figure 5-7.

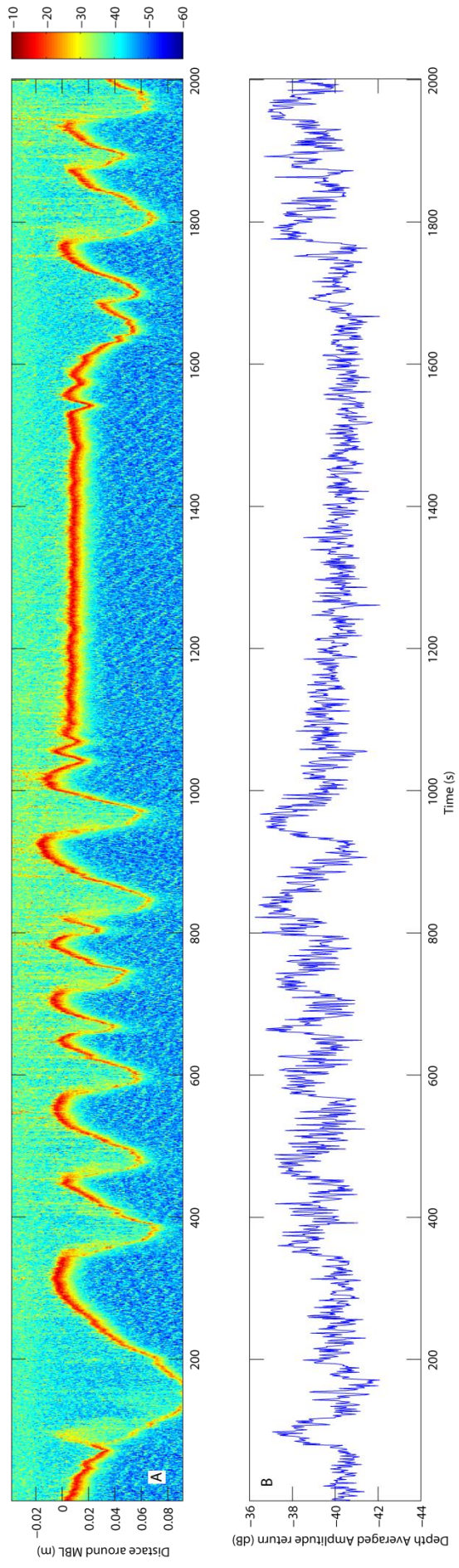


Figure 5-26 A, amplitude of depth sounder return through a dune-USPB-Dune transition. Colour contours in Decibels. B displays the depth averaged dampitude of depth sounder return for the A. The figure demonstrates that higher suspended sediment (inferred from amplitude) is a consequence of dunes. USPB produces little suspended sediment. Flow right to left.

5.4 Discussion

Equilibrium river dune scaling has generally been attributed, via theory and numerous experiments, over the past 60 years to flow depth (Simons *et al.* 1960; Yalin 1964, 1977; Guy *et al.* 1966; Raudkivi 1966; Simons & Richardson 1966; Allen 1968; Allen 1982; Engelund & Fredsoe 1982; Fredsoe 1982; McLean 1990). Yet a detailed process understanding of the interactions and mutual adjustments between flow, sediment transport and bedform properties is still lacking, due to the complexity of these closely interrelated variables producing a dynamic equilibrium that is perturbed with any change in boundary conditions.

The present research aims to examine the complexity and dependent relationships via removing flow depth and discharge as important variables in the system. This objective was achieved by the addition of roughness to the flow surface via a foam cover and wooden skewers whilst maintaining a consistent mean flow depth and discharge. The added surface roughness changed the mean velocity profile shape (Figure 5-15) toward that of rivers with an ice cover (Demers *et al.* 2011), strong secondary circulation or submarine density currents. It was found that the distance of the point of maximum mean downstream velocity to mean bed level scaled linearly to bed shear stress calculated using the water surface slope in the test section (Figure 5-12). This outcome shows a clear dependency between velocity profile shape and bed shear stress, rather than flow depth (Figure 5-12).

In the fluvial environment, most rivers are not straight and therefore do not fully develop an fully developed open channel flow structure, nor equilibrium flow. Examples include meanders, which have strong secondary circulation effects on the mean velocity profile (Bridge & Jarvis 1977; Dietrich *et al.* 1979) and around mid-channel bars (Szupiany *et al.* 2009). In polar latitudes winter ice cover has been found to change mean velocity profiles toward that of parabolas (e.g. Prowse & Ferrick 2002; Ettema & Daly 2004; Demers *et al.* 2011). Smith & Ettema (1997) found that ice covered rivers produce longer, slower dunes with deep trough scour. EXP2, the Foam Cover condition, is the closest to an ice covered river, and the low migration rate, longer bedform wavelength (when compared to EXP1) and considerably higher amplitude of

bedform matches Smith & Ettema (1997)'s findings. The lack of a similarly large increase dune wavelength is very likely due to the increase in flow depth that accompanied formation of fixed ice (Smith & Ettema, 1997), whilst flow depth remained largely constant (± 5 mm) in the present study. Alternatively, the effects of form roughness from the ice cover may well be higher than the foam used in this study (Demers *et al.*, 2013).

5.4.1 Dune scaling

Dune height was found to scale well with bed shear stress. Figure 5-20B shows this parabolic trend which is also reported in Yalin (1977) and Allen (1982) (Figure 5-27). Importantly, this trend has been found by varying only bed shear stress though redistribution of flow momentum in the velocity profile, rather than water depth or discharge as in Guy *et al.* (1966). This difference makes the results comparable and applicable to flows without the log-normal mean velocity profiles found in fully developed open channel flows (Nezu & Nakagawa 1993).

The level of detail in the measurement of the bed through time presented herein allows for interrogation of the formative processes behind the change in the two key areas that produce dune height; the crest and trough with the variation in bed shear stress produced. Figure 5-20 displayed the normalised histograms and mean downstream velocity profiles together around the same mean bed level. Here, several important changes are revealed when the velocity profile shape changes. The addition of the foam cover (EXP2) changes the distribution of bed elevations dramatically, with a considerably greater range produced and a less clear peak for crest and trough elevations. Figure 5-21 shows that the mean crest height continues to increase above the mean bed level with the further increases in bed shear stress. However, this rate is half that found for the increase in trough scour distance from the mean bed level. The increase in bedform length seen in Figure 5-19C indicates that the lack of a peak in crest height in the bed histograms is due to the longer and flatter stoss slope that essentially produces a more kurtosed bed elevation histogram.

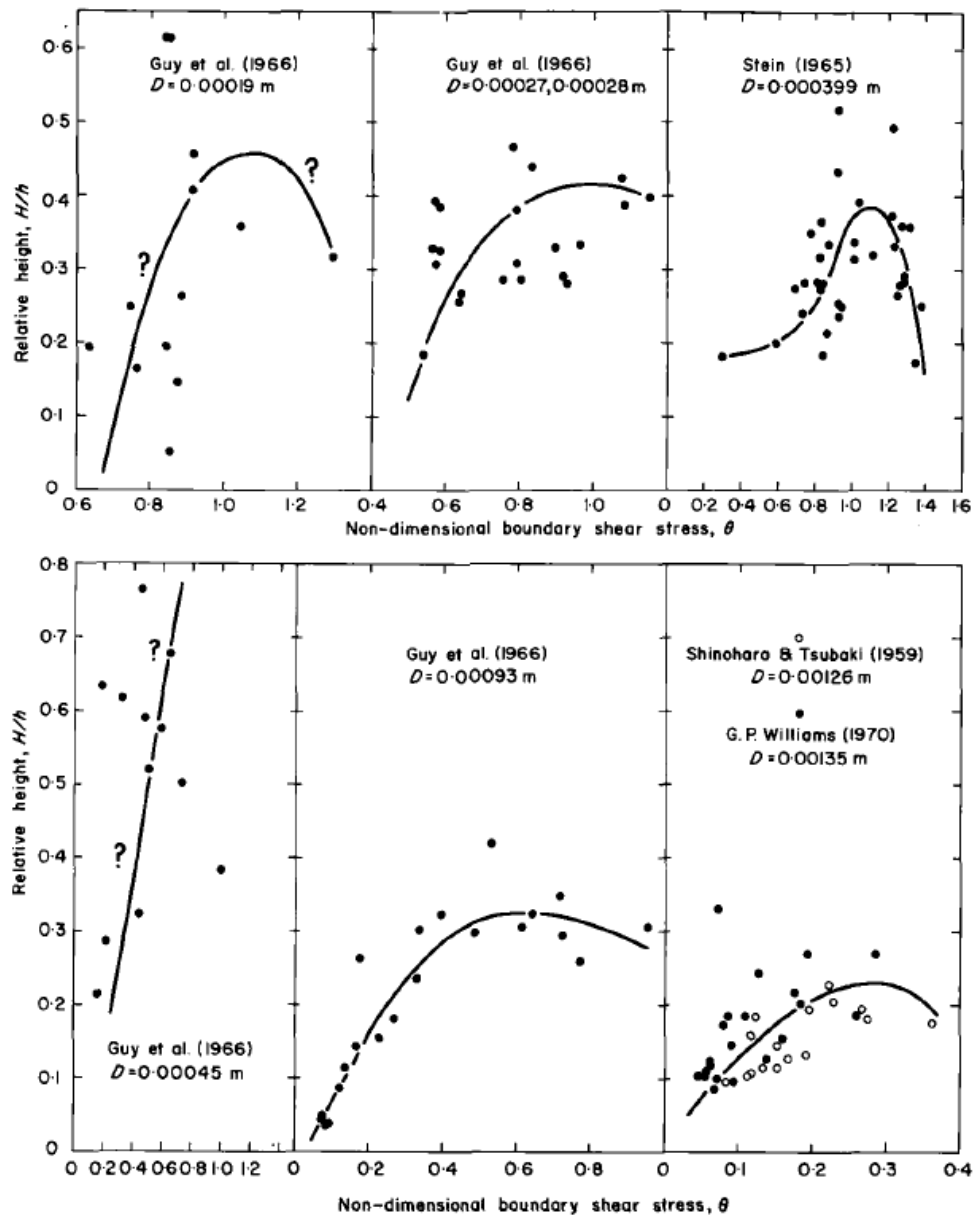


Figure 5-27. Group mean height relative to mean water depth as a function under equilibrium conditions of the non-dimensional boundary shear stress and sediment calibre. Stress corrected for the wall effects by procedure of G.P. Williams (1970) (From Allen (1982, page 334)).

It is interpreted that the bed shear stress was increased sufficiently at the dune crests to effectively wash-out the dunes and produce upper stage plane beds along the dune stoss and crests just from the addition of the foam cover, therefore producing humpback dunes similar to those seen in flood conditions (Carling *et al.*, 2000a) and under ice (Smith & Ettema 1997). With the higher levels of roughness and higher bed shear stress in EXP 3&4 three other changes are produced; 1) deeper troughs, 2) longer, less steep, dunes, and 3) higher

migration rates. The additional increases in dune height are mostly accommodated by increasing trough depth away from the mean bed level. The lower rate of increase in dune crest height above the mean bed level with increasing bed shear stress is likely due to higher sediment transport rate accommodating any excess bed shear stress - a condition commonly defined in one-dimensional sediment continuity equations (Exner 1920).

There is another key difference in the distribution of bed heights at the crest. The open channel condition (EXP1) shows a comparatively gradual decline in bed revelation counts toward the mean bed level from of the peak at 0.01 m. This finding indicates that the maximum crest height above the mean bed level is considerably lower in the open channel condition and is also rarely reached. The small dunes EXP1 are likely due to secondary circulation produced from the flume side walls. These effects are well known to reduce dune height in narrow flumes (Williams 1970). The addition of a no-slip boundary at the free surface is very likely to have changed the nature of secondary circulation from classic open channel flow to pipe/square duct flow type secondary circulation (e.g. Rice *et al.*, 2012; Rice, 2013).

The bed shear stress wall correction procedure of Williams (1970) was produced using equation 4.3;

$$\text{Wall Corrected Bed Shear stress} = W^2/W^2 + 0.055d \quad (5.4)$$

where W =flume width and d =flow depth. This correction produced changes to the calculated bed shear stress (from depth-slope product, Table 4-1) of the order of <0.01% and were thus disregarded. The width to depth ratio of the flume (0.30/0.125=2.4) is just outside the region where wall effects have no measurable effect on dune size (Williams 1970). Unfortunately, Williams (1970) only has correction factors for flow depths of 15 cm and 9 cm depths (Figure 5-28), so a dune height adjustment factor of 1.3 was chosen as this fell equally between these depths. Applied to the open channel condition (EXP1), this correction factor changes mean dune height from 0.026 m to 0.033 m. It is notable that the crest height (above mean bed level) difference between the

EXP1 to EXP2 conditions (Figure 5-20 & 5-21, Table 4-1) is also a change of ~0.01 m.

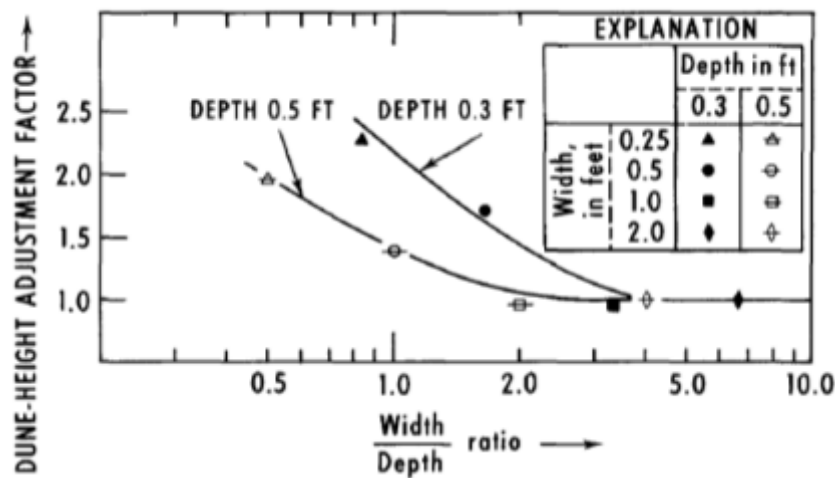


Figure 5-28 Dune height adjustment factors. From Williams 1970, pp20

Unfortunately, the cross-stream mean velocity profiles (not shown) showed no clear trend with the incremental increases in surface roughness and change in dune geometry. However, as the maximum mean downstream velocity is forced toward the bed, the influence of any secondary or cross stream flow on bedload sediment transport must be reduced compared with the downstream vector, which is commonly two orders of magnitude larger than cross stream or vertical flow velocity components in straight channels (Nezu & Nakagawa 1993). The bed scans (Figure 5-16) show that there is still side wall enhanced scour in the EXP4 condition, but these scours are considerably less common and are smaller in size compared with the EXP1 condition. Although secondary circulation structures were not successfully measured, it is clear that their influence on sediment transport direction is greatly reduced when the downstream velocity maximum is closer to the bed.

The influence of secondary circulation on dune geometry have been observed in rivers with width to depth ratios >10. It has been argued that above a crucial aspect ratio the form roughness of dunes prevents formation of channel width secondary circulation (McLelland *et al.* 1999; Parsons *et al.* 2007); whilst Williams (1970) showed that dune height becomes influenced by wall effects/secondary circulation for aspect ratios less than ~2.5. Here, the dune

height correction factor is of very similar magnitude to the difference in crest height above mean bed level between the Open Channel (EXP1) and Foam Cover (EXP2) conditions. It would therefore seem that there is a direct link between open-channel secondary circulation and the maximum height of dune crests above the mean bed level. By reducing the significance of secondary circulation relative to downstream velocity (in this instance by lowering the downstream velocity maximum toward the bed) reduces the significance of secondary circulation effects on sediment transport direction and therefore producing less sinuous dune crest lines. An implicit assumption here is that secondary circulation effects on sediment transport lower the maximum possible dune crest height above the mean bed level. The mechanism is as yet unclear, but is possibly due to higher sediment transport capacity / erosivity added by cross-stream velocities when entraining sediment (Keylock *et al.* 2014).

The dune trough produced the largest proportion of increase in dune height observed here (Figures 5-20 & 5-21). This change in dune geometry is much simpler to explain. Trough scour is dependent upon the intensity of turbulent Reynolds stress produced by flow separation. This intensity is proportional to the relative height of the dune with flow depth and incoming downstream flow velocity (see Chapter 4, (Engel 1981; Kadota & Nezu 1999)). An additional factor is the proximity and steepness of the downstream dune lee slope, which can shorten the reattachment length and produce higher Reynolds stress for the same boundary conditions (Engel 1981). Smith & Ettema (1997) show that the introduction of surface roughness produces more intense Reynolds stresses in the shear layer, and Chapter 4 demonstrated how having a higher gradient of downstream velocity at the crest greatly increased Reynolds shear stress in the shear layer in and around reattachment. The effect of this extra reattachment shear stress that was measured in these fixed dune studies is manifested here, in mobile bedform conditions, through the lowering of velocity maximum closer to the mean bed level and a flow separation shear layer.

Dune length is classically associated with flow depth through the distance required to produce depth-scale eddies after flow reattachment (Yalin 1977). Flume width has no effect on length for the flume size used here (Williams

1970) and therefore secondary circulation effects are of little consequence to bedform length. Here, the change in bed shear stress better describes dune wavelength than flow depth ($r=0.48$ for just depth, not shown) compared an $r=0.96$ for bed shear stress in Figure 5-19C. This outcome throws into doubt the depth controlled process on dune wavelength. Figure 5-18 showed that when downstream velocity is scaled against the shear velocity, velocity profiles near the mean bed levels collapsed for the dune forming conditions. This linear collapse of velocity profiles therefore indicates that dune wavelength, which scaled linearly with bed shear stress (and thus u^*), is controlled by a grain size – bed shear stress relationship, rather than flow depth. Consequently, dune wavelength may have a relationship with the Rouse number.

The linear increase in mean wavelength (Figure 5-19C), combined with the parabolic relationship of dune height (Figure 5-19B) with bed shear stress therefore show two different processes producing dune length and height. Therefore dune height, and thus flow separation, is the primary control for the stability of dunes as it appears that, for bedload dominated laboratory dunes, dune wavelength is an independent process that appears to control the spatial development of flow along the dune stoss. Chapter 4 found that the spatial extent of flow recovery after flow separation could be controlled by adjusting boundary conditions and keeping bedform geometry the same. This procedure implies, for the present mobile bedform case, that longer bedforms were produced primarily due to outer flow control on the turbulent dissipation rate. As higher bedforms produce more intense flow separation, the independence of dune height and wavelength therefore indicates that flow recovery is independent of flow separation height and intensity. The present chapter and Chapter 4 results therefore demonstrate an extension of Engel's (1981) description of bedform geometry affecting flow recovery rates, showing that under bedload dominated conditions more intense flow separation only effects dune height and wavelength is unaffected.

5.4.2 Upper stage plane bed transitions

The transition to upper stage plane bed occurs when the location of maximum bed shear stress across a dune form moves past the dune crest, therefore not facilitating fallout from sediment relaxation and having the bed shear stress maximum before the crest (Bennett *et al.* 1998). This transition was seen repeatedly at a spike length of 30 mm (EXP5) when attempting to achieve the roughness required for constant upper stage planed equilibrium conditions. The eventual spike length of 50 mm (EXP6) produced a consistent upper stage plane bed and was recorded in detail. The transitions seen in EXP5, however, did not involve washing out of dunes but involved a lack of dune formation for long periods of time (~20 minutes). This bed state was typified by a large lee face moving downstream with no bedform development upstream of it. The re-formation of dunes was near spontaneous, but initial bed waves could be seen to build up on the upper stage plane bed prior to dune development (Figure 5-25 & 5-26). These seed waves are a result of a build-up of sediment pulse recirculating and self-propagating throughout the recirculating flume. These pulses of sediment can be seen in the depth sounder data at 1 m downstream of the inlet (Figure 5-25) and are of the scale of 1 cm. The dunes form when there is an increase in depth on the order of 1 cm below the mean bed level at 1 m downstream. This increased depth reduces the bed shear stress enough to enable sediment pile up and flow separation further downstream. The subsequent decrease in flow depth by ~1 cm above the mean bed level at 1 m downstream prevents any further initiation of sediment hysteresis and flow separation, therefore stopping the development of new bedforms at the upstream end of the flume which eventually propagated through the flume channel. Figure 5-26 implies that suspended sediment is reduced during periods of USPB conditions compared to when dunes are present. The ability to measure the bedload layer, or traction carpet, is not possible and thus a comparison between bedload and suspended load with Nasqaband *et al.* (2014a) cannot be performed. It appears that in this instance, the dune-USPB transition was more a result of small (<10%) changes in depth and thus bed shear stress due to circulating pulse of sediment in the flume, rather than substantial increases in suspended sediment inhibiting flow separation (cf. Kostaschuk and Best 2002).

5.5 Addendum

The use of depth-slope product to estimate bed shear stress is anomalous in this chapter, as this calculation is giving the total channel roughness in the test section- that including the rough surface, walls and bed, rather than that energy expelled at the bed- which is the focus of this study. This measurement is therefore measurement of the flume state rather than energy expenditure moving sediment. Therefore, the values used in the above chapter are not applicable to a discussion on the movement of sediment or dunes in this study, but it can be used to describe the overall flume state created. Post thesis (once corrections to the Vectrino II firmware software had been produced) Reynolds shear stress profiles were calculated for each condition and extrapolated to the bed to produce estimated value of bed shear stress (c.f. Nezu & Nakagawa, 1993; Bennett & Best 1995). These values are shown in table 5-2.

Condition	Depth slope (total flume stress), Nm ⁻²	Bed shear stress (From Reynolds stress extrapolation), Nm ⁻²	Bedform state estimated from Leeder 2009, using the Reynolds stress method.
EXP1	3.18	3.42	Ripple/Dune
EXP2	7.61	3.44	Ripple/Dune
EXP3	14.3	7.36	Dune/Upper stage plane bed
EXP4	16.6	7.85	Dune/Upper stage plane bed
EXP5	18.5	Too unsteady for representative profile	Upper stage plane bed
EXP6	27.7	6.23	Upper stage plane bed

The Reynolds stress estimated bed shear stress in table 5-2 is likely to have a minimum error of ± 0.5 Nm⁻² (Bagherimiyab & Lemmin, 2013), with greater error induced from the bedforms in the region of 15% (McLean et al, 1999). Nevertheless, these values are considerably more likely to represent the forces acting on the bed than the depth-slope-product values, as illustrated when they are compare to the bedform stability diagram of Leeder (2009) (table 5-2).

Figure 5-29 displays the mean downstream velocity profile and Reynolds Stress profile shapes, with accompanying final bed topography and illustrates the flow-morphology relationships present in the research. Notably, the gradient of mean

velocity and Reynolds stress near the bed displays the relationship shown in Figure 5-18 where U/u^* near the bed collapsed for all velocity profiles, indicating that skin friction dominates the lower third of the velocity profile. The point of maximum Reynolds stress in Figure 5-29A is at the dune crest, whilst successive increases in surface roughness increase the intensity of flow separation and they measured Reynolds stress, eventually removing the peak in Reynolds stress at the height of the dune crest (and subsequent variation in velocity profile shape), lowering the vertical position of maximum Reynolds stress toward the mean bed level until an upper stage plane bed is reached (Figure 5-29, A-D). The Reynolds stress method of estimating bed shear stress produces an estimate lower than that of the preceding condition, which produced dunes (Table 5-2, Figure 5-29). Whilst this may seem counter-intuitive, it can be easily explained: 1), dune flow separation artificially increases the Reynolds stress produced by as much as 15% (which would produce roughly equal values of bed shear stress between EXP4 & 6)(McLean *et al*, 1999), 2) the position of maximum Reynolds stress in the water column is so close to the mean bed level that accumulations of sediment are suppressed. As seen in EXP 5, this condition sat on the boundary of allowing and not allowing accumulations of sediment to build up and where temporary increases in depth occurred, dune production existed. The upper stage plane bed in EXP6 is a result of sediment accumulations never being allowed to form anywhere in the flume due to the position of highest shear stress being supposed to $\sim 0.01\text{m}$ from the mean bed level.

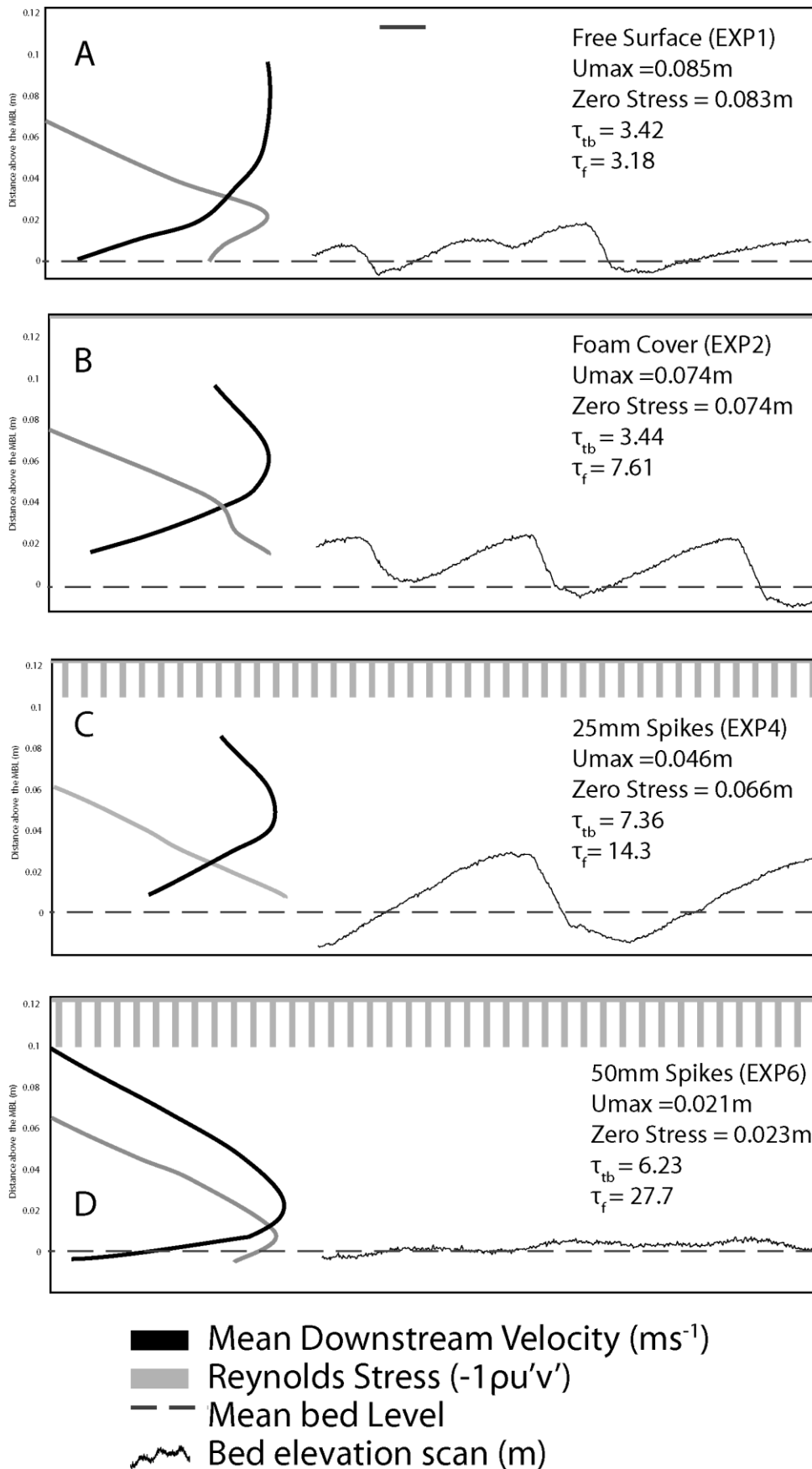


Figure 5-29. Summary diagram of the experimental results. The mean velocity profile and Reynolds stress profiles are scaled from their maximum and minimum values, rather than absolute values, so as to clearly illustrate the profile's gradient. The bed profile was captured from an overhead laser scanner (Figure 5-14).

5.6 Limitations

One significant limitation of this laboratory work is the singular grain size used in the flume experiments. This limits the discussion on bedform stability as it has been shown that bi-modal distributions of grain size can change bedform size, shape and three-dimensionality (Kleinhans 2002)- this is largely thought the disruption of the viscous sublayer from fine gravels on the stoss slopes of dunes. The applicability of the bedform and bed shear stress tests here also does not extend toward the finer sand sizes, which are known to produce low-angle bedforms (Kostaschuck & Villard, 1996) from higher suspension of sediment along the stoss and at the crest (Kostaschuck *et al*, 2009). Therefore the results here are grain size and distribution dependent and a non-dimensionalised parameter, similar to shields cannot be produced from this data. One possible alternative parameter is the critical shields parameter, however measurement of the critical shear stress for entrainment of the sediment used was not performed nor was the data available from the suppliers of the sediment. These results therefore should form the basis of a wider investigation into the effects of velocity profile shape and grain size on bedform morphology.

One result that was unexpected was the reduction in dune three-dimensionality with greater suppression of the velocity maximum. This result has also been found in studies of flow and bedforms under ice (Smith & Ettema 1997, Muste *et al*, 2000; Demers *et al*, 2013) and they allude to the change in secondary circulation patterns as a cause. Measurement of cross stream velocities was undertaken in the laboratory measurements but the results are of poor quality and are not shown here. As such, processes responsible for the change in bedform three-dimensionality can only be inferred from the result and previous research.

5.7 Conclusions

It has been shown that dune height scales in a parabola of stability with bed shear stress, and not flow depth. This result was found by changing the downstream mean velocity profile shape whilst maintaining constant depth and

depth-averaged velocity. This finding has particular significance for flows where the downstream velocity profile is not a classical log-normal open channel shape, such as rivers with any curvature or ice cover.

Changing the velocity profile shape from classical open channel to debris flow (without the density contrast) shape produced an upper stage plane bed whilst maintaining constant depth and depth averaged velocity. This can explain the lack of dune cross strata in debris flow deposits through the incorrect hydraulic interpretations made with the assumption of comparable velocity profile.

Dune wavelength and flow recovery after flow separation is dependent upon outer flow properties. Substantial increases in dune height and thus flow separation intensity did not affect the linear relationship between wavelength and bed shear stress.

The transition from dune to upper stage plane bed was measured repeatedly and measurement of the majority of the flume length found that <10% changes in flow depth, rather than suspended sediment reducing flow separation intensity, was the key driver in the transition.

5.8 Synthesis

The present chapter described laboratory experiments that aimed to provide mobile sediment examples of the outcomes of Chapter 4, specifically: changes to dune shape with an imposed velocity profile of steeper gradient than equilibrium open channel flow log-law velocity profiles. One of the major findings of the present chapter is the increase in trough scour when bed shear stress increased via suppression of the velocity maximum toward the bed. Suppression of the velocity maximum in the flow profile may seem un-natural but it has been found for rivers in arctic regions, where ice forms on the free surface and suppresses the velocity maximum toward the bed – principally through form roughness (Smith & Ettema 1997, Muste *et al*, 2000; Dimers *et al*, 2013). However the studies of flow and sediment transport under ice all produced greater flow depths than their ice free/ free surface e cover free

counterparts. In this present chapter the flow depth was held constant and thus the higher energy slope induced from the surface roughness required the flume slope to be increased to produce equilibrium conditions. With flows under ice, the greater water depth is due to water surface slope remaining constant – due to the valley scale morphological control on the river. Therefore the flow depth increased to compensate for the higher roughness. In this situation, Smith & Ettema (1997) and Muste *et al*, (2000) found that bed shear stress and sediment transport decreased with the presence of ice cover- similar to the EXP2 condition studied here. Therefore the morphological change of the dunes is highly likely to be due to the difference in secondary circulation pattern between open and closed channels (Demers *et al*, 2013; Rice *et al*, 2012). The cause of three dimensionality of bedform plan shape has been a subject of much debate since Allen's (1968) publication, with some defining the transition from 2D to 3D crestline curvature to be only a matter of time for small scale instabilities to feedback and produce a morphological change (Bass *et al*, 1993; Venditii 2005) in flumes. Yet the present research indicates that the ratio of downstream to cross stream velocities near the bed is the critical factor, and future research on the matter should focus on the internal and external controls of this ratio.

In addition, log jams are hypothesised to have been considerably more common along rivers in pre-industrial and mass agricultural times (<1500) (Gibling *et al*. 2010). The presence of frequent log jams and their suppression of the velocity maximum toward the bed may well have produced deeper trough scours than estimated using the model of Leclair (2002), thus impacting the appropriateness of this scaling law on paleo-hydraulic estimations. Based on this study trough scours produced under ice or a log jams could be as much as twice as deep as estimated from equilibrium open channel flow experiments (e.g. Bridge 1997, Leclair 2002).

Of wider implication is the direct testing of the assumption that in open channel flows, the log law assumption can be used to estimate bedform size. Bedform size is commonly estimated from flow depth, as equilibrium open channel flow satisfies conservation laws and thus depth slope-product can be used to estimate bed shear stress. The implication of the present chapter is that, in any flow that is not in equilibrium, is not straight and does not have fully developed

flow, this assumption will produce bedform sizes that are unrepresentative – even in steady state- due to the re-distribution of energy in the profile. Such conditions include, any secondary circulation effects, inclusion of surface roughness and flow that is not well developed- which is highly common in large rivers due to the huge Reynolds numbers involved, and km scale widths, which requires multiple km's of straight channel for full development of a turbulent boundary layer.

Dune Dynamics at the Field Scale

Abstract

River dunes are a fundamental and ubiquitous product of sediment transport in the Worlds' Rivers. Dunes exist on a range of scales, from centimeters to 100's of meters and minutes to years. This range of scales often results in smaller dune bedforms being superimposed onto larger dunes. Despite acknowledgement of this superimposition, little is yet understood of the relative influence of these superimposed dunes on their host bedform, and vice-versa. Here, high-resolution (0.4m²) repeated bathymetric surveys combined with concurrent measurements of the 3D flow velocities and suspended sediment concentrations of a section of the Mekong River in Cambodia, are used to describe the relationships between superimposed bedforms and their host dune. The superimposed bedforms were found to change their morphology to the prevailing hydraulic conditions whilst host bedform size remained unchanged by the varying flow depth and discharge. It is postulated that secondary bedforms buffer the host bedform from scales of hydraulic changes on the order of the secondary bedform size, and that the larger bedforms represent morphological response to similarly large changes in hydraulic condition. Mean large bedform height was half that estimated via empirical scaling relationships, yet mean dune height consistently decreased thought the survey period, and mean wavelength was longer (but much closer) to depth scaling empirical predictors. Additionally, mean suspended sediment concentration matched values of U/u^* near the bed with similar relative bedform depth (bedform height/depth), across variations in depth and discharge. This outcome indicates that these dunes were very close to being depth-limited, without displaying upper stage plane beds at the crests or free surface interaction and were half the height predicted from flume studies.

6.1. Introduction

As a flood wave migrates through a reach, a dune's response lags the change in depth and velocity, producing the well-known hysteresis curve (see literature review section on hysteresis). Martin & Jerolmack (2013) recently demonstrated this hysteresis in a laboratory by showing that when the rate of change of

discharge is equal to the rate of change of the bed there is no hysteresis, whilst large differences in the respective rates will produce a lag in bedform response over flow conditions. This lag results in falling flood flow conditions existing a bed composed of the largest dunes. The falling leg of a flood wave in sand bed rivers is often not a steady, uniform decline to non-flood levels, but a drop that varies over time (Wilbers & Ten Brinke 2003). Stage variation during a falling flood is not solely due to changes in water supply but also adjustment in river bed state (Shimizu *et al.*, 2009). Bed roughness strongly effects stage height and dunes often become largest during a falling flood (Van Rijn 1984c, 2007; Prent & Hickin 2001; Amsler *et al.* 2009; Aberle *et al.* 2010; Robert 2011; Sandbach *et al.* 2012).

A key question for dune modelling is how do the dunes respond, how fast do they adapt to a new flow condition and how will this transient state effect the form roughness produced by the bed and thus river stage levels? These questions are amplified for rivers in monsoonal climates, where stage can change by 5-10m in a week (MRC 2005). Moreover, the rate of change of bedforms during periods of flow unsteadiness is difficult to predict due to the presence of secondary dunes altering the distribution of bed shear stress along the host dune and changing the ratio of bedload to suspended load over host bedforms (Julien & Klasssen 1995; Yen & Lee 1995; Amsler & Garcia 1997; Carling, *et al.*, 2000a; Best 2011; Naqshband *et al.*, 2014a).

Bedform adaption rates can be strongly controlled by the amount of sediment suspended along the host stoss slope during the high flow periods – sediment that would normally fall onto the lee face of a dune and add to its migration (Naqshband *et al.* 2014a). It has been shown that dunes produce considerable macro turbulent flow structures (boils as seen of the flow surface) that mix the entire flow depth (Jackson 1976b; Kostaschuk & Church 1993; Kadota & Nezu 1999; Kostaschuk 2000; Prent & Hickin 2001; Mao 2003; Best 2005a,b; Best *et al.* 2010; Shugar *et al.* 2010; Amsler *et al.* 2009; Szupiany *et al.* 2012; Bradley *et al.* 2013; Demers *et al.* 2013). These bedform-related coherent flow structures are very important in driving the suspension of bed sediment in sand bed rivers and therefore its distribution in a channel. Whilst the above studies have measured these periodic coherent flow structures (CFS) over dunes, how these

CFS change during the course of a flood wave has achieved little focused research, with notable exceptions of boil measurements over a sill through a tidal cycle (Chickadel *et al.* 2009, 2011; Talke *et al.* 2010, 2013). Dune related macro turbulence is formed along the dune stoss slope (Chang & Constantinescu 2013) and “ejected” into the bulk of the flow at flow separation and reattachment (Jackson 1976b; Muller & Gyr 1986, 1996; Laponite 1992, 1996; Kadota & Nezu 1999; Best 2005b) and is therefore strongly dependent upon dune height and length. However, their existence and ability to pick up near bed sediment on dunes stoss slopes can reduce dune size or migration rate; through reducing the sediment supply at the crest and lee slope (e.g. Naqshband *et al.*, 2014a).

Acoustic Doppler current profilers (aDcp) can be used to measure 3D flow velocities in a water column in the field (Kostaschuk *et al.* 2004; Sime *et al.* 2007; Czuba *et al.* 2009; Szupiany *et al.* 2009, 2011). The intensity of acoustic reflection through the water column can also be calibrated to produce concurrent suspended sediment concentrations (Kostaschuk & Church 1993; Kostaschuk *et al.* 2009; Bradley *et al.* 2013). Combining aDcp with high-resolution bathymetry measurements provides an excellent method for viewing these important flow structures and how they are related to bedform morphology (e.g. Parsons *et al.* 2005; Kostaschuk *et al.* 2009; Szupiany *et al.* 2012; Bradley *et al.* 2013). Much of the measurements made of flow over dunes have been aimed at trying to understand the existence of low angle dunes that do not scale well with bed shear stress or depth (Kostaschuk & Villard, 1996). In fact most world’s river dunes do not scale well with either depth or shear stress (Flemming, 2000). Flemming (2000) asserts that depth and grain size both need to be accounted for in determining dune size; however the processes behind this assertion have not been thoroughly investigated. The complex flow structure over dunes does not readily allow for simple interpretations of average bed shear stress and sediment transport (McLean *et al.*, 1999). Understanding the processes that affect the relative amounts of dune bedload and suspended load transport and their effects on dune geometry are crucial in advancing the ability to model these complex river features.

This chapter presents measurements from the falling leg of a significant wet-season flood on the Mekong River in Cambodia. The Mekong catchment receives large amount of rainfall in very short periods of time due to tropical typhoons hitting the catchment often in late summer. The stage level at the town of Kratie (Cambodia) can rise and fall quickly, and by 5m (72%) in 10 days. This chapter presents fieldwork results from the Mekong River during a steady period in the falling leg of the wet season flood. Repeated bathymetric, flow velocity and suspended sediment measurements are reported here and are used to discuss the influences of sediment supply, suspended bed sediment to bedload ratio on the adaption of bedforms to a relatively steady hydraulic condition.

6.2. Methods

6.2.1. Study Area

The Mekong is one of the world's largest rivers, with a mean annual discharge of 457 km³ draining an area of 795,000 km² and a mean annual sediment load of 1.68 MT (Milliman & Meade 1983; Gupta & Liew 2007; MRC 2010). Annual rainfall is high over the northern and eastern basin (2000–4000+ mm yr⁻¹), decreasing over the lowland areas, (~1000 mm a year) (Gupta & Liew, 2007). However, this rainfall is highly seasonal with 85-90% falling between June and October in the south-western monsoon season (Gupta & Liew, 2007). This seasonality produces large flood events on the order of 30,000 to 60,000 m³s⁻¹ that provide 80% of the mean annual discharge for the river (MRC 2005). The Mekong River basin north of the town of Kratie, Cambodia, is largely bedrock controlled. The Mekong travels 4000km from its source (out of a total length of 4880km) before reaching the alluvial plain near Kratie, Cambodia (Gupta & Liew 2007). By this point, 95% of the total Mekong flow has entered the river (MRC 2005) and the mostly bedrock controlled upper reaches results in the Mekong at Kratie receiving the peak flood flows with little upstream attenuation. Whilst the channel bed and banks are constructed of alluvium, it is possible that the general river course is still bedrock confined (Gupta & Liew 2007) causing its long, straight sections in and around the area of study. The inter-annual river discharge changes dramatically between monsoon and dry

seasons, with changes in stage of 20-30m being common and corresponding discharge changes from $<5,000 \text{ m}^3\text{s}^{-1}$ in the dry season to an average of $35,000 \text{ m}^3\text{s}^{-1}$ in the wet with peak discharge at $\sim 60,000 \text{ m}^3\text{s}^{-1}$. Annual bedload sediment discharge at Kratie is estimated to be on the order of 1.5MT yr^{-1} (Bravard *et al.* 2014).

Repeat field observations were made in the Mekong river, Cambodia $\sim 12\text{km}$ south of the transition from bedrock channel to gravel and sand ($12^\circ 29' 16.75''\text{N}$, $106^\circ 0' 45.97''\text{E}$) (Figure 6-1). The overall gradient of the last 650 km of the Mekong is 0.00005 (Gupta & Liew 2007), however the slope over the measured area was two orders of magnitude higher than that during this steady part of the falling flood leg (Table 6-1). Measurements were made on the true left channel of a large highly stable mid channel bar near the town of Kratie.

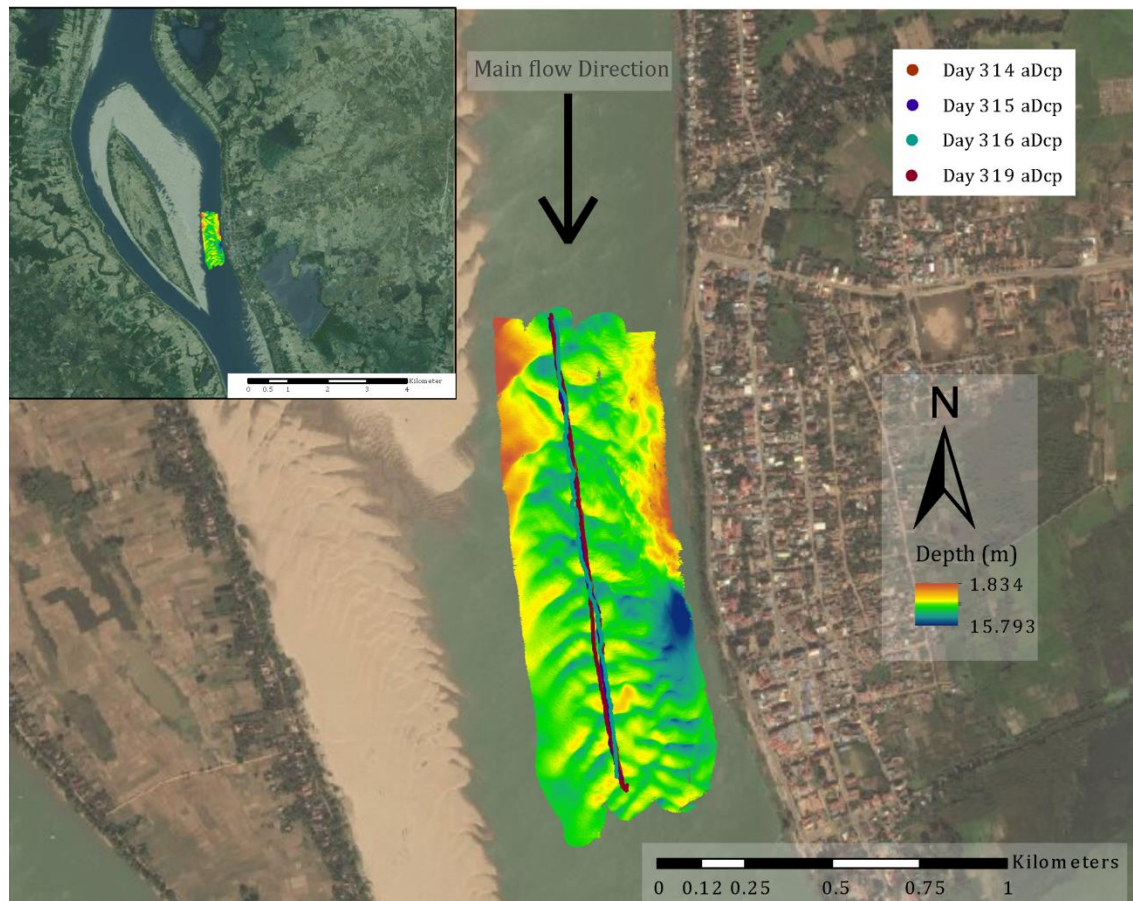


Figure 6-1. Overview of the field site with an inset view of the wider river. The town of Kratie is to the east of the channel. Satellite imagery from the dry season shows the sand bar with relict dunes that extend into the water and the bed survey MBES data from Day 314. The DEM presented here is MBES data from Day 31, contoured to depth below water surface. Flow in top to bottom. Satellite imagery credit: Esri, DigitalGlobe, GeoEye, i-cubed, Earthstar Geographics, CNES/Airbus DS, USDA, USGS, AEX, Getmapping, Aerogrid, IGN, IGP, swisstopo, and the GIS User Community

6.2.2. Data collection instruments, accuracy and correction

The complex river bed bathymetry was measured with a Reson© SeaBat© SV2 7125 Multibeam (MBES) system. The head generates 512 equidistant beams and measures relative water depths over a 165° wide swath perpendicular to the vessel track. Navigation, orientation, and attitude data (heave, pitch, and roll) were provided using an Applanix© POS MV V3 gyroscope inertial guidance system mounted close to the center of the vessel. Vessel positioning was provided using a Leica 1230 real-time kinematic differential GPS, with corrections administered using a SAT6L D64 high-power 35W radio system, accurate to 0.02 m horizontally and 0.03 m vertically. Measurement dates for MBES surveys were 10/11/2013, 11/11/2013, 12/11/2013 and 15/11/2013 (days 314 to 319 herein). The MBES data was measured and corrected concurrently using this dGPS and POS MV setup, with additional acoustic correction of speed of sound of beam steering from a RESON SVP sound velocity profiler.

Three-dimensional flow velocities were recorded using a Teledyne© RD Instruments© 1200 kHz Rio Grande Workhorse© acoustic Doppler current profiler (aDcp) mounted on a second vessel and were recorded concurrently with the MBES. The position of the aDcp was also recorded using the Leica 1230 Real-Time Kinematic (RTK) dGPS system.

Three-dimensional flow velocities were measured on individual track lines at a vertical resolution of 0.25 m (vertical bin size). Velocities are calculated relative to the instrument head and are corrected using the dGPS calculated boat speed and heading (Mueller & Wagner 2009). Mean error velocity was -0.074 ms^{-1} and the aDcp manufacturer reports an accuracy of $\pm 0.05 \text{ ms}^{-1}$ for velocity measurements, producing a combined mean error of $\sim 0.01 \text{ ms}^{-1}$ (0.7% mean flow velocity, Table 1). Recorded echo intensity has a precision of $\pm 1.5 \text{ dB}$ (Teledyne RD Instruments, 2001). The aDcp was set to ping at 1 Hz, and pings were averaged in ensembles every 3 seconds to improve the signal-to-noise ratio. Average vessel velocity for the transects was $\sim 0.5 \text{ ms}^{-1}$, resulting in profiles every 0.85 m along the transect on average. Averaging in the water column occurs over different volumes of water because each beam is oriented at an orthogonal angle of 20° in the vertical and beam spreading occurs at 1.5°,

resulting in deeper bins being horizontally larger than shallow bins and thus having greater velocity error (Teledyne RD Instruments, 2001).

6.2.3. Collection area

The MBES survey area was approximately 1,400 m long by 470 m whilst the aDcp transects were piloted in the centre of this transect taking both upstream and downstream boat direction samples. The river stage downstream of the bar is plotted in Figure 6-2. The measurement period herein takes place during the falling leg of the Mekong wet season in 2013 which contained effects from several category five typhoons: Usagi (24/09/2013); Wutip (30/09/2013); Nari (05/10/2013). The input of water into the catchment from the aftermath of typhoon Hyian (10/11/2013) halted the decline and maintained discharge levels for ~1 week, during which the measurements were taken. Discharge dropped $2142 \text{ m}^3\text{s}^{-1}$ (~7%) and stage dropped 0.73 m (~5.5%), over the survey. Each day consisted of 4 aDcp transects, 2 upstream and 2 downstream and concurrent MBES surveys, except for day 316 where no MBES was taken.

The straightness of the eastern, true left, channel and constant submergence thought out the year meant that well developed dunes under a flow with minimal secondary circulation effects (Jackson 1975b) was likely. During the wet season the sandy bar to the west of this channel is submerged and large dunes form, however most of the year this sandy bar is emergent and these dunes can be seen in satellite images (Figure 6-1). Three surveys of the riverbed were conducted and gridded horizontal resolution of 0.4 m².

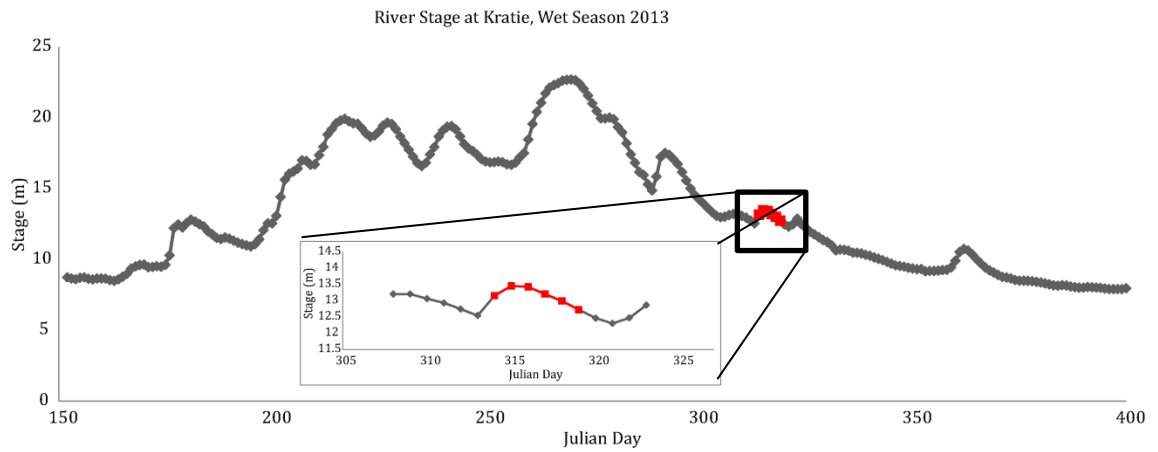


Figure 6-2. River stage Levels at Kratie during the wet season of 2013. Measurement period is highlighted in red. Inset graph is a closer view of the measurement period. Mekong River Commission, http://ffw.mrcmekong.org/historical_rec.htm

Grain size and distribution at Kratie was measured via a boat mounted bed sampler on the 16/01/2013 (day 16). Figure 6-3 shows the frequency distribution and cumulative fraction of grain sizes measured from this bed sample. The bimodal distribution of grain sizes, from fine sand to fine gravel reflects presence of reworking of terrace deposits (MRC 2010). The site is only 12 km south of where the Mekong is bedrock confined. Minor gravel and sand extraction occurs ~5 km north of Kratie. The median grain size is 220 μm and, based upon dry season satellite imagery, the gravel fraction is not obvious on the tops of the ubiquitous sand bars (Figure 6-1); this likely indicates that the coarser fraction is confined to the deeper parts of the channel.

Histogram of Grain Size at Kratie

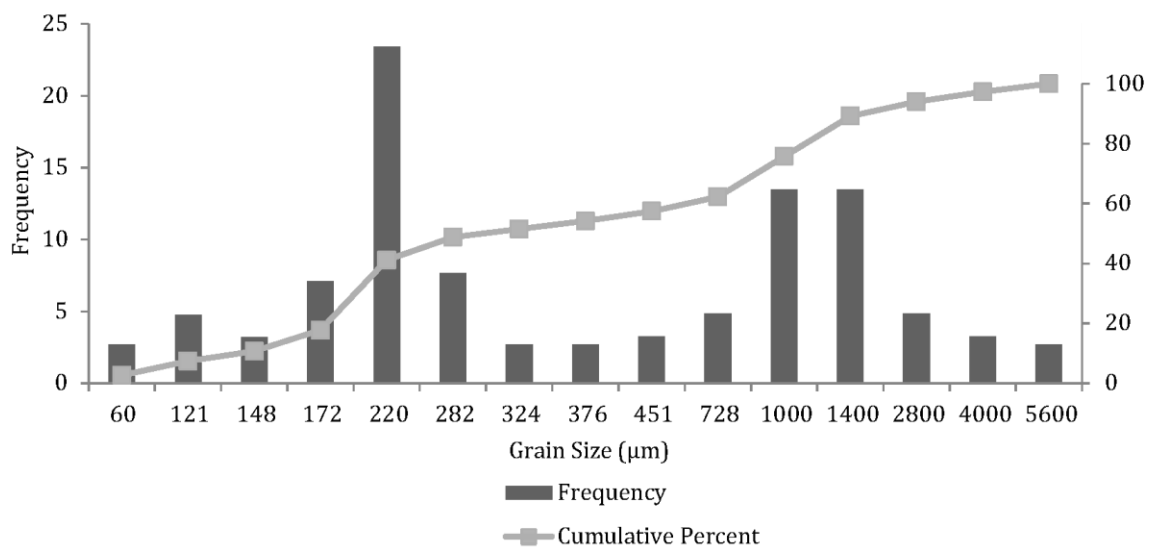


Figure 6-3. Grain size distribution of bed sediment measured at Kratie obtained on the 16/01/2013.

Table 6-1. Grain size distribution data			
Grain Size (μm)	Percent volume coarser	Frequency	Cumulative Sum
60	100.00	2.69	2.69
121	95.24	4.76	7.46
148	92.02	3.22	10.67
172	84.93	7.09	17.76
220	61.52	23.41	41.18
282	53.87	7.65	48.83
324	51.17	2.69	51.52
376	48.48	2.69	54.21
451	45.25	3.23	57.44
728	40.40	4.85	62.29
1000	26.93	13.47	75.76
1400	13.47	13.47	89.23
2800	8.62	4.85	94.07
4000	5.39	3.23	97.31
5600	2.69	2.69	100.00
Median Grain size = 220 μm (d_{50})			
Mean Grain Size = 418 μm			
d_{84} = 1384.1 μm			
d_{16} = 181.3 μm			

The aDcp transects were taken over the dry season channel area, where most developed dunes exist. As the river stage drops the flow moves to the true left, away from the bar, and a large relict dune field can be observed in satellite imagery during the dry season (Figure 6-1, which also shows aDcp transects in the main channel of the true left). Figure 6-1 shows that the repeat aDcp transects have good spatial consistency and are within <15 m of any other aDcp transect. aDcp transects are cut off at the top and bottom extent so that each line starts and finishes at the same place. The upstream transects are shown in this chapter as the upstream boat speed is well below ($\leq 50\%$) the flow speed, ensuring that the velocity error is minimised (Kostaschuk *et al.*, 2005; Sime *et al.*, 2007). Each upstream transect took between 40 minutes to an hour to complete the 1300 m transect, with peak velocity magnitudes of 2.5 ms^{-1} . Dunes

migrated downstream at a peak rate of ~4.4 m per day, so a single dune is unlikely to have moved more than 0.3 m during each transect. Therefore it is considered that the flow measurement transects are over a stationary bed for each measurement period. However, there would certainly be a moving bedload layer.

6.2.4. MBES and aDcp Post-Processing

Post-processing of the MBES data was achieved using CARIS HIPS®, in which all lines and soundings were merged and combined so that area-based filtering and editing could be employed to produce the final DEM for analysis. Post-processing of aDcp data used the Velocity Mapping Toolbox (Parsons *et al.* 2013) to set the data to a regular grid (~0.85 m x 0.25 m), calculate discharge, convert spatial coordinates to UTM, set the data to a grid and output to Matlab® for suspended sediment calibration and plotting. Data were also output to ArcMap® for plotting the transect location alongside the MBES data. For brevity, only one aDcp transect is shown here for each day. As four transects were collected each day, the transect with the highest spatial resolution was used.

6.2.5. Calibration of aDcp backscatter to suspended sediment concentrations

Acoustic backscatter intensity can be correlated with *in situ* measured suspended sediment concentration (Holdaway *et al.* 1999; Kostaschuk *et al.* 2005; Shugar *et al.* 2010; Guerrero & Szupiany, 2013). To convert the acoustic backscatter intensity (dB) from the aDcp into a concentration (mg/l), measured sediment concentrations are needed, which correspond to aDcp transects. As there is no standardised manufacturing calibration for aDcp units, a unique calibration is required for each unit used. In order to calibrate each unit, a series of bulk samples were taken with a Ruttner water sampler of 2.2 litre capacity. A series of three water samples were taken through the water column (top, middle and bottom) of each profile. At the same time the aDcp unit recording acoustic backscatter readings. The aDcp ensemble at which the sample was taken is recorded to enable calibration of the filtered sample. For the 1200 kHz aDcp

herein, a total of 42 concurrent measurements of suspended sediment concentration were used to build a correlation with backscatter intensity (Figure 6-4).

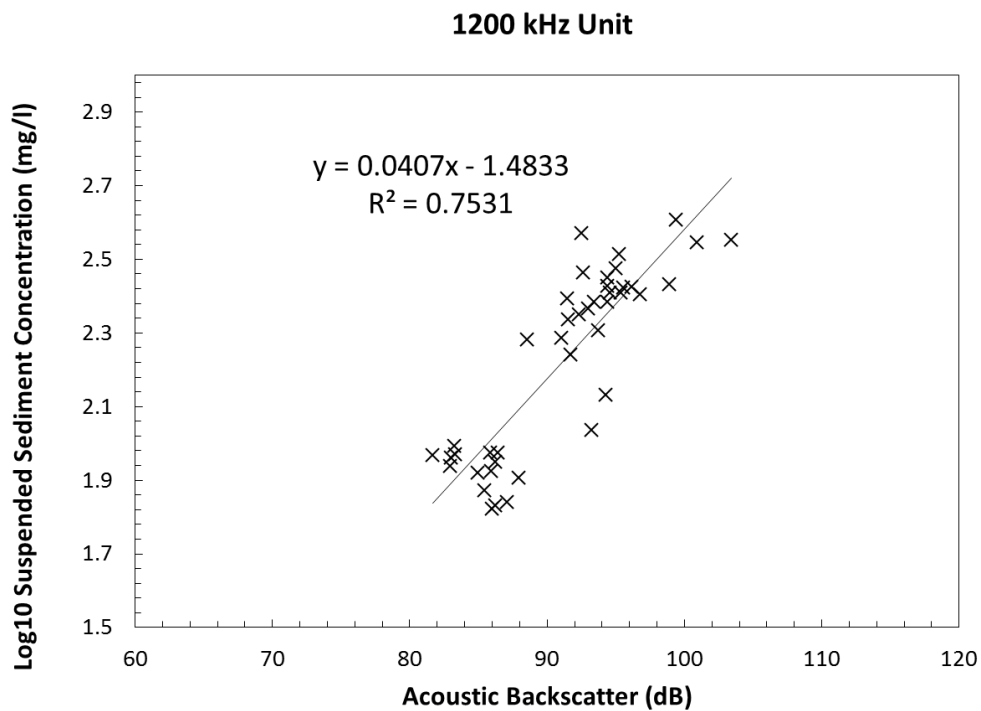


Figure 6-4. Calibration curve of acoustic backscatter (dB) and suspended sediment concentration (mg/l) for the 1200 kHz ADCP unit. $P < 0.05$. Courtesy of C. Hackney.

Table 6-2. aDcp transect collection statistics and hydraulic measurements				
Date	10/11/2013	11/11/2013	12/11/2013	15/11/2013
ID	314	315	316	319
Transect time (s)	1382	2067	3998	1400
GPS transect length (m)	1338	1281	1249	1297
Double average U (ms^{-1})	1.3919	1.3771	1.3299	1.357
Double average V (ms^{-1})	-0.0317	-0.0355	-0.028	-0.0383
Double average W (ms^{-1})	1.3919	1.3771	1.3299	1.357
Pressure (Pa)	88.1	89.1	88.2	87.7
Mean SSC (mg/L)	332	280	271	302
Average Transect Depth (m)	12.58	12.64	12.58	11.5
Water Surface Slope (m/m) (over transect)	-0.00192	-0.00146	n/a	-0.00146
Bed slope (m/m)	0.0006	0.0006	0.0006	0.0007

Bed shear stress (log law) (pa)	10.227	8.21	8.28	8.08
Kratie Discharge (m ³ s ⁻¹) (rating curve)	15811	16874	16812	14732
Kratie stage measurement (m)	13.15	13.45	13.42	12.72

6.3 Results

6.3.1 Dune field morphology

Figure 5 displays the river bed on the 10th November 2013 (Day 314 herein), revealing a channel boarded to the east by outcropping bedrock and a sand bar of roughly equal elevation to the west of the channel. In the channel a series of large dunes running down the centre of mean height ~2 m and wavelength ~98 m with angle of repose lee sides in the centre (Figure 6-6). Toward the shallower edges of the channel (e.g. near the bar) dune crestlines tend to have advanced further downstream than in the centre of the dune. Downstream of the bedrock at the East bank the dunes encounter a large bank related scour ~18 m deep which disrupts the bedform crestlines.

Large lee side scours tend to be aligned with the general flow direction and not with the dune crestlines that developed during the flood on the sand bar (west side of the channel). The steepest dune lee sides (Figure 6-6) are perpendicular to the bedform crestlines, rather than show a saddle and lobe structure that is common with 3D dune shapes (Maddux *et al.*, 2003a; Parsons *et al.* 2005; Venditti 2007). The lateral crestline curvature, and reduction in dune height towards the boundaries of the channel are somewhat similar to wall effects found in laboratory flumes (Williams 1970). However, the cause here is more likely due to a mix of local variation in sediment supply and local depth reduction inducing higher hydraulic roughness and consequently lower flow velocities.

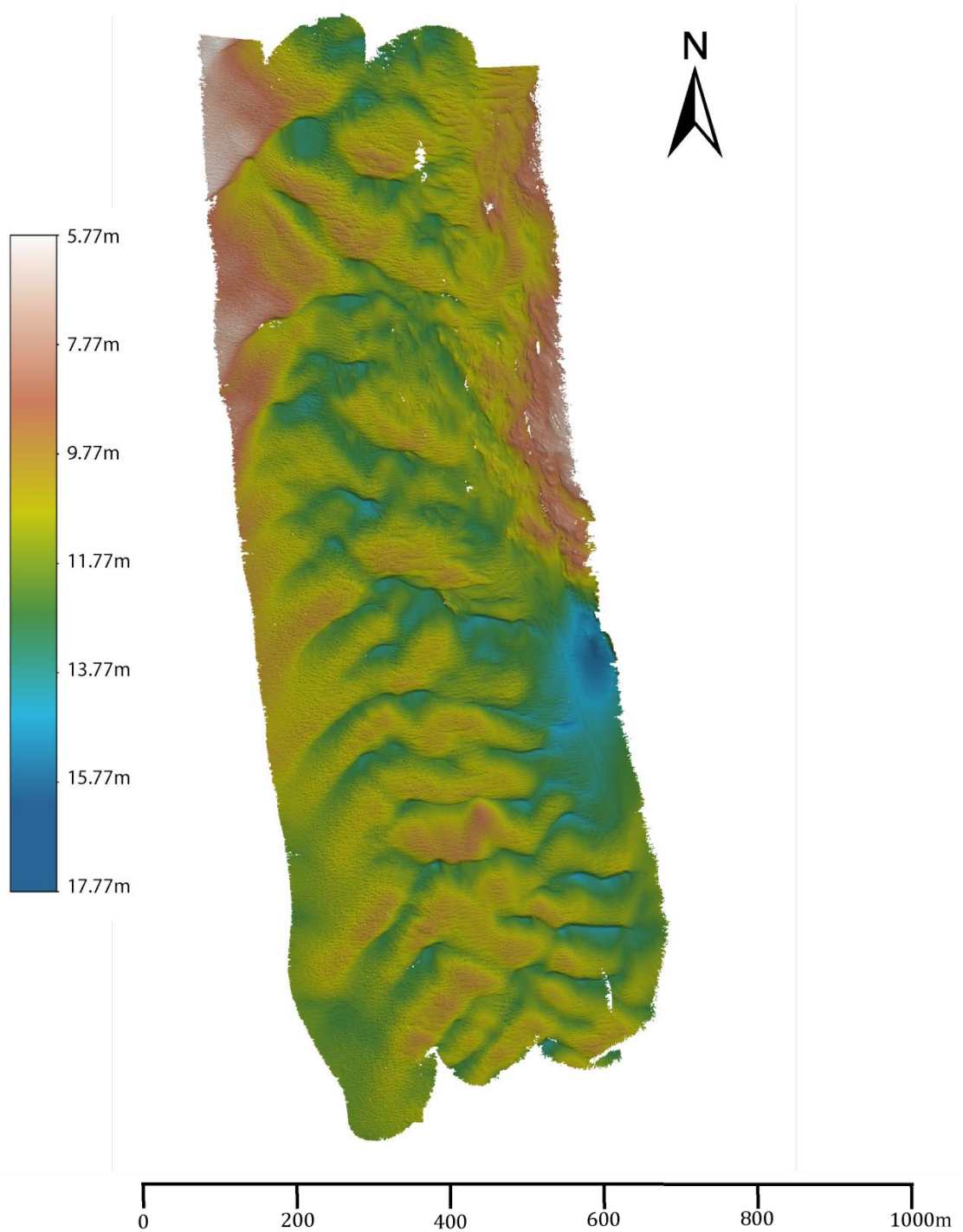


Figure 6-5. Multibeam bathymetry measured on day 314 in the channel near Kratie (seen in Figure 1). Flows is from top to bottom of the page. Depth is scaled to meters below water surface at the time of measurement. Grid resolution is 0.40 m.



Figure 6-6. Local bed slope measured in degrees of the MBES bathymetry in Figure 6-5.

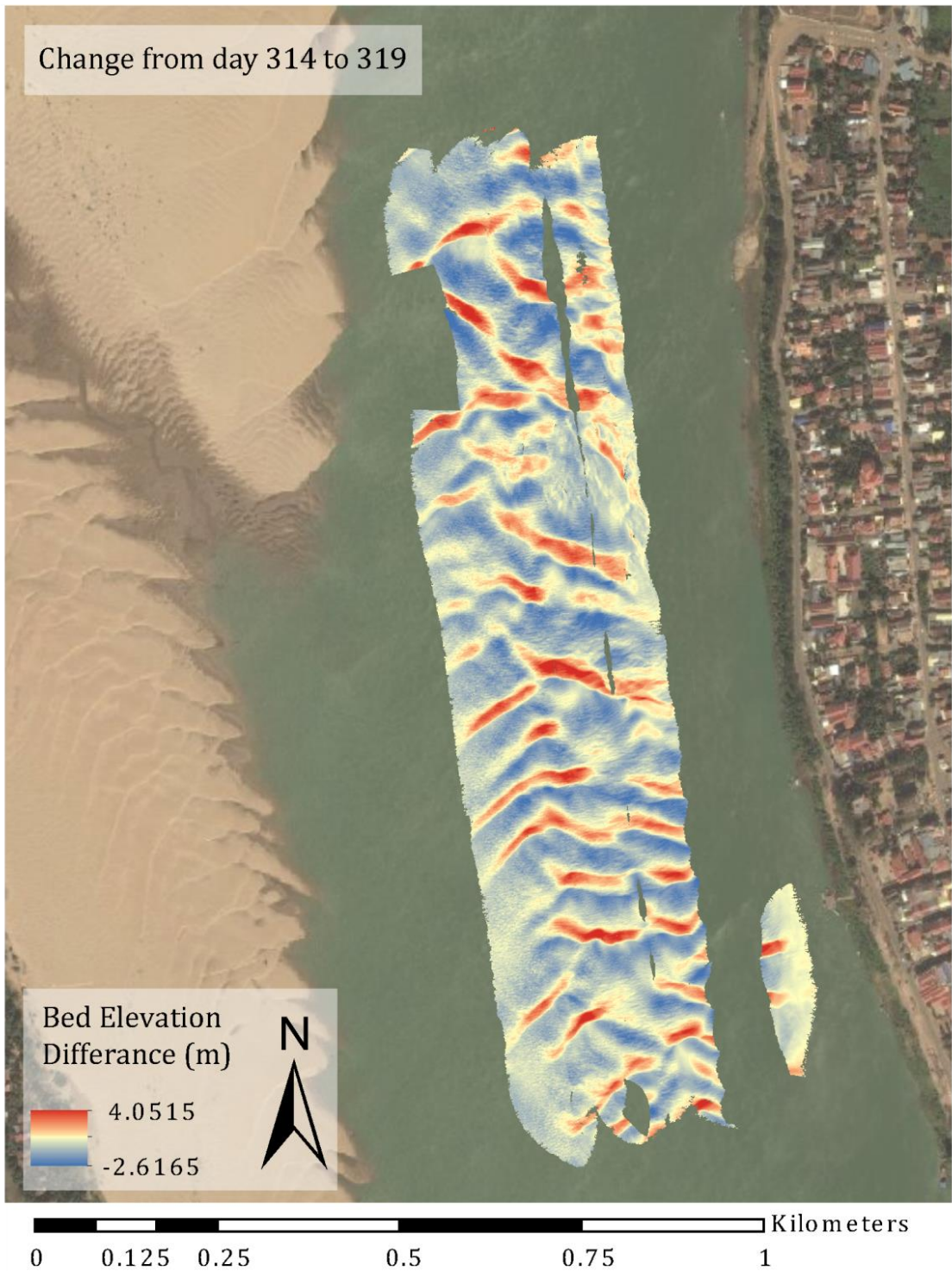


Figure 6-7. Bed translation measured by repeated MBES surveys between days 314 and 319. The gap near the top of the survey is due to error on day 319 corrupting that line of data.

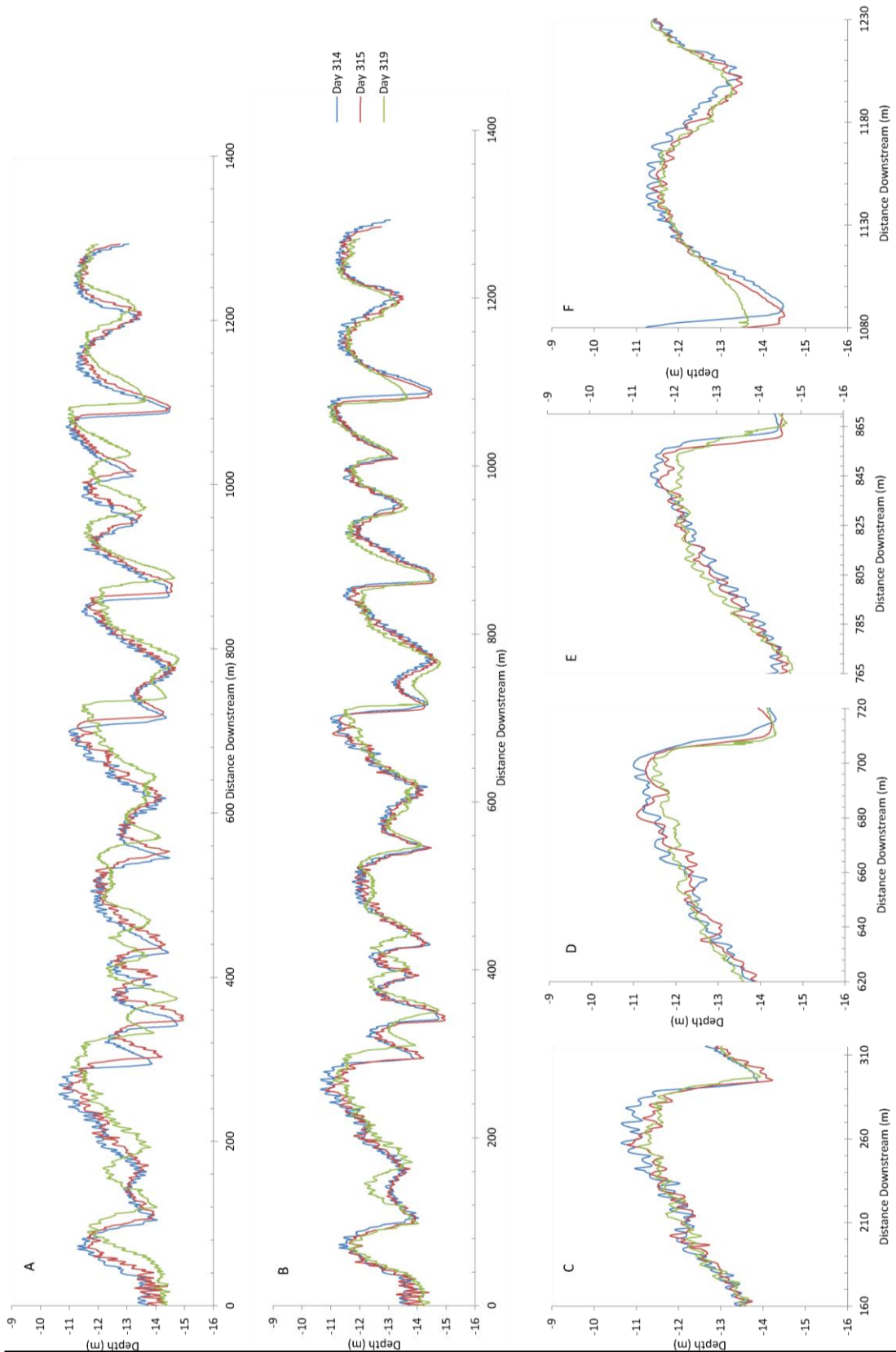


Figure 6-8. Bedform translation and adaption. Profiles taken from the three MBES surveys, along the axis of aDcp transects displayed in Figure 1. 6-8(A) displays the flow stage corrected profiles of bedforms along the aDcp transect. 6-8(B) shows the same profile with the translation removed. Between day 314 and 315 8 m of translation was removed, and between day 314 and 319 22 m of translation was removed. Figures 6- 8 C,D,E and F shows selected larger dunes from Figure 6-8(B) to highlight the secondary bedforms on the stoss and crests of these larger dunes. Their location in Figure 6-8(B) can be found on their y axis distances.

Figure 6-8 displays selected transects, on the same line as the aDcp transects in Figure 6-1, from the MBES elevation surface. Figure 6-8A shows the stage corrected transect, whilst Figure 6-8B shows stages and migration corrected profiles. Bedform translation over the five days ranges between 10 and 25 m. The larger dunes display no clear change in height or length (Table 6-3) compared with the smaller dunes which undergo geometrical change as well as translation (Figure 6-8B). These smaller bedforms have either added in volume (e.g. ~150 m) or had volume eroded away (e.g. 750 m). The dune crestline at 150 m (Figure 6-8B) is aligned more perpendicular to the flow direction than the dune upstream of it in the transect, which is attached to the sand bar (Figure 6-7). The dune losing mass over time at 750 m is downstream of a large and steep lee face ($>30^\circ$, Figure 6-6), and upstream of a large and steep stoss slope. Conversely this dune continued to translate at a constant rate relative to the large lee slope upstream, rather than become amalgamated into the larger bedform.

The larger dunes only show a significant change (at 95% confidence) in height when day 314 is compared with the other surveys (Table 6-4), as day 314 produced the largest difference in dune height (0.15 m) relative to the other survey days. There was no significant change in dune lengths across these bed transects over the five day survey period (Table 6-4). Despite the hydraulic conditions entering the week of measurement being of considerable change (Figure 6-2), little alteration of the major bedforms to the new steady condition has been found. This observation suggests that bedform adaption rates are either very fast and were missed, or are very slow; relative to the time-scale of a week. Whilst the average dune height diminished across the survey period, the change in dune height was only significant when comparing with day 314, even though water depth in the channel dropped 1 m (~8%) by the last survey day (Table 6-2). Erosion of dune crests is a common and rapid way of bedform geometry adaption to lower flow depth (Nelson *et al.*, 2011) and this morphodynamic process reduces dune heights. Large dune height constantly decreased across the survey period, despite flow depth peaking on day 315 and falling >1 m by 319. The mean dune height of 2 m is half that of the empirical predictions for the flow depth of 12.5 m, yet the trend is for decreasing dune height, rather than increasing to the empirically predicted ~4 m height.

Height				
	Day 314	Day 315	Day 316 (aDcp)	Day 319
Mean	2.17	2.02	1.92	1.91
Standard deviation	0.68	0.60	0.61	0.59
Dune number 1	2.30	1.91	2.15	2.03
2	2.74	2.40	2.43	2.21
3	2.11	2.04	1.72	1.68
4	1.06	1.02	0.75	1.12
5	1.75	1.45	1.27	0.98
6	2.22	2.05	2.04	2.07
7	3.01	2.68	2.69	2.83
8	2.72	2.54	2.44	2.49
9	1.31	1.43	1.86	1.86
10	1.42	1.54	1.15	1.17
11	3.18	3.11	2.65	2.59
Length				
	Day 314	Day 315	Day 316 (aDcp)	Day 319
Mean	98.87	98.80	98.46	98.73
Standard deviation	52.76	53.49	50.49	55.01
Dune number 1	201.92	204.04	198.19	218.05
2	47.98	42.90	53.05	37.49
3	48.98	53.90	55.05	58.19
4	38.99	35.20	37.04	42.59
5	103.46	105.60	111.11	95.08
6	179.43	178.74	171.16	178.46
7	152.44	151.24	151.15	144.57
8	79.97	77.00	80.08	78.58
9	64.98	66.55	67.06	71.68
10	79.97	76.45	72.07	69.58
11	89.47	95.15	87.08	91.78

Table 6-4. Significance of large dune geometrical shape change				
Dune heights				
Paired sample Student t-test	Number of dunes	Null Hypotheses	P value	Confidence intervals
Day 314 v 315	11	False	0.0193	0.0297 to 0.2703
Day 314 v 316	11	False	0.0505	0.0505 to 0.4349
Day 314 v 319	11	False	0.0386	0.0163 to 0.4910
Day 315 v 316	11	True	0.2817	-0.0888 to 0.3743
Day 315 v 319	11	True	0.2812	-0.0991 to 0.3063
Day 316 v 319	11	True	0.8146	-0.1076 to 0.1294
Dune Lengths				
Paired sample Student t-test	Number of dunes	Null Hypotheses	P value	Confidence intervals
Day 314 v 315	11	True	0.9469	-2.3593 to 2.5084
Day 314 v 316	11	True	0.8005	-3.1376 to 3.9649
Day 314 v 319	11	True	0.9586	-5.7205 to 6.0005
Day 315 v 316	11	True	0.8420	-3.4765 to 4.1546
Day 315 v 319	11	True	0.9770	-4.8764 to 5.0073
Day 316 v 319	11	True	0.9322	-7.2611 to 6.7138

Table 6-5: Comparison of large dune size with empirical estimations				
Transect day	314	315	316	319
Mean dune height (m)	2.17	2.02	1.92	1.91
Mean dune wavelength (m)	98.87	98.80	98.46	98.73
Number of bedforms	11	11	11	11
Dune steepness (height/length)	0.0219	0.0204	0.0195	0.0194
Mean depth at Kratie (m)	13.15	13.45	13.42	12.72
Mean profile depth (m) (aDcp)	12.56	12.64	12.51	11.5
Equilibrium height = $d \cdot 0.33$ (m)	4.14	4.17	4.12	3.79
Equilibrium length = $d \cdot 5$ (m)	63.0	63.2	62.5	57.5
Allen (1970) = $1.66 \cdot d^{1.55}$ (m)	59.2	58.2	51.1	59.76
Equilibrium length = $d \cdot 7$ (m)	85.7	86.2	85.3	78.4
Yalin (1972) = $2 \cdot \pi \cdot d$ (m)	88.5	87.6	80.5	86.75
Bed shear stress (log law estimated) (Pa)	10.23	8.21	8.28	8.08
Mean SSC (mg/L)	332	280	271	302
Mean short wavelengths (m)	64.3	63.9	64.5	64.3
Mean long wavelengths (m)	159.3	159.9	157.9	159.0

Mean dune wavelength is slightly under-predicted by most of the empirical predictors (Table 6-5). The wavelengths of these larger dunes is roughly bimodal, with two groups of bedforms either <100 m or >100 m long (Table 6-3). The <100 m mean wavelength is ~64 m, and the >100 m wavelengths are ~159 m. The 64 m wavelengths are well predicted with the mean survey depth of 12.3 m. For the longer wavelength group of bedforms, a depth of 23 m is required to produce equilibrium wavelengths of ~150 m. The 2013 flood peak measured at Kratie (Figure 6-1 & 6-2, ~2.5 km south of this survey area) reached a stage of 22.6 m for four days, 43 days before this survey.

Secondary bedforms are superimposed onto larger dunes are shown in Figure 6-8 (C,D,E&F). The stoss and crests of three larger dunes (Figure 6-8 C,D,E) and an off-centre dune (Figure 6-8 F, making it look symmetrical) are viewed more closely to observe the change in size and shape of these two scales of dunes through time. Figure 6-8B indicates that the height of large dune crests over time is reduced. The size of the larger secondary bedforms (days 314 and 315) increases slightly (Figure 6-9 & Table 6-6), particularly at the crests (e.g. at 260 m in Figure 6-8C, 690 m in Figure 8D and 845 m in Figure 6-8E). The secondary bedform size remains largely similar between day 314 and 315 along these dunes' stoss slopes. Day 319 displays a significant decrease in secondary bedform size at the crest and stoss of the four bedforms shown in Figure 6-8 C,D,E, as well as overall (Figure 6-9 & Table 6-6).

The height of the secondary bedforms decreases significantly by ~0.7 m (~33%) on day 319, when compared with day 314 and 315 (at the 95% confidence, Table 6-6). The distribution of secondary bedforms (Figure 6-9) on day 319 shows that the shorter secondary bedforms are more frequent and bedform heights >0.4 m are less common than on day 314 or 315. Therefore, there is a statistically significant change in secondary dune height that occurs in time alongside a 1 m drop in flow depth, whilst the host dune geometry remains essentially constant. Mean secondary bedform lengths increase with the greater flow depth between day 314 and 315, but not significantly (Table 6-6). The reduction in secondary bedform length between day 315 and 319 of 1.2 m (21%) is also significant at the 95% confidence, showing that both secondary bedform height and lengths decreased appreciably between day 315 and 319 whilst under the largest

hydraulic change. Large dune geometry did not alter in response to this hydraulic change.

Figure 6-8F displays an off-centre bedform profile, with secondary bedforms on the stoss and lee sides of the dune. There is no obvious decrease in secondary dune size toward the crest for this dune, in fact the largest secondary bedforms are found at the crest and lee slope of this dune profile. This fact indicates that the secondary bedform dynamics described above may be spatially restricted to the centreline axis of these bedforms.

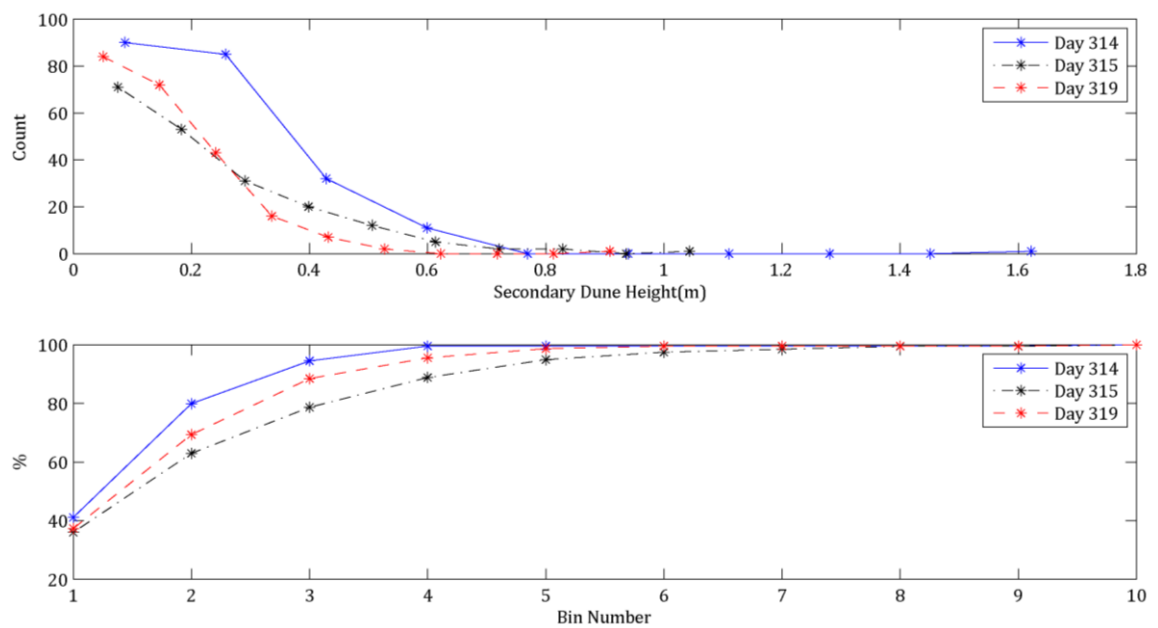


Figure 6-9. Distribution of secondary bedform height (top) and cumulative percentage of secondary bedform height (bottom) for days 314,315 and 319 (MBES survey days). Bedform sizes are measured from all the profiles shown in Figure 6-8.

Secondary dune heights	Number of dunes	Mean	Standard deviation
Day 314	219	0.2344	0.1717
Day 315	197	0.2293	0.1764
Day 319	225	0.1574	0.1214
Paired sample student t-test	Null hypotheses	P value	Confidence intervals
Day 314 V 315	True	0.6701	-0.0267 To 0.0415
Day 314 V 319	False	8.6963e-08	0.0497 To 0.1046
Day 315 V 319	False	7.3180e-06	0.0416 To 0.1039

Secondary dune lengths	Number of dunes	Mean	Standard deviation
Day 314	219	4.93	3.74
Day 315	197	5.58	4.39
Day 319	225	4.38	3.69
Paired sample Student t-test	Null hypotheses	P value	Confidence intervals
Day 314 v 315	True	0.1445	-1.4385 to 0.2123
Day 314 v 319	True	0.1106	-0.1341 to 1.2984
Day 315 v 319	False	0.0027	0.4461 to 2.0982

6.3.2 Overall Flow Field

To investigate the changes in bedform geometry, the aDcp derived flow data from days 314, 315 and 319 are detailed below, and are used to indicate the causal mechanisms behind the changes in secondary dune size, and examine why the larger host bedform heights are so much lower than empirically predicted.

Figure 6-10 displays aDcp data from Day 314, Figure 6-11 displays the transect-averaged velocity profiles, direction and suspended sediment concentration profile whilst Figures 6-12, 6-13 & 6-14 displays flow magnitude and vertical velocity as deviations from the local depth averaged mean on days 314, 315 & 319 respectively. The colour axis for each plot is scaled the same for ease of comparison. The overall flow structure for each day shows a slight higher velocity magnitude in the upper half of the transects, (northern end) and more westerly flow direction (Figure 6-10). As seen in the satellite imagery (Figure 6-1), the sand bar to the west constricts the flow in the upper half of the transect and is the probable cause in this trend; despite this, dunes still instigate high magnitude velocity peaks over dune crests downstream. The vertical velocity across the three transects shows consistent patterns of rising fluid over dunes' stoss slopes and down-welling fluid in the dune lees' (Figure 6-10). Suspended sediment concentration varies over the three transects, with day 315 showing the smallest pulses of suspended sediment concentration in size, frequency and magnitude (Figure 6-11F & Figure 6-13). Transects 314 and 319 (Figures 6-12 &

6-14) both show full depth suspended sediment events and generally higher suspended sediment concentrations than day 315. Several key aspects of the flow over these dunes will be described in more detail; flow direction and dune lee side flow and the relationships between suspended sediment concentration and hydraulic condition.

Flow direction changes along the transect by 16-20° (Figure 6-10) due to flow steering from the large compound bar to the west of the section/transect (Figure 6-1). Therefore the mean flow vector is not perfectly parallel to the dune field orientation or transect path (which was set orthogonal to the dune field orientation).

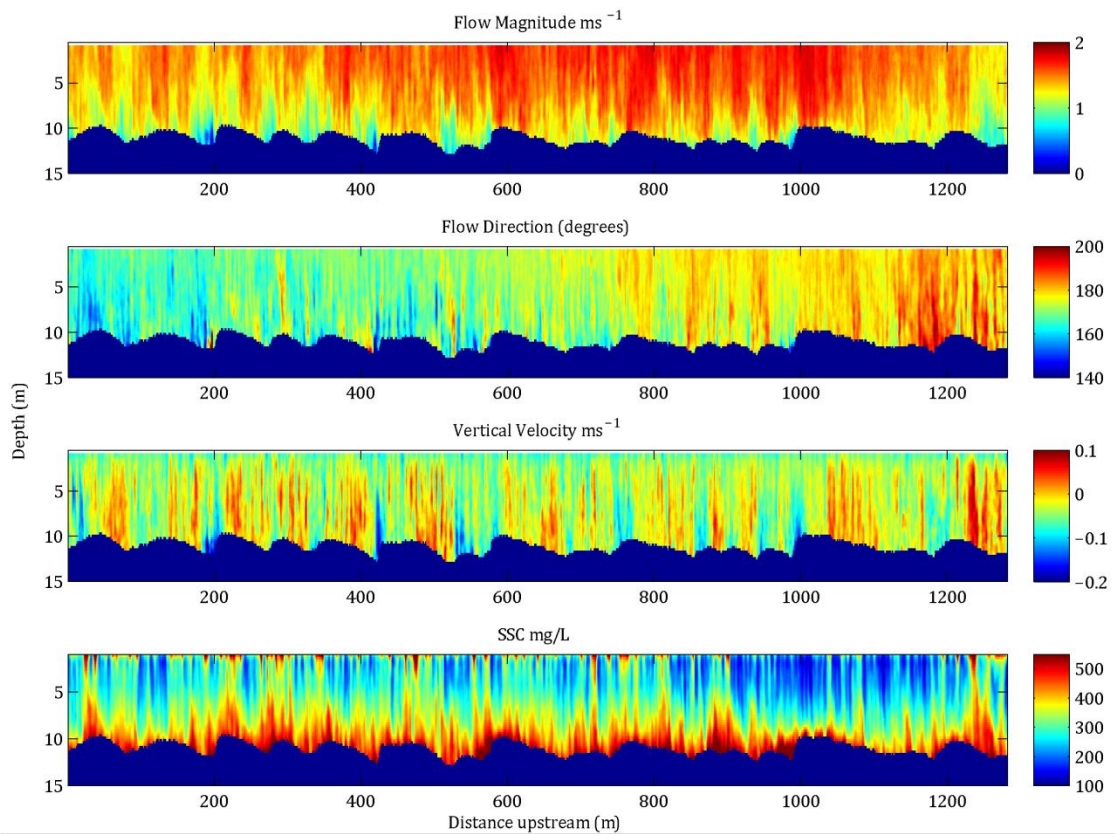


Figure 6-10. aDcp transect from day 314. aDcp transect location is shown in Figure 6-1, 0 m at the southern extent of the dune field in Figure 6-1. Flow magnitude and direction shows a variation across the transect due to flow convergence and steering at the northern extent (~700 to 1300 m)

From day 314 to 319 the downstream velocity (Figure 6-11A) and gradient of downstream velocity (Figure 6-11B) display near log-linear profile shapes. Vertical flow velocity (Figure 6-11C) and cross-stream velocity (calculated from the rotated downstream velocity vector, Figure 6-11D) display near zero values in the middle of each profile with little change through the survey period.

Overall, the change in flow direction with depth is consistent in magnitude and direction for all transects, except a slight difference in the last transect (Day 319) where a greater change from 174.7° to 170.9° was recorded. A slightly greater rotational change is likely caused by the reduced flow depth (1 m) confining the flow further into the dry season channel. The instantaneous bedload transport direction itself is not measured, unlike in studies in smaller rivers (Dietrich *et al.* 1979) and so a description of the effect of the flow rotation change on sediment transport direction not provided. Suspended sediment concentration (Figure 6-11F) shows two distinct trends, with high SSC on days 314 and 319, whilst day 315 and day 316 display distinctly lower SSC near the bed (~150 mg/L less), despite the increase in discharge on day 315.

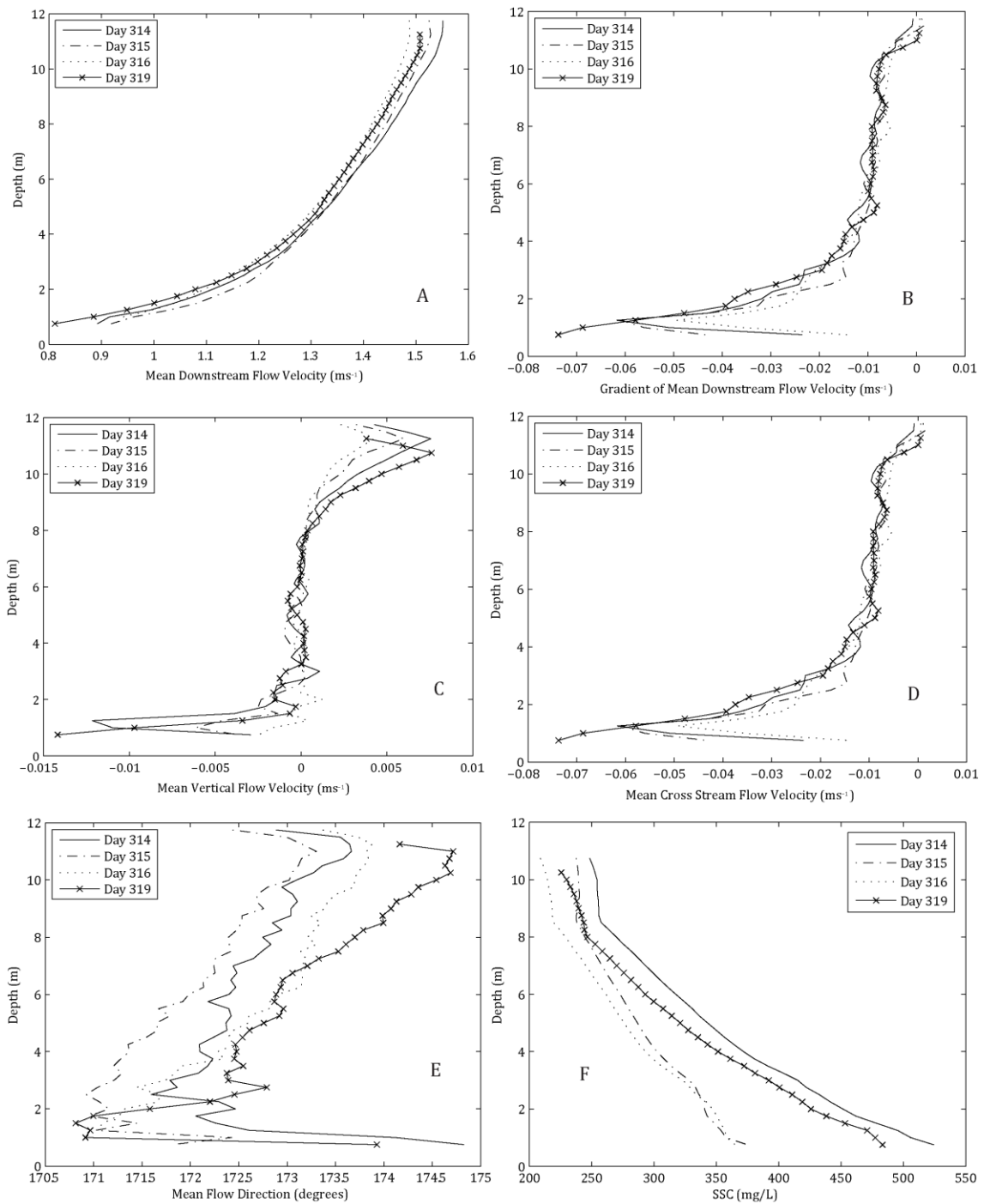


Figure 6-11. Mean flow profiles for selected aDcp transects. Multiple profiles for days 314 and 315 are displayed to show the measurement range for similar flow conditions. Cross stream velocities (F) were calculated from rotating the downstream (A) vector to the mean streamline for each transect

6.3.3 Dune lee side flow

One of the areas in the transect where flow direction changes considerably is in the lee side of dunes, where flow steering by bedform shape can induce

significant lateral flow, as shown in laboratory experiments (Allen 1968; Maddux, *et al.* 2003a,b; Venditti 2007; Blanckaert 2010), observed in the field (Dietrich *et al.* 1979; Bridge 1993; Walker & Nickling, 2002; Parsons *et al.* 2005) and in modelling studies (Omidyeganeh & Piomelli 2013a,b). In this transect there are two main flow directional changes in dune lee sides, the upper half of the transect (>650m) is dominated with high (200-220°) flow directions (SW) whereas for 0-650m dune lee sides have a more easterly flow rotation (140-160°) (Figure 6-10). This pattern is an interesting example of the flow separation vortex being controlled by the channel forced flow direction, in that the lee side flow separation vortex appears to be in an enhanced direction at variance from the mean local flow direction. Similar findings have been found in meanders (Dietrich *et al.* 1979) braided rivers (Bridge 1993), aeolian dunes (e.g. Walker & Nickling, 2002), and laboratories (Allen 1968) where dune crestlines were oblique to the flow, but the dune trough-spurs from rotated flow separation vortices were parallel to the mean flow direction. Oblique crestline-flow direction produces helical flow vortices (Omid & Piomelli 2013a,b), rather than roller vortices (Muller & Gur, 1996), and this distributes lee slope sediment laterally (Walker & Nickling, 2002). Mean lateral velocity (Figure 6-11 D) shows a distinct and consistent move to more negative (western) values closer to the bed, whilst the mean vertical velocity is more negative with depth due to the influence of flow recirculation in dune lees on the mean value. The negative mean vertical velocities (Figure 6-11 C) closer to the bed are due to flow separation behind dune lee sides biasing the mean values toward the negative. Dune lee side flow direction (relative to the depth averaged mean value) in Figures 6-12, 6-13 and 6-14 is an exaggeration of the depth-averaged flow direction at that point. For example in the dune lee sides ~200,400 and 1200 m in Figures 6-12 and 6-13 where deviations are commonly ~10 degrees positive; although it is notable that day 319 (Figure 6-14) does not present such a clear trend. Overall, this suggests lee slope sediment is distributed laterally along these dunes lee sides.

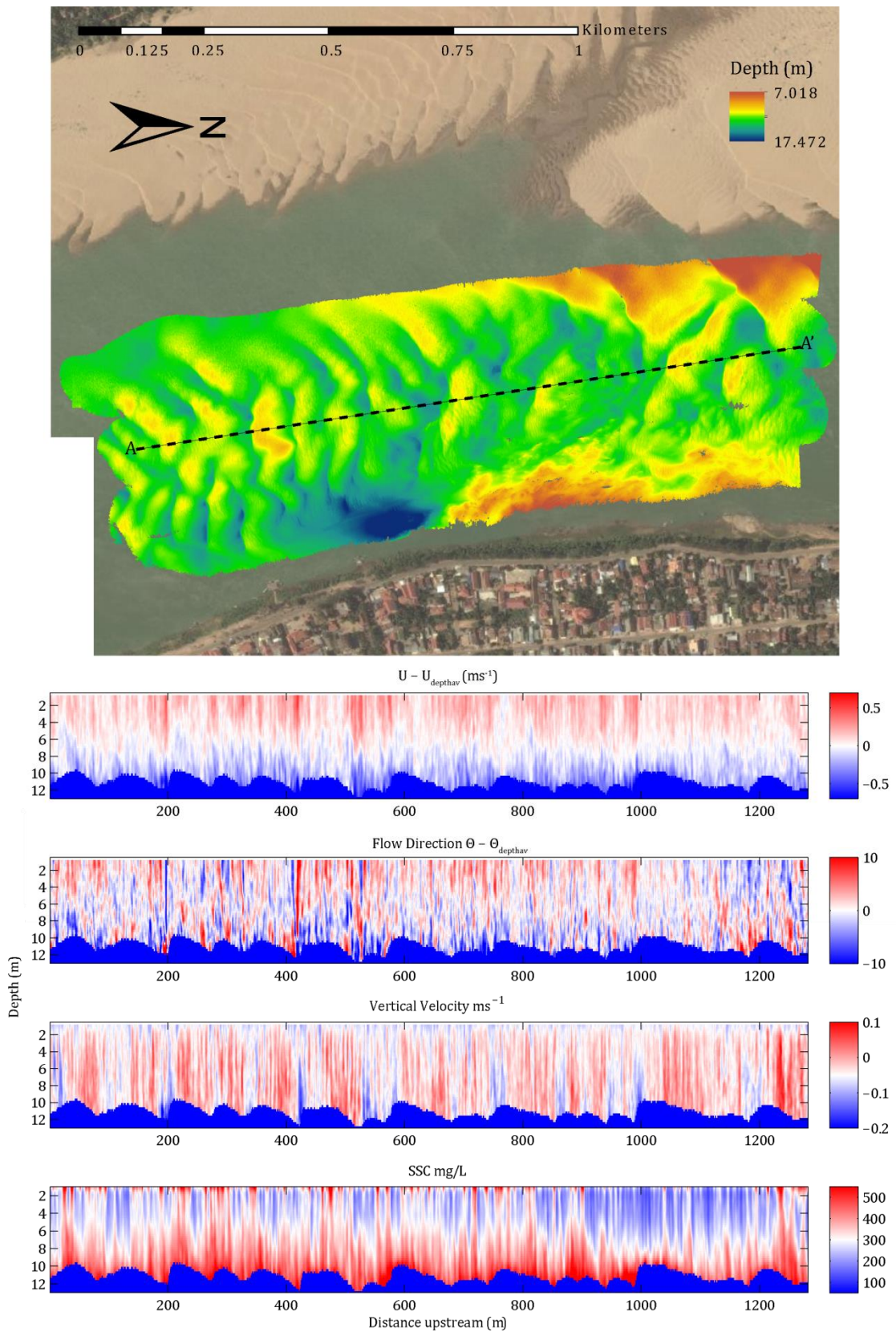


Figure 6-12. MBES bathymetry and aDcp transect data from day 314. aDcp transect location is shown as A to A', with A at 0 m and A' at 1250 m

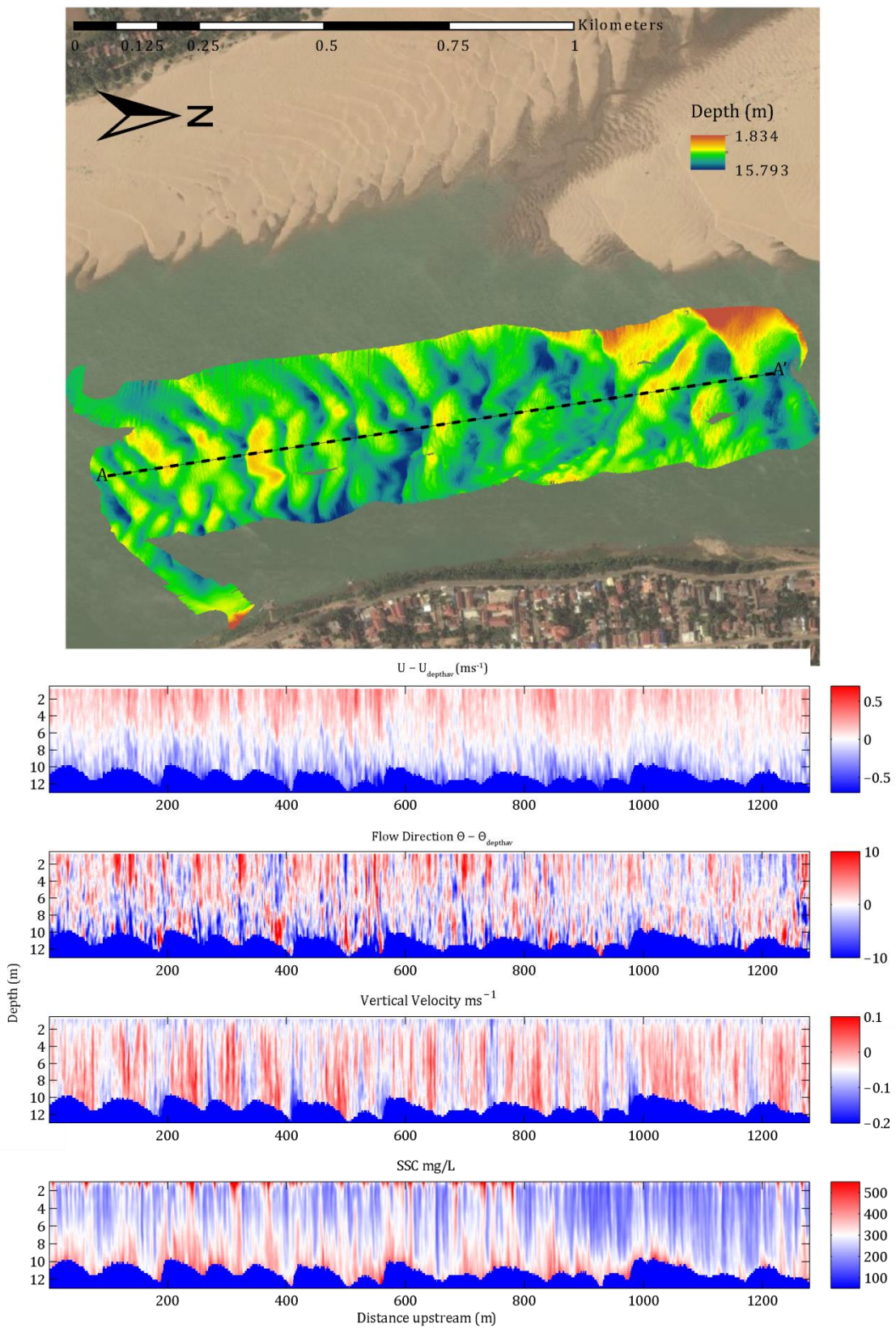


Figure 6-13. MBES bathymetry and aDcp transect data from day 315. aDcp transect location is shown as A to A', with A at 0 m and A' at 1250 m

Dune lee side flow separation itself has been extensively studied, but many aDcp moving boat field surveys often do not detect areas of flow separation, possibly resulting from several factors; firstly, bedform lee sides in rivers and estuaries often have quite low angle of repose ($<20^\circ$) producing intermittent flow separation (Kostaschuk & Villard 1996; Kostaschuk 2000; Best & Kostaschuk 2002; Best *et al.* 2004; Bradley *et al.* 2013;). With intermittent flow separation, there is the possibility that during the period of measurement there is no flow separation, thus making moving boat surveys prone to missing this time dependent phenomenon. Secondly, due to the aDcp beam spread, bin sizes expand with depth and with greater spatial averaging. It is quite possible that small flow recirculation vortices from low angle dunes are spatially-averaged out or missed by the blanking distance. Nevertheless, in transect 314 there are several places where flow separation has been detected (Figure 6-12). Flow magnitudes are particularly low inside the flow separation vortices and this can be seen for the dune at 300 m and 420 m (Figure 6-10). Negative vertical velocity in dune lee sides indicates further that dunes have active lee side flow separation. However, negative vertical velocity over dune lee sides is not uncommon for dunes without flow separation (Best *et al.* 2004). Flow separation produces turbulent eddies that hit the bed, producing large variations in bed shear and pressure where the separated flow reattaches to the bed (roughly 5-7 DH downstream). This phenomenon has been shown to produce higher than average quantities of suspended sediments locally around flow reattachment (Nelson *et al.* 1995). In these field surveys, SSC is highest in the dune lee, peaking at 550 mg/L, e.g. in Figure 6-12 at ~490 m and Figure 6-14 at ~550 m.

From combining the above aDcp data it can be shown that 12 of the 18 dunes in the Day 314 aDcp transect have a measured lee side vortex (Figure 6-15). This conclusion is based upon depth averaged vertical velocity and SSC, where the red bars indicate a negative relationship between vertical velocity (more negative) and SSC (more positive) along the transect (Figure 6-15). The relationships between SSC and vertical velocity with the bedforms is also shown for clarity (Figure 6-15).

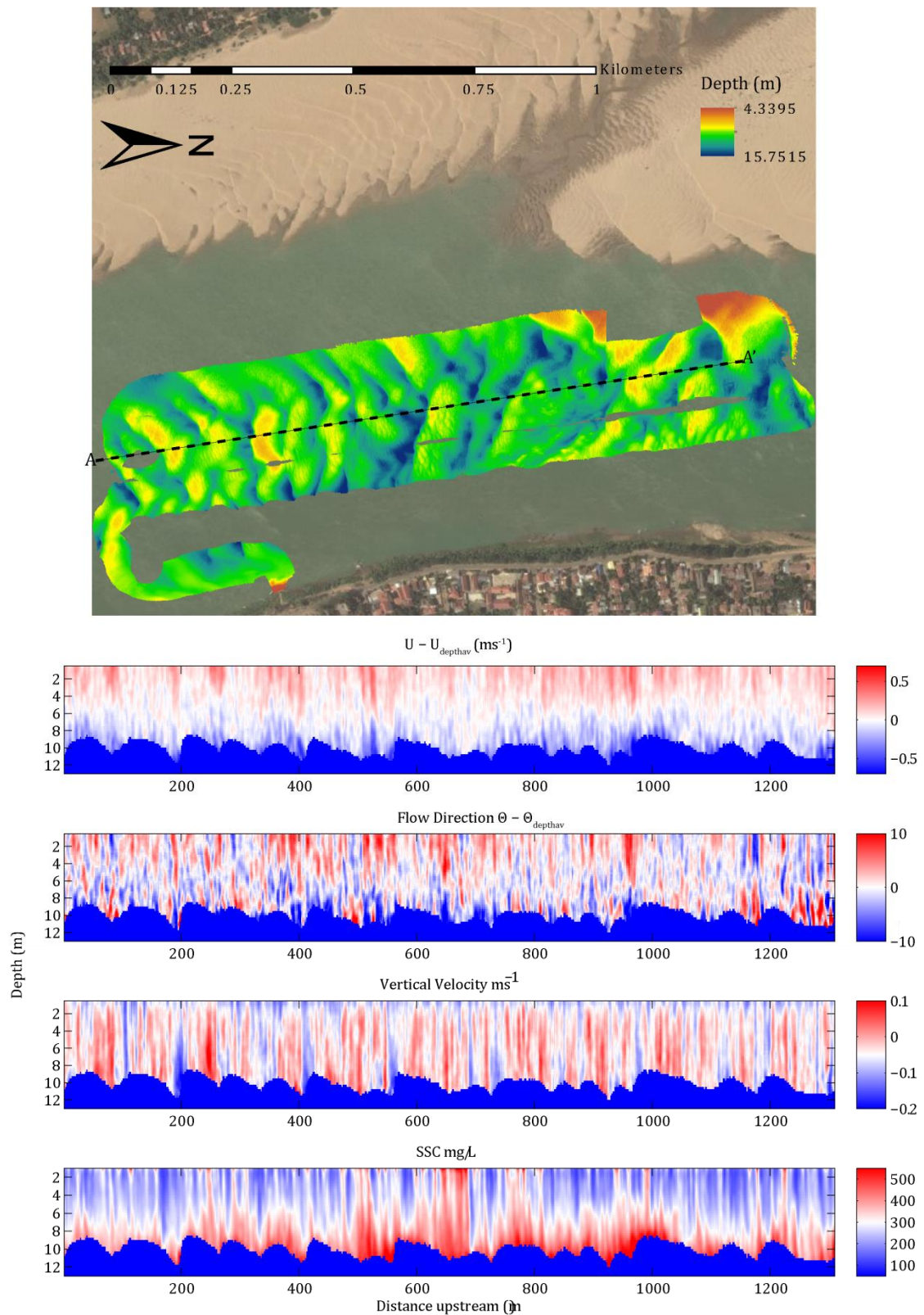


Figure 6-14. MBES bathymetry and aDcp transect data day 319. aDcp transect location is shown as A to A', with A at 0 m and A' at 1250 m

Along transect 314, depth-averaged vertical velocity cross-correlates well with the bed elevation producing an R of 0.68 (with a lag of ~15 m), indicating

synchronisation with the increasing elevation along the stoss slope and positive vertical velocity, and vice versa (Figure 6-15). Stoss side flow convergence and positive vertical velocity also produce high velocity magnitudes, highest at dune crests where depth is shallowest and local Froude number highest. In transect 314 the highest dune crests result in the highest velocity magnitudes in the transect (Figure 6-10).

Depth-wise the effects of bedform form roughness can be seen to reduce flow magnitudes intermittently in Figure 6-12 & Figure 6-14 and in the spatially-averaged mean downstream velocity profiles (Figure 6-11). This roughness effect produces a non-log-law reduction in velocity magnitude close to the mean bed level, commonly found over dunes due to form drag from flow separation (Smith & McLean 1977; McLean & Smith 1979; Nelson *et al.* 1993; McLean *et al.* 1994; Bennett & Best 1995; Omidyeganeh & Piomelli 2011).

Roughness due to intermittent macro turbulent structures (Best 2005b; Grigoriadis *et al.* 2009; Hardy *et al.* 2009;2010a; Omidyeganeh & Piomelli 2011) is harder to see in mean, spatially or temporally averaged profiles. Vertical columns of high-low-high magnitude flow events occur throughout the transect. The low velocity magnitude flow commonly rises to half flow depth, and occasionally near the free surface (e.g. near the end of transect 314, Figure 6-10). These columns of high velocity magnitude coincide with high SSC and have a negative correlation of $R^2=0.42$ to SSC (but a large lag of ~ 150 m). There is a lower correlation between SSC and vertical velocity ($R^2=0.31$), and this is likely to be due to the high amount of SSC along the whole transect near the bed whilst vertical velocity fluctuates between +ve and -ve with dune shape. This consistently high near bed SSC is due to the intense mixing caused by the turbulence produced by bedform roughness, and secondary bedforms (Best 2010). Suspended sediment concentration (SSC) across the transect is highest nearest the bed, with a considerable area roughly at half depth, with values above 400 mg/L. This structure demonstrates the considerable impact dune related turbulence has on flow mixing of suspended sediment levels near the bed in bedload dominated conditions.

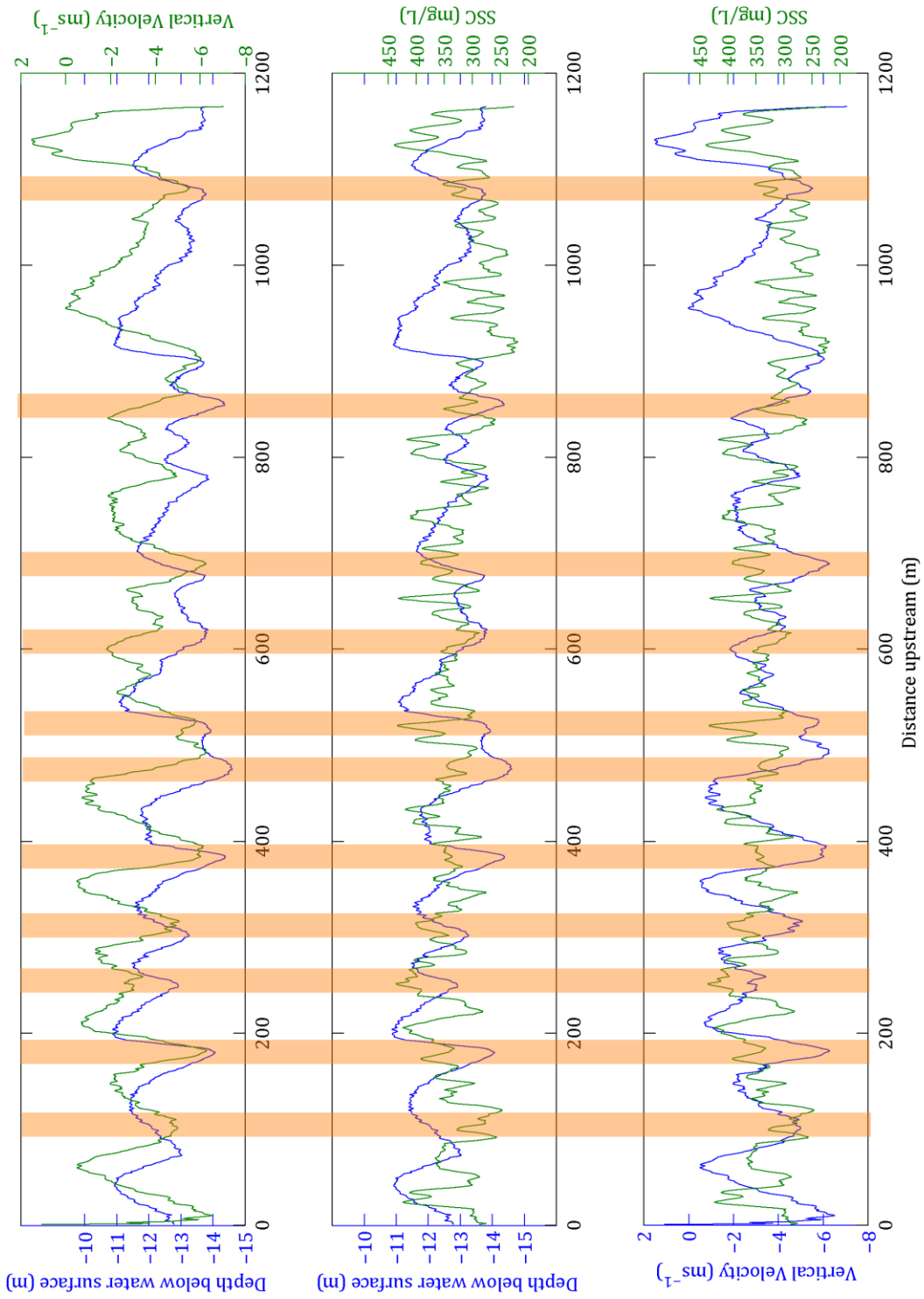


Figure 6-15. Correlations between vertical velocity, bed shape and suspended sediment for the day 314 aDcp transect. Orange bars identify periods where lee side separation can be identified where the value of vertical velocity drops and suspended sediment rises. Although the majority of dunes have measured lee side flow separation, not all dunes measured here had identifiable lee side separation and appear vertical rather than closer 45° due to vertical exaggeration

6.3.4 Bed shear stress, depth and suspended sediment

To further assess the change in suspended sediment concentration with flow depth and flow velocity, the bed shear stress and shear velocity was calculated from the mean (over the length of the transect) downstream velocity profile (Table 6-7). The day 314 transect has the highest bed shear stress and lowest Rouse number. The primary sediment transport mode across all of the surveys suggests sediment transport for the median grain size (212 μm) is increasingly bedload dominated over time (Table 6-7). This assertion is supported by the mean suspended sediment concentrations determined between surveys 314, 315 & 316 (Table 6-7, Figures 6-2 & 6-13). However, day 319 produced the second highest mean suspended sediment concentration measured in this field survey (Figure 6-14), whilst the Rouse number was highest; thus indicating more bedload dominated sediment transport (Table 6-7). As discussed in Chapter 4, flow depth has considerably greater influence on the flow structure over dunes than flow magnitude. The lower depth will have induced greater topographic acceleration, which can be seen in the high velocity magnitudes above the crests of the larger dunes in Figure 6-14 and the higher downstream velocity gradient in the lower half the mean profile for 319 (Figure 6-11), thus, producing greater shear near the boundary. The empirically low mean dune height should indicate that these dunes are not depth-limited as in the laboratory dunes in Chapter 4, yet changes in depth are having a measurable effect on the entire velocity profiles, and importantly near the bed.

Transect day	314	315	316	319
Mean dune height (m)	2.17	2.02	1.92	1.91
Mean dune wavelength (m)	98.87	98.80	98.46	98.73
Dune Steepness (height/length)	0.0219	0.0204	0.0195	0.0194
Mean depth at Kratie (m)	13.15	13.45	13.42	12.72
Mean profile depth (m) (aDcp)	12.56	12.64	12.51	11.5
Depth/Dune height	5.78	6.25	6.5	6.02
Mean downstream velocity (ms^{-1})	1.383	1.377	1.347	1.357
Bed shear stress (log law estimated) (Nm^{-2})	10.23	8.21	8.28	8.08
Shear velocity	0.10	0.09	0.09	0.09
Rouse number	2.50	2.79	2.78	2.81

Mean SSC (mg/L)	332	280	271	302
-----------------	-----	-----	-----	-----

6.4 Discussion

6.4.1 Controls on large dune height and secondary bedforms

For large rivers, dune height has been found to not match the empirically produced scaling derived from laboratory experiments (Guy *et al.* 1966; Allen 1982; Ashley 1990). In some instances, this disparity has been suggested to be due to an overall difference in dune shape; where dune lee sides are $<10^\circ$ (Kostaschuk & Villard 1996). Here dune lee sides are generally greater than 20° (Figure 6-6) and there is evidence that $\sim 66\%$ of the flow over dune lee sides was separated at the time of measurement (Figure 6-15). Yet dune heights are roughly half that from empirical-laboratory predictions; whilst the reduction in secondary bedform size and the observed increase in downstream velocity gradient near the free surface (Figure 6-11) across all surveys indicate that the large host dunes' are experiencing processes more commonly found in depth-limited conditions (e.g. Carling *et al.*, 2000a,b).

Flow depth was seen as a control on dune height in laboratories as flow depth is usually parsimonious with the height of the turbulent boundary layer. Despite dune heights' measured here being half that estimated from empirical equations, it is clear that free flow does not exist in the aDcp transects in these surveys, with coherent flow structures still propagating the entire flow depth (Figure 6-10), and the gradient of downstream and vertical velocity near the free surface being non-zero (Figure 6-11). As chapter 4 detailed, the vertical extent of the form roughness portion of mean velocity profiles over dunes will shorten when depth decreases, producing a higher gradient velocity profile as flow has to accelerate to maintain conservation of momentum. This finding is manifest in the present field dataset, where high velocity magnitudes above the crests of the larger dunes in Figure 6-14 are seen. The mean velocity profile for day 319 produced a higher downstream velocity gradient in *the lower half* of the mean profile for day 319 (Figure 6-11), indicating greater topographic acceleration over the dune stoss slopes and shear close to the boundary. The response of the velocity profile occurred during reduction in absolute depth and mean large bedform height (Table 6-7) but translates into a change in depth from 5.7 (Day

314) to 6.5 (Day 316) to 6.05 (Day 319) dune heights. These values are roughly two and half dune heights of depth more than studied in chapter 4, yet the response of the velocity profile shape between day 316 and 319 is remarkably similar. Interestingly, the mean downstream velocity increased on day 319 (table 6-7), despite the drop in discharge, this may be indicative of discharge partitioning around the bar, or that higher velocity magnitudes exist in the transect over dune crests (Figure 6-10).

The changes in secondary bedforms detailed in section 6.3.1, where secondary dune height and length response to the hydraulic changes during this survey, correspond to the interpretation of flow structure detailed above, in that the reduced secondary bedform size, and higher gradient in the mean downstream velocity profile, indicate that on day 319 the dune field was in fact experiencing depth-limited conditions despite normalised depth being two times higher than empirical predictions and the study in chapter 4.

Reduced dune heights have been found consistently across a large suite of rivers in large rivers (Venditti et al (in review)), this observation implies that factors such as width:depth ratio, hydrograph character, and bedform morphological adaption times exert a consistent control on dune height not found in laboratory studies. The upper limit of dune height, based upon laboratory studies, is the production of an upper stage plane bed at the dunes' crest (chapter 5), usually controlled by the amount of topographic acceleration, flow convergence and grain size at a dune crest (see chapter 4 & 5). In the present surveys, secondary dunes were found consistently at large dunes crests (Figure 6-8), and has been also found at dune crests that are in equilibrium in the field (Parsons *et al.*, 2007). It would therefore appear that there is a different control on dune height in these larger rivers when compared to laboratory studies and smaller rivers.

6.4.2 Suspended sediment

To explore the role of altering flow depth and secondary dunes on this dune field, the suspended sediment concentration will be discussed. Figure 6-16A displays the spatially-averaged downstream velocity normalised by the shear velocity, calculated from the temporal and spatial average of the aDcp transects

(Table 6-7). Here we see the hydraulic relationship that best describes the non-linear changes in suspended sediment seen in aDcp transects 314, 315, 316 and 319 (Figures 6-12 to 6-14). The higher suspended sediment conditions (day 314 & 319) both have similar U/u^* values closer the mean bed level. To illustrate this further U/u^* is plotted against the spatially-averaged suspended sediment concentration in Figure 16 B. Whilst the ratio of U/u^* in the upper flow for day 319 is lower than that at 314, it still reaches similar values of U/u^* at the bed due to the higher gradient in downstream velocity near the boundary. This result indicates that the change in mean downstream flow velocity and reduction in discharge (Table 6-2) is more than compensated by the increased topographic acceleration over the dunes and has consequently pushed U closer to u^* for a greater proportion of flow depth near the bed and as a result increased sediment transport rates and the amount of sediment suspension, reinforcing the above interpretation of the secondary dune sizes and mean velocity profiles.

The Rouse number indicates the dominant mode of sediment transport type is bedload. However it has been less successful in describing smaller scale variations in sediment transport mode during the surveys shown here, due to the above described high gradient of downstream velocity near the bed (e.g. day 319). In this situation the ratio of downstream velocity to shear velocity can be used as a better indicator of the amount of sediment suspension within the bedload dominated regime (Figure 6-16C), as this accounts for the relative effect of depth on the velocity profile over dunes.

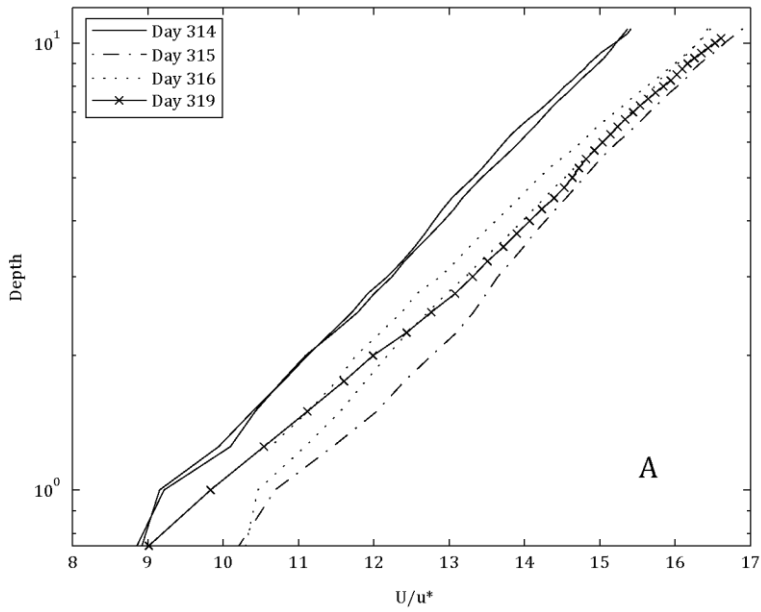


Figure 6-16A. Mean flow profiles for selected aDcp transects. Multiple profiles for day 314 and 315 are displayed to show the measurement range for similar flow conditions, Day 319 shows a higher gradient toward lower U/u^* values that are comparable to day 314.

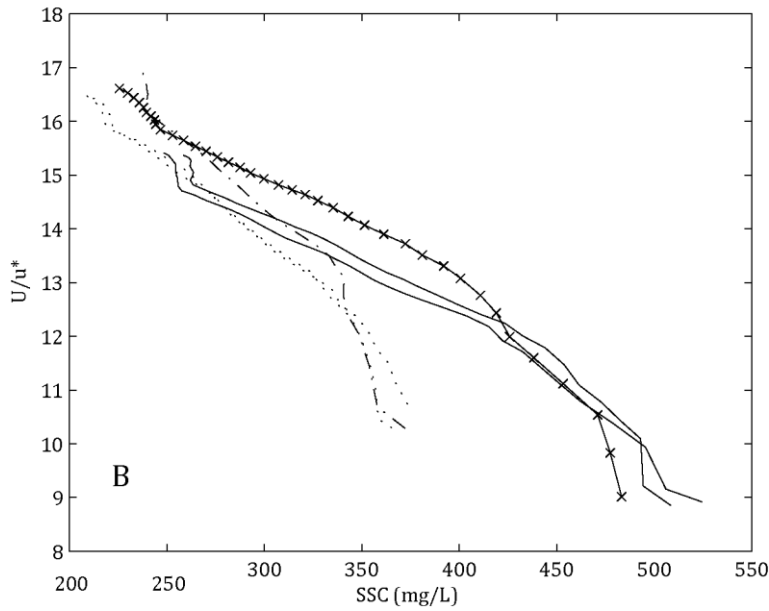


Figure 6-16B. The relationship between U/u^* and suspended sediment concentration.

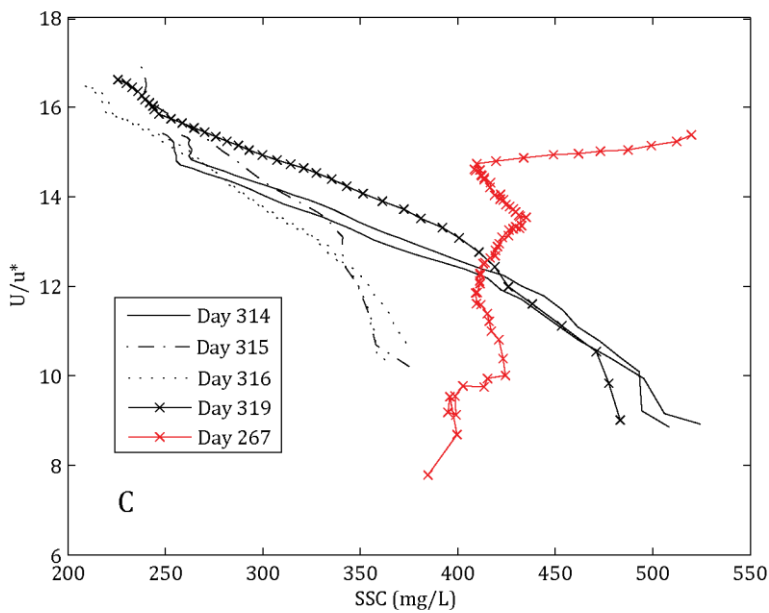


Figure 6-16C. An aDcp profile measured at peak flood (day 267) at Krate is plotted alongside the data of Figure 6-16B to show how a change in Rouse number affects the relationship found in Figure 6-16B.

For comparison against flow conditions at a different Rouse number, Figure 6-16C plots the U/u^* vs SSC values for an aDcp transect acquired at peak flood alongside those in Figure 6-16B. It was calculated that the mode of sediment transport (Rouse number) during the flood peak indicated that sediment was being transported at ~50% suspension for this transect (day 267). Figure 6-16C shows that the full depth-mixing of the suspended sediment has produced no relation between suspended sediment concentration and U/u^* , in contrast to the more bedload-dominated flow fields recorded in the falling leg. This potentially indicates that topographic acceleration over dunes has little impact on the production of suspended sediment when the reach averaged shear velocity is high enough to induce sediment transport at 50% suspension.

Prescribing cause and effect in dune systems is particularly difficult as there are very few variables that are independent and inherent variability is high. Figure 17 displays the relationship between relative submergence (mean large dune height / mean depth) plotted against mean suspended sediment concentration for the aDcp profiles taken on days 314 to 319. The relative submergence of the dunes appears to provide a strong relationship with the concentration of suspended sediment across the survey. This is because submergence is essentially a proxy for topographic acceleration (for the large dunes). Dune steepness can also be used and is more intuitive as a proxy for topographic acceleration, but as wavelength did not change in this survey there is little difference in the relationship produced from this data. Additionally, dune steepness would not produce a dimensionless comparison. It is as yet unclear how to integrate dune submergence into Rouse number calculation (and therefore also account for fall velocity and shear) when the reach averaged shear velocity indicates sediment transport conditions are bedload dominated.

The high quantity of sediment suspended and presence of secondary bedforms at dune crests here, across all conditions that are meant to be bedload dominated, may indicate that the crests of these dunes are more erosive rather than depositional as in traditional dune theory (Exner 1920). The presence of secondary bedforms increasing sediment suspension along the dune stoss slope may well have a direct cause on the empirically low dune height of the large bedforms via a reduction in bedload sediment supply, and the creation of a

temporary suspended load conditions at the host dune crest. This mechanism provides a plausible method to explain the reduced dune height of these dunes.

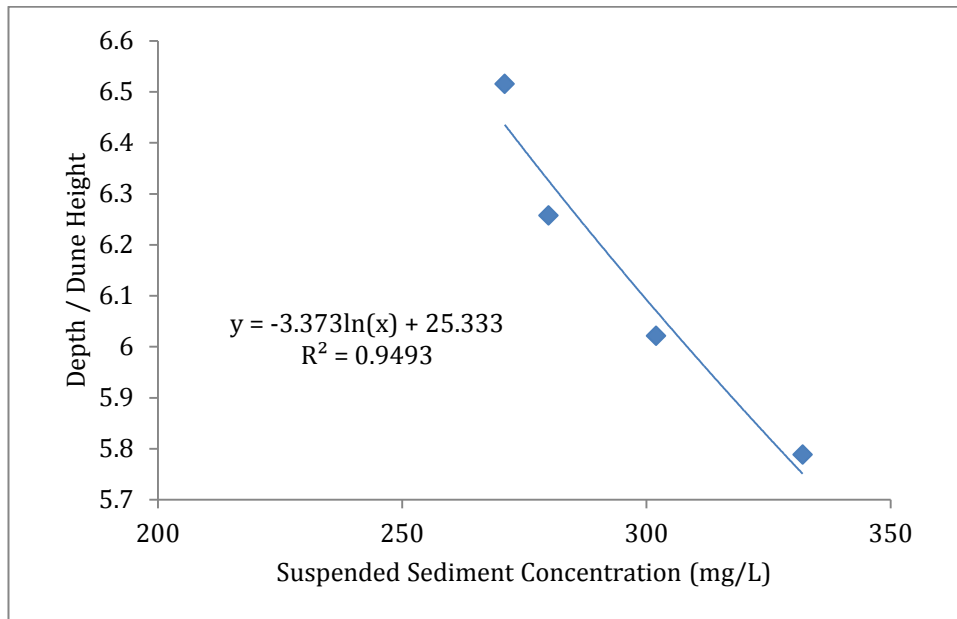


Figure 6-17. Mean large dune height / depth for the corresponding day vs. suspended sediment concentration for the corresponding day. A log fitted line is applied to attempt to show how well these variables are related.

One key aspect of the discussion on suspended sediment concentration and dune height is that the majority of techniques used here effectively assume two-dimensional flow. Whilst aDcp profiles were taken across the centreline of the dunes, where they are at their steepest and most two-dimensional, it is perhaps not representative of the wider 3D dune field, and assumes that the large dune centreline controls the wider dune field morphodynamics. Yet the changes in flow direction in the dune lee's described above indicates the presence of three-dimensionality in the flow structure, and this turbulent three-dimensionality will be transmitted downstream in the dune's turbulent wake. Recently, the effect of strong flow three-dimensional structures of the initiation of sediment transport has been investigated (Keylock *et al.* 2014). This research found that 3D flow structures, particularly the change in flow direction perpendicular to the main flow direction, are more able to move sediment for a given average bed shear stress. Two and three dimensional bedform features can produce strong three dimensional Coherent Flow Structures and it has been observed that these highly turbulent structures suspended large amount of sediment (Kostaschuk & Church 1993; Shugar *et al.* 2010).

Local bed shear stress, shear velocity and Rouse number were calculated across the transects. A linear fit of the log-normal velocity profile was made and a threshold of $R=0.95$ was applied to the bed shear stress and shear velocity calculation as otherwise extremely erroneous values were predicted, profiles that did not have sufficient linear correlation were not used to estimate u^* . No attempt was made to spatially interpolate between erroneous values along the transect. The results (Figure 6-18) were in line with McLean's (1999a) assertion that non-spatially averaged instantaneous profiles of velocity over dunes will overestimate the bed shear stress at reattachment, and underestimate at dunes crests. Consequently, using the Rouse number derived from law of the wall estimated of the shear velocity using instantaneous aD_{cp} data is unwise. The Rouse number is more applicable to larger scales, and small scale definitions are needed to advance our understanding of sediment transport modes at the scale of individual dunes. The impact of non-linear bedform production of suspended sediment at individual dunes scale are important in large scale evolution models as this suspended sand responds to gravity in ill-defined ways (Szupiany et al 2012) that are poorly parameterised; an effect the predicted quantity of sand transport onto lateral bar slopes and then the nature of bar evolution at channel scale (Nicholas, 2013, Nicholas et al 2013).

6.4.2 Scale of bed features and their rates of change

The bi-modal distribution of large dunes in this survey can be attributed in two distinct ways: 1, a transient condition existing from the flood: 2, a steady state that characterises both flood peak and falling leg conditions. Both of these possibilities exist in and excess of a month scale, and greatly longer than this survey period.

1: The bi-modal distribution could represent an unsteady bed state produced from the hysteresis of the large flood 48 days before (Figure 6-2). This timescale would indicate that the adjustment time required for bedforms to reach new equilibrium condition is greater than the six days of this measurement season, as no change in mean wavelength was found (Table 6-4 & 6-5). Whilst the mean dune wavelengths found in these surveys was consistent in time (Figure 6-8, Table 6-3 & 6-5), individual dune wavelength varied by as much as 10 m (20% dune length) over 24 hours (Table 6-3, Dune 2, day 315 to 316). Although some

dunes consistently increase in length (e.g. Dune 10, Table 6-3) or decrease in length (Dune 3, Table 6-3) over the survey period, there is no consistent change in mean dune wavelength over the survey period and therefore it is only possible to attribute these variations to individual dune transience as they migrate downstream, rather than dune calving or amalgamation processes.

2: The bi-modal distribution of wavelengths found in this survey could indicate two separate regimes of dunes formed under inter-annual timescales that represent wet and dry season hydraulic conditions (Coleman 1969; Allen 1978; Fielding & Alexander 1996; Fielding *et al.* 2009). Therefore it is a possibility that this assemblage of dune lengths is stable and common for this river and represents the two major hydraulic conditions of falling flood (shorter dunes and depths in this survey period) and wet seasons (longer dune wavelengths most well match flood peak depths), measurements of dune size is required at other times of year to validate this assertion.

The adaption of dunes' wavelengths to new hydraulic conditions takes longer than dune height change, as the process of shortening or lengthening bedform wavelength requires superimposed bedforms of sufficient size to erode or deposit onto the host bedform (Fredsoe 1979; Nelson 2011; Warmink *et al.* 2014, see discussion in chapter 4). In Figure 6-8 there are two bedforms that could be described as undergoing erosion or being amalgamated (at ~150 m and 750 m respectively, Figure 6-8), yet as noted above, these dunes were found to migrate at a very similar rate to the larger surrounding bedforms, rather than overtake and amalgamate/erode the host bedform. These two bedforms are notable as one dune gained in volume (dune at 150 m) or lost volume (dune at 750 m) over the survey period (Figure 6-8), whilst the other bedforms effectively remain constant in volume. Sediment bypassing and starvation through sheltering of bedforms by nearby lee slopes has recently been investigated in the laboratory (Best *et al.* 2013) and this sheltering is a probable explanation for the loss of sediment for the dune at 750 m (Figure 6-8). This indicates that volume change rather than migration rate change is preferred method of bedform adaption here, so that bed defect amalgamation is via diffusion of the sediment volume rather than through size-dependent translation differences producing amalgamation of bedforms (e.g. Paola & Borgman 1991; Leclair 2002). However, the three-dimensional nature of the bedform field indicates these

three dimensional morphodynamics of amalgamation and diffusion of sediment volume (e.g. Venditti *et al.* 2005c) differ from these traditional two-dimensional laboratory experiments (Leclair 2002; Best *et al.* 2013), as also noted by (Warmink *et al.* 2014).

Figure 6-7 displayed the bedform translation recorded between day 314 and 319. With an average translation of 22 m downstream over five days and a mean wavelength of 98 m, it would take 22.2 days for the mean dune to migrate one wavelength. Yet, with mean wavelength essentially unchanging over the survey period, small and large dunes migrating at similar rates, and longer than predicted wavelengths for equilibrium conditions, after a flood peak, it is more likely this assemblage of wavelengths has reached a steady mean distribution and represents the two distinct conditions recently present in the river. Whether this state exists though the dry season, with depth reducing another ~5 m from the present survey depths, requires further survey.

Interestingly, this dataset has shown that secondary dune dynamics respond quickly to changes in hydraulic conditions, principally in the reduction of secondary dune size, particularly at dune crests, on day 319 (Table 6-6). This adjustment indicates that these secondary bedforms are responding to changes in hydraulic conditions much more rapidly than their host bedform; principally because the hydraulic change was of self-similar scale to the bedforms themselves in space and time (Table 6-8). It is postulated that bedforms primarily react to hydraulic changes that are self-similar in scale to themselves. For example, Villard & Kostaschuk (1998) found that superimposed dunes migrated the faster at low flow, whilst the host, asymmetric dunes, migrated the most at peak flow conditions. The lack of large dune geometrical change on day 319 in response to the reduction in flow depth is because the timescale of this change is more similar to the scale of secondary bedforms than the host, large bedform (Table 6-8). The secondary bedforms are buffering the effects of the smaller scale changes in hydraulic conditions to the larger host bedforms, with both bedform scales responding to different hydraulic states.

Table 6-8. Self-Similar characteristic scales of bedform features

	Large Dunes	Secondary Dunes
Time (days)	1×10^1 to 1×10^2	1×10^1
Depth (m)	$>1 \times 10^1$ $<1 \times 10^2$	1×10^1
Wavelength (m)	$\sim 1 \times 10^2$	1×10^1
Height (m)	$\sim 1 \times 10^1$	1×10^{-1}
Slope	?	?

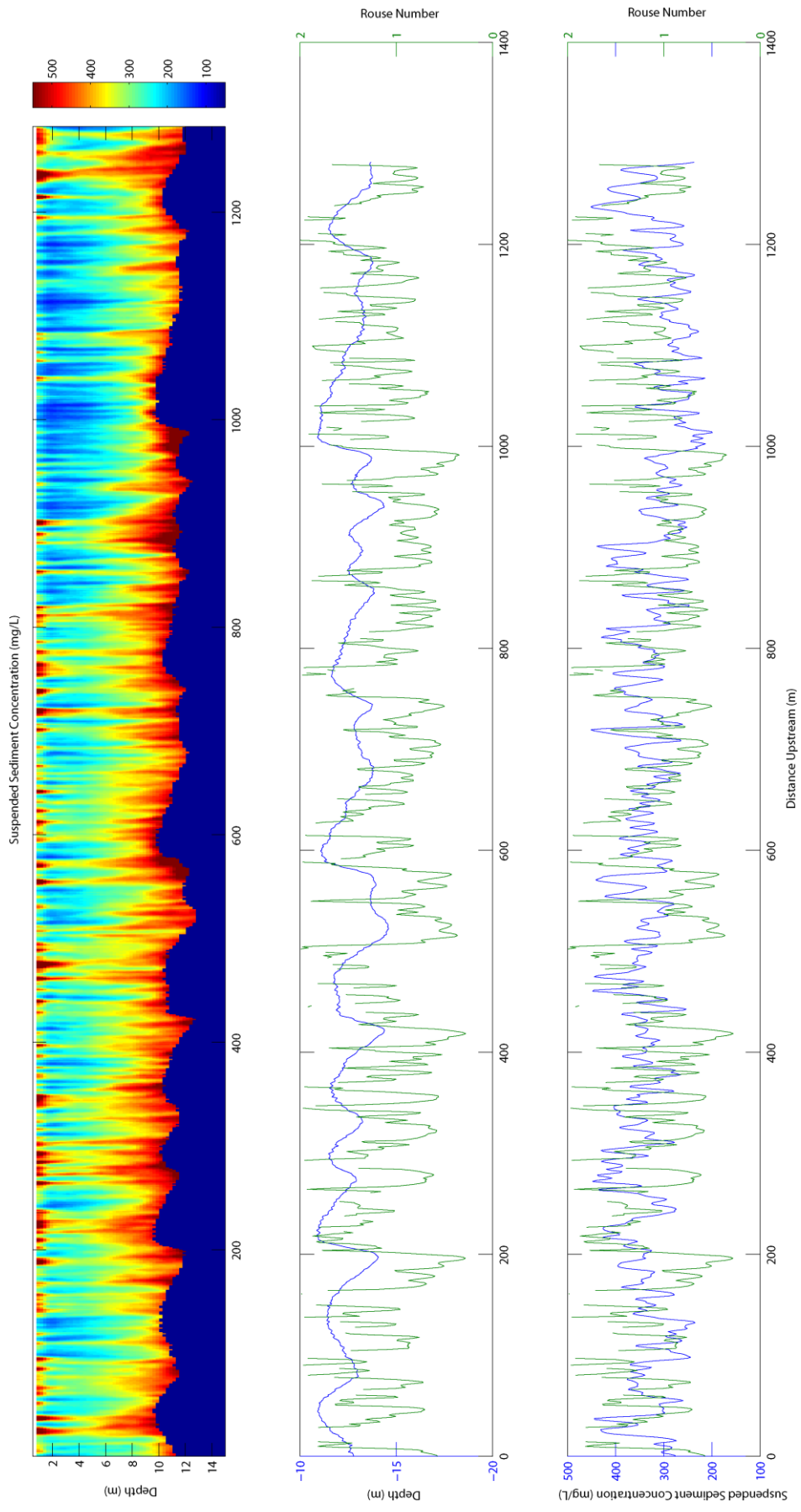


Figure 6-18. An attempt to correlate suspended sediment concentration over dunes (top) with Rouse number (middle) and the depth averaged suspended sediment concentration across an aDcp transect (bottom). Using day 314. Rouse number was calculated using the shear velocity estimated from the law of the wall on each profile. Rouse number inversely and incorrectly matches the changes in suspended sediment concentration

6.5. Limitations

The present chapter used acoustic methods to measure the bed state, 3D velocities and suspended sediment concentration of a section of the Mekong River, Cambodia. Whilst the MBES data is able to measure the bathymetry for nearly the entire width of the river, the aDcp transect only provides us with data of that transect. With the slow boat velocities required to obtain good aDcp data, multiple transects across the width of the channel were not possible. Therefore measurement of secondary flow structures, which may or may not exist in large river channels (Parsons et al 2007) but can greatly affect sediment transport (Bridge & Jarvis 1982; Dietrich *et al.*, 1988; Bridge, 1993; Maddux *et al.*, 2003b; Ettema & Daly, 2004) is untenable here, a significant drawback as the morphology of the bedforms here is highly three-dimensional. In addition, the data collected is only transient, rather than mean flow at each point (e.g. chapter 4), thus estimation of bed shear stress derived from individual profiles in the transect is highly spurious (Figure 6-18)- with only transect averaged profile useable. This limitation restricts the discussion on production of suspended sediment over the dunes to larger scale relationships, such and dune height/ flow depth, rather than assessing local controls on suspension- which could be secondary bedform dependent, and control overall dune shape (Kostaschuk & Villard 1996).

The time between bathymetry measurement surveys is longer than that of the migration rate of the superimposed bedforms. As such, tracking the superimposed bedforms is not possible as they have migrated further than one wavelength, and thus estimation of sediment transport is not possible. Such data would be very useful as it would allow measurement of the volume of superimposed bedforms adds to the host bedform, rather than bypasses it.

Whilst this survey of the river Mekong during the falling leg of the wet season has revealed similarities to the results of chapter 4, the small range of discharges, depths and time scale of the survey means that larger scale variation in bedform response to unsteady flow conditions was not measured. This survey was measured at a comparably a steady state to the preceding flood. For bedforms on the scale of 100's of meteres long, repeated surveys over multiple weeks is required to be able to measure large dune morphodynamics in

response to unsteady flow conditions. As such, the main conclusions from this work are related to the shorter scale superimposed bedforms.

6.6. Conclusions

Dune morphology, flow structure and suspended sediment concentration were measured in the stable portion of a falling leg of a flood wave on the Mekong River. It was found that:

1. A rise in suspended sediment concentration and reduction in flow depth occurred simultaneously with a statistically significant reduction in superimposed (secondary) dune height and wavelength. Large dune mean geometry showed no consistent relationship with the hydraulic conditions present at the timescale of this survey. It is postulated that secondary bedforms buffer the host bedform from scales of hydraulic changes on the order of the secondary bedform size.
2. Mean suspended sediment concentration is well predicted by values of U/u^* near the bed, with similar relative bedform submergence (bedform height/depth), across variations in discharge.
3. Despite dune height being half that predicted from empirical equations, mean velocity profiles were affected by variation in flow depth and produced suspended sediment concentrations that did not match those predicted by the Rouse number. The reduction in superimposed bedforms size, and increase in suspended sediment concentration when depth reduced indicates that the secondary bedforms are affected by flow depth. In addition, the increase in suspended sediment at dunes crests (due to the presence of secondary bedforms) may well reduce the deposition of sediment at the dune crest, thus limiting host dune height.
4. Cross-correlating vertical velocity and suspended sediment concentration suggests that lee side flow separation was successfully measured for 66% of the dunes in the aDcp transects. These dunes were not low-angle dunes with intermittent flow separation.
5. A bi-modal distribution of dune wavelengths was found, similar to other rivers in monsoonal climates. Larger dune wavelengths have equilibrium depths of ~ 23 m, whereas the short dunes were in equilibrium with the flow depth at the time of survey (~ 12 m). However, over the six day survey, amalgamation or carving of bedforms was not observed, and

smaller dunes migrated at very similar rates to the larger bedforms surrounding them. This observation suggests that the bi-modal distribution of wavelengths could be a stable configuration.

6.7 Synthesis

One of the major questions in dune research at present is understanding, measuring and being able to predict the proportion of sediment that is deposited on the lee slope- and adding to the bedform volume and its' migration downstream, and what proportion overpasses dune flow separation and does not add the bedform volume (Mohrig, & Smith 1996; Naqshband et al 2014). This question is expanded and complicated further when considering superimposed bedforms, which can add to the host dune (Reesink & Bridge 2007) or pass over dunes (Venditti et al 2005b). The character and behavior of these superimposed bedforms has been found in this chapter to be dependent on fluctuations in boundary conditions on the timescale of a single day (same order that creates them), and as such the proportion of the superimposed bedform that deposits onto the host lee slope is likely strongly controlled by transient fluctuations in the boundary conditions as much as any individual morphological processes (c.f. Reesink & Bridge 2007).

Moreover, the increased production of suspended sediment over large dunes from the presence of secondary dunes will change the distribution of suspended sediment that is entrained into the flow separation bubble and eventually contributes to host bedform migration. In addition the increase in suspended sediment production may well reduce sediment supply to the host dune crest, thus artificially keeping it lower than empirical predications without producing low angle dunes. Short dunes have been found in many of the world's large rivers (Best 2005a) that tend to scale as $1/6^{\text{th}}$ flow depth rather than $1/3^{\text{rd}}$ (Garica 2008) and the process that controls this has yet to be confirmed (Venditti et al., in review), quite probably due to the larger scales needed to measure this phenomenon, flumes are just too small for larger scale ($>10\text{m}$ long wavelength) superimposed dunes to emerge (Conlan *et al.*, 2008).

Lastly, of potential significant importance is the lack of variation in large bedform migration rate found in this survey. Bedform migration rate is proportional to the sediment transport rate and their height (Paola & Borgman 1991). However, the variation in dune height found here did not produce

different migration rates. This could be due to the aDcp transects being off the axis of the sediment transport rate; or there could be local, individual bedform dependent, variation in the proportion of superimposed bedforms passing over or entraining into their host dunes.

Thesis Synthesis

7.1 Hypotheses and Conclusions

- 1. The turbulent flow structure over bedforms in non-equilibrium conditions is considerably different from the turbulent flow structure for equilibrium conditions which has been previously researched, and that measuring these non-equilibrium flow states will illuminate why bedforms change shape to new flow conditions.*

This hypothesis was answered in chapter four. It was found that the spatial location of turbulence over fixed dunes in unsteady conditions varies considerably with those reported over dunes in equilibrium conditions, particularly over the stoss slope of dunes. This can lead to a stacked-wake: wake interaction that alters the locations of quadrant events around the stoss slope non-linearly. Additionally, the stacking of turbulent wake structures compresses a dunes' wake closer to the bed, increasing the Reynolds stress over the stoss slope of dunes. This wake stacking was observed without a change in bedform geometry.

- 2. That dune leeside reattachment length over dunes varies with relative submergence.*

Variation in median reattachment length with mean downstream velocity only occurred at flow depths below that of standard equilibrium conditions, and when the mean velocity profile shape at the crest was not a log-law. This indicated that grain roughness had become dominant for much of the velocity

profile when relative submergence increased. To account for variation in grain roughness across all conditions, the influence of varying velocity profile shape was summarised via producing U/u^* at the dune crest, this was measured against median reattachment length and found to show a good correlation. Therefore varying the relative submergence did affect the reattachment length, but the process found to be responsible for low relative submergence affecting reattachment length was found to exist across all conditions.

3. *That the relative effects of flow convergence and acceleration over a dune stoss slope is non-linear and affects the stability of dunes.*

These effects were described via the depth averaged mean velocity at the dune crest, and these were measured across a suit of conditions in chapter 4 showed that mean vertical velocity scales non-linearly with mean downstream velocity. It was interpreted that this is a process controlling dune shape and stability, as the relative proportion of vertical to downstream velocity will strongly affect deposition and erosion of sediment at the dune crest.

4. *That using flow depth is a poor proxy for dune height and overall dune geometry, with bed shear stress being more representative of the processes that control dune height and length.*

The experiments displayed in chapter five found that dune height scales in a parabola with bed shear stress, and not flow depth for bedload transport dominated dunes. This finding has particular significance for flows where the downstream velocity profile is not a log-law open channel shape, such as rivers with any curvature (secondary circulation) or ice cover. In the same experiments dune wavelength was linearly scaled with bed shear stress, indicating that upper stage plane beds are akin to an infinitely long dune. The parabola of dune height therefore did not impact on dune wavelength suggesting that these two processes are independent. Velocity profiles were found to collapse near the bed when plotted as U/u^* over relative depth, again indicating a strong grain roughness control over dunes despite a wide range of imposed velocity profile shapes.

5. *That superimposed bedforms and their host bedform respond differently to changes in hydraulic conditions, i.e. they do not act as one single-or join- unit of bedform.*

Large dune geometry showed no consistent relationship with the hydraulic conditions present at the timescale of this survey; however it was found that the secondary dunes significantly increased and then decreased their height and length with increases and decrease in flow depth. At the same time, their host dunes shows no statistically significant changes in their shape. The larger host dunes displayed a bi-modal wavelength with one mode scaling well with peak flood depth, yet, there was no variation in dune wavelength either as a group or individually that was consistent with the changes in hydraulic conditions at the time of survey, or with bedform adaption processes that usually occur during periods of unsteadiness. All large bedforms migrated at similar rates despite their variation in size. It is postulated that secondary bedforms buffer the host bedform from scales of hydraulic changes on the order of the secondary bedform size, and additionally, they may distribute sediment transport across a bedform field, producing more even large bedform migration rates.

6. *That superimposed bedforms can affect the maximum host dune height (rather than flow depth) though greater suspension of sediment along the host dune stoss slope.*

Mean large dune height was found to be half that prediction from empirical equations using flow depth. Despite this, the mean large dune height consistently decreased through the survey, even though temporary increases in flow depth. The variation of suspended sediment over the dunes in the Mekong River did not match those predicted via the Rouse number, instead suspended sediment concentration was better matched by plotting U/u^* , across variations in discharge and depth. Similar relative bedform depths (bedform height/depth), across the variations in depth and discharge also showed a good relationship with suspended sediment. This relationship between flow structure and suspended sediment, with the concurrent variation secondary dune size indicated that these dunes were depth limited. This is despite the consistent presence of secondary dunes at the crest of the host bedform (and not an upper stage plane bed) or strong free surface interaction.

7.2 Key Thesis Synthesis

One of the major key themes found across the research undertaken in this thesis was the ability of using the relationship of U/u^* to describe the processes that control dunes. The implication of this is that the processes dominating dunes are strongly governed by relative grain roughness and that relative submergence is a secondary factor that affects sediment transport though altering the grain roughness (see mean velocity profiles in chapters 4, and 5). Many bedform stability diagrams describe dunes being hydraulically rough bedforms (e.g. Van Rijn 1987c), so that the sediment sizes reach into the buffer layer. Therefore whilst form drag produces more resistance to the flow, it contributes comparatively little to sediment transport processes. When form roughness does affect sediment transport- it is primarily through inadvertently increasing the grain resistance over the dunes. Potentially, this leads to the conclusion that dunes act as hydraulically smooth roughness elements, contrary to most stability diagrams (e.g. Van Rijn 1997c). This conclusion is evidenced in chapter 4, there the turbulent wake produced from flow separation protects the bed from the higher magnitude outer or free flow velocities, producing a skimming flow effect over the bed similar to that of flow over gravel, that protects the sediment at the bed from the free stream velocities, similarly to the viscous sublayer and sand grains, one to two orders of magnitude smaller (Grass 1971; Nowell & Church, 1979; Hardy et al., 2009). Importantly, this was measured at relatively shallow depths. The flows in Chapter 6 are considerably deeper and the presence of superimposed bedforms may buffer their host bedform from transient hydraulic boundary conditions, adding yet another scale of smoothing between order of magnitude scales.

Reference list

- Aalto, R., Maurice-Bourgoin, L., Dunne, T., Montgomery, D. R., Nittrouer, C. A., Guyot, J-L. (2003). Episodic sediment accumulation on Amazonian flood plains influenced by El Niño/Southern Oscillation. *Nature*, 425(6957), pp. 493–497.
- Aberle, J., Nikora, V., Henning, M., Ettmer, B., Hentschel, B. (2010). Statistical characterization of bed roughness due to bed forms: A field study in the Elbe River at Aken, Germany. *Water Resources Research*, 46, pp.W03521.
- Aberle, J., Coleman, S.E., Nikora, V.I. (2012). Bed load transport by bed form migration. *Acta Geophysica*, 60(6), pp. 1720–1743.
- Adrian R.J., Yao C.S. (1985). Pulsed laser technique application to liquid and gaseous flows and the scattering power of seed materials. *Applied Optics*, 24 (1), pp. 44-52.
- Adrian, R.J. (1991). Particle imaging techniques for experimental fluid-mechanics. *Annual Review of Fluid Mechanics*, 23 (1), pp. 261–304.
- Adrian, R. (1997). Dynamic ranges of velocity and spatial resolution of particle image velocimetry. *Measurement Science and Technology*, 8, pp. 1393.
- Adrian, R.J., Christensen, K.T., Liu, Z.C. (2000a). Analysis and interpretation of instantaneous turbulent velocity fields. *Experiments in Fluids*, 29(3), pp. 275–290.
- Adrian, R.J., Meinhart, C.D., Tomkins, C.D. (2000b). Vortex organization in the outer region of the turbulent boundary layer. *Journal of Fluid Mechanics*, 422, pp. 1–54.
- Adrian, R.J. (2005). Twenty years of particle image velocimetry. *Experiments in Fluids*, 39(2), pp. 159–169.
- Adrian, R.J. (2007). Hairpin vortex organization in wall turbulence. *Physics of Fluids*, 19(4), pp. 41301.

- Adrian, R.J., Westerweel, J. (2011). *Particle Imaging Velocimetry*, Cambridge: Cambridge Aerospace Series.
- Aleixo, R., Zech, Y., Soares-Frazão S. (2012). Turbulence measurements in dam-break flows, *Proceedings Of The River Flow 2012 Conference*, Edited by R. E. Murillo Munoz. San Jose, Costa Rica, Vol. 1, pp. 311-318.
- Allen, J.R.L. (1968). *Current Ripples; Their Relation To Patterns Of Water And Sediment Motion*, Amsterdam,: North-Holland Pub. Co.
- Allen, J.R.L. (1976). Bed forms and unsteady processes : some concepts of classification and response illustrated by common one-way types. *Earth Surface Processes*, 1, pp. 361–374.
- Allen, J.R.L. (1978a). Computational models for dune time-lag calculations using Stein’s rule for dune height. *Sedimentary Geology*, 20, pp. 165–216.
- Allen, J.R.L. (1978b). Polymodal dune Assemblages: An interpretation in terms of Dune Creation-Destruction in periodic flows. *Sedimentary Geology*, 20, pp. 17–28.
- Allen, J.R.L. (1980). Sand waves: a model of origin and internal structure. *Sedimentary Geology*, 26, pp. 281–328.
- Allen, J.R.L. (1982). *Sedimentary Structures: Their character and Physical Basis, Volume I. Developments in Sedimentology 30*, Amsterdam: Elsevier Science Publishers.
- Amaral, S., Jónatas, R., Bento, A.M., Palma, J. Viseu, T., Cardoso, R., & Ferreira R.M.L. 2014. Failure by overtopping of earth dams. Quantification of the discharge hydrograph. In, *Proceedings of the 3rd IAHR Europe Congress, 14-15 April, Porto, Portugal*, pp. 182-193,
- Amir, M., Nikora, V. I., Stewart, M. T., (2014). Pressure forces on sediment particles in turbulent open-channel flow: a laboratory study. *Journal of Fluid Mechanics*. 757. pp. 459-497.
- Amsler, M.A., Garcia, H.M.,(1997). Discussion: Sand-dune geometry of large rivers during floods. *Journal of Hydraulic Engineering*, 121(9), pp. 582–585.

Amsler, M.L., Blettler, M.C.M., de Drago, I.E. (2009). Influence of hydraulic conditions over dunes on the distribution of the benthic macroinvertebrates in a large sand bed river. *Water Resources Research*, 45, pp. W06426.

An Heyvaert, V.M., Baeteman, C. (2008). A middle to late Holocene avulsion history of the Euphrates River: a case study from Tell ed-Dēr, Iraq, Lower Mesopotamia. *Quaternary Science Reviews*, 27(25-26), pp. 2401–2410.

Arnott, R. (2010). Turbidites, and the case of the missing dunes (and sometimes ripples). *GeoCanada 2010 – Working with the Earth*, pp. 1–4.

Arroyo, M.P., Greated, C.A. (1991). Stereoscopic particle image velocimetry. *Measurement Science and Technology*, 2(12), pp. 1181–1186.

Ashley, S.M. (1990). Classification of large-scale subaqueous bedforms: A new look at an old problem-SEPM bedforms and bedding structures. *Journal of Sedimentary Research*, 60(1).

Ashworth, P., Best, J., Roden, J. (2000). Morphological evolution and dynamics of a large, sand braid-bar, Jamuna River, Bangladesh. *Sedimentology*, 47, pp. 533–555.

Ashworth, P.J., Lewin, J. (2012). How do big rivers come to be different? *Earth-Science Reviews*, 114(1-2), pp. 84–107.

Baas, J.H., Best, J.L. (2008). The dynamics of turbulent, transitional and laminar clay-laden flow over a fixed current ripple. *Sedimentology*, 55(3), pp. 635–666.

Baas, J. H., Oost, A. P., Sztano, O. K., Deboer, P. L., Postma, G. (1993). Time as an Independent Variable for Current Ripples Developing Towards Linguoid Equilibrium Morphology. *Terra Nova*, 5 (1), pp 29-35

Baas, J.H., Best, J.L. (2008). The dynamics of turbulent, transitional and laminar clay-laden flow over a fixed current ripple. *Sedimentology*, 55(3), pp. 635–666.

- Baas, J.H., Best, J. L., Peakall, J., Wang, M. (2009). A Phase Diagram for Turbulent, Transitional, and Laminar Clay Suspension Flows. *Journal of Sedimentary Research*, 79, pp. 162–183.
- Baas, J.H., Best, J.L., Peakall, J. (2011). Depositional processes, bedform development and hybrid bed formation in rapidly decelerated cohesive (mud-sand) sediment flows. *Sedimentology*, 58(7), pp. 1953–1987.
- Baas, J.H., Davies, A.G., Malarkey, J. (2013). Bedform development in mixed sand–mud: The contrasting role of cohesive forces in flow and bed. *Geomorphology*, 182, pp. 19–32.
- Babakaiff, C.S., Hickin, E.J. (1996). Coherent flow structures in Squamish River Estuary, British Columbia, Canada. In *Coherent Flow Structures in Open Channels*, edited by P. J. Ashworth *et al.*, pp. 321-342, Wiley. Chicester.
- Bagherimiyab, F., Lemmin, U. (2013). Shear velocity estimates in rough-bed open-channel flow. *Earth Surface Processes and Landforms*, 38 (18), pp. 1714-1724
- Bagnold, R.A. (1956). The flow of cohesionless grains in fluid. *Philosophical Transactions of the Royal Society London, Series A.*, 249, pp. 235–297.
- Bagnold, R.A. (1960). *Some Aspects of the Shape of River Meanders* Some Aspects of the Shape of River Meanders, USGS Professional Paper: 282-E, Reston, VA.
- Bagnold, R.A. (1966). *An approach to the sediment transport problem from general physics*, Washington,: U. S. Govt. Print. Off.
- Balachandar, R., Hyun, B.S., Patel, V.C. (2007). Effect of depth on flow over a fixed dune. *Canadian Journal of Civil Engineering*, 34(12), pp. 1587–1599.
- Barnhart, D.H., Adrian, R.J., Papen, G.C. (1994). Phase-conjugate holographic system for high-resolution particle-image velocimetry. *Applied Optics*, 33(30), pp. 7159–7170.

- Bartholdy, J., Bartholomae, A., Flemming, B. (2002). Grain-size control of large compound flow-transverse bedforms in a tidal inlet of the Danish Wadden Sea. *Marine Geology*, 188, pp. 391–413.
- Belt, C.B. (1975). The 1973 flood and man's constriction of the Mississippi River. *Science (New York, N.Y.)*, 189(4204), pp. 681–684.
- Bennett, S., Best, J. (1995). Mean flow and turbulence structure over fixed, two-dimensional dunes: implications for sediment transport and bedform stability. *Sedimentology*, 42, pp. 491-513.
- Bennett, J.L., Best, J. (1996). Mean flow and turbulence structure over fixed ripples and the ripple dune transition. In P. J. . B. Ashworth J.L.: Best,J; McLelland, S.J., ed. *Coherent Flow Structures In Open Channels*. Chichester: Wiley.
- Bennett, S.J., Bridge, J.S. , Best, J.L. (1998). Fluid and sediment dynamics of upper stage plane beds. *Journal of Geophysical Research*, 103(C1), pp. 1239–1274.
- Berkooz, G., Holmes, P., Lumley, J.L. (1993). The proper orthogonal decomposition in the analysis of turbulent flows. *Annual Review of Fluid Mechanics*, 25, 539-575.
- Best, J.L., Roy, A.G. (1991). Mixing-layer distortion at the confluence of channels of different depth. *Nature*, 350, 411–413.
- Best, J.L. (1992). On the entrainment of sediment and initiation of bed defects: insights from recent developments within turbulent boundary layer research. *Sedimentology*, 39, pp. 797–811.
- Best, J.L., Bridge, J.S. (1992). The morphology and dynamics of low amplitude bedwaves upon upper stage plane beds and the preservation of planar laminae. *Sedimentology*, 39, pp. 737–752.
- Best, J.L. (1996). The fluid dynamics of small scale alluvial bedforms. In P. Carling A; Dawson, Martin, R, ed. *Advances in Fluvial Dynamics and Stratigraphy*. Chichester: John Wiley and Sons.

- Best, J.L., Kostaschuk, R. (2002). An experimental study of turbulent flow over a low-angle dune. *Journal of Geophysical Research*, 107(C9), p.3135.
- Best, J.L., Kostaschuk, R., Hardy, R.J. (2004). The fluid dynamics of low angle river dunes. *Marine Sandwave and River Dune Dynamics*.
- Best, J.L. (2005). The kinematics, topology and significance of dune related macroturbulence: Some observations from the laboratory and field. In *Fluvial Sedimentology VII*. Edited by M. D. Blum, S. B. Marriott, ., S. Leclair, Special Publication of the International Association of Sedimentologists, 41–60.
- Best, J.L. (2005). The kinematics, topology and significance of dune related macroturbulence: Some observations from the laboratory and field. In M. D. Blum, S. B. Marriott, S. Leclair, eds. *Fluvial Sedimentology VII*. Special Publication of the International Association of Sedimentologists, pp. 41–60.
- Best, J.L., Simmons, S., Parsons, D., Oberg, K., Czuba, J., Malzone, C. (2010). A new methodology for the quantitative visualization of coherent flow structures in alluvial channels using multibeam echo-sounding (MBES). *Geophysical Research Letters*, 37(6), L06405.
- Best, J.L., (2011). Flow fields and coherent structures associated with superimposed and amalgamating bedforms J. G. Venditti *et al.*, eds. *Coherent Flow Structures in Geophysical flows near Earths surface*.
- Best, J.L., Blois, G., Barros, J., Christensen, K. (2013). The dynamics of bedform amalgamation: new insights from a very thin flume. In *Marine and River Dune Dynamics IV*. Eds. V. Van Lancker & T. Garlan. Bruges, Belgium: VLIZ special publication numer 65, pp. 81–88.
- Bintliff, J. (2002). Time, process and catastrophism in the study of Mediterranean alluvial history: A review. *World Archaeology*, 33(3), pp. 417–435.
- Biron, P., Roy, A., Best, J. (1996). Turbulent flow structure at concordant and discordant open-channel confluences. *Experiments in Fluids*, 21, 437–446.
- Biron, P.M. Lane, S. N., Roy, A. G., Bradbrook, K. F., Richards, K. S. (1998). Sensitivity of bed shear stress estimated from vertical velocity profiles : the

problem of sampling resolution. *Earth Surface Processes and Landforms*, 23, pp. 133–139.

Blanckaert, K., Kleinhans, M.G., McLelland, S.J., Uijttewaal, W.S.J., Murphy, B.J., van de Kruijs, A., Parsons, D.R., Chen, Q. (2013). Flow separation at the inner (convex) and outer (concave) banks of constant-width and widening open-channel bends. *Earth Surface Processes and Landforms*, 38(7), 696–716.

Blanckaert, K. (2010). Topographic steering, flow recirculation, velocity redistribution, and bed topography in sharp meander bends. *Water Resources Research*, 46(9), p.W09506.

Blanckaert, K. (2011). Hydrodynamic processes in sharp meander bends and their morphological implications. *Journal of Geophysical Research*, 116 (F1), F01003.

Blois, G. Barros, J.M. Christensen, K.T. Best, J.L. (2012). An experimental investigation of 3D subaqueous barchan dunes and their morphodynamic processes. In *Marine and River Dune Dynamics 4*. . 35–38.

Blois, G., J. L. Best, G. H. Sambrook Smith, and R. J. Hardy. (2014). Effect of bed permeability and hyporheic flow on turbulent flow over bed forms. *Geophysical Research Letters*, 41, 6435–6442.

Blum, M.D., Roberts, H.H., (2009). Drowning of the Mississippi Delta due to insufficient sediment supply and global sea-level rise. *Nature Geoscience*, 2(7), pp. 488–491.

Bogard, D.G., Tiederman, W.G. (1986). Burst detection with single point velocity measurements. *Journal of Fluid Mechanics*, 162, pp. 389–413.

Bolle, A., Mathys, M., Haerens, P. (2013). How the Belgian wind farm business made us discover the challenging environment of marine sand dunes. In V. Van Vlancker & T. Garlan, eds. *Marine and River Dune Dynamics 4*. Bruges, Belgium: VLIZ special publication number 65, pp. 45–52.

Bradley, R.W. *et al.* (2013). Flow and sediment suspension events over low-angle dunes: Fraser Estuary, Canada. *Journal of Geophysical Research: Earth Surface*, 118(3), pp. 1693–1709.

- Bravard, J.P., Goichot, M. , Tronchère, H. (2014). An assessment of sediment-transport processes in the Lower Mekong River based on deposit grain sizes, the CM technique and flow-energy data. *Geomorphology*, 207, pp. 174–189.
- Bridge, J., Best, J. (1988). Flow, sediment transport and bedform dynamics over the transition from dunes to upper-stage plane beds: implications for the formation of planar laminae. *Sedimentology*, 35, pp. 753–763.
- Bridge, J.S., Jarvis, J. (1977). Velocity profiles and bed shear stress over various bed configurations in a river bend. *Earth surface Processes*, 2, 281–294.
- Bridge, J.S., Jarvis, J. (1982). The dynamics of a river bend : a study in flow and sedimentary processes. *Sedimentology*, 29(4), pp. 499–541.
- Bridge, J.S. (1985). Paleochannel patterns inferred from alluvial deposits - a critical-evaluation. *Journal of Sedimentary Petrology*, 55(4), pp. 579–589.
- Bridge, J.S. (1993). The interaction between channel geometry, water flow, sediment transport and deposition in braided rivers. In J. B. Best., C. S. Bristow, eds. *Braided rivers*. Bath: Geological Society Publishing House, pp. 13–71.
- Bridge, J.S. (1997). Thickness of sets of cross strata and planar strata as a function of formative bed-wave geometry and migration, and aggradation rate. *Geology*, 25(11), pp. 971–974.
- Bridge, J.S., Tye, R.S. (2000). Interpreting the dimensions of ancient fluvial channel bars, channels, and channel belts from wireline-logs and cores. *Aapg Bulletin-American Association of Petroleum Geologists*, 84(8), pp. 1205–1228.
- Bridge, J. (2003). *Rivers and Floodplains: Forms, Processes, and Sedimentary Record.*, Oxford: Blackwell Publishing.
- Brownlie, W.R. (1983). Flow depth in sand bed channels. *Journal of Hydraulic Engineering*, 109(7), pp. 959–990.
- Buffin-Bélanger, T., Roy, A.G. (2005). 1 Min in the life of a river: selecting the optimal record length for the measurement of turbulence in fluvial boundary layers. *Geomorphology*, 68(1-2), .77–94.

Caldwell, R.L. & Edmonds, D.A., (2014). The effects of sediment properties on deltaic processes and morphologies: A numerical modelling study. *Journal of Geophysical Research: Earth Surface*, 119, pp. 961–982.

Cameron, S.M. Nikora, V. I. Albayrak, L. Miler, O. Stewart, M. Siniscalchi, F. (2013). Interactions between aquatic plants and turbulent flow: a field study using stereoscopic PIV. *Journal of Fluid Mechanics*. 731, 10, 345-372.

Carling, P., Dawson, M.R. (1996). *Advances In Fluvial Dynamics And Stratigraphy*, Chichester: Wiley.

Carling, P.A. (1999). Subaqueous gravel dunes. *Journal of Sedimentary Research*, 69(3), pp. 534-545.

Carling, P.A., Golz, E., Orr, H. G., Radecki-Pawlik, A., (2000). The morphodynamics of fluvial sand dunes in the River Rhine, near Mainz, Germany. I, Sedimentology and morphology. *Sedimentology*, 47, pp. 227–252.

Carling, P.A. Williams, J.J., Golz, E., Kelsey, A D. (2000). The morphodynamics of fluvial sand dunes in the River Rhine, near Mainz, Germany. II, Sedimentology and morphology. *Sedimentology*, 47, pp. 253-278

Cea, L., Puertas, J. ., Pena, L. (2007). Velocity measurements on highly turbulent free surface flow using ADV. *Experiments in Fluids*, 42(3), pp. 333–348

Chakraborty, P. Balachandar, S. , Adrian, R.J. (2005). On the relationships between local vortex identification schemes. *Journal of Fluid Mechanics*, 535, pp. 189–214.

Chang, K., Constantinescu, G. (2013). Coherent structures in flow over two-dimensional dunes. *Water Resources Research*, 49(5), pp. 2446–2460.

Chapman, C.A., Walker, I.J., Hesp, P, A., Bauer, B. O., Davidson-arnott, R. G. D. Geomorphology Turbulent Reynolds stress and quadrant event activity in wind flow over a coastal foredune. (2012). *Geomorphology*, 151-152, pp. 1–12.

Chapman, C.A., Walker, I.J., Hesp, P. A., Bauer, B. O., Davidson-arnott, R. G. D., Ollerhead, J. (2013). Reynolds stress and sand transport over a foredune. *Earth Surface Processes and Landforms*, 38(14), pp. 1735–1747.

Chen, J., Wang, Z., Li, M., Wei, T., Chen, Z. (2012). Bedform characteristics during falling flood stage and morphodynamic interpretation of the middle–lower Changjiang (Yangtze) River channel, China. *Geomorphology*, 147-148, pp. 18–26.

Chézy, A. de, (1775). Memoire sur la vitesse de l'eau conduite dans une régole. *Reprinted in Annals des Ponts et Chaussées*. 1921, 60.

Chickadel, C., Horner-devine, A. R., Talke, S. A., Jessup, A T. (2009). Vertical boil propagation from a submerged estuarine sill. *Geophysical Research Letters*, 36(10), pp. L10601.

Chickadel, C.C. Talke, S.A. Horner-devine, A.R. Jessup, A.T. (2011). Infrared-based measurements of velocity, turbulent kinetic energy, and dissipation at the water surface in a tidal river. *Geoscience Remote Sensing Letters*, 8(5), pp. 849–853.

Cohen, S., Kettner, A.J. , Syvitski, J.P.M. (2014). Global suspended sediment and water discharge dynamics between 1960 and 2010: Continental trends and intra-basin sensitivity. *Global and Planetary Change*, 115, pp. 44–58.

Coleman, K.M. (1969). Brahmaputra River: Channel processes and sedimentation. *Sedimentary Geology*, 3, pp. 129–239.

Coleman, S., Fenton, J. (2000). Potential-flow instability theory and alluvial stream bed forms. *Journal of Fluid Mechanics*, 418, pp. 101–117.

Coleman, S.E. Nikora, V. I., McLean, S. R., Clunie, T. M., Schlicke, T., Melville, B. W. (2006). Equilibrium hydrodynamics concept for developing dunes. *Physics of Fluids*, 18(10), pp. 105104.

Coleman, S.E., Nikora, V.I. (2009). Bed and flow dynamics leading to sediment wave initiation. *Water Resources Research*, 45(4). pp W04402

- Coleman, S.E., Nikora, V.I. (2011). Fluvial dunes: initiation, characterization, flow structure. *Earth Surface Processes and Landforms*, 36(1), pp. 39–57.
- Coleman, S.E., Nikora, V.I., Aberle, J. (2011). Interpretation of alluvial beds through bed-elevation distribution moments. *Water Resources Research*, 47(11), pp. W11505.
- Conlan, I.A., Rutherford, B.L., Finlayson, B.L., Western, A.W. (2008). Sediment transport through a forced pool on the Mekong River: sand dunes superimposed on a larger sediment wave? In *Marine and River Dune Dynamics IV*. Eds. V. Van Lancker & T. Garlan. Bruges, Belgium: VLIZ special publication number 65, pp. 81–88.
- Cooper, J.R., Tait, S.J. (2010). Examining the physical components of boundary shear stress for water-worked gravel deposits. *Earth Surface Processes and Landforms*, 35, pp. 1240-1246.
- Coz, J. Le. Jodeau, M. Hauet, A. Marchand, B. Le Boursicaud, R. (2014). Image-based velocity and discharge measurements in field and laboratory river engineering studies using the free Fudaa-LSPIV software. In *River Flow 2014*. Edited by Schleiss, A J.de Cesare, G. Franca, M. J. Pfister, M. Taylor & Francis Group. London. 1961–1967.
- Creutin, J.D., Muste, M. Bradley, A.A. Kim, S.C. Kruger, A. (2003). River gauging using PIV techniques: a proof of concept experiment on the Iowa River. *Journal of Hydrology*, 277(3-4), pp. 182–194.
- Czuba, A. J. Oberg, K.A., Best, J.L., Parsons, D. R., Simmons, S. M., Johnson, K. K., Malzone, C. (2009). Coherent flow structures generated over alluvial sand dunes, Mississippi River, revealed by Acoustic Doppler Current Profiling and Multibeam Echo Sounding. In *Marine and River Dune Dynamics IV*. Eds. V. Van Lancker & T. Garlan. Bruges, Belgium: VLIZ special publication number 65, pp. 81–88.
- Dantec Website (accessed 29/12/2014).
http://www.dantecdynamics.com/docs/products-and-services/fluid-mechanics/piv/Flow_Velocity_and_Turbulence_239.pdf

Demers, S., Buffin-Bélanger, T., Roy, A.G. (2011). Helical cell motions in a small ice-covered meander river reach. *River Research and Applications*, 1125(August 2010), pp. 1118–1125.

Demers, S., Buffin-Bélanger, T. & Roy, A.G., 2013. Macroturbulent coherent structures in an ice-covered river flow using a pulse-coherent acoustic Doppler profiler. *Earth Surface Processes and Landforms*, 38(9), pp. 937–946.

Dietrich, W.E., Smith, J.D., Dunne, T. (1979). Flow and sediment transport in a sand bedded meander. *The Journal of Geology*, 87(3), pp305–315.

Dimas, A. A. (2008). Effect of bed dunes on spatial development of open-channel flow. *Journal of Hydraulic Research*, 46(6), pp. 802

Dinehart, R.L. (1992). Evolution of coarse gravel bed forms: Field measurements at flood stage. *Water Resources Research*, 28(10), pp. 2667–2689.

Dorst, L., Dehling, T., Howlett, C. (2013). Developments in North Sea wide resurveying and charting of dynamics sand wave areas. In *Marine and River Dune Dynamics IV*. Eds. V. Van Lancker & T. Garlan. Bruges, Belgium: VLIZ special publication number 65, pp. 81–88.

Drake, T.G. Shreve, R L. Dietrich, William E. Whiting, Peter J. Leopold, Luna B. (1988). Bedload transport of fine gravel observed by motion-picture photography. *Journal of Fluid Mechanics*, 192, pp. 193–217.

Edmonds, D. a. & Slingerland, R.L., (2009). Significant effect of sediment cohesion on delta morphology. *Nature Geoscience*, 3(2), pp. 105–109.

Einstein, H.A., Barbarossa, N.L. (1952). River channel roughness. *Transactions of the American Society of Civil Engineers*, 117, pp. 1121–1146.

Elsinga, G.E. Scarano, F. Wieneke, B. van Oudheusden, B. W. (2006). Tomographic particle image velocimetry. *Experiments in Fluids*, 41(6), pp. 933–947.

Engel, P. (1981). Length of flow separation over dunes. *Journal of Hydraulic Division. American Society of Civil Engineers*, 107(HY10), pp. 113–1143.

- Engelund, F., Fredsoe, J. (1982). Sediment ripples and dunes. *Annual Review of Fluid Mechanics*, 14, pp. 13–37.
- Ettema, R., Daly, S.F. (2004). *Sediment Transport Under Ice*, U.S. Army Corps of Engineers. Washington, DC.
- Ewing, R.C., Kocurek, G. (2010). Aeolian dune-field pattern boundary conditions. *Geomorphology*, 114(3), pp. 175–187.
- Exner, F.M. (1920). Zur physik der dunen. *Sitzungs Bericht Akad. Wiss. Wien. Wien.*, Mathemathi(IIa), p.Band 129.
- Fahringer, T., Thurow, B. (2012). Tomographic Reconstruction of a 3-D Flow Field Using a Plenoptic Camera. In *42nd AIAA Fluid Dynamics Conference and Exhibit*. Pp. 2826.
- Falco, R.E. (1991). A coherent structure model of the turbulent boundary layer and its ability to predict Reynolds number dependence. *Philosophical Transactions: Physical Sciences and Engineering*, 336(1641), pp. 103 –129.
- Fedele, J.J., Garcia, M.H. (2001). Alluvial roughness in streams with dunes: A boundary-layer approach. In G. Seminara & P. Blondeaux, eds. *River, Coastal and Estuarine Morphodynamics*. New York.: Springer, pp. 37–60.
- Ferguson, R.I. Parsons, D.R. Lane, S.N. Hardy, R.J. (2003). Flow in meander bends with recirculation at the inner bank. *Water Resources Research*, 39(11), WR001965.
- Ferguson, R.I., Church, M. (2004). A simple universal equation for grain settling velocity. *Journal of Sedimentary Research*, 74(6), pp. 933–937.
- Fernandez, R., Best, J., López, F. (2006). Mean flow, turbulence structure, and bed form superimposition across the ripple-dune transition. *Water Resources Research*, 42(5), pp. W054063
- Ferreira, R.M.L., Ferreira, L., Ricardo, A. M. ., Franca, M.J. (2010). Impacts of sand transport on flow variables and dissolved oxygen in gravel-bed streams suitable for salmonid spawning. *River Research and Applications*, 26(4), pp: 414-438.

- Ferreira, R.M.L. (2011) *Turbulent flow hydrodynamics and sediment transport. Laboratory research with LDA and PIV*. In *Experimental Methods in Hydraulic Research, GeoPlanet-Earth and Planetary Sciences*. Edited by Pawel Rowinski, Polish Acad Sci, Inst Geophys. pp. 67-111.
- Fielding, C.R., Alexander, J. (1996). Sedimentology of the Upper Burdekin River of North Queensland, An Australian example of a tropical, variable discharge river. *Terra Nova*, 8(5), pp. 447-457.
- Fielding, C.R. Allen, J. P., Alexander, J., Gibling, M. R. (2009). Facies model for fluvial systems in the seasonal tropics and subtropics. *Geology*, 37(7), pp. 623-626.
- Flemming, B.W. (2000). The role of grain size, water depth and flow velocity as scaling factors controlling the size of subaqueous dunes. (March), pp. 55-61.
- Fredsoe, J. (1979). Unsteady flow in straight alluvial streams modification of individual dunes. *Journal of Fluid Mechanics*, 91(3), pp. 497-512.
- Fredsoe, J. (1982). Shape and dimensions of stationary dunes in rivers. *Journal of the Hydraulics Division of the American Society of Civil Engineers.*, 108, pp. 932-947.
- Fryberger, S.G., Ahlbrandt, T.S., Andrews, S. (1979). Origin, sedimentary features, and significance of low-angle Eolian "sand sheet" deposits, Great Sand Dunes National Monument and Vicinity, Colorado. *Journal of Sedimentary Research*, 3(9), pp. 733-746.
- Fujita, I., Muste, M., Kruger, A. (1998). Large-scale particle image velocimetry for flow analysis in hydraulic engineering applications. *Journal of Hydraulic Research*, 36(3), 397-414.
- Furbish, D.J., Schmeeckle, M.W. (2013). A probabilistic derivation of the exponential-like distribution of bed load particle velocities. *Water Resources Research*, 49(3), pp. 1537-1551.
- Gabel, S.L. (1993). Geometry and kinematics of dunes during steady and unsteady flows in the Calamus River, Nebraska, USA. *Sedimentology*, 40, pp. 237-269.

- Garcia, M.H., Nino, Y., Lopez, F. (1996). Laboratory observations of particle entrainment into suspension by turbulent bursting P. J. Ashworth *et al.*, eds. *Coherent flow Structures in Open Channel Flows*.
- Garcia, M.H. (2008). *Sedimentation Engineering*. ASCE Manuals and Reports on Engineering Practice, No. 110.
- Garcia, D. (2011). A fast all-in-one method for automated post-processing of PIV data. *Experiments in fluids*, 50(5),1247–1259.
- Gibling, M. R., Bashforth, A. R., Falcon-Lang, H. J., Allen, J. P., Fielding, C. R., (2010). Log jams and flood sediment buildup caused channel abandonment and avulsion in the Pennsylvanian of Atlantic Canada. *Journal of Sedimentary Research*, 80(3), pp 268-287.
- Gioia, G. Guttenberg, N. Goldenfeld. Chakraborty, P. (2010). spectral theory of the turbulent mean-velocity profile. *Physical Review Letters*, 105(18), 184501.
- Gmeiner, P. *et al.* (2011). Development of a device for direct bed shear stress measurement in a gravel bed river. 13, pp. 12342.
- Gollub, J.P., Benson, S. V. (2006). Many routes to turbulent convection. *Journal of Fluid Mechanics*, 100(03), pp. 449.
- Goring, D., Nikora, V. (2002). Despiking acoustic Doppler velocimeter data. *Journal of Hydraulic Engineering*, 128(1), pp. 117–126.
- Grass, J. (1970). Initial instability of fine bed sand. *Journal of Hydraulic Division. American Society of Civil Engineers*, 93, pp. 619–631.
- Grass, J. (1971). Structural features of turbulent flow over smooth and rough boundaries. *Journal of Fluid Mechanics*, 50 (02), pp. 233-255.
- Grass, J. (1983). The influence of boundary layer turbulence on the mechanics of sediment transport. In B. Sumer M: Muller, A, ed. *Mechanics of sediment transport : proceedings of Euromech 156, Mechanics of sediment transport, Istanbul, 12-14 July 1982*. Rotterdam: A.A.Balkema.
- Gray, A.B. Pasternack, G. B., Watson, E. B., Warrick, J. A., Goñi, M, A. (2014). The effect of El Niño Southern Oscillation cycles on the decadal scale suspended

sediment behavior of a coastal dry-summer subtropical catchment. *Earth Surface Processes and Landforms*, pp. 272-284.

Grigoriadis, D.G.E., Balaras, E., Dimas, A. A. (2009). Large-eddy simulations of unidirectional water flow over dunes. *Journal of Geophysical Research*, 114(F2), pp. F02022.

Gruen, A.W. (1985). Adaptive least squares correlation: a powerful image matching technique. In *Proc. ACSM-ASP Convention*, Washington DC, pp. 175–187.

Guerrero, M., Szupiany, R.N. (2013). Multi-frequency acoustics for suspended sediment studies : an application in the Parana River Multi-frequency acoustics for suspended sediment studies : an application in the Parana River. *Journal of Hydraulic Research*, 51(6), pp. 696–707.

Gupta, A., Hock, L., Xiaojing, H., Ping, C. (2002). Evaluation of part of the Mekong River using satellite imagery. *Geomorphology*, 44, pp. 221–239.

Gupta, A., Liew, S.C. (2007). The Mekong from satellite imagery: A quick look at a large river. *Geomorphology*, 85(3-4), pp. 259–274.

Guy, H.P., Simons, D.B., Richardson, E.V. (1966). *Summary of Alluvial Channel Data From Flume Experiments* , 1956-61, Washington DC.

Haller, G., Yuan, G. (2000). Lagrangian coherent structures and mixing in two-dimensional turbulence. *Physica D: Nonlinear Phenomena*, 147(3-4), pp. 352–370.

Haller, G., Sapsis, T. (2011). Lagrangian coherent structures and the smallest finite-time Lyapunov exponent. *Chaos*. 21(2), pp. 023115.

Hand, B.M., Bartberger, C.E. (1988). Leaside sediment fallout patterns and the stability of angular bedforms. *Journal of Sedimentary Petrology*, 58(1), pp. 33–43.

Hardy, R.J. Lane, S.N. Lawless, M.R. Best, J.L. Elliott, L. Ingham, D.B. (2005). Development and testing of a numerical code for treatment of complex river

channel topography in three-dimensional CFD models with structured grids. *Journal of Hydraulic Research*, 43(5), pp. 468–480.

Hardy, R.J. Best, J.L. Lane, S.N. Carbonneau, P.E. (2009). Coherent flow structures in a depth-limited flow over a gravel surface: The role of near-bed turbulence and influence of Reynolds number. *Journal of Geophysical Research*, 114(F1), pp. F01003.

Hardy, R.J., Best, J.L., Lane, S.N., Carbonneau, P.E. (2010a). Coherent flow structures in a depth-limited flow over a gravel surface: The influence of surface roughness. *Journal of Geophysical Research*, 115(F3), pp. F03006.

Hardy, R.J. Best, J.L., Parsons, D.R., Keevil, G.M. (2010b). On determining the geometric and kinematic characteristics of coherent flow structures over a gravel bed: a new approach using combined PLIF-PIV. *Earth Surface Processes and Landforms*, 36(2), pp. 279–284.

Hardy, R.J., Lane, S.N. , Yu, D. (2011). Flow structures at an idealized bifurcation: a numerical experiment. *Earth Surface Processes and Landforms*, 36(15), pp. 2083–2096.

Harris, C.D., Ullman, E.L. (1945). The Nature of Cities. *American Academy of Political and Social Science*, 242, pp. 7–17.

Hay, A.E. (2011). Geometric bed roughness and the bed state storm cycle. *Journal of Geophysical Research*, 116(C4), pp. C04017.

Heslot, F., Casting, B. , Libchaber, A. (1987). Transitions to turbulence in helium gas. *Physical Review A*, 36(12), pp. 5870–5873.

Hjelmfelt, A. T., Mockros, L. F. (1966). Motion of discrete particles in a turbulent fluid. *Applied Scientific Research*. 16,pp. 1,149-161

Holdaway, G.P. Thorne, P. D., Flatt, D., Jones, S. E., Prandle, D. (1999). Comparison between ADCP and transmissometer measurements of suspended sediment concentration. *Continental Shelf Research*, 19, pp. 421–441.

Holleman, I. , Beekhuis, J. (2003). Analysis and correction of dual-PRF velocity data. *Journal of Atmospheric and Oceanic Technology*, 20, pp. 443–453.

- Holmes, R.R., Garcia, M.H. (2008). Flow over bedforms in a large sand-bed river: A field investigation. *Journal of Hydraulic Research*, 46(3), pp. 322–333.
- Hooke, J.M. (2006). Human impacts on fluvial systems in the Mediterranean region. *Geomorphology*, 79(3-4), pp. 311–335.
- Hooke, R.L. (1975). Distribution of sediment transport and shear stress in a meander bend. *The Journal of Geology*, 83(5), pp. 543–565.
- Hurther, D., Lemmin, U. (2000). Shear stress statistics and wall similarity analysis in turbulent boundary layers using a high-resolution 3-D ADV. *IEEE Journal of Oceanic Engineering*, 25(4), pp. 446–457.
- Hurther, D., Lemmin, U. (2008). Improved turbulence profiling with field-adapted acoustic Doppler velocimeters using a bifrequency Doppler noise suppression method. *Journal of Atmospheric and Oceanic Technology*, 25(3), pp. 452–463.
- Huybrechts, N., Luong, G. V., Zhang, Y. F., Villaret, C., Verbanck, M. A. (2011). Dynamic routing of flow resistance and alluvial bed-form changes from the lower to the upper regime. *Journal of Hydraulic Engineering*, (September), pp. 932–945.
- IPCC Working Group 2. (2014). *Climate Change 2014: Impacts, Adaptation, and Vulnerability. Working Group II Contribution to the IPCC 5th Assessment Report - Changes to the Underlying Scientific/Technical Assessment. Chapter 5*,
- Jackson, R.G. (1975a). Hierarchical attributes and a unifying model of bed forms composed of cohesionless material and produced by shearing flow. *Geological Society of America Bulletin*, 86(11), pp. 1523–1533.
- Jackson, R.G. (1975b). Velocity - bed-form - texture patterns of meander bends in the lower Wabash River of Illinois and Indiana. *Geological Society of America Bulletin*, 86(11), pp. 1511–1522.
- Jackson, R.G. (1976a). Large-scale ripples of the lower Wabash River. *Sedimentology*, 23, pp. 593–623.

- Jackson, R.G. (1976b). Sedimentological and fluid-dynamic implications of the turbulent bursting phenomenon in geophysical flows. *Journal of Fluid Mechanics*, 77(3), pp. 531–560.
- Jerolmack, D.J., Mohrig, D. (2005a). A unified model for subaqueous bed form dynamics. *Water Resources Research*, 41(12), p.n/a–n/a.
- Jerolmack, D.J., Mohrig, D. (2005b). Frozen dynamics of migrating bedforms. *Geology*, 33, pp. 57-60.
- Jerolmack, D.J., Mohrig, D. (2005c). Interactions between bed forms: Topography, turbulence, and transport. *Journal of Geophysical Research*, 110(F2).
- Jerolmack, D.J., Mohrig, D. (2005d). Palaeoclimatology: formation of Precambrian sediment ripples. *Nature*, 436(7049), p.E1; discussion E1–2.
- Jerolmack, D.J., Mohrig, D., Mcelroy, B. (2006). A unified description of ripples and dunes in rivers. *River, Coastal and Estuarine Morphodynamics: RCEM 2005*, pp. 843–852.
- Jodeau, M. Hauet, A. Paquier, A. Le Coz, J. Dramais, G. (2008). Application and evaluation of LS-PIV technique for the monitoring of river surface velocities in high flow conditions. *Flow Measurement and Instrumentation*, 19(2), pp. 117–127.
- Joe, P. ., May, P.T. (2003). Correction of Dual PRF Velocity Errors for Operational Doppler Weather Radars. *Journal of Atmospheric and Oceanic Technology*, 20, pp. 429–442.
- Johannesson, H., Parker, G. (1989). Linear Theory of River Meanders. In S. Ikeda & G. Parker, eds. *River Meandering*. Water Resources Monograph. Washington, D. C.: American Geophysical Union.
- Jordan, B.P.R. (1965). *Fluvial Sediment of the Mississippi River at St . Louis , Missouri*, Washington,.
- Julien, P.Y., Klasssen, G.J. (1995). Sand-dune geometry of large river during floods. *Journal of Hydraulic Engineering*, 121(9), pp. 657–633.

- Kadota, A., Nezu, I. (1999). Three-dimensional structure of space-time correlation on coherent vortices generated behind dune crest. *Journal of Hydraulic Research*, 37(1), 59–80.
- Keane, R.D., Adrian, R.J. (1992). Theory of cross-correlation analysis of PIV images. *Applied scientific research*, 46, pp. 191–215.
- Keylock, C.J. (2008). A criterion for delimiting active periods within turbulent flows. *Geophysical Research Letters*, 35(11), pp. L11804.
- Keylock, C.J. (2009). Evaluating the dimensionality and significance of “active periods” in turbulent environmental flows defined using Lipschitz/Hölder regularity. *Environmental Fluid Mechanics*, 9(5), pp. 509–523.
- Keylock, C.J., Nishimura, K. , Peinke, J. (2012). A classification scheme for turbulence based on the velocity-intermittency structure with an application to near-wall flow and with implications for bed load transport. *Journal of Geophysical Research*, 117(F1).
- Keylock, C.J., Singh, A. , Fofoula-Georgiou, E. (2013). The influence of migrating bed forms on the velocity-intermittency structure of turbulent flow over a gravel bed. *Geophysical Research Letters*, 40(7), pp. 1351–1355.
- Keylock, C.J., Lane, S.N. , Richards, K.S. (2014). Quadrant/octant sequencing and the role of coherent structures in bed load sediment entrainment. *Journal of Geophysical Research: Earth Surface*, 119(2), pp. 264–286.
- Kitzhofer, J., Nonn, T., Brücker, C. (2011). Generation and visualization of volumetric PIV data fields. *Experiments in Fluids*, 51(6), pp. 1471–1492.
- Kleinhans, M.G. (2002). Upstream sediment input effects on experimental dune trough scour in sediment mixtures. *Journal of Geophysical Research: Earth Surface*. 110, pp. F04S06
- Kostaschuk, R., Church, M.A. (1993). Macroturbulence generated by dunes: Fraser River, Canada. *Sedimentary Geology*, 85(1-4), pp. 25–37.
- Kostaschuk, R., Villard, P. (1996). Flow and sediment transport over large subaqueous dunes: Fraser River, Canada. *Sedimentology*, 43(5), pp. 849–863.

- Kostaschuk, R. (2000). A field study of turbulence and sediment dynamics over subaqueous dunes with flow separation. *Sedimentology*, 47, pp. 519–531.
- Kostaschuk, R., Villard, P., Best, J. (2004). measuring velocity and shear stress over dunes with acoustic Doppler profiler. , (September), pp. 932–936.
- Kostaschuk, R., Best, J. (2005). Response of sand dunes to variations in tidal flow: Fraser Estuary, Canada. *Journal of Geophysical Research*, 110(F4), pp. F04S04.
- Kostaschuk, R. Shugar, D. H., Best, J., Parsons, D. R., Lane, S. N., Hardy, R. J., Orfeo, O. (2009). Suspended sediment transport and deposition over a dune : Río Paraná , Argentina. *Earth Surface Processes and Landforms*, 1611(July), pp. 1605–1611.
- Kuhnle, R.A. (1992). Bed load transport during rising and falling stages on two small streams. *Earth Surface Processes and Landforms*, 17, pp. 191–197.
- Kuhnle, R.A., Wren, D.G. (2009). Size of suspended sediment over dunes. *Journal of Geophysical Research*, 114(F2), pp. 1–9.
- Kuru, W.C., Leighton, D.T., McCreedy, M.J. (1995). Formation of waves on a horizontal erodible bed of particles. *International Journal of Multiphase Flow*, 26(6), pp. 1123–1140.
- Lane, S.N., Richards, K.S. (1997). Linking river channel form and process: time, space and causality revisited. *Earth Surface Processes and Landforms*, 22(3), pp. 249–260.
- Lane, S.N. Biron, P.M. Bradbrook, K.F. Butler, J.B. Chandler, J.H. Crowell, M.D. (1998). Three-dimensional measurement of river channel flow processes using acoustic Doppler velocimetry. *Earth Surface Processes and Landforms*. 23, pp. 1247-1267
- Langbein, W.B., Leopold, L.B. (1968). *River channel bars and dunes: theory of kinematic waves*, Washington, U.S. Govt. Print. Off.
- Lapointe, M.F, (1992). Burst-like sediment suspension events in a sand bed river. *Earth Surface Processes and Landforms*, 17(3), 253–270.

- Lapointe, M.F. (1996). Frequency spectra and intermittency of the turbulent suspension process in a sand-bed river. *Sedimentology*, 43(3), pp. 439–449.
- Leclair, S.F. (2002). Preservation of cross-strata due to the migration of subaqueous dunes : an experimental investigation. pp. 1157–1180.
- Leclair, S.F. (2006). New pieces to the puzzle of reconstructing sediment paleofluxes from river dune deposits. *Geology*, 34(5), p.401.
- Leclair, S.F. (2011). Interpreting fluvial hydromorphology from the rock record: Large-river peak flows leave no clear signature. In: Davidson, S.K., Leleu, S. North, C.P. (eds.), *From River to Rock Record: the Preservation of Fluvial Sediments and their Subsequent Interpretation*: SEPM Special Publication, 97, pp. 113-124.
- Leeder, M.R. (1983). On the interactions between turbulent entrainment of sediment and initiation of bed defects flow, sediment transport and bedform mechanics in channelized flows. In J. D. Collinson, J. Lewin, eds. *Modern and Ancient Fluvial Systems*. Special Publication of the International Association of Sedimentologists, pp. 5–18.
- Leeder, M. (2009). On the interactions between turbulent flow, sediment transport and bedform mechanics in channelized flows. In J. D. Collinson and J. Lewin, ed. *Modern and Ancient Fluvial Systems*. Oxford, UK.: Blackwell Publishing Ltd.
- Lefebvre, A., Ernstsens, V.B., Winter, C. (2011). Influence of compound bedforms on hydraulic roughness in a tidal environment. *Ocean Dynamics*, 61(12), pp. 2201–2210.
- Lefebvre, A., Paarlberg, A.J., Winter, C. (2014). Flow separation and shear stress over angle-of-repose bed forms: A numerical investigation. *Water Resources Research*, pp. 986–1005.
- Levi, E. (1983). A Universal Strouhal Law. *Journal of Engineering Mechanics-Asce*, 109(3), pp. 718–727.
- Levi, E. (1991). Vortices in Hydraulics. *Journal of Hydraulic Engineering-Asce*, 117(4), pp. 399–413.

- Lourenco, L., Krothapalli, A. (1995). On the accuracy of velocity and vorticity measurements with PIV. *Experiments in Fluids*, 18(6), 421–428.
- Lu, S.S., Willmarth, W.W. (1973). Measurements of the structure of the Reynolds stress in a turbulent boundary layer. *Journal of Fluid Mechanics*, 60(3), 481–511.
- Lunt, I.A. Sambrook Smith, G. H., Best, J. L., Ashworth, P. J., Lane, S. N., Simpson, C. J. (2013). Deposits of the sandy braided South Saskatchewan River: Implications for the use of modern analogs in reconstructing channel dimensions in reservoir characterization. *AAPG Bulletin*, 97(4), pp. 553–576.
- Lynch, K., Fahringer, T., Thurow, B. (2012). Three-dimensional particle image velocimetry using a plenoptic camera. In *50th AIAA Aerospace Sciences Meeting including the New Horizons Forum and Aerospace Exposition*. 1056.
- Macklin, M.G., Lewin, J., Woodward, J.C. (1995). Macklin, M.G., Lewin, J., Woodward, J.C., 1995. Quaternary fluvial systems in the Mediterranean basin. In: Lewin, J., Macklin, M.G., Woodward, J.C. (Eds.), *Mediterranean Quaternary River Environments*. Balkema, Rotterdam, pp. 1–25. In J. Lewin, M. G. Macklin, & J. C. Woodward, eds. *Mediterranean Quaternary River Environments*. Rotterdam, pp. 1–25.
- Maddux, T.B., Nelson, J.M., McLean, S.R. (2003a). Turbulent flow over three-dimensional dunes: 1. Free surface and flow response. *Journal of Geophysical Research*, 108(F1), pp. 6009.
- Maddux, T.B., McLean, S.R., Nelson, J.M. (2003b). Turbulent flow over three-dimensional dunes: 2. Fluid and bed stresses. *Journal of Geophysical Research*, 108(F1), pp. 6010.
- Malkiel, E. (2003). The three-dimensional flow field generated by a feeding calanoid copepod measured using digital holography. *Journal of Experimental Biology*, 206(20), pp. 3657–3666.
- Manning, R. (1891). On the flow of water in open channels and pipes. *Transactions Inst. Civ. Eng. of Ireland*, 20, pp. 161–207.

- Mao, Y. (2003). The effects of turbulent bursting on the sediment movement in suspension *International Journal of Sediment Research*, 18(2), pp. 148–157.
- Marquis, G.A., Roy, A.G. (2011). Bridging the gap between turbulence and larger scales of flow motions in rivers. *Earth Surface Processes and Landforms*, 36(4), pp. 563–568.
- Martin, R.L., Jerolmack, D.J. (2013). Origin of hysteresis in bed form response to unsteady flows. , 49(January), pp. 1–20.
- Matthes, G.H. (1947). Macroturbulence in natural stream flow. *Transactions of the American Geophysical Union*, 28, pp. 255–262.
- McLean, D.G., Church, M., Tassone, B. (1999). Sediment transport along lower Fraser River: 1. Measurements and hydraulic computations. *Water Resources Research*, 35(8), pp. 2533–2548.
- McLean, S.R., Smith, J.D. (1979). Turbulence measurements in the boundary-layer over a sand wave field. *Journal of Geophysical Research-Oceans and Atmospheres*, 84(Nc12), pp. 7791–7808.
- McLean, S.R., Smith, J.D. (1986). A model for flow over two-dimensional bed forms. *Journal of Hydraulic Engineering*, 112(4), pp. 300–317.
- McLean, S.R. (1990). The stability of Ripples and Dunes. *Earth Science Reviews*, 29, pp. 131–144.
- McLean, S.R., Nelson, J., Wolfe, S.R. (1994). Turbulence structure over two-dimensional bed forms Implications for sediment transport. *Journal of Geophysical Research*, 99(6), pp. 12,712–729,747.
- McLean, S.R., Wolfe, S.R., Nelson, J.M. (1999b). Predicting boundary shear stress for the purpose of estimating sediment transport over twodimensional bedforms. *Journal of Hydraulic Engineering*, 125(7), pp. 725–736.
- McLean, S.R., Wolfe, S.R., Nelson, J.M. (1999a). Spatially averaged flow over a wavy boundary revisited. *Journal of Geophysical Research*, 104(C7), pp. 15,743–15,753.

McLean, S.R., Nelson, J.M., Gary, L. (2008). Suspended sediment in the presence of dunes. , pp. 611–618.

McLelland, S.J. Richards, K.S. Roy, A.G. (1998). Three-dimensional measurement of river channel flow processes using acoustic Doppler velocimetry. *Earth Surface Processes and Landforms*, 23, pp. 1247–1267.

McLelland, S., Ashworth, P.J., Best, J. (1999). Flow structure and transport of sand-grade suspended sediment around an evolving braid bar, Jamuna River. In N. D. Smith & J. Rogers, eds. *Fluvial Sedimentology VI*. Oxford: Blackwell, pp. 43–57.

Meinart, R. (1983). *Mesure de champs de vitesse d'écoulements fluides par analyse de suites d'images obtenues par diffusion d'un feuillet lumineux*: Université Libre de Bruxelles.

Melling, A. (1997). Tracer particles and seeding for particle image velocimetry. *Measurement Science and Technology*, 8 (12), pp. 1406–1416.

Meneveau, C., Sreenivasan, K. (1987). Simple multifractal cascade model for fully developed turbulence. *Physical Review Letters*, 59(13), pp. 1424–1427.

Milliman, J.D., Meade, R.H. (1983). World-wide delivery of river sediment to the oceans. *The Journal of Geology*, 91(1), pp. 1–21.

Milburn, D., Prowse, T. (2002). Under-ice movement of cohesive sediments before river- ice breakup. *Hydrological Processes*, 834(November 1999), pp. 823–834.

Mohrig, D., Smith, J.D. (1996). Predicting the migration rates of subaqueous dunes. *Water Resources Research*, 32(10), pp. 3207–3217.

Moog, D.B., Whiting, P.J. (1998a). Annual hysteresis in bed load rating curves. *Water Resources Research*, 34(9), pp. 2393–2399.

Moog, D.B., Whiting, P.J. (1998b). Temporal characteristics of coherent flow structures generated over alluvial sand dunes, Mississippi River, revealed by Acoustic Doppler Current Profiling and Multibeam Echo Sounding. *Water Resources Research*, 34(9), pp. 2393–2399.

MRC, (2005). *Overview of the Hydrology of the Mekong Basin*.

MRC, (2010). *State of the Basin Report*.

Muller, A., Gyr, A. (1986). On the vortex formation in the mixing layer behind dunes. *Journal of Hydraulic Research*, 24(5), pp. 359–375.

Muller, A., Gyr, A. (1996). The role of coherent flow Structures in developing bedforms during sediment transport. P. J. Ashworth *et al.*, eds. *Coherent Flow Structures in Open Channel Flows*.

Muste, M., Braileanu, F. & Ettema, R., (2000). Flow and sediment transport measurements in a simulated ice-covered channel. *Water Resources Research*, 36(9), pp.2711–2720.

Muste, M., Fujita, I., Hauet, A. (2008). Large-scale particle image velocimetry for measurements in riverine environments. *Water Resources Research*. 44(4), pp. W00D19.

Nabi, M. de Vriend, H. J., Mosselman, E., Sloff, C. J., Shimizu, Y. (2012). Detailed simulation of morphodynamics: 1. Hydrodynamic model. *Water Resources Research*, 48(12), pp. W12523

Nabi, M. de Vriend, H. J., Mosselman, E., Sloff, C. J., Shimizu, Y. (2013a). Detailed simulation of morphodynamics: 2. Sediment pickup, transport, and deposition. *Water Resources Research*, 49(8), pp. 4775–4791.

Nabi, M. de Vriend, H. J., Mosselman, E., Sloff, C. J., Shimizu, Y. (2013b). Detailed simulation of morphodynamics: 3. Ripples and dunes. *Water Resources Research*, 49(9), pp. 5930–5943.

Nakagawa, H., Nezu, I. (1981). Structure of space-time correlations of bursting phenomena in an open channel flow. *Journal of Fluid Mechanics*, 104, pp. 1–43.

Naqshband, S. Ribberink, J. S., Hurther, D., Hulscher, S. J. M. H. (2014a). Bed load and suspended load contributions to migrating sand dunes in equilibrium. *Journal of Geophysical Research: Earth Surface*, 119, pp. 1043-1063

Naqshband, S., Ribberink, J.A., Hulscher, S.J.M.H. (2014b). Using both free surface effect and sediment transport mode parameters in defining the

morphology of river dunes and their evolution to upper stage plane beds.

Journal of Hydraulic Engineering-ASCE, pp. 1–6.

Nelson, J.M., Smith, J.D. (1989). Mechanics of flow over ripples and dunes.

Journal of Geophysical Research, 94(C6), pp. 8146–8162.

Nelson, J., McLean, S.R., Wolfe, S.R. (1993). Mean flow and turbulence fields

over two dimensional bed forms. *Water Resources Research*, 29(12), pp. 3935–3953.

Nelson, J.M., Shreve, R. L., McLean, S. R., Drake, T. G. (1995). Role of near-bed turbulence structure in bed load transport and bed form mechanics. *Water*

Resources Research, 31(8), pp. 2071–2086.

Nelson, J.M. Logan, B. L., Kinzel, P. J., Shimizu, Y., Giri, S., Shreve, R. L.,

McLean, S. R., Barbara, S. (2011). Bedform response to flow variability. *Earth Surface Processes and Landforms*, 1947(September), pp. 1938–1947.

Nezu, I., Nakagawa, H. (1993). *Turbulence in Open Channel Flows.*, Rotterdam: A.A. Balkema.

Nezu, I., Nakagawa, H. (1995). Turbulence measurements in unsteady free-surface flows. *Flow measurement and instrumentation*, 6(1), pp. 49–59.

Nicholas, A.P. Sandbach, S. D., Ashworth, P. J., Amsler, M. L., Best, J. L.,

Hardy, R. J., Lane, S. N., Orfeo, O., Parsons, D. R., Reesink, A. J.H., Sambrook-Smith, G. H., Szupiany, R. N. (2012). Modelling hydrodynamics in the Rio

Paraná, Argentina: An evaluation and inter-comparison of reduced-complexity and physics based models applied to a large sand-bed river. *Geomorphology*, 169-170, pp. 192–211.

Nicholas, A.P. Nicholas, A. P., Ashworth, P. J., Sambrook Smith, G. H.,

Sandbach, S. D.. (2013). Numerical simulation of bar and island morphodynamics in anabranching megarivers. *Journal of Geophysical Research: Earth Surface*, 118(4), pp. 2019–2044.

Nicholas, A.P. (2013). Modelling the continuum of river channel patterns. *Earth Surface Processes and Landforms*, 38(June), pp. 1187–1196.

- Niemann, S.L., Fredsoe, J., Jacobsen, N.G. (2011). Sand dunes in steady flow at low froude numbers: Dune height evolution and flow resistance. *Journal of Hydraulic Engineering*, 137(1), pp. 5–14.
- Ninto, Y., Garcia, M.H. (1996). Experiments on particle–turbulence interactions in the near–wall region of an open channel flow: implications for sediment transport. *Journal of Fluid Mechanics*, 326, pp. 285–319.
- Nittrouer, J.A., Allison, M.A., Campanella, R. (2008). Bedform transport rates for the lowermost Mississippi River. *Journal of Geophysical Research*, 113(F3).
- Nowell, A. & Church, M.A., 1979. Turbulent flow in a depth-limited boundary layer. *Journal of Geophysical Research-Oceans*, 84(C8), pp.4816–4824.
- Nystuen, J.D., Dacey, M.F. (1961). A graph theory interpretation of nodal regions. *Papers of the Regional Science Association*, 7(1), pp. 29–42.
- Okamoto, T., Nezu, I. (2013). Spatial evolution of coherent motions in finite-length vegetation patch flow. *Environmental Fluid Mechanics*, 13(5), 417–434.
- Omidyeganeh, M.H, Piomelli, U. (2011). Large-eddy simulation of two-dimensional dunes in a steady, unidirectional flow. *Journal of Turbulence*, 12, p.N42.
- Omidyeganeh, M.H., Piomelli, U. (2013a). Large-eddy simulation of three-dimensional dunes in a steady, unidirectional flow. Part 1. Turbulence statistics. *Journal of Fluid Mechanics*, 721, pp. 454–483.
- Omidyeganeh, M.H., Piomelli, U. (2013b). Large-eddy simulation of three-dimensional dunes in a steady, unidirectional flow. Part 2. Flow structures. *Journal of Fluid Mechanics*, 734, pp. 509–534.
- Omidyeganeh, M.H., Piomelli, U., Christensen, K. T., Best, J. L. (2013). Large eddy simulation of interacting barchan dunes in a steady, unidirectional flow. *Journal of Geophysical Research: Earth Surface*, 118(4), pp. 2089–2104.
- Paarlberg, A.J. Dohmen-Janssen, C. M., Hulscher, S. J. M. H., Termes, P. (2007). A parameterization of flow separation over subaqueous dunes. *Water Resources Research*, 43(12).

- Paarlberg, A.J. Dohmen-Janssen, C. M., Hulscher, S. J. M. H., Termes, P. (2009). Modeling river dune evolution using a parameterization of flow separation. *Journal of Geophysical Research*, 114(F1), pp. 1–17.
- Paarlberg, A.J. Dohmen-Janssen, C. M., Hulscher, S. J. M. H., Termes, P., Schielen, R. (2010). Modelling the effect of time-dependent river dune evolution on bed roughness and stage. *Earth Surface Processes and Landforms*, 35(15), pp. 1854–1866.
- Paola, C., Borgman, L. (1991). Reconstructing random topography from preserved stratification. *Sedimentology*, 38(4), pp. 553–565.
- Paola, C., Straub, K., Mohrig, D., Reinhardt, L. (2009). The "unreasonable effectiveness" of stratigraphic and geomorphic experiments. *Earth-Science Reviews*. 97(1-4), pp. 1-43
- Parker, G. (1990). Hydraulic geometry of active gravel rivers. *Journal of the Hydraulics Division*, 105(9), pp. 1185–1201.
- Parker, G. (2014). Teasing out simplicity from complexity: the law of constant bankfull velocity in alluvial rivers. In *AGU Fall Meeting 2014*. San Francisco, EP41D–06.
- Parsons D.R., Best J.L., Orfeo O., Hardy R.J., Kostaschuk R., Lane S.N. (2005). Morphology and flow fields of three-dimensional dunes, Rio Parana Argentina : Results from simultaneous multibeam echo sounding and acoustic Doppler current profiling. *Journal of Geophysical Research*, 110, F04S03.
- Parsons, D.R. *et al.* (2007). Form roughness and the absence of secondary flow in a large confluence – diffluence, Rio Paraná , Argentina. *Earth Surface Processes and Landforms*, 162, pp. 155–162.
- Parsons, D.R. *et al.* (2013). Velocity Mapping Toolbox (VMT): A processing and visualization suite for moving-vessel ADCP measurements. *Earth Surface Processes and Landforms*, 38(February), pp. 1244–1260.
- Peakall, J. Ashworth, P., Best, J. (1996). Physical modelling in fluvial geomorphology : principles, applications and unresolved issues. In *The Scientific Nature of Geomorphology: Proceedings of the 27th Binghamton*

Symposium in Geomorphology. Edited by B. Rhoads & C. Thorn. Wiley. pp. 27-29.

Petit, F. (1987). The relationship between shear stress and the shaping of the bed of a pebble-loaded river la ruelles—Ardenne. *Catena*, 14(5), pp. 453–468.

Phillips, J.D. (2011). Emergence and pseudo-equilibrium in geomorphology. *Geomorphology*, 132(3-4), pp. 319–326.

Pons, A., Davidson-arnott, R.G. (2007). Comparing Different Methods Of Shear Velocity Estimates Under Field Conditions 1 st year of Master internship report. , (July), pp. 1–26.

Prasad, A.K., Adrian, R.J. (1993). Stereoscopic particle image velocimetry applied to liquid flows. *Experiments in Fluids*, 15, pp. 49-60

Prasad, A.K. (2000). Stereoscopic particle image velocimetry. *Experiments in Fluids*, 29(2), .pp. 103–116.

Prent, T.H., Hickin, E.J. (2001). Annual regime of bedforms , roughness and flow resistance , Lillooet River , British Columbia , BC.

Prowse, T.D., Ferrick, M.G. (2002). Preface - Hydrology of ice-covered rivers and lakes: scoping the subject. *Hydrological Processes*, 16(4), pp. 759–762.

Raffel, M. Willert, C.E. Wereley, S.T. Kompenhans, J. (2007). *Particle Image Velocimetry. A Practical Guide*. Springer, New York.

Ramirez, M.T., Allison, M. A. (2013). Suspension of bed material over sand bars in the Lower Mississippi River and its implications for Mississippi delta environmental restoration. *Journal of Geophysical Research: Earth Surface*, 118(2), pp. 1085–1104.

Rao, K.N. Narasimha, R. Badri Narayanan, M.A. (1971). Bursting Phenomenon in a Turbulent Boundary Layer. *Journal of Fluid Mechanics*, 48 Part 2, pp. 339-352.

Raudkivi, A.J. (1963). Study of sediment ripple formation. *Journal of Hydraulic Division. American Society of Civil Engineers*, 86(HY6), pp. 15–33.

- Raudkivi, A.J. (1966). Bed forms in alluvial channels. *Journal of Fluid Mechanics*, 26, pp. 15–33.
- Raudkivi, A.J. (1998). *Loose Boundary Hydraulics*, Rotterdam: Brookfield.
- Reesink, A.J.H., Bridge, J.S. (2007). Influence of superimposed bedforms and flow unsteadiness on formation of cross strata in dunes and unit bars. *Sedimentary Geology*, 202(1-2), pp. 281–296.
- Reesink, A.J.H., Bridge, J.S. (2009). In fluence of bedform superimposition and fl ow unsteadiness on the formation of cross strata in dunes and unit bars — Part 2 , further experiments. *Sedimentary Geology*, 222(3-4), pp. 274–300.
- Ricardo, A.M.; Koll, K.; Franca, M.J.; Schleiss, A.J. and Ferreira, R.M.L. (2014) The terms of the turbulent kinetic energy budget within reaches of emergent vegetation. *Water Resources Research. Res.*, 50, pp. 4131–4148
- Rice, H., Hunter, T. N., Peakall, J., Biggs, S., Fairweather, M. (2012). Behaviour of time-dependent bedforms in closed pipe flow. *Proceeding of THMT-12. Proceedings of the Seventh International Symposium On Turbulence, Heat and Mass Transfer Palermo, Italy, 24-27 September, 2012*, pp. 10.
- Rice, H.P. (2013). *Transport and deposition behaviour of model slurries in closed pipe flow*. PhD Thesis. University of Leeds.
- Robert, A., Uhlman, W. (2001). An experimental study on the ripple dune transition. *Earth Surface Processes and Landforms*, 26, pp. 615–629.
- Robert, A. (2003). *River processes : an introduction to fluvial dynamics*, London: Arnold.
- Robert, A. (2011). Flow resistance in alluvial channels. *Progress in Physical Geography*, 35(6), pp. 765–781.
- Roden, J., 1998. *The Sedimentology and dynamics of mega-dunes, Jamuna River, Bangladesh*. PhD thesis, University of Leeds.
- Rubin, D.M., McCulloch, D.S. (1980). Single and superimposed bedforms a synthesis of sanfrancisco bay and flume observations. *Sedimentary Geology*, 26(26), pp. 207–231.

- Ruddiman, W.F., Raymo, M.E. (2003). A methane-based time scale for Vostok ice. *Quaternary Science Reviews*, 22, pp. 141–155.
- Ruderich, R., Fernholz, H.H. (1986). An experimental investigation of a turbulent shear flow with separation, reverse flow, and reattachment. *Journal of Fluid Mechanics*, 163, pp. 283–322.
- Ryerson, W.G., Schwenk, K. (2012). A simple, inexpensive system for digital particle image velocimetry (DPIV) in Biomechanics. *Journal of Integrative Biology*, 317, pp. 127–140.
- Ryu, D.N., Choi, D.H., Patel, V.C. (2007). Analysis of turbulent flow in channels roughened by two-dimensional ribs and three-dimensional blocks. Part I: Resistance. *International Journal of Heat and Fluid Flow*, 28(5), pp. 1098–1111.
- Sambrook Smith, G.H. Best, J. L., Orfeo, O., Vardy, M. E., Zinger, J. A. (2013). Decimeter-scale in situ mapping of modern cross-bedded dune deposits using parametric echo sounding: A new method for linking river processes and their deposits. *Geophysical Research Letters*, 40(15), pp. 3883–3887.
- Sandbach, S.D. Lane, S. N., Hardy, R. J., Amsler, M. L., Ashworth, P. J., Best, J. L., Nicholas, A. P., Orfeo, O., Parsons, D. R., Reesink, A. J. H., Szupiany, R. N. (2012). Application of a roughness-length representation to parameterize energy loss in 3-D numerical simulations of large rivers. *Water Resources Research*, 48(12), pp. W12501.
- Schindler, R.J., Robert, A. (2004). Suspended sediment concentration and the ripple-dune transition. *Hydrological Processes*, 18(17), pp. 3215–3227.
- Schindler, R.J., Robert, A. (2005). Flow and turbulence structure across the ripple-dune transition: an experiment under mobile bed conditions. *Sedimentology*, 52(3), pp. 627–649.
- Schmeeckle, M.W., Nelson, J.M. (2003). Direct numerical simulation of bedload transport using a local , dynamic boundary condition. *Sedimentology*., 50, pp. 279–301.

- Schmeeckle, M. W. (2014). The role of velocity, pressure, and bed stress fluctuations in bed load transport over bed forms: numerical simulation downstream of a backward-facing step. *Earth Surface Dynamics*, 2,(2), pp. 715-732.
- Schröder, A. Geisler, R. Staack, K. Elsinga, G. E. Scarano, F. Wieneke, B. Henning, A. Poelma, C. Westerweel, J. (2011). Eulerian and Lagrangian views of a turbulent boundary layer flow using time-resolved tomographic PIV. *Experiments in Fluids*, 50(4), pp. 1071–1091.
- Schumm, R.W., Lichty, S.A. (1965). Time, space and causality in Geomorphology. *American Journal of Science*, 263, pp. 110–119.
- Seminara, G. (2010). Fluvial sedimentary patterns. *Annual Review of Fluid Mechanics*, 42(1), pp. 43–66.
- Sequeiros, O.E. Spinewine, B., Beaubouef, R, T., Sun, T., Garcia, M. H., Parker, G. (2010). Bedload transport and bed resistance associated with density and turbidity currents. *Sedimentology*, 57(6), pp. 1463–1490.
- Sheng, J., Malkiel, E., Katz, J. (2008). Using digital holographic microscopy for simultaneous measurements of 3D near wall velocity and wall shear stress in a turbulent boundary layer. *Experiments in Fluids*, 45(6), 1023–1035.
- Shimizu, Y. Giri, S., Yamaguchi, S., Nelson, J., (2009). Numerical simulation of dune-flat bed transition and stage-discharge relationship with hysteresis effect. *Water Resources Research*, 45. W04429
- Shugar, D.H. Kostaschuk, R., Best, J. L., Parsons, D. R., Lane, S. N., Orfeo, O., Hardy, R. J. (2010). On the relationship between flow and suspended sediment transport over the crest of a sand dune, RÃo ParanÃi, Argentina. *Sedimentology*, 57(1), pp. 252–272.
- Sills, G.L. Vroman, N. D., Wahl, R. E., Schwanz, N. T. (2008). Overview of New Orleans Levee Failures: Lessons Learned and Their Impact on National Levee Design and Assessment. *Journal of Geotechnical and Geoenvironmental Engineering*, 134(5), pp. 556–565.

- Sime, L.C., Ferguson, R.I., Church, M. (2007). Estimating shear stress from moving boat acoustic Doppler velocity measurements in a large gravel bed river. *Water Resources Research*, 43(October 2006), pp. 1–12.
- Simons, D., Richardson, E.V., Nordin, A.F. (1960). Sedimentary structures generated by flow in alluvial channels. AAPG-SEPM. Primary Sedimentary Structures (SP12), pp. 34–52
- Simons, D.B., Richardson, E.V. (1962). *The effect of bed roughness on depth-discharge relations in alluvial channels*. Geological Survey Water-Supply Paper 1498-E
- Simons, D.B., Richardson, E.V. (1966). *Alluvial Channels Resistance to Flow in Alluvial Channels*, Geological Survey Professional Paper 422-J
- Simpson, R.L. (1989). Turbulent boundary-layer separation. *Annual Review of Fluid Mechanics*, 21, pp. 205–234.
- Simpson, R.L. (1996). Aspects of turbulent boundary-layer separation. *Progress in Aerospace Science*, 32, pp. 457–521.
- Smith, B., Ettema, R. (1995). A method for calculating flow resistance in ice-covered alluvial channels. *Journal of Hydraulic Engineering*, 123(7), pp. 592–599.
- Smith, B.T., Ettema, R. (1997). Ice-cover influence on flow structure over dunes. Ice-cover influence on flow structure over dunes. *Journal of Hydraulic Research*, 35(5), pp. 37–41.
- Smith, C.R. (1996). Coherent flow structures in smooth-wall turbulent boundary layers: facts, mechanisms and speculation. In P. J. Ashworth *et al.*, eds. *Coherent Flow Structures in Open Channels*. Chichester: Wiley.
- Smith, J., McLean, S.R. (1977). Spatially averaged flow over a wavy surface. *Journal of Geophysical Research*, 82(12), pp. 1735–1746.
- Soloff, S.M., Adrian, R.J., Liu, Z.C. (1997). Distortion compensation for generalized stereoscopic particle image velocimetry. *Measurement Science and Technology*, 8(12), pp. 1441–1454.

- Southard, J.B., Boguchwal, L.A. (1990). Bed configurations in steady unidirectional water flows. Part 2. Synthesis of flume data. *Journal of Sedimentary Petrology*, 60(5), pp. 658–679.
- Straub, K.M. Ganti, V., Paola, C., Foufoula-Georgiou, E. (2012). Prevalence of exponential bed thickness distributions in the stratigraphic record: Experiments and theory. *Journal of Geophysical Research*, 117(F2). F02003
- Sukhodolov, A.N., Fedele, J.J., Rhoads, B.L. (2006). Structure of flow over alluvial bedforms : an experiment on linking field and laboratory methods. *Earth Surface Processes and Landforms*, 1310(March), pp. 1292–1310.
- Sumner, E.J., Talling, P. J., Lawrence A.A., Wynn, R. B. Stevenson, C. J., Frenz, M., (2012). Facies architecture of individual basin-plain turbidites: Comparison with existing models and implications for flow processes. *Sedimentology*, 59(6), pp. 1850–1887.
- Syvitski, J.P.M. Vörösmarty, C. J., Kettner, A. J., Green, P. (2005). Impact of humans on the flux of terrestrial sediment to the global coastal ocean. *Science (New York, N.Y.)*, 308(5720), pp. 376–80.
- Syvitski, J.P.M. Kettner, A. J., Overeem, I., Hutton, E. W. H., Hannon, M. T., Brakenridge, G. R. Day, J., Vörösmarty, C., Saito, Y., Giosan, L., Nicholls, R. J. (2009). Sinking deltas due to human activities. *Nature Geoscience*, 2(10), pp. 681–686.
- Syvitski, J.P.M. Cohen, S., Kettner, A. J., Brakenridge, G. R. (2014). How important and different are tropical rivers? — An overview. *Geomorphology*, 227(12), pp. 5–17.
- Syvitski, J.P.M., Milliman, J.D. (2014). Geology, geography, and humans battle for dominance over the delivery of fluvial sediment to the coastal Ocean. *The Journal of Geology*, 115(1), pp. 1–19.
- Szupiany, R.N. Amsler, M. L., Parsons, D. R., Best, J. L. (2009). Morphology, flow structure, and suspended bed sediment transport at two large braid-bar confluences. *Water Resources Research*, 45(5), pp. W05415.

- Szupiany, R.N. Amsler, M. L., Hernandez, J., Parsons, D. R., Best, J. L., Fornari, E., Trento, A. (2012). Flow fields, bed shear stresses, and suspended bed sediment dynamics in bifurcations of a large river. *Water Resources Research*, 48(11), pp. W11515.
- Talke, S.A., Horner-Devine, A.R., Chickadel, C.C. (2010). Mixing layer dynamics in separated flow over an estuarine sill with variable stratification. *Journal of Geophysical Research*, 115(C9). C09004
- Talke, S.A., Devine, A.R.H., Chickadel, C.C., Jessup, A.T. (2013). Turbulent kinetic energy and coherent structures in a tidal river. *Journal of Geophysical Research: Oceans*, 118, (12), pp. 6965-6981
- Talling, P.J. Masson, D. G., Sumner, E. J., Malgesini, G. (2012). Subaqueous sediment density flows: Depositional processes and deposit types. *Sedimentology*, 59(7), pp. 1937–2003.
- Tayfur, G., Singh, V. (2012). Transport capacity models for unsteady and non-equilibrium sediment transport in alluvial channels. *Computers and Electronics in Agriculture*, 86, pp. 26–33.
- Theunissen, R., Scarano, F., Riethmuller, M.L. (2007). An adaptive sampling and windowing interrogation method in PIV. *Measurement Science and Technology*, 18(1), pp. 275–287.
- Theunissen, R. Scarano, F., Riethmuller, M.L. (2010). Spatially adaptive PIV interrogation based on data ensemble. *Experiments in Fluids*, 48, pp. 875–887.
- Thielicke, W. (2014). PIVlab - time-resolved particle image velocimetry (PIV) tool. <http://www.mathworks.co.uk/matlabcentral/fileexchange/27659-pivlab-time-resolved-particle-image-velocimetry--piv--tool>.
- Thomas, B.F., Watt, D.A. (1903). *The Improvement of Rivers A Treatise on the Methods Employed for Improving Streams for Open Navigation, and for Navigation by means of Locks and Dams*, New York.: Wiley.
- Tobin, G.A. (1995). The levee love affair: a stormy relationship? *Journal of the American Water Resources Association*, 31(3), pp. 359–367.

- Tomkins, C.D., Adrian, R.J. (1999). Characteristics of vortex packets in wall turbulence. In *Turbulence and Shear Flow Phenomena*. Edited by S. Banerjee & J. Eaton, New York.: Begell House, pp. 31–36.
- Torrence, C., Compo, G.P. (1998). A practical guide to wavelet analysis. *Bulletin of the American Meteorological Society*, 79(1), pp. 61–78.
- Turcotte, B. Morse, B., Bergeron, N. E., Roy, A. G. (2011). Sediment transport in ice-affected rivers. *Journal of Hydrology*, 409(1-2), pp. 561–577.
- Ullman, E.L. (1941). A theory of location for cities. *American Journal of Sociology*, 46(6), pp. 853–864.
- Unger, J., Hager, W.H. (2007). Down-flow and horseshoe vortex characteristics of sediment embedded bridge piers. *Experiments in Fluids*, 42, 1-19.
- Unverricht, D., Nguyen, T., (2014). Suspended sediment dynamics during the inter-monsoon season in the subaqueous Mekong Delta and adjacent shelf, southern Vietnam. *Journal of Asian Earth Science*. 79, pp. 509–519.
- Van den Berg, J.H., Van Gelder, A. (1993). A new bedform stability diagram, with emphasis on the transition of ripples to plane bed in flows over fine sand and silt. *Special Publication of the International Association of Sedimentologists*, 17, pp. 11–21.
- Van den Berg, J.H., Van Gelder, A. (1998). Flow and sediment transport over large subaqueous dunes: Fraser River, Canada. *Sedimentology*, 45(1), pp. 217–219
- Van Rijn, L. (1982). Equivalent roughness of alluvial bed. *Journal of Hydraulic Engineering*, 108(10), pp. 1215–1218.
- Van Rijn, L.C. (1984a). Sediment transport Part I Bed load transport. *Journal of Engineering Mechanics*, 110(10), pp. 1431–1456.
- Van Rijn, L.C. (1984b). Sediment transport Part II suspended load transport. *Journal of Hydraulic Engineering*, 110(11), pp. 1613–1641.
- Van Rijn, L.C. (1984c). Sediment transport Part III Bed forms and alluvial roughness. *Journal of Hydraulic Engineering*, 110(12), pp. 1733–1754.

- Vanoni, V.A., Brooks, H. (1957). *Laboratory studies of the roughness and suspended load of alluvial streams*, Missouri.
- Venditti, J.G., Bennett, S.J. (2000). Spectral analysis of turbulent flow and suspended sediment transport over fixed dunes. *Journal of Geophysical Research*, 105(C9), pp. 22–35.
- Venditti, J.G. (2003). *Initiation and development of sand dunes in river channels*, Ph.D. thesis., Vancouver, B. C., Canada.: Department of Geography., University. of B. C., Vancouver.
- Venditti, J.G., Bauer, B.O. (2005). Turbulent flow over a dune: Green River, Colorado. *Earth Surface Processes and Landforms*, 30(3), pp. 289–304.
- Venditti, J.G., Church, M., Bennett, S.J. (2005a). Bed form initiation from a flat sand bed. *Journal of Geophysical Research: Earth Surface*, 110, pp. 1–19.
- Venditti, J.G., Church, M., Bennett, S.J. (2005b). Morphodynamics of small-scale superimposed sand waves over migrating dune bed forms. *Water Resources Research*, 41(10). W10423
- Venditti, J.G., Church, M., Bennett, S.J. (2005c), On the transition between 2D and 3D dunes. *Sedimentology*, 52(6), pp. 1343–1359.
- Venditti, J.G., Church, M., Bennett, S.J. (2006). On interfacial instability as a cause of transverse subcritical bed forms. *Water Resources Research*, 42, pp. 1–10.
- Venditti, J. (2007). Turbulent flow and drag over fixed two and three-dimensional dunes. *Journal of Geophysical Research: Earth Surface*, 112, 1–21.
- Verhagen, I.T.E. Baas, J. H., Jacinto, R. S., McCaffrey, W. D., Davies, A. G. (2013). A first classification scheme of flow-bed interaction for clay-laden density currents and soft substrates. *Ocean Dynamics*, 63(4), pp. 385–397.
- Villard, P., Kostaschuk, R. (1998). The relation between shear velocity and suspended sediment concentration over dunes: Fraser Estuary, Canada. *Marine Geology*, 148, pp. 71–81.

- Wahl, T.L. (2003). Discussion of “Despiking Acoustic Doppler Velocimeter Data” by Derek G. Goring and Vladimir I. Nikora. *Journal of Hydraulic Engineering*, 129(6), pp. 474–487.
- Walker, I.J., Nickling, W.G. (2002). Dynamics of secondary airflow and sediment transport over and in the lee of transverse dunes. *Progress in Physical Geography*, 26(1), pp. 47–75.
- Warmink, J. J., Dohmen-Janssen, C. C., Lansink, J., Naqshband, S., van Duin, O. J. M., Termes, A.P.P., Hulscher, S.J.M.H. (2014). Understanding river dune splitting through flume experiments and analysis of a dune evolution model. *Earth Surface Processes and Landforms*. 39, pp. 1208-1220.
- Westerweel, J. (1993). Analysis of PIV interrogation with low pixel resolution. In *SPIE’s 1993 International Symposium on Optics, Imaging, and Instrumentation*. Edited by S. S. Cha & J. D. Trolinger, International Society for Optics and Photonics, pp. 624–635.
- Westerweel, J. (1997). Fundamentals of digital particle image velocimetry, *Measurement Science and Technology*, 8, 1379–1392.
- Westerweel, J., Scarano, F. (2005). Universal outlier detection for PIV data. *Experiments in Fluids*, pp. 1096–1100.
- Wheatstone, C. (1838). Contributions to the Physiology of Vision. Part the First. On Some Remarkable, and Hitherto Unobserved, Phenomena of Binocular Vision. *Philosophical Transactions of the Royal Society of London*, 128, pp. 371–394.
- Whiting, P.J. Dietrich, W. E., Leopold, L. B., Drake, T. G., Shreve, R. L. (1988). Bedload sheets in heterogeneous sediment. *Geology*, 16(2), pp. 105.
- Whiting, P.J., Dietrich, W.E. (1990). Boundary Shear Stress and Roughness Over Mobile Alluvial Beds. *Journal of Hydraulic Engineering*. 116 (12), pp. 1495-1511.
- Wiberg, P.L., Smith, J.D. (1991). Velocity distribution and bed roughness in high-gradient streams. *Water Resources Research*, 27(5), 825–838.

- Wilbers, A.W.E., Ten Brinke, W.B.M. (2003). The response of subaqueous dunes to floods in sand and gravel bed reaches of the Dutch Rhine. *Sedimentology*, 50(6), pp. 1013–1034.
- Wilbers, A.W.E. (2004). *The development and hydraulic roughness of subaqueous dunes*. Phd thesis, University of Utrecht, Neatherlands.
- Wilcock, P.R. (1996). Estimating local bed shear stress from velocity observations. , 32(11), pp. 3361–3366.
- Wilkinson, T.J. (1999). Holocene Valley fills of Southern Turkey and Northwestern Syria : Recent geoarchaeological contributions. , 18, pp. 555–571.
- Willert, C.E., Gharib, M. (1991). Digital particle image velocimetry. *Experiments in Fluids*, 193, pp. 181–193.
- Williams, G.P. (1970). *Flume Width and Water Depth Effects in Experiments Flume Width and Water Depth Effects in Sediment-Transport Experiments Geological Survey Professional Paper 562-H*, Washington DC.
- Willians, J. (1996). Turbulent flow in rivers. In P. Carling A; Dawson, Martin,R, ed. *Advances in Fluvial dynamics and stratigraphy*. Chuchester: John Wiley and Sons.
- Wren, D.G., Kuhnle, R.A., Wilson, C.G. (2007). Measurements of the relationship between turbulence and sediment in suspension over mobile sand dunes in a laboratory flume. , 112(April), pp. 1–14.
- Yager, E. M. Schmeeckle, M. W. (2013). The influence of vegetation on turbulence and bed load transport. *Journal of Geophysical Research: Earth Surface*. 118, (3), pp. 1585-1601
- Yalin, M.S. (1964). Geometrical properties of sand waves. *Journal of Hydraulic Division. American Society of Civil Engeiners ASCE*, 90, pp. 105–19.
- Yalin, M.S. (1977). *Mechanics of sediment transport* 2d ed., Oxford ; New York: Pergamon Press.

Yao C.-S., Adrian R.J. (1984). Orthogonal compression and 1-D analysis technique for measurement of 2-D particle displacements in pulsed laser velocimetry. *Applied Optics*, 23,(11),pp. 1687-9.

Yen, C., Lee, K.T. (1995). Bed Topography and Sediment Sorting in Channel Bend with Unsteady Flow. *Journal of Hydraulic Engineering*, 121(8).pp. 591-599

Zedel, L., Hay, A.E. (2010). Resolving Velocity Ambiguity in Multifrequency, Pulse-to-Pulse Coherent Doppler Sonar. *IEEE Journal of Oceanic Engineering*, 35(4), pp. 847–851.

Zinger, J.A. Rhoads, B.L. Best, J.L. Johnson, K.K. Zinger, J. (2013). Flow structure and channel morphodynamics of meander bend chute cutoffs: A case study of the Wabash River, USA. *Journal of Geophysical Research: Earth Surface*, 118(4), pp. 2468–2487.